

# ornl

**OAK RIDGE  
NATIONAL  
LABORATORY**

**MARTIN MARIETTA**

MARTIN MARIETTA ENERGY SYSTEMS LIBRARIES



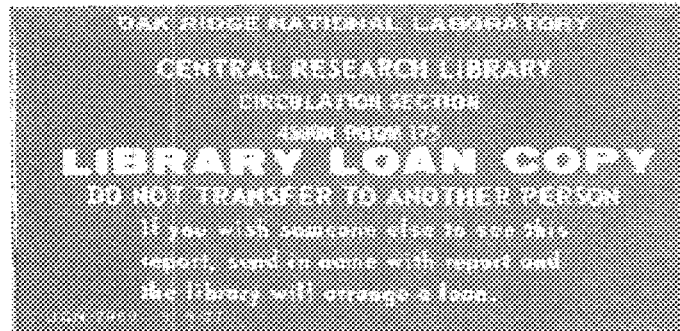
3 4456 0269915 9

ORNL/TM-10570

## The Seasonal Exchange of Carbon Dioxide Between the Atmosphere and the Terrestrial Biosphere: Extrapolation from Site-Specific Models to Regional Models

A. W. King  
D. L. DeAngelis  
W. M. Post

Environmental Sciences Division  
Publication No. 2988



OPERATED BY  
MARTIN MARIETTA ENERGY SYSTEMS, INC.  
FOR THE UNITED STATES  
DEPARTMENT OF ENERGY

Printed in the United States of America. Available from  
National Technical Information Service  
U.S. Department of Commerce  
5285 Port Royal Road, Springfield, Virginia 22161  
NTIS price codes—Printed Copy: A14 Microfiche A01

This report was prepared as an account of work sponsored by an agency of the United States Government. Neither the United States Government nor any agency thereof, nor any of their employees, makes any warranty, express or implied, or assumes any legal liability or responsibility for the accuracy, completeness, or usefulness of any information, apparatus, product, or process disclosed, or represents that its use would not infringe privately owned rights. Reference herein to any specific commercial product, process, or service by trade name, trademark, manufacturer, or otherwise, does not necessarily constitute or imply its endorsement, recommendation, or favoring by the United States Government or any agency thereof. The views and opinions of authors expressed herein do not necessarily state or reflect those of the United States Government or any agency thereof.

ENVIRONMENTAL SCIENCES DIVISION

THE SEASONAL EXCHANGE OF CARBON DIOXIDE BETWEEN THE ATMOSPHERE  
AND THE TERRESTRIAL BIOSPHERE: EXTRAPOLATION FROM  
SITE-SPECIFIC MODELS TO REGIONAL MODELS\*

A. W. King, D. L. DeAngelis, and W. M. Post

Environmental Sciences Division  
Publication No. 2988

---

\*Submitted as a dissertation by A. W. King to the Graduate Council of  
the University of Tennessee in partial fulfillment of the requirements  
for the degree of Doctor of Philosophy.

Date of Issue: December 1987

Prepared for the  
Office of Energy Research  
HA 02 05 00 0

Prepared by the  
OAK RIDGE NATIONAL LABORATORY  
Oak Ridge, Tennessee 37831  
operated by  
MARTIN MARIETTA ENERGY SYSTEMS, INC.  
for the  
U.S. DEPARTMENT OF ENERGY  
under contract DE-AC05-84OR21400



3 4456 0269915 9



## TABLE OF CONTENTS

	<u>Page</u>
1. INTRODUCTION . . . . .	1
1.1 THE SEASONAL CYCLE OF ATMOSPHERIC CO <sub>2</sub> . . . . .	3
1.1.1 The Source of Seasonal Variations in Atmospheric CO <sub>2</sub> . . . . .	3
1.1.2 Latitudinal Variations in the Seasonal CO <sub>2</sub> Cycle . . . . .	6
1.1.3 An Increase in the Amplitude of the Seasonal CO <sub>2</sub> Cycle . . . . .	13
1.2 MODELING THE SEASONAL CYCLE OF ATMOSPHERIC CO <sub>2</sub> . . . . .	17
1.2.1 Tracer Transport Models and CO <sub>2</sub> Source Functions . . . . .	17
1.2.2 A Review of CO <sub>2</sub> Source Functions . . . . .	20
1.2.3 The Need for Ecologically Derived CO <sub>2</sub> Source Functions . . . . .	36
2. THE SITE-SPECIFIC MODELS . . . . .	42
2.1 TEMPERATE BROADLEAF DECIDUOUS FOREST MODEL . . . . .	47
2.1.1 Structure of the Model . . . . .	47
2.1.1.1 Compartments . . . . .	47
2.1.1.2 Driving Variables . . . . .	52
2.1.1.3 Flows or Rate Processes . . . . .	52
2.1.1.4 Photosynthesis and Respiration . . . . .	55
2.1.1.5 Release of Carbon Through Decomposition . . . . .	60
2.1.2 Seasonal Photosynthesis and Respiration . . . . .	60
2.2 TEMPERATE BROADLEAF EVERGREEN FOREST MODEL . . . . .	62
2.2.1 Structure of the Model . . . . .	62
2.2.1.1 Compartments . . . . .	62
2.2.1.2 Driving Variables . . . . .	66
2.2.1.3 Flows or Rate Processes . . . . .	68
2.2.1.4 Photosynthesis and Respiration . . . . .	70
2.2.1.5 Release of Carbon Through Decomposition . . . . .	71
2.2.2 Seasonal Photosynthesis and Respiration . . . . .	71
2.3 COOL CONIFEROUS FOREST MODEL . . . . .	74
2.3.1 Structure of the Model . . . . .	74
2.3.1.1 Compartments . . . . .	74
2.3.1.2 Driving Variables . . . . .	78
2.3.1.3 Flows or Rate Processes . . . . .	78
2.3.1.4 Photosynthesis and Respiration . . . . .	78
2.3.1.5 Release of Carbon Through Decomposition . . . . .	85
2.3.2 Seasonal Photosynthesis and Respiration . . . . .	85

## 2. (Continued)

2.4	WARM CONIFEROUS FOREST MODEL . . . . .	87
2.4.1	Structure of the Model . . . . .	87
2.4.1.1	Compartment	87
2.4.1.2	Driving Variables . . . . .	87
2.4.1.3	Flows or Rate Processes . . . . .	93
2.4.1.4	Photosynthesis and Respiration . . . . .	93
2.4.1.5	Release of Carbon Through Decomposition . . . . .	98
2.4.2	Seasonal Photosynthesis and Respiration . . . . .	98
2.5	TROPICAL MOIST EVERGREEN FOREST MODEL . . . . .	101
2.5.1	Structure of the Model . . . . .	101
2.5.1.1	Compartment	101
2.5.1.2	Driving Variables . . . . .	101
2.5.1.3	Flows or Rate Processes . . . . .	104
2.5.1.4	Photosynthesis and Respiration . . . . .	104
2.5.1.5	Release of Carbon Through Decomposition . . . . .	106
2.5.2	Seasonal Photosynthesis and Respiration . . . . .	106
2.6	TROPICAL DRY DECIDUOUS FOREST MODEL . . . . .	107
2.6.1	Structure of the Model . . . . .	107
2.6.1.1	Compartment	107
2.6.1.2	Driving Variables . . . . .	112
2.6.1.3	Flows or Rate Processes . . . . .	112
2.6.1.4	Photosynthesis and Respiration . . . . .	112
2.6.1.5	Release of Carbon Through Decomposition . . . . .	115
2.6.2	Seasonal Photosynthesis and Respiration . . . . .	115
2.7	TUNDRA MODEL . . . . .	115
2.7.1	Structure of the Model . . . . .	118
2.7.1.1	Compartment	118
2.7.1.2	Driving Variables . . . . .	118
2.7.1.3	Flows or Rate Processes . . . . .	118
2.7.1.4	Photosynthesis and Respiration . . . . .	123
2.7.1.5	Release of Carbon Through Decomposition . . . . .	124
2.7.2	Seasonal Photosynthesis and Respiration . . . . .	125
2.8	GRASSLAND MODEL . . . . .	128
2.8.1	Structure of the Model . . . . .	128
2.8.1.1	Compartment	128
2.8.1.2	Driving Variables . . . . .	131
2.8.1.3	Flows or Rate Processes . . . . .	131
2.8.1.4	Photosynthesis and Respiration . . . . .	131
2.8.1.5	Release of Carbon Through Decomposition . . . . .	137
2.8.2	Seasonal Photosynthesis and Respiration . . . . .	138

	<u>Page</u>
2. (Continued)	
2.9 DESERT AND ARID SHRUBLAND MODEL . . . . .	141
2.9.1 Structure of the Model . . . . .	141
2.9.1.1 Compartments . . . . .	141
2.9.1.2 Driving Variables . . . . .	144
2.9.1.3 Flows or Rate Processes . . . . .	148
2.9.1.4 Photosynthesis and Respiration . . . . .	154
2.9.1.5 Release of Carbon Through Decomposition . . . . .	157
2.9.2 Seasonal Photosynthesis and Respiration . . . . .	157
2.10 CROPLAND MODEL . . . . .	158
2.10.1 Structure of the Model . . . . .	158
2.10.1.1 Compartments . . . . .	158
2.10.1.2 Driving Variables . . . . .	158
2.10.1.3 Flows or Rate Processes . . . . .	163
2.10.1.4 Photosynthesis and Respiration . . . . .	163
2.10.1.5 Release of Carbon Through Decomposition . . . . .	167
2.10.2 Seasonal Photosynthesis and Respiration . . . . .	168
3. A GLOBAL CO <sub>2</sub> EXCHANGE FUNCTION FOR THE TERRESTRIAL BIOSPHERE . . . . .	172
3.1 BIOME IDENTIFICATION AND GEOGRAPHICAL EXTENT . . . . .	172
3.1.1 Model Biome Identification . . . . .	172
3.1.2 Geographical Distribution and Areal Extent . . . . .	177
3.2 SIMULATION OF GLOBAL CO <sub>2</sub> EXCHANGES . . . . .	180
3.2.1 Extrapolation From Site-specific to Regional CO <sub>2</sub> Fluxes: An Hypothesis . . . . .	180
3.2.2 Global CO <sub>2</sub> Exchange Functions: A Test of the Hypothesis . . . . .	182
4. EXTRAPOLATION FROM SITE-SPECIFIC MODELS TO REGIONAL MODELS . . . . .	192
4.1 EXTRAPOLATION AND THE EXPECTED VALUE OF A RANDOM VARIABLE . . . . .	193
4.2 A RECIPE FOR EXTRAPOLATION OF THE SITE-SPECIFIC MODELS . . . . .	198
4.2.1 Ingredient 1: The Site-specific Models . . . . .	199
4.2.2 Ingredient 2: The Region of Extrapolation . . . . .	200
4.2.3 Ingredient 3: The Frequency Distributions . . . . .	201
4.2.4 Ingredient 4: Calculation of the Expected Value . . . . .	201

	<u>Page</u>
4. (Continued)	
4.3 AN APPLICATION OF EXTRAPOLATION BY EXPECTED VALUE . . .	202
4.3.1 The Tundra Between 64°N and 90°N Latitude . . . .	204
4.3.1.1 Driving Variables and Their Frequency Distributions . . . . .	204
4.3.1.2 Monte Carlo Simulation . . . . .	212
4.3.1.3 Expected Net Seasonal CO <sub>2</sub> Exchange . . .	213
4.3.2 The Cool Coniferous Forest Between 64°N and 90°N Latitude . . . . .	216
4.3.2.1 Driving Variables and Their Frequency Distributions . . . . .	216
4.3.2.2 Monte Carlo Simulation . . . . .	225
4.3.2.3 Expected Net Seasonal CO <sub>2</sub> Exchange . . .	226
4.3.3 Net Seasonal Biosphere-Atmosphere CO <sub>2</sub> Exchange for 64°N to 90°N . . . . .	228
5. SUMMARY, SYNTHESIS, AND CONCLUSION . . . . .	246
LIST OF REFERENCES . . . . .	256
APPENDIX . . . . .	271

## LIST OF TABLES

<u>Table</u>	<u>Page</u>
1.1 The increase in amplitude of the seasonal CO <sub>2</sub> cycle . . .	14
1.2 Junge and Czeplak's (1968) estimates of total CO <sub>2</sub> uptake by the terrestrial biosphere for 10° latitude belts . . . . .	24
1.3 Machta's (1972) estimates of seasonal CO <sub>2</sub> exchange (10 <sup>15</sup> g CO <sub>2</sub> month <sup>-1</sup> ) for 20° latitude belts . . . . .	28
1.4 Pearman and Hyson's (1981b) estimates of seasonal CO <sub>2</sub> exchange (10 <sup>15</sup> g CO <sub>2</sub> month <sup>-1</sup> ) for latitude belts of equal area (2.55 x 10 <sup>7</sup> km <sup>2</sup> ) . . . . .	30
1.5 Azevedo's (1982) estimates of seasonal CO <sub>2</sub> exchange (10 <sup>15</sup> g CO <sub>2</sub> month <sup>-1</sup> ) for 10° latitude belts . . . . .	33
2.1 State variables of the temperate broadleaf deciduous forest model . . . . .	53
2.2 Driving variables and seasonal forcings of the temperate broadleaf deciduous forest model . . . . .	54
2.3 The flows of organic matter simulated by the temperate broadleaf deciduous forest model . . . . .	56
2.4 State variables of the temperate broadleaf evergreen forest model . . . . .	65
2.5 Driving variables of the temperate broadleaf evergreen forest model . . . . .	67
2.6 The flows of organic matter simulated by the temperate broadleaf evergreen forest model . . . . .	69
2.7 State variables of the cool coniferous forest model . . . . .	77
2.8 Driving variables and phenology parameters of the cool coniferous forest model . . . . .	79
2.9 The flows of carbon and water simulated by the cool coniferous forest model . . . . .	80
2.10 State variables of the warm coniferous forest model . . . . .	92

<u>Table</u>	<u>Page</u>
2.11 Driving variables and seasonal forcings of the warm coniferous forest model . . . . .	94
2.12 The flows of carbon, phosphorus, and water simulated by the warm coniferous forest model . . . . .	95
2.13 State variables of the tropical moist evergreen forest model . . . . .	103
2.14 The flows of organic matter simulated by the tropical moist evergreen forest model . . . . .	105
2.15 State variables of the tropical dry deciduous forest model . . . . .	111
2.16 Time-varying rate coefficients of the tropical dry deciduous forest model . . . . .	113
2.17 The flows of organic matter simulated by the tropical dry deciduous forest model . . . . .	114
2.18 State variables of the tundra model . . . . .	120
2.19 Driving variables of the tundra model . . . . .	121
2.20 Flows of organic matter simulated by the tundra model . . . . .	122
2.21 State variables of the grassland model . . . . .	130
2.22 Driving variables of the grassland model . . . . .	132
2.23 The flows of organic matter simulated by the grassland model . . . . .	133
2.24 State variables of the desert and arid shrubland model . . . . .	145
2.25 Driving variables of the desert and arid shrubland model . . . . .	147
2.26 The flows of carbon, nitrogen, and ash simulated by the desert and arid shrubland model . . . . .	149
2.27 The flows of carbon and nitrogen simulated by the desert and arid shrubland model that are not depicted in Figure 2.33 . . . . .	155
2.28 State variables of the cropland model . . . . .	162

<u>Table</u>	<u>Page</u>
2.29 Driving variables of the cropland model . . . . .	164
2.30 The flows of carbon and water simulated by the cropland model . . . . .	165
3.1 The correspondence between the site-specific models and Olson's land cover categories . . . . .	175
3.2 Area of the terrestrial biosphere represented by each of the land cover categories, by hemisphere and globally, from 80°N to 60°S . . . . .	181
3.3 Estimates of seasonal CO <sub>2</sub> exchange (10 <sup>15</sup> g CO <sub>2</sub> month <sup>-1</sup> ) derived from the simple extrapolation of the site-specific models for 10° latitude belts . . . . .	188
3.4 Estimates of seasonal CO <sub>2</sub> exchange (10 <sup>15</sup> g CO <sub>2</sub> month <sup>-1</sup> ) derived from the simple extrapolation of the site-specific models for 20° latitude belts . . . . .	189
3.5 Estimates of seasonal CO <sub>2</sub> exchange (10 <sup>15</sup> g CO <sub>2</sub> month <sup>-1</sup> ) derived from the simple extrapolation of the site-specific models for latitude belts of equal area (ca. 2.55 x 10 <sup>7</sup> km <sup>2</sup> ) . . . . .	190
4.1 Climate stations and IBP Tundra Biome sites used in describing the spatial heterogeneity of the tundra model's driving variables . . . . .	205
4.2 Input to PRISM used to describe frequency distributions of the tundra model's driving variables for the 64°N to 90°N latitude belt . . . . .	209
4.3 Predicted net CO <sub>2</sub> exchange between the atmosphere and the tundra of the 64°N to 90°N latitude belt . . . . .	217
4.4 Climate stations used in describing the spatial heterogeneity of the cool coniferous forest model's driving variables . . . . .	219
4.5 Input to PRISM used to describe frequency distributions of the cool coniferous forest model's driving variables for the 64°N to 90°N latitude belt . . . . .	222

<u>Table</u>		<u>Page</u>
4.6	Predicted net CO <sub>2</sub> exchange between the atmosphere and the cool coniferous forest of the 64°N to 90°N latitude belt . . . . .	229
4.7	Predicted net CO <sub>2</sub> exchange between the atmosphere and the terrestrial biosphere of the 64°N to 90°N latitude belt . . . . .	230

## LIST OF FIGURES

<u>Figure</u>	<u>Page</u>
1.1 The global carbon cycle . . . . .	2
1.2 The records of atmospheric CO <sub>2</sub> from (a) Mauna Loa, Hawaii and (b) Canadian Weather Station P . . . . .	4
1.3 The seasonal cycle of atmospheric CO <sub>2</sub> at various latitudes . . . . .	7
1.4 Latitudinal variation of the mean peak-to-peak amplitude of the seasonal CO <sub>2</sub> cycle . . . . .	8
1.5 Phase characteristics of the seasonal CO <sub>2</sub> cycle . . . . .	11
1.6 The change in relative amplitude of the seasonal CO <sub>2</sub> cycle at Mauna Loa Observatory, Hawaii . . . . .	15
1.7 Seasonal variation in the intensity of the CO <sub>2</sub> source for selected latitudes . . . . .	22
1.8 Amplitude of the seasonal component of Junge and Czeplak's CO <sub>2</sub> source function . . . . .	26
1.9 Azevedo's curves describing the seasonality of biospheric uptake (-) and release (+) of CO <sub>2</sub> . . . . .	32
2.1 Geographical distribution of the site-specific models . . . . .	45
2.2 Compartmental structure of the temperate broadleaf deciduous forest model - ecosystem overview . . . . .	48
2.3 Compartmental structure of the temperate broadleaf deciduous forest model - canopy subsystems . . . . .	49
2.4 Compartmental structure of the temperate broadleaf deciduous forest model - understory subsystem . . . . .	50
2.5 Compartmental structure of the temperate broadleaf deciduous forest model - litter/soil subsystem . . . . .	51
2.6 Seasonal total ecosystem photosynthesis (P) and respiration (R) for a temperate broadleaf deciduous forest stand . . . . .	61
2.7 Seasonal net CO <sub>2</sub> exchange between the atmosphere and a temperate broadleaf deciduous forest stand . . . . .	63

<u>Figure</u>	<u>Page</u>
2.8 Compartmental structure of the temperate broadleaf evergreen forest model . . . . .	64
2.9 Seasonal total ecosystem photosynthesis (P) and respiration (R) for temperate broadleaf evergreen forest stand . . . . .	72
2.10 Seasonal net CO <sub>2</sub> exchange between the atmosphere and a temperate broadleaf evergreen forest stand . . . . .	73
2.11 Compartmental structure of the cool coniferous forest model - carbon submodel . . . . .	75
2.12 Compartmental structure of the cool coniferous forest model - water submodel . . . . .	76
2.13 Seasonal total ecosystem photosynthesis (P) and respiration (R) for a cool coniferous forest stand . . . . .	86
2.14 Seasonal net CO <sub>2</sub> exchange between the atmosphere and a cool coniferous forest stand . . . . .	88
2.15 Compartmental structure of the warm coniferous forest model - carbon flow submodel . . . . .	89
2.16 Compartmental structure of the warm coniferous forest model - phosphorus cycling submodel . . . . .	90
2.17 Compartmental structure of the warm coniferous forest model - water flow submodel . . . . .	91
2.18 Seasonal total ecosystem photosynthesis (P) and respiration (R) for a warm coniferous forest stand . . . . .	99
2.19 Seasonal net CO <sub>2</sub> exchange between the atmosphere and a warm coniferous forest stand . . . . .	100
2.20 Compartmental structure of the tropical moist evergreen forest model . . . . .	102
2.21 Seasonal total ecosystem photosynthesis (P) and respiration (R) for a tropical moist evergreen forest stand . . . . .	108
2.22 Seasonal net CO <sub>2</sub> exchange between the atmosphere and a tropical moist evergreen forest stand . . . . .	109

<u>Figure</u>	<u>Page</u>
2.23 Compartmental structure of the tropical dry deciduous forest model . . . . .	110
2.24 Seasonal total ecosystem photosynthesis (P) and respiration (R) for a tropical dry deciduous forest stand . . . . .	116
2.25 Seasonal net CO <sub>2</sub> exchange between the atmosphere and a tropical dry deciduous forest stand . . . . .	117
2.26 Compartmental structure of the tundra model . . . . .	119
2.27 Seasonal total ecosystem photosynthesis (P) and respiration (R) for a tundra ecosystem . . . . .	126
2.28 Seasonal net CO <sub>2</sub> exchange between the atmosphere and a tundra ecosystem . . . . .	127
2.29 Compartmental structure of the temperate grassland model . . . . .	129
2.30 Seasonal total ecosystem photosynthesis (P) and respiration (R) for a temperate grassland plot . . . . .	139
2.31 Seasonal net CO <sub>2</sub> exchange between the atmosphere and a temperate grassland plot . . . . .	140
2.32 Compartmental structure of the desert and arid shrubland model - production submodel . . . . .	142
2.33 Compartmental structure of the desert and arid shrubland model - decomposition submodel . . . . .	143
2.34 Compartmental representation of carbon components in living plant compartments of the desert and arid shrubland model . . . . .	153
2.35 Seasonal total ecosystem photosynthesis (P) and respiration (R) for a stand of arid land vegetation . . . . .	159
2.36 Seasonal net CO <sub>2</sub> exchange between the atmosphere and a stand of arid land vegetation . . . . .	160
2.37 Compartmental structure of the cropland model . . . . .	161
2.38 Seasonal photosynthesis (P) and respiration (R) for a corn crop . . . . .	169

<u>Figure</u>	<u>Page</u>
2.39 Seasonal net CO <sub>2</sub> exchange between the atmosphere and a corn crop . . . . .	171
3.1 Digitized land cover map for the area between 30°N-40°N and 75°-85°W using (a) the Olson classification and (b) the aggregated cover types defined by the site-specific models . . . . .	179
3.2 World map of 10° latitude belts . . . . .	183
3.3 World map of 20° latitude belts . . . . .	184
3.4 World map of equal-area latitude belts . . . . .	185
3.5 World map of 8° by 10° grid cells . . . . .	186
4.1 An abstract area, heterogeneous in X, and the frequency distribution of the random variable X . . . . .	196
4.2 Map of the climate stations and IBP Tundra Biome sites used in describing the spatial heterogeneity of the tundra model's driving variables . . . . .	207
4.3 Seasonal net biosphere-atmosphere CO <sub>2</sub> exchange from the site-specific tundra model and the mean of the Monte Carlo simulation of that model . . . . .	214
4.4 Map of the climate stations used in describing the spatial heterogeneity of the cool coniferous forest model's driving variables . . . . .	220
4.5 Seasonal net biosphere-atmosphere CO <sub>2</sub> exchange from the site-specific cool coniferous forest model and the mean of the Monte Carlo simulation of that model . . . . .	227
4.6 Net CO <sub>2</sub> exchange between the atmosphere and the terrestrial biosphere of the 64°N to 90°N latitude belt . . . . .	232

LIST OF PLATES

<u>Plate</u>		<u>Page</u>
3.1	World map of the model biomes . . . . .	273



## ACKNOWLEDGMENTS

We wish to thank Dr. A. C. Echternacht, Dr. L. J. Gross, and Dr. E. C. Clebsch of the University of Tennessee, Knoxville (UTK) and Dr. R. V. O'Neill and Dr. W. R. Emanuel of the Environmental Sciences Division, Oak Ridge National Laboratory, (ESD/ORNL) for their critical reviews during the preparation of this manuscript. We also thank Dr. W. R. Emanuel (ESD/ORNL), and Dr. J. S. Olson (ESD/ORNL retired) for their important assistance with the global land use data. Discussions with Dr. R. V. O'Neill (ESD/ORNL), Dr. D. L. Urban (University of Virginia, Charlottesville), and A. R. Johnson (ESD/ORNL) helped clarify many of the ideas expressed here. We appreciate their interest.

This research was sponsored by the Carbon Dioxide Research Division, Office of Energy Research, U.S. Department of Energy, and by the National Science Foundation's Ecosystem Studies Program under Interagency Agreement BSR-8417923 with the U.S. Department of Energy.



## ABSTRACT

Ecological models of the seasonal exchange of carbon dioxide ( $\text{CO}_2$ ) between the atmosphere and the terrestrial biosphere are needed in the study of changes in atmospheric  $\text{CO}_2$  concentration. In response to this need, a set of site-specific models of seasonal terrestrial carbon dynamics was assembled from open-literature sources. The collection was chosen as a base for the development of biome-level models for each of the earth's principal terrestrial biomes or vegetation complexes. The primary disadvantage of this approach is the problem of extrapolating the site-specific models across large regions having considerable biotic, climatic, and edaphic heterogeneity. Two methods of extrapolation were tested.

The first approach was a simple extrapolation that assumed relative within-biome homogeneity, and generated  $\text{CO}_2$  source functions that differed dramatically from published estimates of  $\text{CO}_2$  exchange. The differences were so great that the simple extrapolation was rejected as a means of incorporating site-specific models in a global  $\text{CO}_2$  source function.

The second extrapolation explicitly incorporated within-biome variability in the abiotic variables that drive seasonal biosphere-atmosphere  $\text{CO}_2$  exchange. Simulated site-specific  $\text{CO}_2$  dynamics were treated as a function of multiple random variables (i.e., the model driving variables). The predicted regional  $\text{CO}_2$  exchange is the computed expected value of simulated site-specific exchanges for that region times the area of the region. The extrapolation was tested

for the circumglobal latitude belt between 64°N and 90°N. The test involved the regional extrapolation of a tundra and a coniferous forest carbon exchange model. Comparisons between the CO<sub>2</sub> exchange estimated by extrapolation and published estimates of regional exchange for the latitude belt support the appropriateness of extrapolation by expected value. Extrapolation by mathematical expectation is a promising technique for extrapolating from site-specific models to regional and biome-level models.

## CHAPTER 1

### INTRODUCTION

The carbon dioxide ( $\text{CO}_2$ ) concentration of the Earth's atmosphere is increasing. This well publicized upward trend is generally attributed to the release of  $\text{CO}_2$  by fossil fuel combustion, although contributions from deforestation are also likely. Carbon dioxide is presumably an important element of the global radiation balance. As one of the so-called "green-house gases",  $\text{CO}_2$  functions to retain sensible heat in the lower atmosphere, and consequently influences the Earth's climate. Uncertainties surrounding the potential for significant changes in the Earth's climate as a consequence of increasing levels of atmospheric  $\text{CO}_2$  have fueled considerable interest in the sources and consequences of anthropogenic perturbations to the global carbon cycle, and in the global cycle itself (Figure 1.1). Here, we focus on an important component of that cycle, the seasonal exchange of  $\text{CO}_2$  between the atmosphere and the terrestrial biosphere.

Mathematical models are the primary analytical tools in the study of the global carbon cycle. They are means of synthesizing and integrating data and concepts from diverse sources. They provide a mechanism for testing hypotheses about the carbon cycle that could otherwise not be evaluated. Further, they allow quantitative predictions of future concentrations of atmospheric  $\text{CO}_2$  for alternative scenarios of fossil fuel emission and land use. In this report we describe a specific approach to the modeling

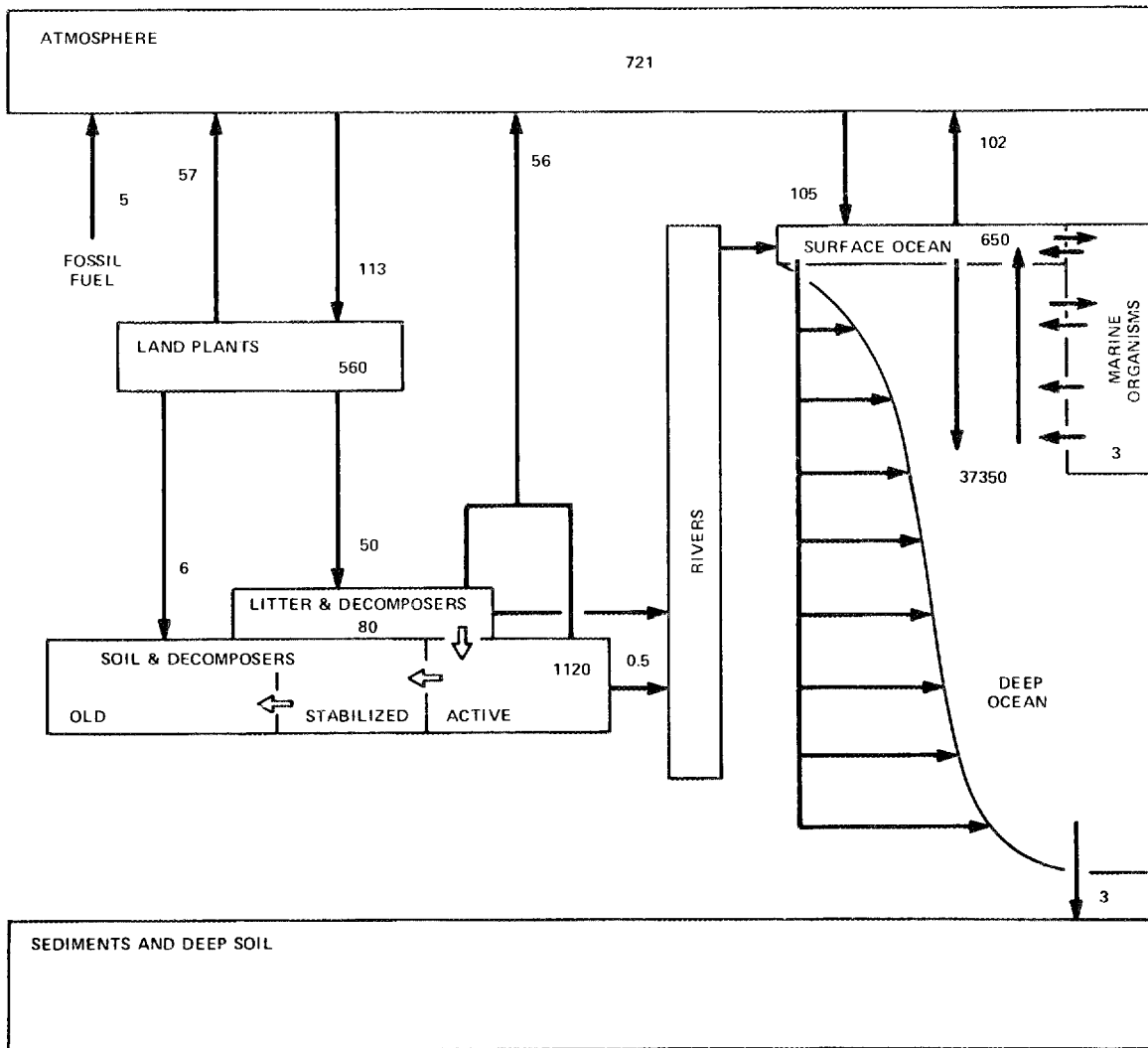


Figure 1.1. The global carbon cycle. Reservoir sizes are in  $10^{15}$  g C and fluxes are in  $10^{15}$  g C year<sup>-1</sup>. Adapted from Emanuel, Killough, and Olson (1981), Dahlman (1984), and Emanuel and O'Neill (1985).

of seasonal CO<sub>2</sub> exchange between the atmosphere and the terrestrial biosphere; namely, the use of ecosystem-level models of carbon metabolism as a basis for a model of larger-scale regional and global biosphere-atmosphere exchanges.

As far as possible long-term effects of increasing CO<sub>2</sub> on the climate are concerned, the seasonal biosphere-atmosphere exchanges of CO<sub>2</sub> may be of minor importance. However, insights into this seasonality will not only improve our general understanding of the global carbon cycle as a biogeochemical cycle, but may also contribute specifically to our understanding of the role of the biosphere in that cycle, an understanding that is critical to predictions of future concentrations of atmospheric CO<sub>2</sub>.

## 1.1 THE SEASONAL CYCLE OF ATMOSPHERIC CO<sub>2</sub>

### 1.1.1 The Source Of Seasonal Variations In Atmospheric CO<sub>2</sub>

The atmospheric CO<sub>2</sub> records from Mauna Loa (Hawaii) Observatory and elsewhere document a seasonality, which appears as nearly sinusoidal excursions around the increasing average annual concentration of CO<sub>2</sub> (Figure 1.2; Bolin and Keeling 1963; Bolin and Bischoff 1970; Keeling, Bacastow et al. 1976; Keeling, Adams et al. 1976; Lowe, Guenther, and Keeling 1979; Bacastow and Keeling 1981; Bischoff 1981; Peterson et al. 1982; Fraser, Pearman, and Hyson 1983; Mook et al. 1983; Tanaka, Nakasaw, and Aoki 1983; Keeling, Carter, and Mook 1984; Pearman and Beardsmore 1984; Keeling et al. 1985; Komhyr et al. 1985). The highest concentrations of CO<sub>2</sub> in this annual or seasonal cycle generally occur just before

ORNL - DWG 86-1758

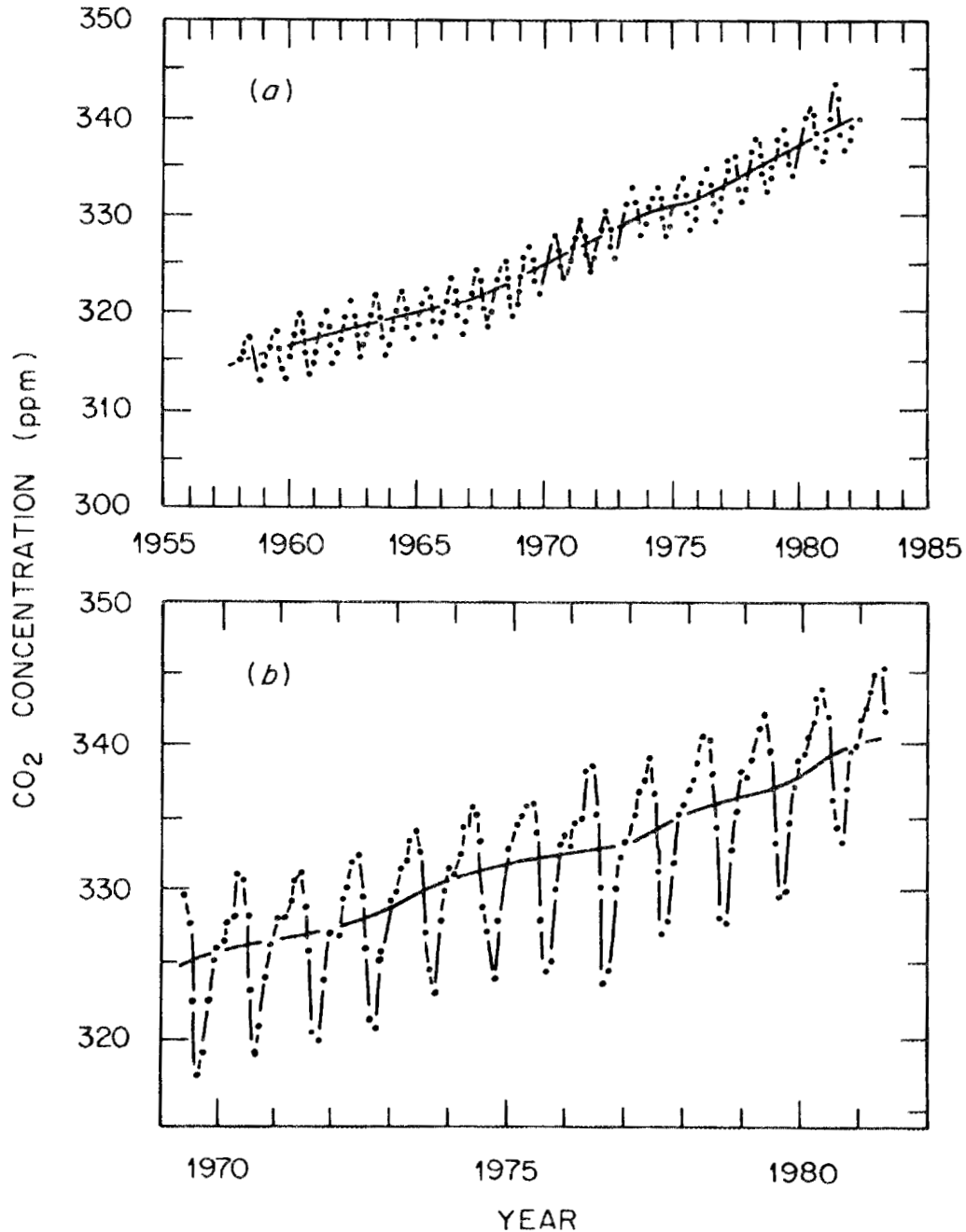


Figure 1.2. The records of atmospheric CO<sub>2</sub> from (a) Mauna Loa, Hawaii and (b) Canadian Weather Station P. The dots indicate monthly average concentrations. The smooth curves represent the long term trend of increasing annual concentrations.

the onset of the region's growing season, and the lowest concentrations occur at the end of the growing season, or the beginning of vegetative dormancy. At Mauna Loa, in the northern hemisphere, the peak concentration occurs in May, the minimum in October (Bacastow, Keeling, and Whorf 1985). Over southeastern Australia, the peak occurs in October and the minimum in April (Pearman and Beardsmore 1984). This pattern and subsequent investigations have led many to conclude that the seasonal cycle of atmospheric CO<sub>2</sub> is primarily the result of the seasonal metabolic activity of the terrestrial biosphere on a regional or hemispheric scale (Bolin and Keeling 1963; Pales and Keeling 1965; Junge and Czeplak 1968; Woodwell, Houghton, and Tempel 1973; Machta 1974; Hall, Ekdahl, and Wartenburg 1975; Keeling, Bacastow et al. 1976; Machta, Hanson, and Keeling 1977; Lowe, Guenther, and Keeling 1979; Pearman and Hyson 1980, 1981a,b; Azevedo 1982; Gillette 1982; Houghton 1982; Cleveland, Freeny, and Graedel 1983; Fraser, Pearman, and Hyson 1983; Fung et al. 1983; Mook et al. 1983; Pearman, Hyson, and Fraser 1983; Woodwell 1983; Keeling, Carter, and Mook 1984; Keeling et al. 1985; Komhyr et al. 1985; Tucker et al. 1986).

During the growing season the photosynthetic activity of the terrestrial vegetation results in a net withdrawal of CO<sub>2</sub> from the atmosphere, and a decline in the background concentration of CO<sub>2</sub>. During periods of vegetative dormancy the respiratory activity of heterotrophs, especially decomposers, results in a net release of CO<sub>2</sub>, and atmospheric concentrations rise. Seasonal variations in fossil fuel use, ocean temperatures, and the biological activity of

the ocean may contribute slightly to seasonal CO<sub>2</sub> concentrations, but their relative contribution to the seasonal pattern appears to be very minor, at least in the northern hemisphere (Junge and Czeplak 1968; Machta, Hanson, and Keeling 1977; Bacastow, Keeling, and Whorf 1981; Pearman and Hyson 1981a; Azevedo 1982; Cleveland, Freeny, and Graedel 1983; Keeling, Carter, and Mook 1984). In polar regions and in the southern hemisphere, seasonal ocean-atmosphere exchange of CO<sub>2</sub> may be more important (Machta, Hanson, and Keeling 1977; Gillette 1982; Keeling, Carter, and Mook 1984; Komhyr et al. 1985). Holdridge (1980) has questioned the primacy of the seasonal biosphere-atmosphere exchange hypothesis, suggesting the seasonal variations in CO<sub>2</sub> concentration are the result of temperature related variations in global atmospheric density, and Lugo and Brown (1980) have raised some ecological issues involved in the interpretation of seasonal atmospheric CO<sub>2</sub> data. However, the consensus is that the seasonal pattern evident in the atmospheric CO<sub>2</sub> records is predominantly a reflection of seasonal variations in the net exchange of CO<sub>2</sub> between the atmosphere and the terrestrial biosphere.

#### 1.1.2 Latitudinal Variations In The Seasonal CO<sub>2</sub> Cycle

The amplitude of the seasonal cycle of atmospheric CO<sub>2</sub> concentration varies with latitude. Figure 1.3 (Keeling 1983) illustrates the decrease in amplitude from north to south. Figure 1.4 summarizes this variation for a larger number of stations. The decrease in peak-to-peak amplitude across the

ORNL-DWG 86-16757

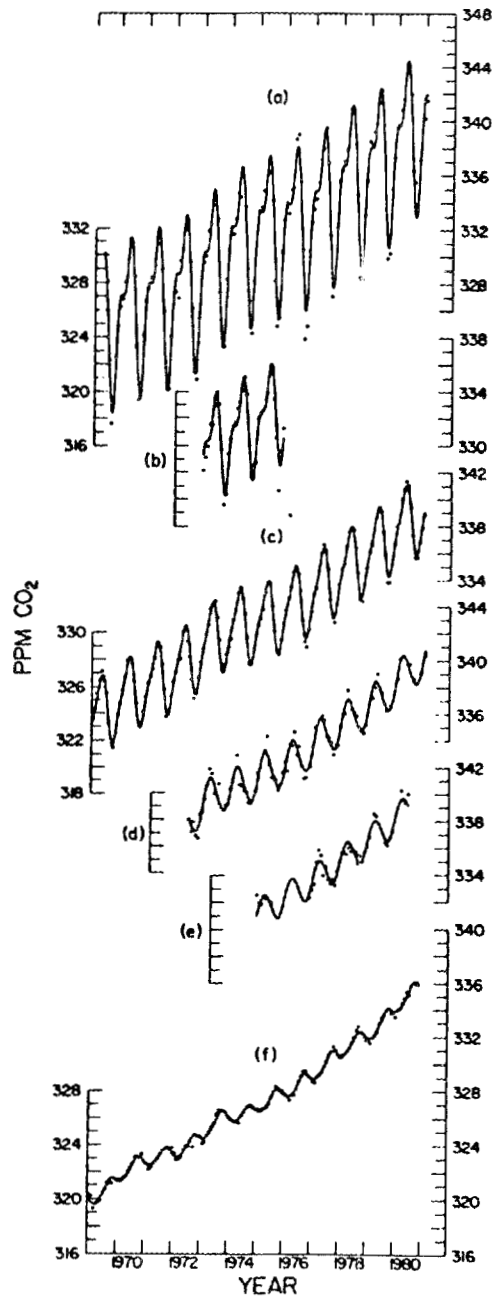


Figure 1.3. The seasonal cycle of atmospheric  $\text{CO}_2$  at various latitudes. (a) Canadian Weather Station P,  $50.0^\circ\text{N}$ ; (b) La Jolla, California,  $32.9^\circ\text{N}$ ; (c) Mauna Loa Observatory, Hawaii,  $19.5^\circ\text{N}$ ; (d) Fanning Island,  $3.9^\circ\text{N}$ ; (e) Christmas Island,  $2.0^\circ\text{N}$ ; and (f) the South Pole. The oscillating curves are fits to a spline function plus harmonics with periods of 12, 6, 4, and 3 months. From Keeling (1983).



northern hemisphere is generally assumed to be due to a pole to equator decline in the seasonality of net biosphere-atmosphere  $\text{CO}_2$  exchange (Machta, Hanson, and Keeling 1977; Keeling 1983; Azevedo 1982; Fung et al. 1983). According to this interpretation, the strong seasonality of the growing season in higher latitudes of the northern hemisphere is responsible for the large seasonal amplitude of the seasonal  $\text{CO}_2$  cycle. The weak seasonality of equatorial regions results in a smaller seasonal variation.

The reduced peak-to-peak amplitudes (1.0-2.0 ppm) of the southern hemisphere are presumably due to the smaller land mass of the southern hemisphere, particularly in the middle to high latitudes. With relatively less land area and more ocean area, the influence of the terrestrial biosphere on atmospheric  $\text{CO}_2$  is much reduced in the southern hemisphere. Seasonal variations in  $\text{CO}_2$  as far south as 10-15°S may be the result of intrusions of northern hemisphere air (Keeling, Carter, and Mook 1984; Komhyr et al. 1985). Pearman and Hyson (1980) and Pearman and Beardsmore (1984) suggest that as much as two-thirds of the seasonal variation in the southern hemisphere is the result of transport from the northern hemisphere rather than surface exchange. At higher latitudes in the southern hemisphere half or more of the small seasonal variation may be caused by air-sea exchange (Keeling, Carter, and Mook 1984). The source of the increase in amplitude from middle to high southern latitudes is uncertain, but seasonal variations in ice cover and upwelling events may contribute (Machta, Hanson, and Keeling 1977; Keeling, Carter, and Mook 1984; Komhyr et al. 1985).

The phase of the seasonal CO<sub>2</sub> cycle also varies with latitude. Following Fraser, Pearman, and Hyson (1983) and Komhyr et al. (1985), phase is defined by the dates on which the CO<sub>2</sub> concentration increases and decreases through the annual mean concentration. Carbon dioxide drawdown (relative to the CO<sub>2</sub> secular trend levels) begins in the northern hemisphere on about the first day of summer between 50°N and 60°N (Komhyr et al. 1985). Drawdown propagates northward and southward with time, such that drawdown at mid-latitudes precedes drawdown in both higher and lower latitudes (Figure 1.5). The buildup of CO<sub>2</sub> in the northern hemisphere (again, relative to the CO<sub>2</sub> secular trend levels) begins in mid-autumn and follows a similar pattern of propagation with time.

As expected, CO<sub>2</sub> drawdown in the southern hemisphere lags drawdown in the northern hemisphere by approximately six months (Figure 1.5). The buildup of CO<sub>2</sub> in the southern hemisphere begins in late June or early July. The pattern of propagation with time is similar to that in the northern hemisphere. The intrusion of northern hemisphere air across the equator extends the northern phasing of drawdown and buildup some 10° into the southern hemisphere (Figure 1.5) and produces anomalous patterns at Seychelles (4°40'S) and American Samoa (14°15'S).

The apparently counterintuitive phasing of CO<sub>2</sub> drawdown in the northern hemisphere, where tropical and subtropical stations lag behind those at mid-latitudes and coincide with or lag behind high latitudes, is indeed more apparent than real. If the photosynthetic

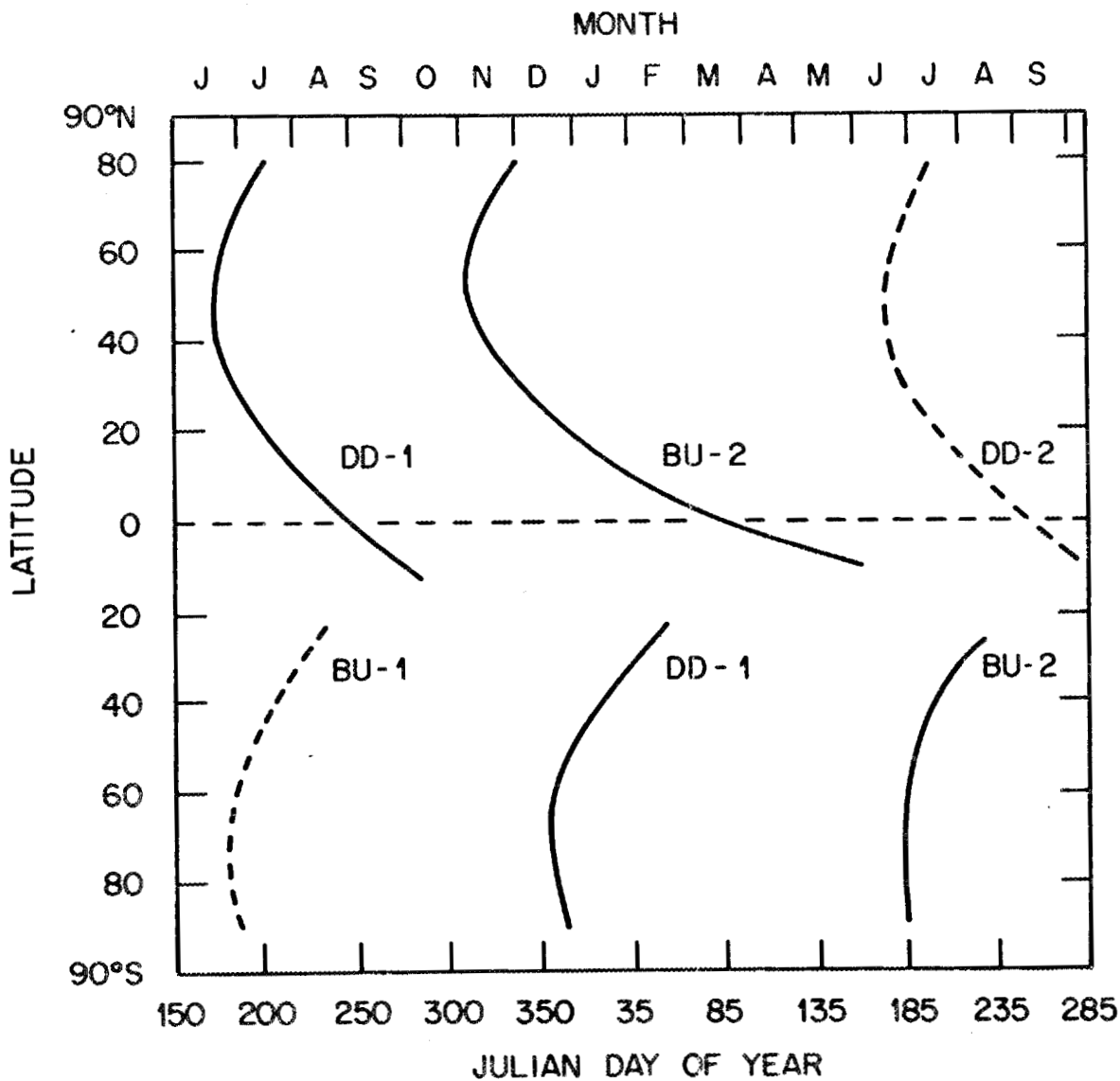


Figure 1.5. Phase characteristics of the seasonal CO<sub>2</sub> cycle. The curves indicate the times of the year when CO<sub>2</sub> drawdown (DD) and buildup (BU) begin relative to secular-trend CO<sub>2</sub> levels. After Komhyr et al. (1985).

activity of terrestrial plants is responsible for seasonal reductions in atmospheric CO<sub>2</sub>, one would expect that stations in lower latitudes of the northern hemisphere would record drops in concentration before those at high latitudes, in coincidence with the northward progression of the onset of the growing season. Examination of the CO<sub>2</sub> records (e.g., those provided by Komhyr et al. 1985) suggests that this is indeed the case. High latitude CO<sub>2</sub> concentrations fall below maximum concentrations slightly later than those from middle to low latitudes. The rate of change from seasonal maximum to seasonal minimum concentrations appears to increase with latitude and accounts in part for the phase pattern of Figure 1.5, since phase is defined by the date on which CO<sub>2</sub> concentrations fall below the secular trend level (i.e., the mean annual concentration). Thus, the counterintuitive results are due in part to the particular definition of phase used by Fraser, Pearman and Hyson (1983) and Komhyr et al. (1985). Further analyses of these patterns are planned.

Because of mixing, the amplitude and phase of the seasonal CO<sub>2</sub> cycle also varies with altitude (Bolin and Keeling 1963; Bolin and Bischoff 1970; Pearman and Beardsmore 1984). The amplitude of the seasonal variation appears to decrease with altitude (from the middle to upper troposphere) in the northern hemisphere (Bolin and Bischoff 1970), while it appears to increase with altitude in the southern hemisphere (Pearman and Beardsmore 1984). In the southern hemisphere the seasonal cycle of the middle troposphere lags behind that of the upper troposphere (Pearman and Beardsmore 1984); the

opposite is seen in the northern hemisphere (Bolin and Bischoff 1970). These differences are possibly due to the high altitude transport of northern hemisphere air into the southern hemisphere (see Pearman and Beardsmore 1984). The influence of terrestrial vegetation is most obvious in the lower (below 2 km) troposphere (Pearman and Beardsmore 1984). The latitudinal trends discussed above include corrections for these elevational gradients.

### 1.1.3 An Increase In The Amplitude Of The Seasonal CO<sub>2</sub> Cycle

The amplitude of the seasonal CO<sub>2</sub> cycle is apparently increasing with time. Hall, Ekdahl, and Wartenburg (1975) saw no evidence for changes in the seasonal cycle using data from Mauna Loa for 1958 to 1972. However, investigations since then have documented increases in the seasonal amplitude at Mauna Loa (Bacastow, Keeling, and Whorf 1981, 1985; Pearman and Hyson 1981a; Cleveland, Freeny, and Graedel 1983; Komhyr et al. 1985), Canadian Ocean Weather Station P (Bacastow et al. 1981; Pearman and Hyson 1981a; Keeling et al. 1985), the South Pole (Cleveland, Freeny, and Graedel 1983), and possible increases at Point Barrow, Alaska (Pearman and Hyson 1981a) and American Samoa (Komhyr et al. 1985). Komhyr et al. (1985) report a decrease in the annual cycle amplitude at the South Pole. Table 1.1 summarizes these results, and Figure 1.6 presents the change in relative amplitude of the seasonal cycle at Mauna Loa (Bacastow, Keeling, and Whorf 1985). The seasonal amplitude in atmospheric CO<sub>2</sub> data is quite variable from year to year, increasing at times and decreasing at other times. The long

Table 1.1. The increase in amplitude of the seasonal CO<sub>2</sub> cycle.

Station	Period of Record	Amplitude Increase (%/year)	Reference <sup>a</sup>
Mauna Loa (20°N,156°W)	1959-1982	0.75	a
	1959-1978	0.45	b
	1959-1978	0.54	c
	1976-1982	1.94	d
Canadian Weather Station P (50°N,145°W)	1969-1981	0.81	e
	1970-1978	0.72	b
South Pole (90°S)	1965-1978	2.31	c
	1975-1982	-4.09	d
Point Barrow (71°N,157°W)	1961-1976	1.79	b
American Samoa (14°S,171°W)	1975-1982	4.28	d

<sup>a</sup>The references are: (a) Bacastow, Keeling, and Whorf (1985); (b) Pearman and Hyson (1981a); (c) Cleveland, Freeny, and Graedel (1983); (d) Komhyr et al. (1985); (e) Keeling et al. (1985).

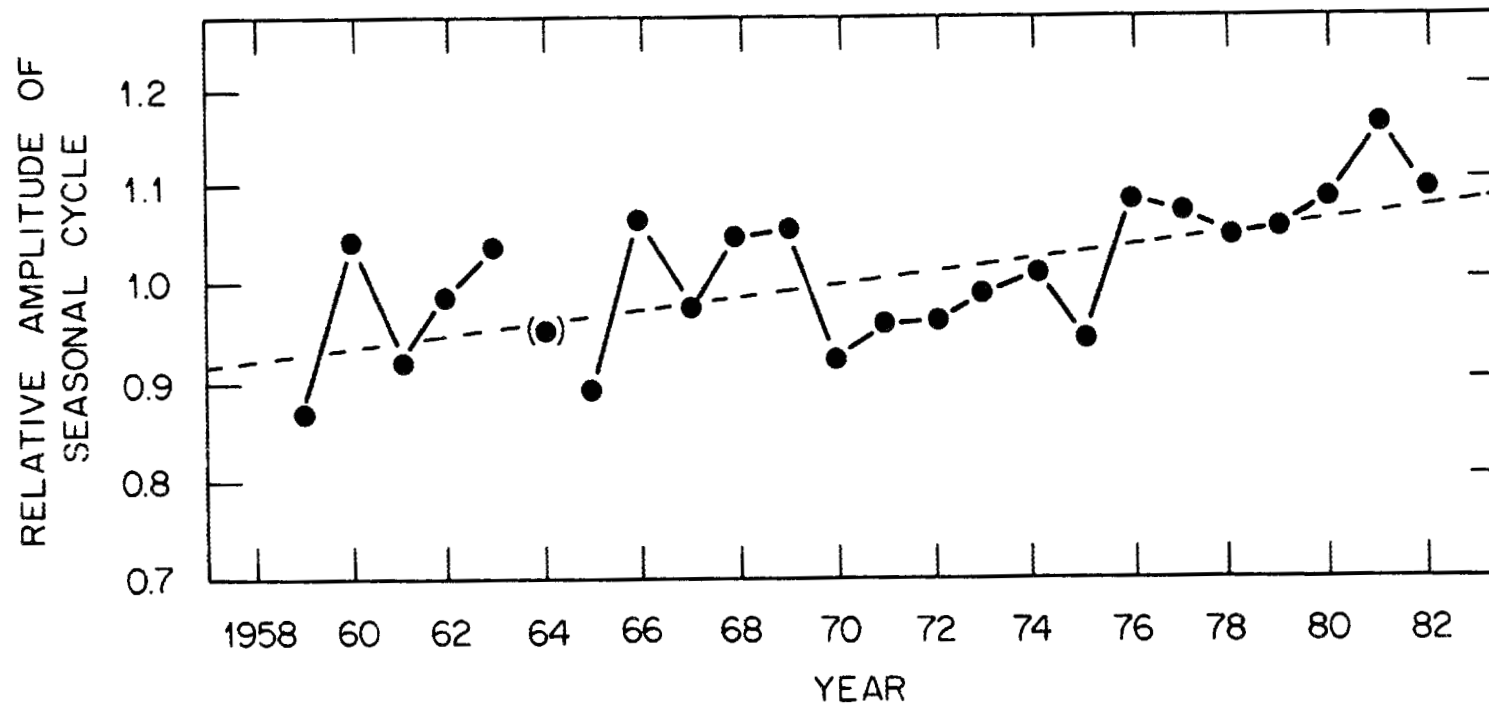


Figure 1.6. The change in relative amplitude of the seasonal CO<sub>2</sub> cycle at Mauna Loa Observatory, Hawaii. From Keeling et al. (1985).

term increases do not necessarily indicate monotonic secular trends, but may reflect transient variations on time scales of decades (Pearman and Hyson 1981a).

There are several possible explanations for the observed increases in seasonal amplitude. For example, it is possible that the increased CO<sub>2</sub> concentration of the lower atmosphere has stimulated the photosynthetic activity of the terrestrial biosphere, either as increased storage and growth or increased annual turnover (Bacastow, Keeling, and Whorf 1981, 1985; Bacastow et al. 1981; Pearman and Hyson 1981a; Cleveland, Freeny, and Graedel 1983; Keeling 1983; Keeling et al. 1985). Abundant evidence for increased photosynthesis with CO<sub>2</sub> fertilization in greenhouses and controlled growth chambers is frequently cited as support for this hypothesis. Alternatively, if ecosystem respiration during periods of vegetative dormancy were to increase or decrease relative to respiration during the growing season (perhaps in response to a temperature change), the amplitude of the seasonal cycle could be increased (Pearman and Hyson 1981a, Cleveland, Freeny, and Graedel 1983). Even in the absence of CO<sub>2</sub> fertilization, an increase in photosynthetic biomass could produce a change in the seasonal amplitude. Despite net deforestation in the tropics (Sieler and Crutzen 1980; Houghton et al. 1983; Woodwell et al. 1983; Detwiler, Hall, and Bogdonoff 1985), reforestation of temperate zones of the northern hemisphere (Armentano and Ralston 1980, Delcourt and Harris 1980) might represent enough increased CO<sub>2</sub> assimilation by the biosphere to produce an increase in the seasonal amplitude of the

CO<sub>2</sub> cycle at certain stations (Pearman and Hyson 1981a). Any CO<sub>2</sub> fertilization effect would enhance this impact. Changes in the seasonality of oceanic exchange and fossil fuel CO<sub>2</sub> release could also explain changes in seasonal amplitude. However, these influences are generally thought to be unlikely or negligible (Bacastow, Keeling, and Whorf 1981; Pearman and Hyson 1981a; Cleveland, Freeny, and Graedel 1983).

Thus, an increase in the metabolic activity of the terrestrial biosphere, in particular increased CO<sub>2</sub> assimilation during the growing season, stands as the principal hypothesis explaining the increase in the amplitude of the seasonal CO<sub>2</sub> cycle. The records of atmospheric CO<sub>2</sub> concentration do not, however, permit a unique separation of this biospheric signal from the influences of other sources and sinks, nor can they identify the nature of the increase in biosphere activity (e.g., CO<sub>2</sub> fertilization, land-use changes, or transient responses to climate variations). The biosphere's seasonal activity must be independently evaluated. This information can then be used in conjunction with atmospheric CO<sub>2</sub> records to more fully evaluate the biosphere's role in the normal seasonal cycle and the hypothesis of increased biospheric activity.

## 1.2 MODELING THE SEASONAL CYCLE OF ATMOSPHERIC CO<sub>2</sub>

### 1.2.1 Tracer Transport Models And CO<sub>2</sub> Source Functions

Tracer transport models of atmospheric CO<sub>2</sub> are important tools in the study of the seasonal CO<sub>2</sub> cycle. These models simulate the distribution of atmospheric CO<sub>2</sub> in response to

large-scale transfer processes and the exchange of CO<sub>2</sub> at the earth's surface. The CO<sub>2</sub> source function, which describes the sources and sinks of atmospheric CO<sub>2</sub>, is a key element in any CO<sub>2</sub> tracer model, and it provides a useful focal point for modeling the seasonal exchange of CO<sub>2</sub> between the atmosphere and the terrestrial biosphere.

The tracer transport equation of a CO<sub>2</sub> tracer model can be expressed in general form as

$$\frac{\partial C}{\partial t} = \text{TRANSPORT}(s,t) + \text{SOURCE}(s,t) , \quad (1.1)$$

where C is the concentration (mole fraction, ppm) of atmospheric CO<sub>2</sub>, TRANSPORT(s,t) describes the diffusion and advection of CO<sub>2</sub> over space (s) and time (t), and SOURCE(s,t) describes the sources and sinks of CO<sub>2</sub> in space and time. We are concerned here with only the SOURCE term. Descriptions of the TRANSPORT term can be found in Bolin and Keeling (1963), Reiter (1971), Hyson, Fraser and Pearman (1980), Eliassen (1980), Hanna, Briggs, and Hosker (1982), Azevedo (1982), and Fung et al. (1983).

For a one or two-dimensional tracer model (latitude only or latitude and altitude; see Bolin and Keeling 1963, Junge and Czeplak 1968, Machta 1972, 1974, Pearman and Hyson 1980, 1981b, Azevedo 1982) SOURCE appears as

$$\text{SOURCE}(s,t) = Q(\theta,t) , \quad (1.2)$$

where Q is a simple change in notation,  $\theta$  is latitude, and t is time. The two-dimensional models simulate zonal mean CO<sub>2</sub>

concentration, often for  $10^\circ$  latitude belts encircling the earth. The spatial distribution of the  $\text{CO}_2$  sources and sinks are also zonal means by latitude belt.

In a three-dimensional tracer model (latitude, longitude, and altitude; see Hansen et al. 1983; Fung et al. 1983; Heimann, Keeling and Mook 1985) the source term of Equation 1.1 appears as

$$\text{SOURCE}(s,t) = Q(\lambda,\theta,t) , \quad (1.3)$$

where  $\lambda$  is longitude and  $\theta$  is latitude. The three-dimensional tracer models are based on three-dimensional General Circulation Models (GCM's) and simulate the  $\text{CO}_2$  concentrations for grid boxes that are distributed globally both horizontally and vertically. The horizontal dimensions of the grid boxes (the grid cell resolution) is usually  $8^\circ$  latitude by  $10^\circ$  longitude, although coarser ( $12^\circ \times 15^\circ$ ) and finer ( $4^\circ \times 5^\circ$ ) resolutions are possible (Hansen et al. 1983). The horizontally distributed grid cells of the three-dimensional models permit a finer resolution of the spatial distribution of  $\text{CO}_2$  sources and sinks than is possible with the two-dimensional models. In particular, they allow incorporation of the longitudinal variations in  $\text{CO}_2$  exchange between the atmosphere and the Earth's surface.

If the source function,  $Q$ , of the  $\text{CO}_2$  tracer model describes the seasonal variations of sources and sinks in the carbon cycle, then  $Q$  expresses the net exchange of  $\text{CO}_2$  between the atmosphere and the Earth's surface over a given period of time, usually a month, for a specified area. The units of  $Q$ , as it appears in the

transport equation, are changes in CO<sub>2</sub> concentration (ppm). However, the CO<sub>2</sub> source function is usually expressed as the mass of CO<sub>2</sub> or carbon released to (positive values) or withdrawn from (negative values) the atmosphere per unit area per unit time (e.g., kg CO<sub>2</sub> km<sup>-2</sup> month<sup>-1</sup>, or 10<sup>15</sup> g CO<sub>2</sub> (latitude belt)<sup>-1</sup> month<sup>-1</sup>). These values are converted to CO<sub>2</sub> concentrations by considering the air masses involved. The annual or seasonal cycle of atmospheric CO<sub>2</sub> is then expressed as the difference between the mean monthly concentration and the background concentration (e.g., annual mean concentration).

### 1.2.2 A Review Of CO<sub>2</sub> Source Functions

Bolin and Keeling (1963) analyzed the seasonal cycle of atmospheric CO<sub>2</sub> with five years of pole-to-pole data. With these data and their one-dimensional model of large-scale meridional mixing in the atmosphere, they derived a seasonal CO<sub>2</sub> source function consistent with observed concentrations. The seasonal sources and sinks of CO<sub>2</sub> were denoted by

$$Q''(\mu, t) = Q(\mu, t) - (\langle Q^*(\mu) + Q^{**}(\mu) \rangle - \langle Q' + \hat{Q} \rangle), \quad (1.4)$$

where

$Q''(\mu, t)$  = the seasonal sources and sinks,

$Q(\mu, t)$  = the immediate sources and sinks,

$Q^*(\mu)$  = the natural sources and sinks,

$Q^{**}(\mu)$  = the industrial source,

$Q'$  = the average increase of CO<sub>2</sub> in the atmosphere,

$\hat{Q}$  = the sink of industrial  $\text{CO}_2$ ,  
 $\mu$  =  $\sin \theta$ ,  $\theta$  being latitude,  
 $t$  = time,

and the angle brackets ( $\langle \rangle$ ) denote the time average.

Expanding  $Q(\mu, t)$  in Legendre polynomials and using their model of latitudinal exchange, Bolin and Keeling (1963) were able to derive sources and sinks as a function of season and latitude. Their source function is illustrated in Figure 1.7. Their derived sources and sinks gave seasonal  $\text{CO}_2$  variations which were in reasonable agreement with the station observations, although there were discrepancies. Bolin and Keeling (1963) did not compare their derived sources and sinks with independent data on biospheric sources and sinks. Furthermore, they provided no physical basis for their exchanges beyond the assumption that seasonal variations of  $\text{CO}_2$  in the atmosphere were predominantly due to the terrestrial vegetation of the northern hemisphere.

Junge and Czeplak (1968) estimated a seasonal  $\text{CO}_2$  source function using data from the terrestrial biosphere. They assumed that the seasonal variation of the  $\text{CO}_2$  source is influenced by the terrestrial biosphere, human activities, ocean surface temperatures, and the biosphere of the ocean surface waters. Junge and Czeplak (1968) screened these potential contributions and concluded that only the terrestrial biosphere and human activities represented non-negligible contributions. However, because of uncertainties,

ORNL-DWG 86-1751

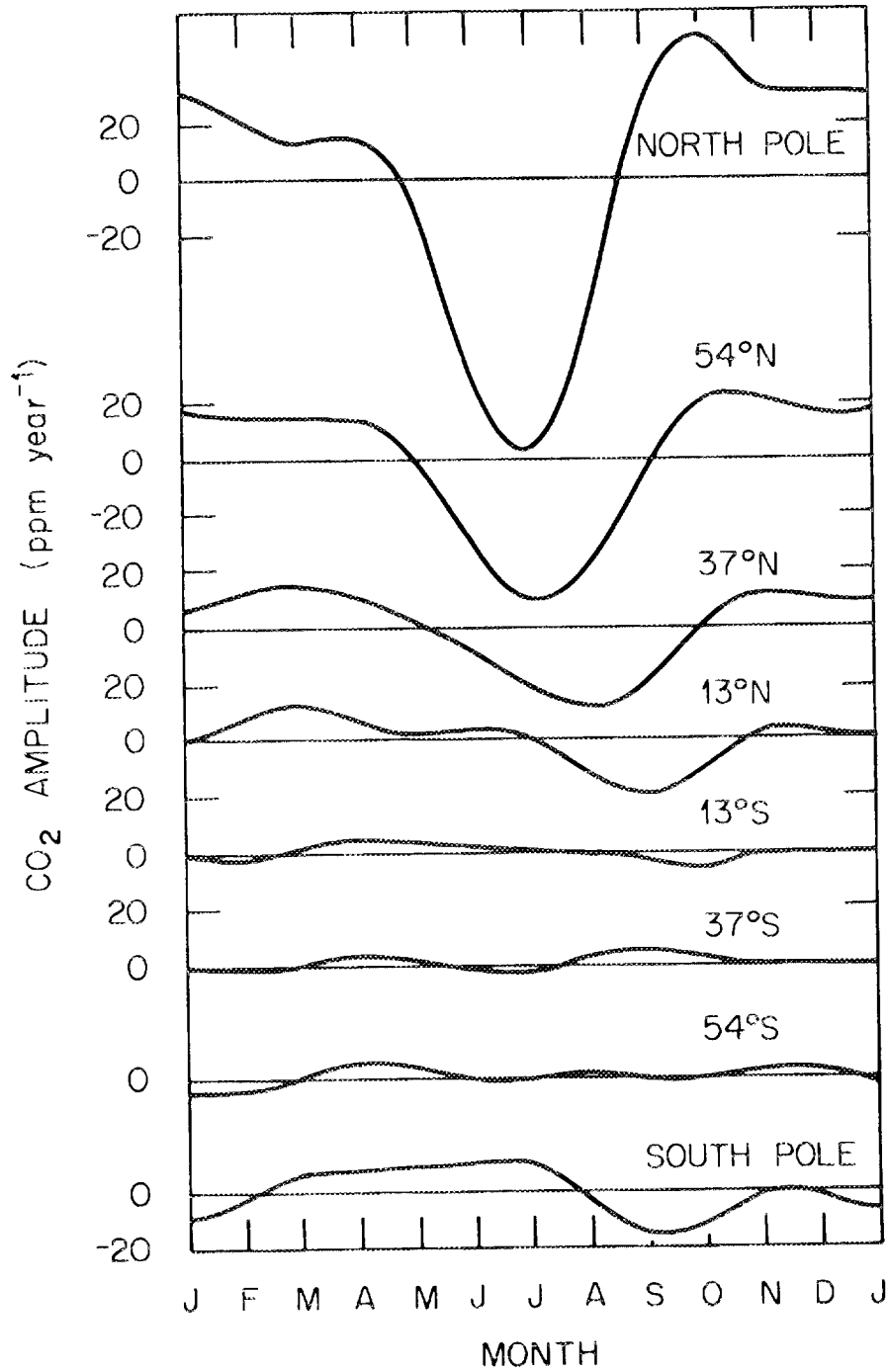


Figure 1.7. Seasonal variation in the intensity of the CO<sub>2</sub> source for selected latitudes. From Bolin and Keeling (1963).

the anthropogenic contributions were not included in the model, leaving only the terrestrial biosphere.

With the aid of some simple ecological assumptions about the biosphere, Junge and Czeplak (1968) derived a seasonal source function with a horizontal resolution of  $10^\circ$  latitude belts. The source function for each latitude is of the form

$$Q(\mu, t) = a(\mu)\cos(2\pi t) , \quad (1.5)$$

where  $\mu$  is  $\sin \theta$ ,  $\theta$  is latitude, and  $0 \leq t \leq 1$  for the year.

The term  $a(\mu)$  represents the amplitude of the seasonal component of the  $\text{CO}_2$  source function ( $\text{ppm CO}_2 \text{ year}^{-1}$ ) and  $\cos(2\pi t)$  represents the time dependence of the source function. The values of  $a(\mu)$  are given by

$$a(\mu) = \text{CO}_2 f(1 - e) . \quad (1.6)$$

The  $\text{CO}_2$  concentration,  $\text{CO}_2$ , in  $\text{ppm year}^{-1}$ , represents the total annual  $\text{CO}_2$  uptake by the terrestrial plants of each  $10^\circ$  latitude belt. These values were obtained from data on net primary production (Table 1.2) mapped by Lieth (1965). Lieth's carbon mass data were converted to atmospheric concentrations by considering the surface area and air masses involved for each latitude belt. The term  $f$  in Equation 1.6 represents the fraction of total uptake which occurs in the summer season as opposed to the winter season. Junge and Czeplak (1968) assumed that at latitudes less than  $30^\circ$  the growing season is determined by rainfall (and by temperature at higher latitudes). Accordingly, they estimated  $f$  by the bias for

Table 1.2. Junge and Czeplak's (1968) estimates of total CO<sub>2</sub> uptake by the terrestrial biosphere for 10° latitude belts.

Latitude Belt	Annual CO <sub>2</sub> Uptake <sup>a</sup> (10 <sup>15</sup> g year <sup>-1</sup> )
80°-90°N	0.00
70°-80°N	0.00
60°-70°N	4.76
50°-60°N	9.15
40°-50°N	10.25
30°-40°N	9.15
20°-30°N	11.71
10°-20°N	14.27
0°-10°N	23.42
0°-10°S	26.35
10°-20°S	17.93
20°-30°S	8.78
30°-40°S	4.03
40°-50°S	0.73
50°-60°S	0.00
60°-70°S	0.00
70°-80°S	0.00
80°-90°S	0.00

<sup>a</sup>The carbon data of Junge and Czeplak (1968) were converted to CO<sub>2</sub> using a conversion factor of 1 g C = 3.66 g CO<sub>2</sub>.

rainy summer months over rainy winter months (number of rainy summer months minus the number of rainy winter months) as a fraction of total rainy months. At the equator  $f = 0$ , and for latitudes greater than  $30^\circ$   $f = 1$ . Junge and Czeplak recognized the crudeness of this parameter, but doubted that much more reliable figures were available at that time.

The release of  $\text{CO}_2$  from the soil which accompanies the decay of organic matter is incorporated as  $e$  in Equation 1.6, where  $e$  is the fraction of soil release which occurs during the summertime. Hence,  $(1 - e)\text{CO}_2$  is the actual uptake of  $\text{CO}_2$  during the growing season, and they assumed the same amount was released from the soil during the winter (i.e., a steady-state assumption of no net annual exchange between the biosphere and the atmosphere). The best fit estimate of  $e$  was 0.39, but Junge and Czeplak went on to conclude that the value of  $e$ , the seasonal variation of soil respiration, was the most uncertain factor in the seasonal  $\text{CO}_2$  exchange.

In Figure 1.8,  $a(\mu)$  in Equation 1.6 is plotted for  $e = 0.39$ . When the resulting source function, Equation 1.5, was applied to a one-dimensional transport model identical to that used by Bolin and Keeling (1963), Junge and Czeplak (1968) predicted seasonal variations in amplitude that agreed "reasonably well" with observations. However, there were deviations in phase. These deviations approached 60 days or more in the northern latitudes. Junge and Czeplak felt that their assumption of a simple trigonometric function for the time dependence of  $Q(\mu, t)$  was responsible for these deviations, since the observations document a

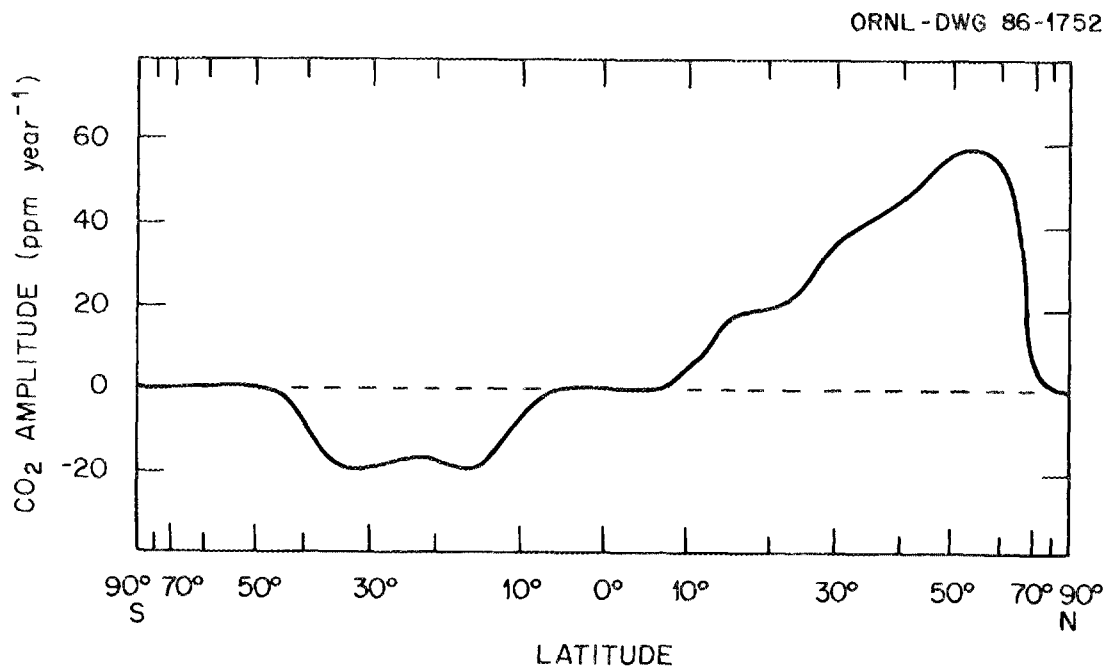


Figure 1.8. Amplitude of the seasonal component of Junge and Czeplak's CO<sub>2</sub> source function. After Junge and Czeplak (1968). Positive values indicate a release of CO<sub>2</sub> to the atmosphere; negative values indicate biospheric uptake.

pronounced asymmetry between summer and winter which their symmetric cosine function could not duplicate.

Junge and Czeplak (1968) also found that seasonal variations in  $\text{CO}_2$  concentration (as determined by a two-dimensional diffusion transport model) were not very sensitive to variations in the source function, and these concentrations were insensitive to latitudinal variations in  $K$ , the horizontal eddy diffusion coefficient in the transport equation. Therefore, they concluded that detailed information on the  $\text{CO}_2$  source function was unlikely to be obtained from atmospheric  $\text{CO}_2$  observations.

Machta (1972, 1974) simulated seasonal surface exchange using estimates of net monthly  $\text{CO}_2$  exchange between terrestrial vegetation and the atmosphere. Data on photosynthetic uptake and decomposition release provided by H. Lieth were extrapolated over  $20^\circ$  latitude belts. Machta used the resulting source function (Table 1.3) in a two-dimensional model of atmospheric mixing. He observed a two-month phase lag between the observed and predicted seasonal  $\text{CO}_2$  cycle at Mauna Loa Observatory (Machta 1972) and concluded (Machta 1974) that the source and sink estimates in the Lieth data (Table 1.3) would have to be increased by 50% in order to accurately simulate the amplitude of the seasonal cycle of atmospheric  $\text{CO}_2$ . Machta (1972, 1974) felt the discrepancy between prediction and observation was due mainly to uncertainties in the  $\text{CO}_2$  source function.

Pearman and Hyson (1980, 1981b) returned to the approach used by Bolin and Keeling (1963), that is, using a two-dimensional model

Table 1.3. Machta's (1972) estimates of seasonal CO<sub>2</sub> exchange (1015 g CO<sub>2</sub> month<sup>-1</sup>) for 20° latitude belts.<sup>a</sup>

Latitude Belt	Jan	Feb	Mar	Apr	May	Jun	Jul	Aug	Sep	Oct	Nov	Dec
70°-90°N	0.00	0.00	0.03	0.04	0.04	-0.09	-0.07	-0.06	0.07	0.03	0.00	0.00
50°-70°N	0.37	0.37	0.44	0.47	0.16	-1.16	-1.76	-1.52	0.67	0.88	0.64	0.44
30°-50°N	0.57	0.57	0.67	0.73	0.25	-1.80	-2.74	-2.36	1.05	1.36	1.01	0.67
10°-30°N	0.41	0.27	0.00	-0.27	-0.41	-0.55	-0.44	-0.27	0.00	0.27	0.45	0.55
10°N-10°S	0.00	0.00	0.00	0.00	0.00	0.00	0.00	0.00	0.00	0.00	0.00	0.00
10°-30°S	-0.36	-0.22	0.00	0.22	0.36	0.45	0.34	0.22	0.00	-0.22	-0.34	-0.45
30°-50°S	-0.60	-0.51	0.22	0.29	0.22	0.15	0.13	0.13	0.15	0.16	0.06	-0.04
50°-70°S	0.00	0.00	0.00	0.00	0.00	0.00	0.00	0.00	0.00	0.00	0.00	0.00
70°-90°S	0.00	0.00	0.00	0.00	0.00	0.00	0.00	0.00	0.00	0.00	0.00	0.00

<sup>a</sup>The carbon data of Machta (1972) were converted to CO<sub>2</sub> using a conversion factor of 1 g C = 3.66 g CO<sub>2</sub>. Positive values indicate release to the atmosphere; negative values indicate uptake by the terrestrial biosphere.

of atmospheric mixing to generate a  $\text{CO}_2$  source function consistent with the observed seasonality of  $\text{CO}_2$  concentration. They first converted Machta's (1974) source-sink data to their model configuration. Then, by assuming that seasonal oceanic  $\text{CO}_2$  exchange does not contribute significantly to observed atmospheric concentration and that the phase of the biosphere-atmosphere exchanges given by the converted Machta data was correct, they ran a series of simulations, tuning the biospheric exchanges until a best fit between predicted and observed seasonal cycles was obtained. The resulting source function, in conjunction with their two-dimensional diffusion model, generated a seasonal cycle that agreed reasonably well with station observations in phase and amplitude for all locations except Mauna Loa. A revised source function (Table 1.4) with changes in the timing of exchanges (particularly in low latitudes,  $10^\circ$ - $30^\circ$ ) was required to increase model accuracy.

The southern hemisphere exchange data were not modified from Machta (1974). The predicted amplitude of seasonal variations at southern hemisphere sites agreed well with observations, but phase agreement was not as good. Pearman and Hyson (1980) concluded these differences were likely due to northern hemispheric influences and seasonality in oceanic exchange.

The seasonal  $\text{CO}_2$  source function produced by Azevedo (1982) was guided by the work of Junge and Czeplak (1968) and Machta (1972). Azevedo estimated net primary production for latitude belts of  $10^\circ$  from data presented by Lieth (1978). The seasonality of the

Table 1.4. Pearman and Hyson's (1981b) estimates of seasonal CO<sub>2</sub> exchange (10<sup>15</sup> g CO<sub>2</sub> month<sup>-1</sup>) for latitude belts of equal area (2.55 x 10<sup>7</sup> km<sup>2</sup>).<sup>a</sup>

Latitude Belt	Jan	Feb	Mar	Apr	May	Jun	Jul	Aug	Sep	Oct	Nov	Dec
64.2°-90.0°N	0.27	0.27	0.34	0.36	0.14	-0.89	-1.30	-1.20	0.53	0.66	0.48	0.33
53.1°-64.2°N	0.36	0.36	0.43	0.46	0.16	-1.10	-1.70	-1.50	0.66	0.85	0.65	0.42
44.9°-53.1°N	0.48	0.47	0.56	0.60	0.19	-1.50	-2.20	-1.90	0.84	1.10	0.82	0.56
36.9°-44.9°N	0.49	0.47	0.54	0.57	0.14	-1.40	-2.10	-1.80	0.71	0.95	0.77	0.55
30.0°-36.9°N	0.41	0.37	0.40	0.39	0.02	-0.88	-1.30	-1.10	0.38	0.49	0.51	0.42
23.6°-30.0°N	0.34	0.28	0.28	0.24	-0.09	-0.48	-0.69	-0.58	0.00	0.09	0.29	0.31
17.5°-23.6°N	0.28	0.22	0.20	0.16	-0.12	-0.26	-0.35	-0.29	-0.14	-0.09	0.17	0.23
11.5°-17.5°N	0.17	0.13	0.11	0.08	-0.08	-0.13	-0.17	-0.14	-0.11	-0.08	0.08	0.14
5.7°-11.5°N	0.05	0.04	0.03	0.02	-0.02	-0.04	-0.05	-0.04	-0.03	-0.02	0.02	0.04
0.0°- 5.7°N	0.00	0.00	0.00	0.00	0.00	0.00	0.00	0.00	0.00	0.00	0.00	0.00
0.0°- 5.7°S	0.00	0.00	0.00	0.00	0.00	0.00	0.00	0.00	0.00	0.00	0.00	0.00
5.7°-11.5°S	-0.02	-0.01	0.00	0.01	0.02	0.02	0.02	0.01	0.00	-0.01	0.02	0.02
11.5°-17.5°S	-0.06	-0.04	0.00	0.04	0.06	0.07	0.05	0.04	0.00	-0.04	-0.05	-0.07
17.5°-23.6°S	-0.10	-0.06	0.00	0.06	0.09	0.11	0.08	0.06	0.00	-0.05	-0.08	-0.11
23.6°-30.0°S	-0.18	-0.09	0.02	0.08	0.10	0.12	0.09	0.06	0.01	-0.04	-0.07	-0.14
30.0°-36.9°S	-0.17	-0.13	0.04	0.09	0.10	0.10	0.08	0.06	0.03	0.00	-0.04	-0.14
36.9°-44.4°S	-0.15	-0.12	0.04	0.07	0.07	0.06	0.05	0.04	0.03	0.02	0.00	-0.11
44.4°-53.1°S	-0.05	-0.04	0.02	0.03	0.02	0.02	0.02	0.01	0.01	0.01	0.00	-0.04
53.1°-64.2°S	0.00	0.00	0.00	0.00	0.00	0.00	0.00	0.00	0.00	0.00	0.00	0.00
64.2°-90.0°S	0.00	0.00	0.00	0.00	0.00	0.00	0.00	0.00	0.00	0.00	0.00	0.00

<sup>a</sup>Positive values indicate release to the atmosphere; negative values indicate uptake by the terrestrial biosphere.

source function was introduced using simple curves of biosphere uptake and release. Three regions, latitudinal zones, per hemisphere were considered, with a different curve for each. In fact there are only two curves since Azevedo assumed an equatorial zone (10°N-10°S) of no seasonality. The curves for the northern hemisphere are shown in Figure 1.9. The curves are shifted by six months for the southern hemisphere. Also, to account for deforestation in southern latitudes since 1950 (the vegetation maps used by Lieth (1978) date from around 1950) and climatic differences from the northern hemisphere, the estimates of the southern balance between assimilation and release were reduced by 50%. These changes were required to obtain a good fit for the amplitude of the southern cycle (Azevedo 1982). The monthly net CO<sub>2</sub> exchange between biosphere and atmosphere predicted by Azevedo's function is given in Table 1.5.

Azevedo (1982) ran his one-dimensional (latitude) CO<sub>2</sub> transport model with only the terrestrial biosphere source function and achieved a good fit for the phase and amplitude of observed seasonal cycles. The additional contribution of modeled seasonal oceanic exchanges was very small, and Azevedo concluded these variations were not a critical component.

The CO<sub>2</sub> source functions discussed to this point involve only latitudinal variations in sources and sinks. Longitudinal variations such as the transition between grassland and deciduous forest in North America are lost in the zonal means of the source functions. The source functions of three dimensional tracer models can, however, incorporate these longitudinal variations.

ORNL-DWG 86-1753

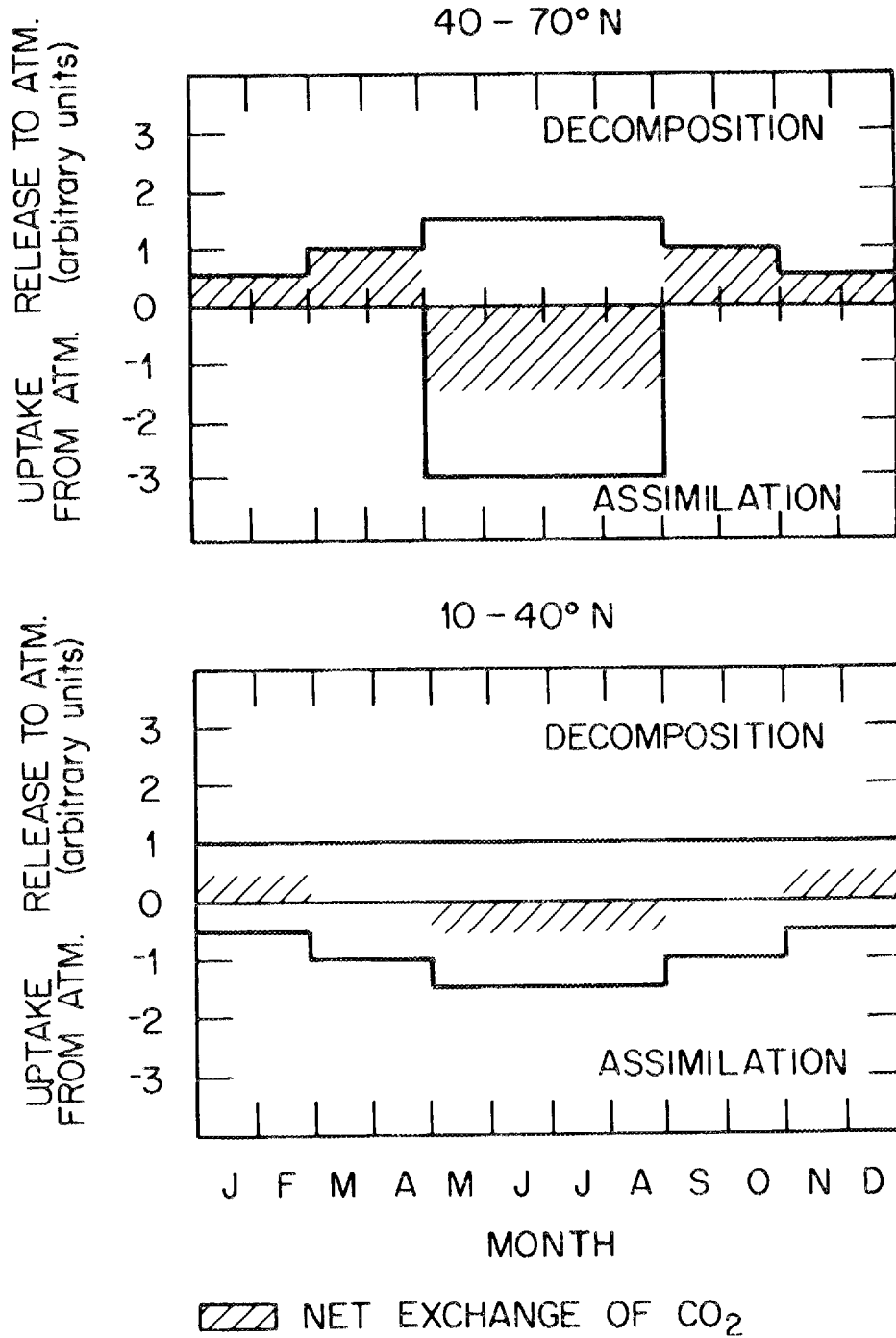


Figure 1.9. Azevedo's curves describing the seasonality of biospheric uptake (-) and release (+) of CO<sub>2</sub>.

Table 1.5. Azevedo's (1982) estimates of seasonal CO<sub>2</sub> exchange (10<sup>15</sup> g CO<sub>2</sub> month<sup>-1</sup>) for 10° latitude belts.<sup>a</sup>

Latitude Belt	Jan	Feb	Mar	Apr	May	Jun	Jul	Aug	Sep	Oct	Nov	Dec
80°-90°N	0.00	0.00	0.00	0.00	0.00	0.00	0.00	0.00	0.00	0.00	0.00	0.00
70°-80°N	0.00	0.00	0.00	0.00	0.00	0.00	0.00	0.00	0.00	0.00	0.00	0.00
60°-70°N	0.36	0.36	0.72	0.72	-1.08	-1.08	-1.08	-1.08	0.72	0.72	0.36	0.36
50°-60°N	0.66	0.66	1.32	1.32	-1.98	-1.98	-1.98	-1.98	1.32	1.32	0.66	0.66
40°-50°N	0.84	0.84	1.68	1.68	-2.52	-2.52	-2.52	-2.52	1.68	1.68	0.84	0.84
30°-40°N	0.87	0.87	0.00	0.00	-0.87	-0.87	-0.87	-0.87	0.00	0.00	0.87	0.87
20°-30°N	0.78	0.78	0.00	0.00	-0.78	-0.78	-0.78	-0.78	0.00	0.00	0.78	0.78
10°-20°N	0.84	0.84	0.00	0.00	-0.84	-0.84	-0.84	0.84	0.00	0.00	0.84	0.84
0°-10°N	0.00	0.00	0.00	0.00	0.00	0.00	0.00	0.00	0.00	0.00	0.00	0.00
0°-10°S	0.00	0.00	0.00	0.00	0.00	0.00	0.00	0.00	0.00	0.00	0.00	0.00
10°-20°S	-0.46	-0.46	0.00	0.00	0.46	0.46	0.46	0.46	0.00	0.00	-0.46	-0.46
20°-30°S	-0.28	-0.28	0.00	0.00	0.28	0.28	0.28	0.28	0.00	0.00	-0.28	-0.28
30°-40°S	-0.12	-0.12	0.00	0.00	0.12	0.12	0.12	0.12	0.00	0.00	-0.12	-0.12
40°-50°S	-0.07	-0.07	0.05	0.05	0.02	0.02	0.02	0.02	0.05	0.05	-0.07	-0.07
50°-60°S	0.00	0.00	0.00	0.00	0.00	0.00	0.00	0.00	0.00	0.00	0.00	0.00
60°-70°S	0.00	0.00	0.00	0.00	0.00	0.00	0.00	0.00	0.00	0.00	0.00	0.00
70°-80°S	0.00	0.00	0.00	0.00	0.00	0.00	0.00	0.00	0.00	0.00	0.00	0.00
80°-90°S	0.00	0.00	0.00	0.00	0.00	0.00	0.00	0.00	0.00	0.00	0.00	0.00

<sup>a</sup>Positive values indicate release to the atmosphere; negative values indicate uptake by the terrestrial biosphere.

Fung et al. (1983) used a CO<sub>2</sub> tracer model in conjunction with the Goddard Institute for Space Studies (GISS) three-dimensional Global Circulation Model (GCM) of Hansen et al. (1983). The two-dimensional source function developed by Fung et al. (1983) combined the global 1° X 1° resolution vegetation map of Matthews (1983) with Azevedo's (1982) curves of CO<sub>2</sub> uptake and release by the terrestrial biosphere. Annual net primary production (NPP) values were assigned to each 1° X 1° cell of Matthews' vegetation map. The resultant NPP map was converted to the 8° latitude by 10° longitude resolution of the tracer model. The monthly flux of carbon to the atmosphere is then given by

$$\text{SOURCE}(\lambda, t) = \text{NPP}(\lambda, \theta) \times (\text{RELEASE}(\theta, t) - \text{UPTAKE}(\theta, t)) , \quad (1.7)$$

where  $\text{NPP}(\lambda, \theta)$  is the annual net primary production of a grid cell of longitude  $\lambda$  and latitude  $\theta$ , and  $(\text{RELEASE}(\theta, t) - \text{UPTAKE}(\theta, t))$  is given by the uptake and release curves of Azevedo (1982, see Figure 1.9). Fung et al. (1983) assumed a steady state biosphere (i.e., no net annual exchange of CO<sub>2</sub>) and normalized the uptake and release curves so that one year's total release equals one year's total uptake, or

$$\sum_{\text{1 year}} \text{RELEASE}(\theta, t) = \sum_{\text{1 year}} \text{UPTAKE}(\theta, t) = 1 . \quad (1.8)$$

Fung et al. (1983) ran their tracer model with this two-dimensional source function and the one-dimensional source functions of Machta (1972) and Pearman and Hyson (1980). The

two-dimensional source function resulted in simulated seasonal cycles at monitoring station locations which matched observed cycles better than those generated with the other two source functions. Noting the influence of model requirements on the form of the source function (each of which does a reasonable job when used as input to their own respective tracer models), Fung et al. (1983) stressed the need for an ecological model of CO<sub>2</sub> exchange with the atmosphere.

Heimann, Keeling, and Tucker (1985) analyzed the seasonal cycle of atmospheric CO<sub>2</sub> using a revised tracer model structured after the GISS model of Hansen et al. (1985). The NPP estimates for their terrestrial source function were computed from remote sensing data recorded by the advanced very-high-resolution radiometer (AVHRR) sensors flown on meteorological satellites of the National Oceanic and Atmospheric Administration (Tucker, Townshend, and Goff 1985; Tucker et al. 1986). The radiatively computed 'vegetation index' of Tucker, Townshend, and Goff (1985) was converted to NPP with the model of Kumar and Monteith (1981). The spatially and temporally distributed AVHRR data were average over the 8° X 10° resolution of the tracer model grid cells.

To account for the combined respiration of plants and soils, a constant respiratory term was combined with a temperature dependent term which used ground temperatures. Heimann, Keeling, and Tucker (1985) assumed a 50% increase in respiration for a 10°C rise in temperature above a monthly mean of -10°C. Respiration below -10°C was assumed to be zero. The model also assumed respiration and photosynthesis at each grid location was balanced over the year.

The three-dimensional tracer model predicted cycles of atmospheric  $\text{CO}_2$  that agreed quite well with observations at six recording stations. The temperature dependent plant respiration and the seasonal oceanic exchanges were adjusted globally to provide a best fit.

### 1.2.3 The Need For Ecologically Derived $\text{CO}_2$ Source Functions

All of the described biospheric  $\text{CO}_2$  exchange functions, when ran in conjunction with their respective tracer models, provide reasonable simulations of observed seasonal  $\text{CO}_2$  cycles. Although there are variations in the level of agreement, none provide predictions so bad that the responsible source function can be completely disregarded. However, the source functions tend to be very model dependent. The approach taken by Bolin and Keeling (1963) and Pearman and Hyson (1980, 1981b) derives seasonal sources and sinks consistent with observations of atmospheric  $\text{CO}_2$ . The source function is that one which, given a model of atmospheric mixing, is required to give the best fit between observation and model prediction; model dependency is explicit and obvious.

The other source functions are derived from information on the terrestrial biosphere, specifically net primary production, but they too may involve terms which are tuned to provide a best fit. Junge and Czeplak (1968) adjusted their  $e$  term, the fraction of  $\text{CO}_2$  released from the soil during the summertime, to generate a source function which provided acceptable predictions of seasonal  $\text{CO}_2$  concentrations, given their model of atmospheric mixing. Machta

(1972, 1974) modified Lieth's biosphere data with his own "liberal extrapolations", and Azevedo (1982) reduced his own estimates of the assimilation-decomposition balance in the southern hemisphere after simulations failed to reproduce the amplitude of the southern seasonal cycle. Heimann, Keeling, and Tucker (1985) adjusted the fraction of plant respiration dependent on temperature to gain a best fit between observed and predicted seasonality. Auspiciously, the source function of Fung et al. (1983) involved little if any tuning of the biosphere, although their source function is dependent on the assignment of NPP values to the  $1^\circ \times 1^\circ$  cells of Matthews' (1983) vegetation map.

Our discussion of tuning in the source functions should not be taken as a criticism. These approaches are reasonable, useful, and necessary; calibration is an inherent part of all modeling. Our purpose is to point out where the tuning takes place, where model dependency is explicit. Adjustments in the source functions are frequently related to uncertainties in the biospheric sources and sinks and may involve sensitive parameters in the model (e.g., the  $e$  of Junge and Czeplak 1968, or the respiratory release of Heimann, Keeling, and Tucker 1985). The model dependency of existing  $\text{CO}_2$  source functions makes discrimination between the influence of myriad uncertainties in the seasonal carbon metabolism of the biosphere and of uncertainties in seasonal atmospheric mixing very difficult. As recognized by Fung et al. (1983), there is a need for an independently derived biospheric  $\text{CO}_2$  exchange function, i.e., one which is derived, to as great an extent as possible, from the

best available information on the seasonal behavior of the global ecosystem-biosphere complex.

In addition to contributing to model independence, an ecologically based source function can address explicitly some of the ecological assumptions found in existing source functions, perhaps allowing some of them to be relaxed. For example, the source functions generally assume a steady-state biosphere, one in which there is no net annual exchange of carbon between the atmosphere and biosphere. This assumption precludes any consideration of questions concerning the net source/sink characteristics of various terrestrial regions. An ecologically derived source function might incorporate information on net ecosystem production (NEP) and permit some progress on this important question.

Existing source functions and their companion transport models appear to simulate more readily the amplitude of the seasonal CO<sub>2</sub> cycle than the phase or timing of the seasonal cycle (see review in Section 1.2.2). This observation suggests that the timing of the biospheric CO<sub>2</sub> exchanges or the shape of the seasonal uptake and release curves are as important as the magnitude of the peak fluxes or the integrated annual exchanges (NPP) in the estimation of net CO<sub>2</sub> flux (also see Fung et al. 1983). Any ecological model of CO<sub>2</sub> exchange will likely involve information on the time of CO<sub>2</sub> fluxes to and from the biosphere. This information might prove useful in improving the fit between predicted and observed seasonal CO<sub>2</sub> concentrations.

Furthermore, the existing source functions involve only superficial sources and sinks, they do not address the partitioning of  $\text{CO}_2$  between carbon reservoirs (Heimann, Keeling, and Mook 1985) or dynamics within the biosphere. The biosphere is a black box. Advances in understanding the global carbon cycle will surely involve explicit within-biosphere dynamics. An ecologically derived source function may have characteristics which will contribute to that description.

Efforts to derive an ecological model of the seasonal exchange of  $\text{CO}_2$  between the biosphere and the atmosphere may approach the problem in a number of different ways:

1. Empirical relationships can be derived between the seasonality of photosynthetic and respiratory fluxes and climatic variables. This method usually makes no attempt to model the terrestrial standing crops.
2. Standardized compartment models can be applied to each biome, life-zone type, or latitudinal zone. These models may be simple, containing several biomass and soil variables, averaged over each of the zones.
3. Models already developed for specific sites may be borrowed and various modifications made in them so they apply to wider areas than the particular sites for which they were originally designed.

Each of the above procedures has advantages and disadvantages. We will outline here the relative advantages and the disadvantage of approach number 3, the elaboration of site-specific models.

Advantages:

1. A large number of site-specific models have already been developed. Computer simulation of these is usually fairly simple.
2. These site-specific models were developed by experts on the particular biome type, and in many cases the models have been validated.
3. Detailed site-specific compartment models have the flexibility to incorporate a variety of scenarios of possible interest in any attempt to investigate changes in seasonal fluxes (see Section 1.1.3). These include (a) land-use changes, (b) changes in harvesting rates, (c) growth stimulation by enhanced CO<sub>2</sub>, (d) changes in climate, and (e) effects of other stresses such as acid rain.
4. It is easy to incorporate new ecological data into improvements of site-specific models.
5. The site-specific models often include the within-biome dynamics or carbon reservoir partitioning referred to above.
6. The site-specific models can provide "ground-truth" data against which other modeling approaches can be compared.

Disadvantage:

The primary disadvantage of site-specific models is that it may be difficult to extend such models to cover whole biomes. This is due to the great amount of heterogeneity, climatic, edaphic and even vegetative, within a biome.

Our purpose here is to describe the derivation of a CO<sub>2</sub> exchange function based on site-specific models of ecosystem-level carbon metabolism. In particular, we address the central problem of extrapolation from site-specific models to biome-level and regional models of CO<sub>2</sub> flux. Chapter 2 describes the site-specific models. In Chapter 3 we use these models to generate a global CO<sub>2</sub> exchange function, and in Chapter 4 we explore the problem of extrapolation. Chapter 5 provides a summary and synthesis. The need for ecologically derived CO<sub>2</sub> source functions is clear. It is also clear that the problem of extrapolation, the problem of translating local, site-scaled information to larger spatial and temporal scales must be addressed as ecologists move increasingly towards investigations at landscape, regional, and global scales.

## CHAPTER 2

## THE SITE-SPECIFIC MODELS

The assembly of a set of terrestrial carbon flux models is made possible by the recent appearance of a number of volumes synthesizing the extensive research efforts of the International Biological Program (IBP). Examples include compilations or summaries of information on forests (Reichle 1981), grasslands (Bremeyer and Van Dyne 1980), arid lands (Goodall and Perry 1979), and tundra (Brown et al. 1980; Bliss, Heal, and Moore 1981). Although these summaries sometimes do not contain detailed seasonal information, many of the primary sources on which they are based do contain such information; many of the 116 IBP sites compiled by DeAngelis, Gardner, and Shugart (1981) are good examples.

In addition to the large amount of data collected, many site-specific models of seasonal carbon dynamics have been constructed, both within and outside the various IBP projects. These models are reviewed by King and DeAngelis (1985). Many of these models are process-oriented compartment models. Seasonality is built into the models through both empirical information on phenology and mechanistic driving of photosynthesis, respiration, and decomposition by climatic variables. These models, and others like them, were scrutinized for their applicability to the problem of modeling the seasonal carbon dynamics of the terrestrial biosphere.

In collecting site-specific models for ultimate integration into an overall model of global CO<sub>2</sub> exchange, we directed our search towards coverage of ten major ecosystem types; tropical evergreen forest, tropical deciduous forest, temperate deciduous forest, temperate broadleaved evergreen forest, grassland, temperate coniferous forest (e.g., pine), boreal coniferous forest (e.g., spruce-fir), tundra, arid lands, and agroecosystems (see King and DeAngelis 1985, 1986). From this compiled set of models, we selected representative models for as many ecosystem types (or subtypes) as possible. The criteria used in the selection process are outlined below.

1. Availability: The selection of representative models was determined by the number of suitable models. For some ecosystem types, few appropriate models are available; for others, such as the temperate grasslands, there exists a relatively large selection of models dealing with some aspect of carbon dynamics.

2. Abiotic driving variables: Models in which seasonal carbon dynamics are driven by seasonally varying climatic factors were favored. For example, decomposition might be modeled as a function of litter (or soil) temperature and moisture. Models in which seasonal dynamics are determined by time-varying rate coefficients specific only to a certain site or data set were selected against. This selection criterion reflects the demands of the site-to-biome extrapolation process described later (Section 3.0).

3. **Simplicity:** Preference was given to models with relatively few state variables and parameters (unless the state variables are repetitive, such as many soil layers). Thus exceptionally complex or detailed models were omitted.

4. **Completeness:** In general, the models chosen were those that trace the flux of carbon from the assimilation of  $\text{CO}_2$  via photosynthesis, through translocation of photosynthate, to the release of  $\text{CO}_2$  during respiration and organic decomposition. When such models were not available, we selected submodels of photosynthetic production and decomposition. These independently derived submodels required coupling in some manner in order to provide complete models of carbon fluxes for some of the ecosystem types.

5. **General applicability:** Preference was given to those models that have already been applied to two or more sites within the ecosystem type or biome, in contrast to those models having been applied to only one site or vegetation stand. This criterion often distinguished between models developed for general application and those developed with only a single site in mind.

6. **Validation:** Preference was given to models that have been validated against independent data sets, or for which model output has been compared against field observations.

This chapter describes the set of site-specific models selected according to the above criteria, that we use in the regional or global model of seasonal carbon dynamics. Figure 2.1 illustrates the geographical distribution of these models.



Figure 2.1. Geographical distribution of the site-specific models. The numbers indicate the sections of Chapter 2 in which the models are described: 1 refers to Section 2.1, 2 refers to Section 2.2, etc.

The model descriptions present the compartmental structure of the models, the intercompartmental carbon or biomass fluxes, the climatic driving forces, and the way in which the driving forces are assumed to affect the fluxes. Special emphasis is given to the effect of the driving forces on photosynthesis, respiration, and the release of  $\text{CO}_2$  during decomposition; these fluxes are the most critical in simulating  $\text{CO}_2$  exchange between the atmosphere and the terrestrial biosphere.

The descriptions also include plots of total stand, or ecosystem, photosynthesis and respiration (including both live plant respiration and decomposer respiration) and plots of net exchange with the atmosphere, as generated by the models. Photosynthesis represents the assimilation of atmospheric  $\text{CO}_2$  by the vegetation; the respiration represents the ecosystem's contribution to atmospheric  $\text{CO}_2$ . Net exchange is respiration minus photosynthesis. Hence, a positive value indicates the stand is acting as a source of atmospheric  $\text{CO}_2$ ; a negative value indicates the stand is acting as a sink. These simulations were verified by comparing our model output with model results (for standing crops and/or fluxes) reported in the literature documenting the model or describing model applications. If this information was not available, pertinent data from the various synthesis volumes or other sources were used to check model output. These data included information on annual net primary productivity, net ecosystem productivity, photosynthetic rates, standing crops, and soil respiratory fluxes.

The models were implemented on the computer facilities at Oak Ridge National Laboratory (ORNL), Oak Ridge, Tennessee. Listings of the the computer programs are available from the author upon request.

## 2.1 TEMPERATE BROADLEAF DECIDUOUS FOREST MODEL

A model of organic matter transfer in a second-growth deciduous forest at Oak Ridge, Tennessee (35°55'N,80°77'W) was developed by Sollins, Reichle, and Olson (1973) and Sollins, Harris, and Edwards (1976). This forest ecosystem is dominated by the tulip poplar (Liriodendron tulipifera L.). The purpose of their model was to improve the ability to predict effects of perturbation of forests. We use the model to predict seasonal carbon dynamics in forests for which we believe the model to be appropriate. The model is described by differential equations, and the solutions involve a time step of approximately one day (0.003 year).

### 2.1.1 Structure Of The Model

#### 2.1.1.1 Compartments

The overall compartmental structure of the model is shown in Figure 2.2. There are four subsystems: (1) subsystem A - tulip poplar component of the stand (Figure 2.3), (2) subsystem B - miscellaneous other canopy species (Figure 2.3), (3) subsystem C - understory species (Figure 2.4), and (4) subsystem D - soil, litter, and decomposers (Figure 2.5).

ORNL - DWG 70-12021AR

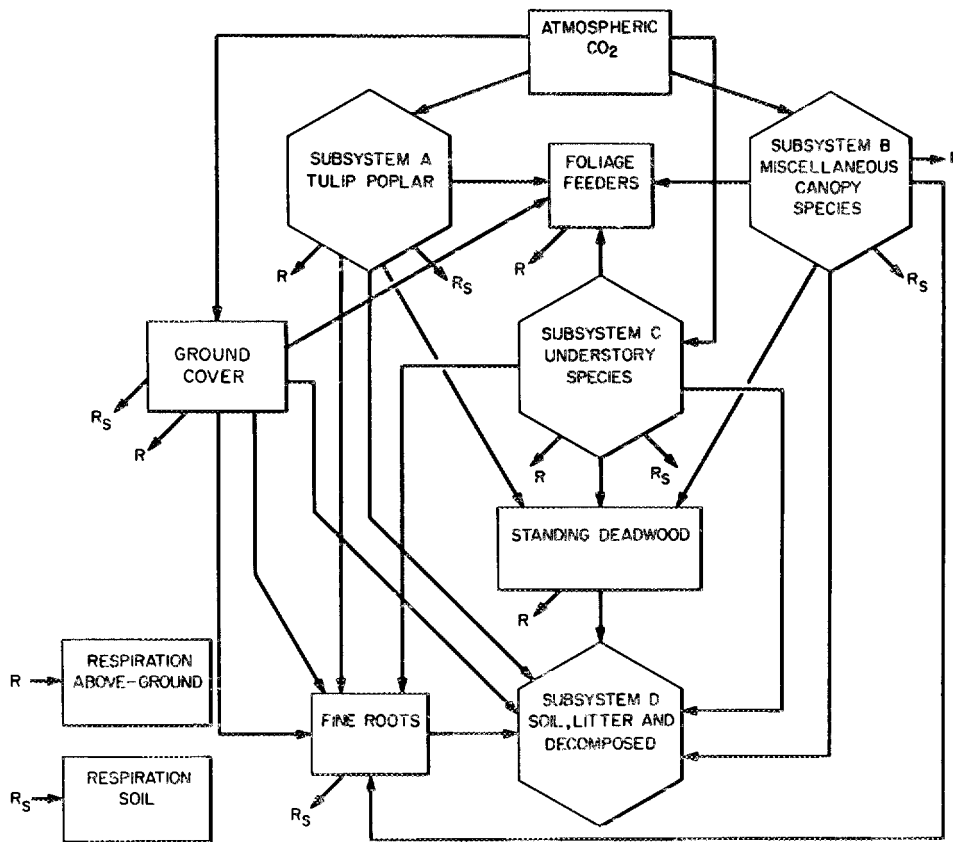


Figure 2.2. Compartmental structure of the temperate broadleaf deciduous forest model - ecosystem overview. The figure shows the four major subsystems (A-D) and various other compartments. R - aboveground respiration; R<sub>s</sub> - belowground respiration. From Sollins, Reichle, and Olson (1973).

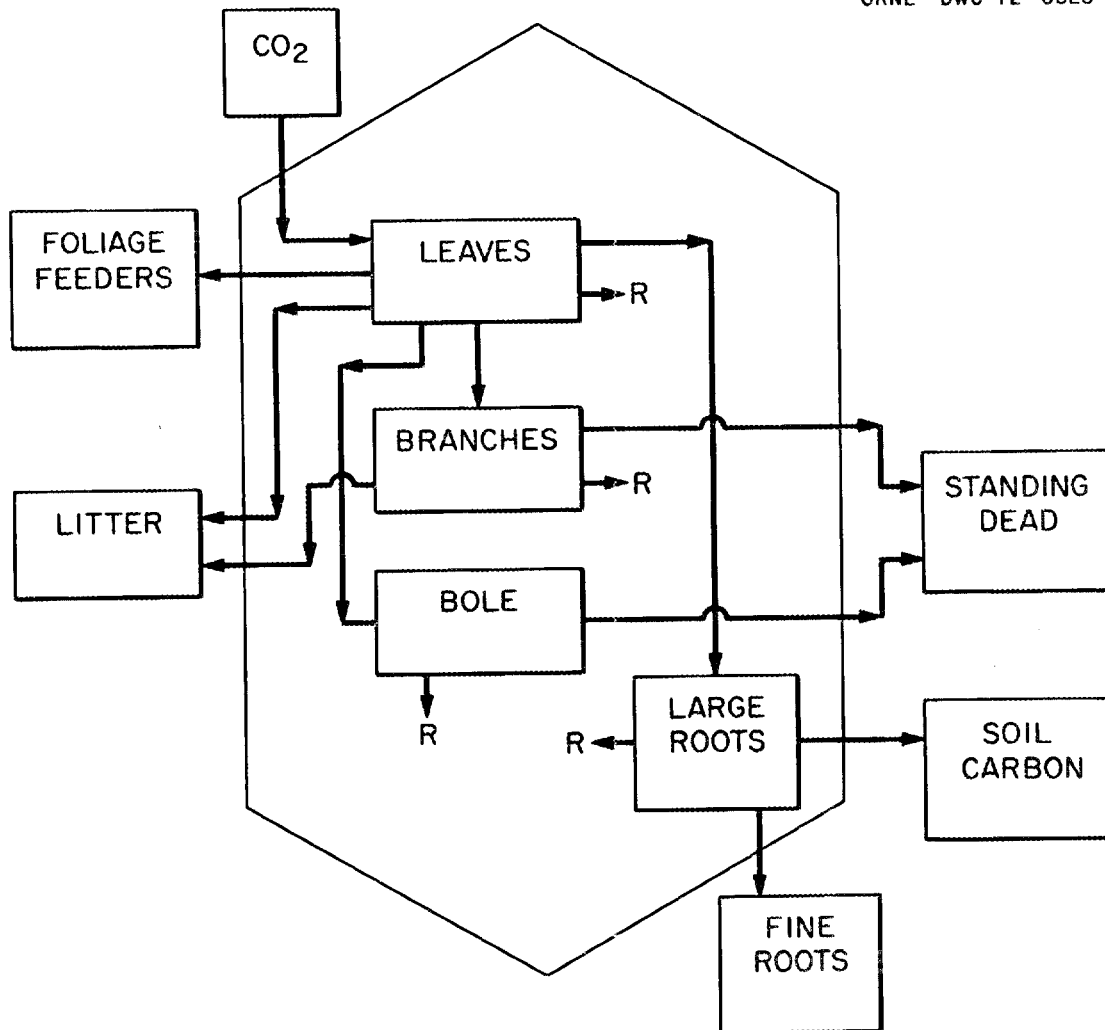


Figure 2.3. Compartmental structure of the temperate broadleaf deciduous forest model - canopy subsystems. Subsystem A -- the dominant species *L. tulipifera* including all individuals greater than 10 m height. Subsystem B -- other overstory trees 10 m height. R - aboveground respiration. From Sollins, Reichle, and Olson (1973).

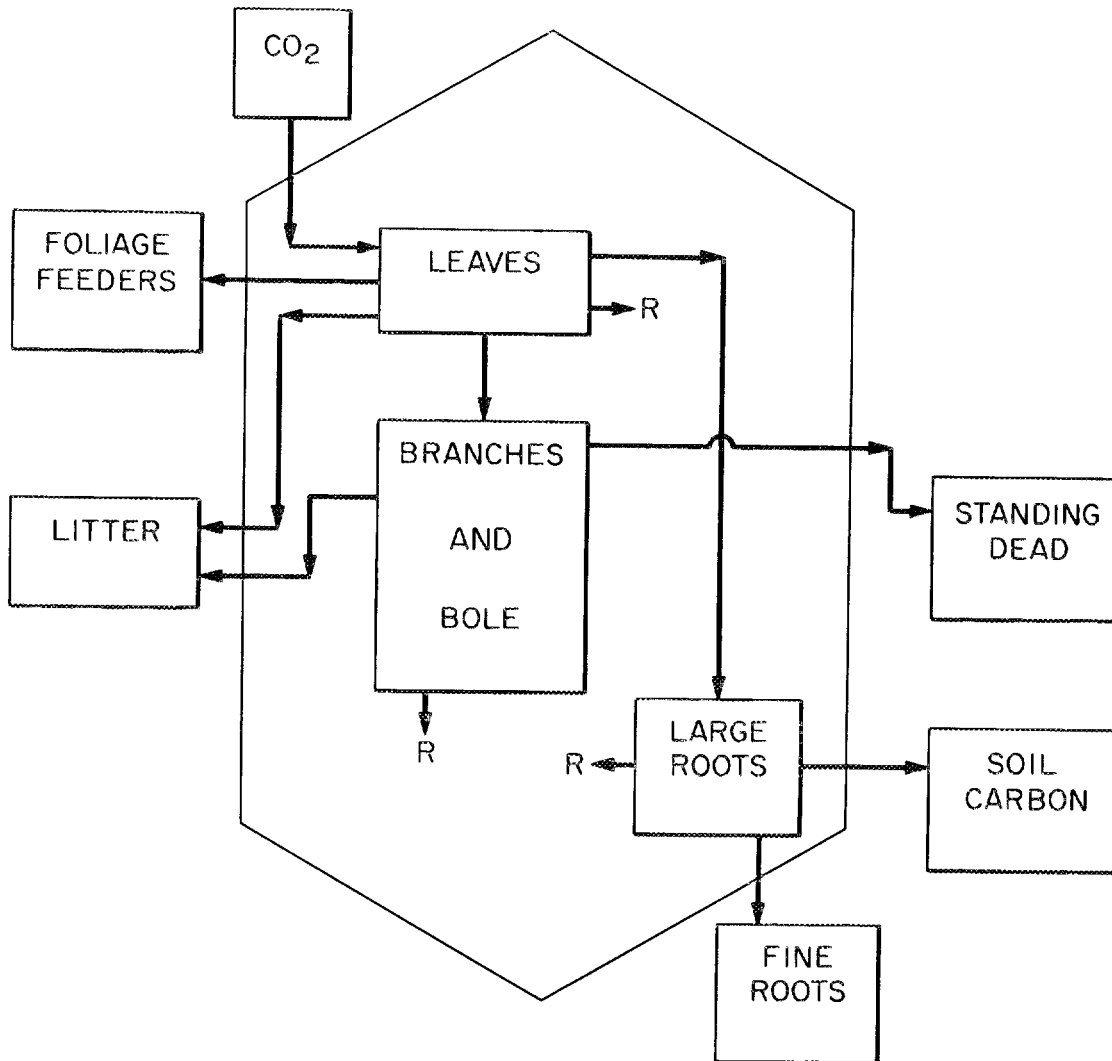


Figure 2.4. Compartmental structure of the temperate broadleaf deciduous forest model - understory subsystem. Understory includes trees 1-10 m height. R - aboveground respiration. From Sollins, Reichle, and Olson (1973).

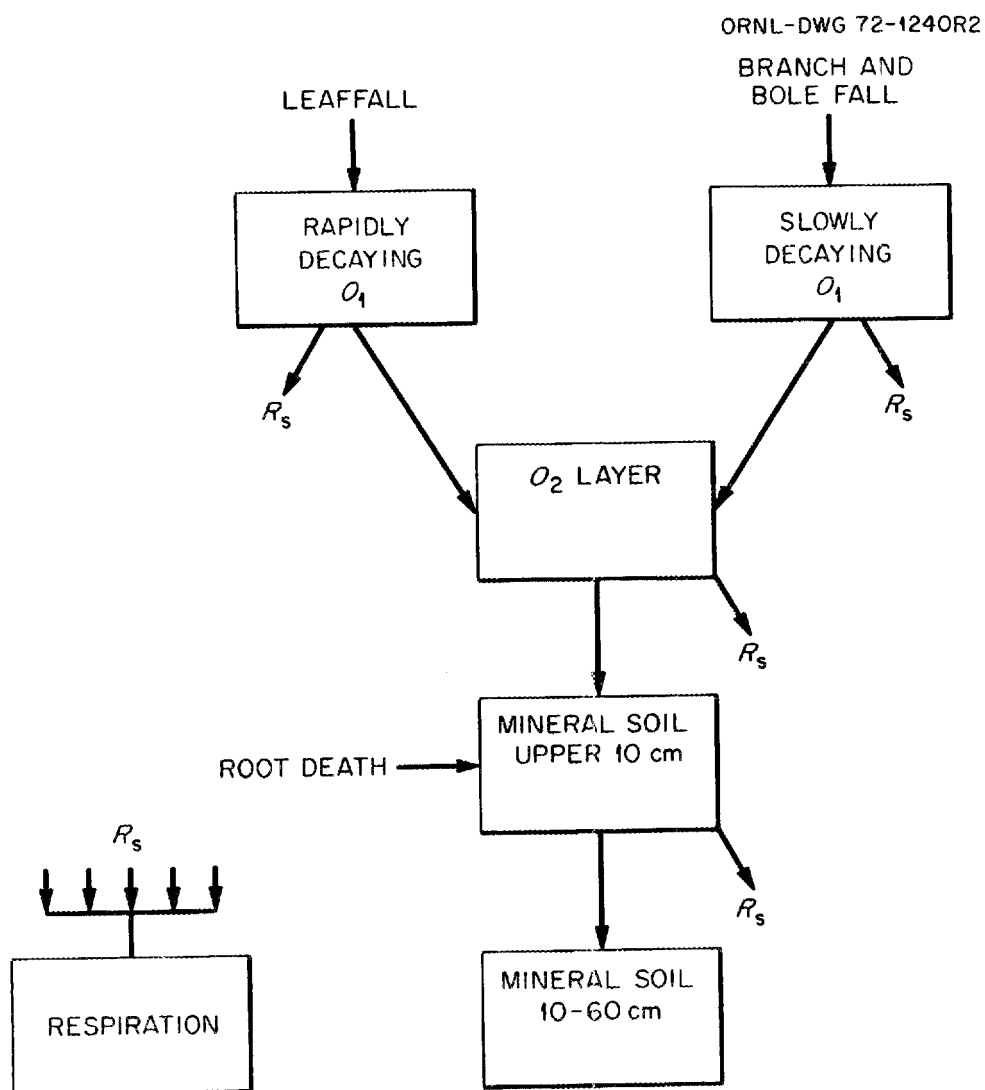


Figure 2.5. Compartmental structure of the temperate broadleaf deciduous forest model - litter/soil subsystem. Decomposer organisms are conceptually combined with their substrate. R - belowground respiration. From Sollins, Reichle, and Olson (1973).

The state variables corresponding to these compartments are defined in Table 2.1. The variables do not correspond to the compartments in Figures 2.3 to 2.5 in a strictly one-to-one manner. For example, the functional component of tulip poplar active tissue,  $X_3$ , occurs in more than one of the structural compartments of Figure 2.3 (i.e, branches, boles, large roots, and fine roots). The values of all state variables are in units of kg biomass  $m^{-2}$ .

#### 2.1.1.2 Driving Variables

Model seasonality is influenced by seasonally variable abiotic factors and phenological events. There are three exogenous driving variables and a pair of phenology switches in the model (Table 2.2).

Daily values of soil moisture and temperature are interpolated from mean monthly empirical values read into the computer program as input data. Light intensity is a constant during the growing season. The leaf fall switch is off ( $Z_4 = 0$ ) during the growing season and on ( $Z_4 = 1$ ) during the dormant period. Similarly, the translocation switch is on when gross photosynthesis is non-zero and off when there is no gross photosynthesis occurring. The beginning and end of the growing season are specified as input data.

#### 2.1.1.3 Flows Or Rate Processes

The flows of organic matter correspond to the arrows between compartments in Figures 2.3 to 2.5. The detailed functional representation of these flows and the assumptions involved are described in Sollins, Reichle, and Olson (1973) and Sollins, Harris and Edwards (1976); here we simply define the flows and indicate

Table 2.1. State variables of the temperate broadleaf deciduous forest model.

State Variable*	Description
X <sub>1</sub>	tulip poplar leaves
X <sub>2</sub>	tulip poplar active tissues
X <sub>3</sub>	tulip poplar woody tissues
X <sub>4</sub>	tulip poplar buds
X <sub>5</sub>	other overstory leaves
X <sub>6</sub>	other overstory active tissues
X <sub>7</sub>	other overstory woody tissues
X <sub>8</sub>	other overstory buds
X <sub>9</sub>	understory leaves
X <sub>10</sub>	understory active tissues
X <sub>11</sub>	understory woody tissues
X <sub>12</sub>	understory buds
X <sub>13</sub>	ground cover
X <sub>14</sub>	standing dead
X <sub>15</sub>	canopy consumers
X <sub>16</sub>	fine roots
X <sub>17</sub>	quickly decomposing O <sub>1</sub> layer
X <sub>18</sub>	slowly decomposing O <sub>1</sub> layer
X <sub>19</sub>	O <sub>2</sub> layer
X <sub>20</sub>	soil organic matter (0-10 cm depth)
X <sub>21</sub>	soil organic matter (10-60 cm depth)

\*Units are kg biomass m<sup>-2</sup>.

Table 2.2. Driving variables and seasonal forcings of the temperate broadleaf deciduous forest model.

---

Driving Variable	Description
$Z_1$	temperature ( $^{\circ}\text{C}$ )
$Z_2$	light intensity ( $\text{langley min}^{-1}$ )
$Z_3$	soil moisture (% wet weight)
$Z_4$	leaffall switch
$Z_5$	translocation switch

---

which, if any, of the driving variables influence a particular flux (Table 2.3). Unless indicated otherwise, the flows are continuous linear functions of the source compartment. The model representation of photosynthesis and respiration is discussed further in Section 2.1.1.4. In Table 2.3, the notation  $F(i,j)$  indicates the flow of material from compartment  $i$  to compartment  $j$ . The number 99 refers to a compartment external to the system. All flows into the system are labelled  $F(99,j)$ , and all flows out of the system are labelled  $F(i,99)$ .

#### 2.1.1.4 Photosynthesis And Respiration

There are four gross photosynthesis functions: (1) tulip poplar leaves, (2) other overstory leaves, (3) understory leaves, and (4) ground cover. The first three of these functions are similar, so we show only the photosynthesis of tulip poplar leaves,  $G_A$ :

$$G_A = \frac{X_4^* + A_{13}}{A_{13} + 0.005} \left( \frac{-3.914B_1}{A_1K_1} \right) \frac{X_1}{X_1 + X_5} \ln \left( \frac{1 + A_1E_1}{1 + A_1I(0)} \right), \quad (2.1)$$

where  $X_4^*$  is the mass of tulip poplar buds at the end of the dormant season;  $A_1$  is a light saturation coefficient;  $B_1$  is the maximum rate of photosynthesis;  $K_1$  is a light extinction coefficient;  $I(0)$  is the incident light intensity ( $Z_2$ , Table 2.2), and

$$E_1 = I(0) \exp [-1000 K_1 (X_1 + X_5)] . \quad (2.2)$$

Equation 2.2 describes the attenuation of light by the forest canopy.

Table 2.3. The flows of organic matter simulated by the temperate broadleaf deciduous forest model.

Flow <sup>a</sup>	Description <sup>b</sup>
Tulip poplar trees	
F(99,1)	photosynthesis of leaves: $Z_1$
F(1,2)	translocation of organic matter from leaves to active tissue
F(1,15)	consumption of leaves
F(1,17) <sub>1</sub>	frass production
F(1,17) <sub>2</sub>	litterfall to quickly decomposing $O_1$ layer: $Z_4$
F(1,99)	respiration of leaves: $Z_1$
F(2,1)	translocation of organic matter from active tissue to leaves: $Z_5$
F(2,3)	translocation of organic matter from active tissue to woody tissue: $Z_1$
F(2,4)	translocation of organic matter from active tissue to buds: $Z_1$
F(2,16)	translocation of organic matter from active tissue to fine roots
F(2,99)	respiration of active tissues: $Z_1$
F(3,14)	transfer to standing dead
F(3,17)	limbfall to quickly decomposing $O_1$ layer
F(3,18)	limbfall to slowly decomposing $O_1$ layer
F(3,20)	transfer of woody biomass to soil organic matter
F(4,99)	respiration of buds
Other overstory trees	
F(99,5)	photosynthesis of leaves: $Z_2$
F(5,6)	translocation of organic matter from leaves to active tissues
F(5,15)	consumption of leaves
F(5,17) <sub>1</sub>	frass production
F(5,17) <sub>2</sub>	litterfall to quickly decomposing $O_1$ layer: $Z_4$
F(5,99)	respiration of leaves: $Z_1$
F(6,5)	translocation of organic matter from active tissues to leaves: $Z_5$
F(6,7)	translocation of organic matter from active tissue to woody tissue: $Z_1$
F(6,8)	translocation of organic matter from active tissue to buds: $Z_1$
F(6,16)	translocation of organic matter from active tissue to fine roots
F(6,99)	respiration of active tissues: $Z_1$
F(7,14)	transfer to standing dead
F(7,17)	limbfall to quickly decomposing $O_1$ layer

Table 2.3. (Continued)

Flow <sup>a</sup>	Description <sup>b</sup>
F(7,18)	limbfall to slowly decomposing O <sub>1</sub> layer
F(7,20)	transfer of woody biomass to soil organic matter
F(8,99)	respiration of buds: Z <sub>1</sub>
Understory trees	
F(99,9)	photosynthesis of leaves: Z <sub>2</sub>
F(9,10)	translocation of organic matter from leaves to active tissue
F(9,15)	consumption of leaves
F(9,17) <sub>1</sub>	frass production
F(9,17) <sub>2</sub>	litterfall to quickly decomposing O <sub>1</sub> layer: Z <sub>4</sub>
F(9,99)	respiration of leaves: Z <sub>1</sub>
F(10,9)	translocation of organic matter from active tissue to leaves: Z <sub>5</sub>
F(10,11)	translocation of organic matter from active tissue to woody tissue: Z <sub>1</sub>
F(10,12)	translocation of organic matter from active tissue to buds: Z <sub>1</sub>
F(10,99)	respiration of active tissue: Z <sub>1</sub>
F(11,14)	transfer to standing dead
F(11,17)	limbfall to quickly decomposing O <sub>1</sub> layer
F(11,18)	limbfall to slowly decomposing O <sub>1</sub> layer
F(11,20)	transfer of organic matter from woody tissues to soil organic matter
F(12,99)	respiration of buds: Z <sub>1</sub>
Ground cover	
F(99,13)	photosynthesis of leaves: Z <sub>2</sub>
F(13,16)	transfer to fine roots
F(13,17)	litterfall to quickly decomposing O <sub>1</sub> layer
F(13,99)	respiration of leaves: Z <sub>1</sub>
Other components	
F(14,18)	transfer of biomass from standing dead to slowly decomposing O <sub>1</sub> layer
F(14,99)	decomposer respiration from standing dead: Z <sub>1</sub>
F(15,99)	respiration of canopy consumers: Z <sub>1</sub>
F(16,20)	transfer of fine roots to soil organic matter: Z <sub>1</sub> , Z <sub>3</sub>
F(16,99)	respiration of fine roots: Z <sub>1</sub>
F(17,19)	transfer of biomass from quickly decomposing O <sub>1</sub> layer to O <sub>2</sub> layer: Z <sub>1</sub> , Z <sub>3</sub>

Table 2.3. (Continued)

Flow <sup>a</sup>	Description <sup>b</sup>
F(17,99)	decomposer respiration from quickly decomposing O <sub>1</sub> layer: Z <sub>1</sub> , Z <sub>3</sub>
F(18,19)	transfer of biomass from slowly decomposing O <sub>1</sub> layer to O <sub>2</sub> layer: Z <sub>1</sub> , Z <sub>3</sub>
F(18,99)	decomposer respiration from slowly decomposing O <sub>1</sub> layer: Z <sub>1</sub> , Z <sub>3</sub>
F(19,20)	transfer of biomass from O <sub>2</sub> layer to soil organic matter: Z <sub>1</sub> , Z <sub>3</sub>
F(19,99)	decomposer respiration from O <sub>2</sub> layer
F(20,21)	transfer of biomass from soil organic matter (0-10 cm) to soil organic matter (10-60 cm)
F(20,99)	decomposer respiration from soil organic matter (0-10 cm)
F(21,99)	decomposer respiration from soil organic matter (10-60 cm)

<sup>a</sup>Units are kg biomass m<sup>-2</sup> year<sup>-1</sup>.

<sup>b</sup>Includes a list of those driving variables (if any) that influence the flow.

The photosynthesis of ground cover is  $G_H$ ;

$$G_H = \frac{-3.914B_{13}}{A_{13}K_{13}} \ln \left( \frac{1 + A_{13}E_1E_2 \exp(-1000K_{13}X_{13})}{1 + A_{13}E_1E_2} \right), \quad (2.3)$$

where  $E_1$  is given by Equation 2.2 and light attenuation by the understory is given by

$$E_2 = \exp(-1000K_gX_g), \quad (2.4)$$

where  $K_g$  is the light extinction coefficient for the understory.

The parameters  $A_{13}$ ,  $B_{13}$ , and  $K_{13}$  are the groundcover equivalents of those in Equation 2.1.

Net photosynthesis, whether for tulip poplar, other overstory, understory, or groundcover, is gross photosynthesis less a constant proportional loss to foliar respiration. This proportionality constant is specific to the vegetation (compartment) involved.

Plant respiration not associated with gross photosynthesis (e.g., F(1,99), Table 2.3) and canopy consumer respiration are described by

$$F(i,99) = R_i F_T X_i, \quad (2.5)$$

where  $R_i$  is a rate parameter specific to compartment  $i$ , and  $X_i$  is the biomass of compartment  $i$ . The temperature dependence of respiration,  $F_T$ , is calculated in the following way:

$$F_T = 0.35(40 - T) \exp(-(40 - T)/8), \quad (2.6)$$

where  $T$  is temperature ( $Z_1$ , Table 2.2). This temperature function also describes the influence of temperature on the translocation fluxes of Table 2.3.

### 2.1.1.5 Release Of Carbon Through Decomposition

As litter material decomposes,  $\text{CO}_2$  is released through decomposer respiration. The Sollins, Reichle, and Olson (1973) model does not model decomposers directly, but it does allow for decomposer respiration. The loss of organic matter from the quickly decomposing  $O_1$  layer through respiration of decomposers,  $F(17,99)$ , is described by

$$F(17,99) = R_{17}F_{TM}X_{17} , \quad (2.7)$$

where  $F_{TM}$  is  $0.2Z_1Z_3$  (Table 2.2);  $R_{17}$  is a rate constant, and  $X_{17}$  is the organic matter of the quickly decomposing  $O_1$  layer. Decomposer respiratory losses from the slowly decomposing  $O_1$  layer and the  $O_2$  layer are of the same functional form. Decomposer loss from the upper soil organic matter layer is not dependent on temperature and moisture, and is given by a constant proportion of the mass of soil organic matter in the 0-10 cm layer.

### 2.1.2 Seasonal Photosynthesis And Respiration

Values of temperature and soil moisture for the Walker Branch watershed site at Oak Ridge were sampled by Sollins, Reichle, and Olson (1973) approximately twice a month during 1971. These values were used to interpolate approximate daily values of the functions for photosynthesis,  $G_A$ ,  $G_B$ ,  $G_C$ , and  $G_H$ , as well as respiration. Graphs of total ecosystem photosynthesis and respiration, as generated by the simulation, are shown in Figure 2.6. The net flux of carbon dioxide (respiration minus photosynthesis) between the

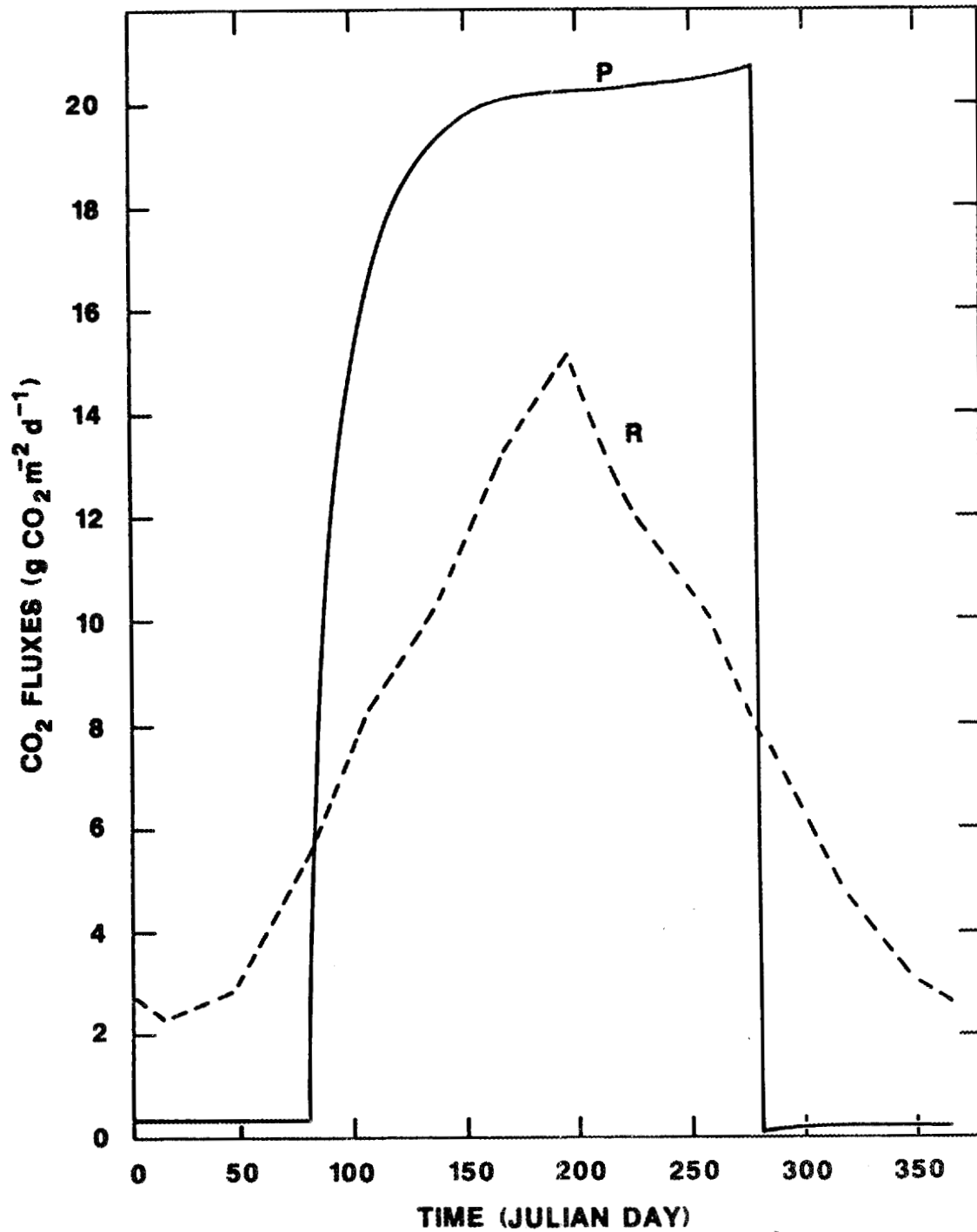


Figure 2.6. Seasonal total ecosystem photosynthesis (P) and respiration (R) for a temperate broadleaf deciduous forest stand. Flux units are g CO<sub>2</sub> m<sup>-2</sup> d<sup>-1</sup>.

atmosphere and the forest stand is plotted in Figure 2.7. Again, a positive value indicates the stand is acting as a source of atmospheric CO<sub>2</sub>; a negative value indicates the stand is acting as a sink. Biomass fluxes generated by the model were converted to CO<sub>2</sub> fluxes using a conversion factor of 1 g dry weight = 1.65 g CO<sub>2</sub> (Lieth 1978).

## 2.2 TEMPERATE BROADLEAF EVERGREEN FOREST MODEL

Seasonal carbon dynamics in a temperate broadleaf evergreen forest are modeled with an adaptation of the Attiwill et al. (1973) model of an Australian eucalyptus forest. The site, located within Mount Disappointment State Forest, Victoria (37°25'S, 145°10'E), is dominated by messmate eucalyptus (Eucalyptus obliqua (L'Herit.)) (see Attiwill (1973) and Burgess (1981) for further site description). Developed during the International Woodlands Workshop (Reichle, O'Neill, and Olson 1973), the seasonal compartment model simulates biomass dynamics using differential equations and a time step of five days (0.014 year).

### 2.2.1 Structure Of The Model

#### 2.2.1.1 Compartments

The model involves nine compartments representing biomass reservoirs in the trees, understory, and litter. The state variables corresponding to the compartments depicted in Figure 2.8 are defined in Table 2.4.

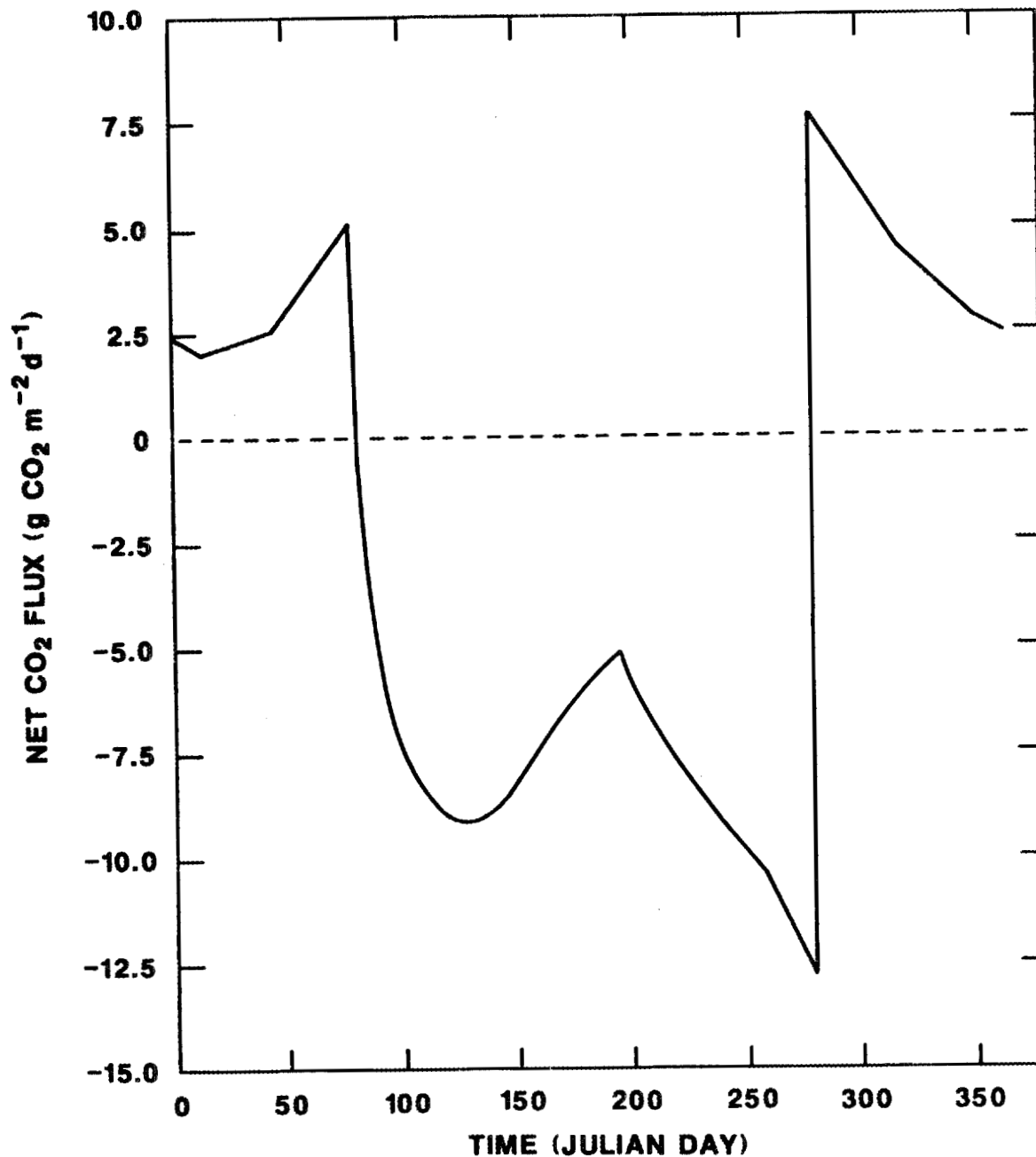


Figure 2.7. Seasonal net CO<sub>2</sub> exchange between the atmosphere and a temperate broadleaf deciduous forest stand. Net flux is respiration minus photosynthesis. Flux units are g CO<sub>2</sub> m<sup>-2</sup> d<sup>-1</sup>.

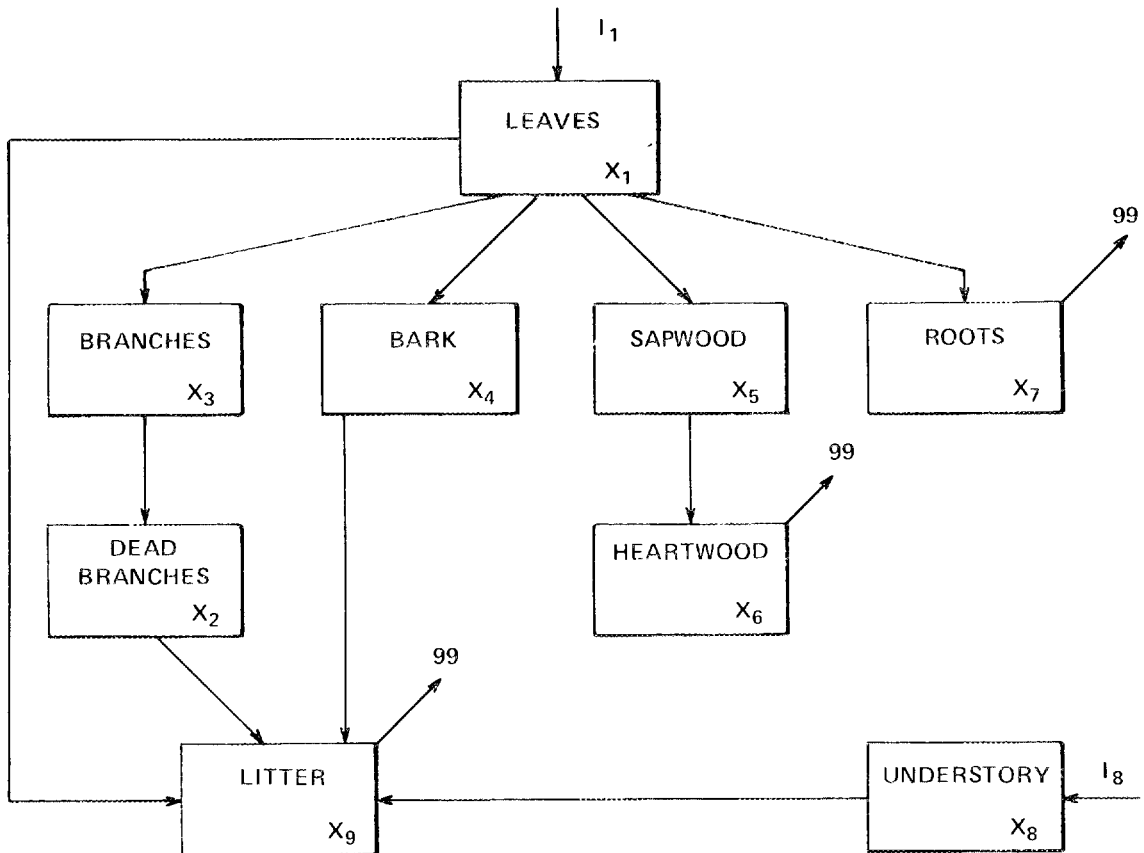


Figure 2.8. Compartmental structure of the temperate broadleaf evergreen forest model. The arrows indicate the flux of biomass from compartment  $i$  to compartment  $j$ . The number 99 indicates a compartment external to the system.

Table 2.4. State variables of the temperate broadleaf evergreen forest model.

State Variable*	Description
$x_1$	tree leaves
$x_2$	dead branchwood
$x_3$	branches
$x_4$	stem bark
$x_5$	sapwood
$x_6$	heartwood
$x_7$	roots
$x_8$	understory
$x_9$	litter

\*Units are g biomass  $m^{-2}$ .

### 2.2.1.2 Driving Variables

Seasonality in the model is influenced by variations in three exogenous abiotic variables (Table 2.5). Rainfall and global radiation are combined to form a composite variable, evapotranspiration (EV, mm month<sup>-1</sup>), using the equation:

$$EV = \begin{cases} aZ_2 & \text{if } Z_1 \geq 18.0 \text{ mm week}^{-1} \\ bZ_1 & \text{if } Z_1 < 18.0 \text{ mm week}^{-1} \end{cases}, \quad (2.8)$$

where  $b$  is the slope of evapotranspiration as a function of rainfall, and  $a$  is a time-varying coefficient relating evapotranspiration and global radiation (see Attiwill et al. 1973).

Rainfall at time  $t$  ( $0 \leq t \leq 1$ ),  $Z_1(t)$ , is given by:

$$Z_1(t) = 19.25 + 7.25 \cos(2\pi(t - 0.0633)) . \quad (2.9)$$

Global radiation,  $Z_2(t)$ , is calculated with the equation:

$$Z_2(t) = \begin{cases} A_0 + B_0t & \text{if } t \leq 0.5 \\ A_1 + B_1t & \text{if } 0.5 \leq t < 0.8333 \\ A_0 & \text{if } 0.8333 < t \leq 1.0 \end{cases}, \quad (2.10)$$

where

$$A_0 = 1400 \text{ kcal m}^{-2} \text{ d}^{-1},$$

$$A_1 = 13,150 \text{ kcal m}^{-2} \text{ d}^{-1},$$

$$B_0 = 9400,$$

$$B_1 = 14,100.$$

These equations were fitted to observations for the Australian forest (Attiwill et al. 1973).

Table 2.5. Driving variables of the temperate broadleaf evergreen forest model.

Driving Variable	Description
$Z_1$	rainfall ( $\text{mm week}^{-1}$ )
$Z_2$	global radiation ( $\text{kcal m}^{-2} \text{d}^{-1}$ )
$Z_3$	temperature ( $^{\circ}\text{C}$ )

### 2.2.1.3 Flows Or Rate Processes

The flows in the model are represented by the arrows in Figure 2.8. In general, these fluxes are constant coefficient donor control processes. Exceptions include leaf litterfall which is a function of temperature (see Attiwill et al. 1973) and the photosynthesis forcings which are functions of evapotranspiration (see Attiwill et al. 1973 and Section 2.2.1.2). The model described by Attiwill et al. (1973) includes a photosynthesis allocation function to partition the production input into growth of various tree compartments. This function determines the average fractional allocation to a particular tree compartment as a function of expected and actual biomass in that compartment (actual biomass was in turn a function of tree bole biomass) and a proportional input flux for that compartment determined from a precedent linear annual version of the model. We have not included this allocation function in our implementation. A flux representing activation of storage reserves in the roots is also excluded from the implementation. These omissions serve to linearize the model and simplify the solutions.

The flows included in the model are defined in Table 2.6. The notation  $F(i,j)$  indicates the flux of biomass from compartment  $i$  to compartment  $j$ . The number 99 represents a carbon or biomass sink, generally the atmosphere. Table 2.6 also indicates which, if any, of the driving variables (Table 2.5) influence a given flow.

Table 2.6. The flows of organic matter simulated by the temperate broadleaf evergreen forest model.

Flow <sup>a</sup>	Description <sup>b</sup>
I1	tree leaves production forcing: $Z_1, Z_2$
I8	understory production forcing: $Z_1, Z_2$
F(1,3)	leaf to branch translocation
F(1,4)	leaf to stem bark translocation
F(1,5)	leaf to sapwood translocation
F(1,7)	leaf to root translocation
F(1,9)	leaf litterfall: $Z_3$
F(2,9)	fall of dead branches
F(3,2)	branch mortality
F(4,9)	fall of dead stem bark
F(5,6)	transfer from sapwood to heartwood
F(6,99)	heartwood respiration
F(7,99)	root respiration
F(8,9)	fall of understory litter
F(9,99)	litter decomposition

<sup>a</sup>Units are  $g \text{ biomass } m^{-2} \text{ year}^{-1}$ .

<sup>b</sup>Includes a list of those driving variables (if any) that influence the flow.

#### 2.2.1.4 Photosynthesis And Respiration

Photosynthesis is simulated by forcings of monthly net production,  $I_1$  and  $I_8$ , applied to tree leaves,  $X_1$ , and understory vegetation,  $X_8$ , respectively. The forcings are calculated by:

$$I_1(t) = 12.0G(t) , \quad (2.11)$$

and

$$I_8(t) = pI_1(t) , \quad (2.12)$$

where  $p$  is a constant ratio of understory production to tree leaf production, and  $G(t)$  is the growth function,  $G$ , evaluated at time  $t$ . The value of  $G(t)$  is given by:

$$G(t) = g(t)/1.0 + ag(t) , \quad (2.13)$$

where  $g(t)$  is potential growth at time  $t$  as a function of evapotranspiration,  $EV$  (see Section 2.2.1.2), at time  $t$ , and  $a$  is a growth altering coefficient. This parameter reflects the reduction in growth associated with reduced leaf area (see Attiwill et al. 1973).

The potential growth rate,  $g = f(EV)$ , is given by:

$$g(t) = \begin{cases} bEV(t) & \text{if } 0.0 \leq EV \leq 60 \text{ mm} \\ 60b & \text{if } EV > 60 \text{ mm} , \end{cases} \quad (2.14)$$

where  $b$  is an empirically derived parameter relating growth and evapotranspiration ( $EV$ ). For the eucalyptus forest of Attiwill et al. (1973),  $b = 6.25$ .

Respiration,  $F(i,0)$ , from living compartments is calculated by:

$$F(i,0) = r_i X_i \quad i = 6, 7, \quad (2.15)$$

where  $r_i$  is a constant rate coefficient, and  $X_i$  is the biomass of compartment  $i$ . Live respiration losses are assumed to apply only to heartwood,  $X_6$ , and roots,  $X_7$ .

#### 2.2.1.5 Release Of Carbon Through Decomposition

As litter,  $X_9$ , decomposes,  $CO_2$  is evolved according to the relationship:

$$F(9,0) = r_9 X_9, \quad (2.16)$$

where  $r_9$  is a linear constant rate coefficient, and  $F(9,0)$  is the flux of  $CO_2$  as biomass is decomposed.

#### 2.2.2 Seasonal Photosynthesis And Respiration

Rainfall,  $Z_1$ , and global radiation,  $Z_2$ , values were generated using the empirically derived equations of Attiwill et al. (1973) (also see Section 2.2.1.2). These input data were used to drive the simulation model and generate total ecosystem photosynthesis and respiration values for an "average" year. A plot of daily fluxes sampled at 5-day intervals is shown in Figure 2.9. Biomass fluxes generated by the model were converted to  $CO_2$  fluxes using the conversion factor of 1 g dry matter = 1.65 g  $CO_2$  (Lieth 1978). Seasonal net  $CO_2$  exchange between the forest stand and the atmosphere is plotted in Figure 2.10.

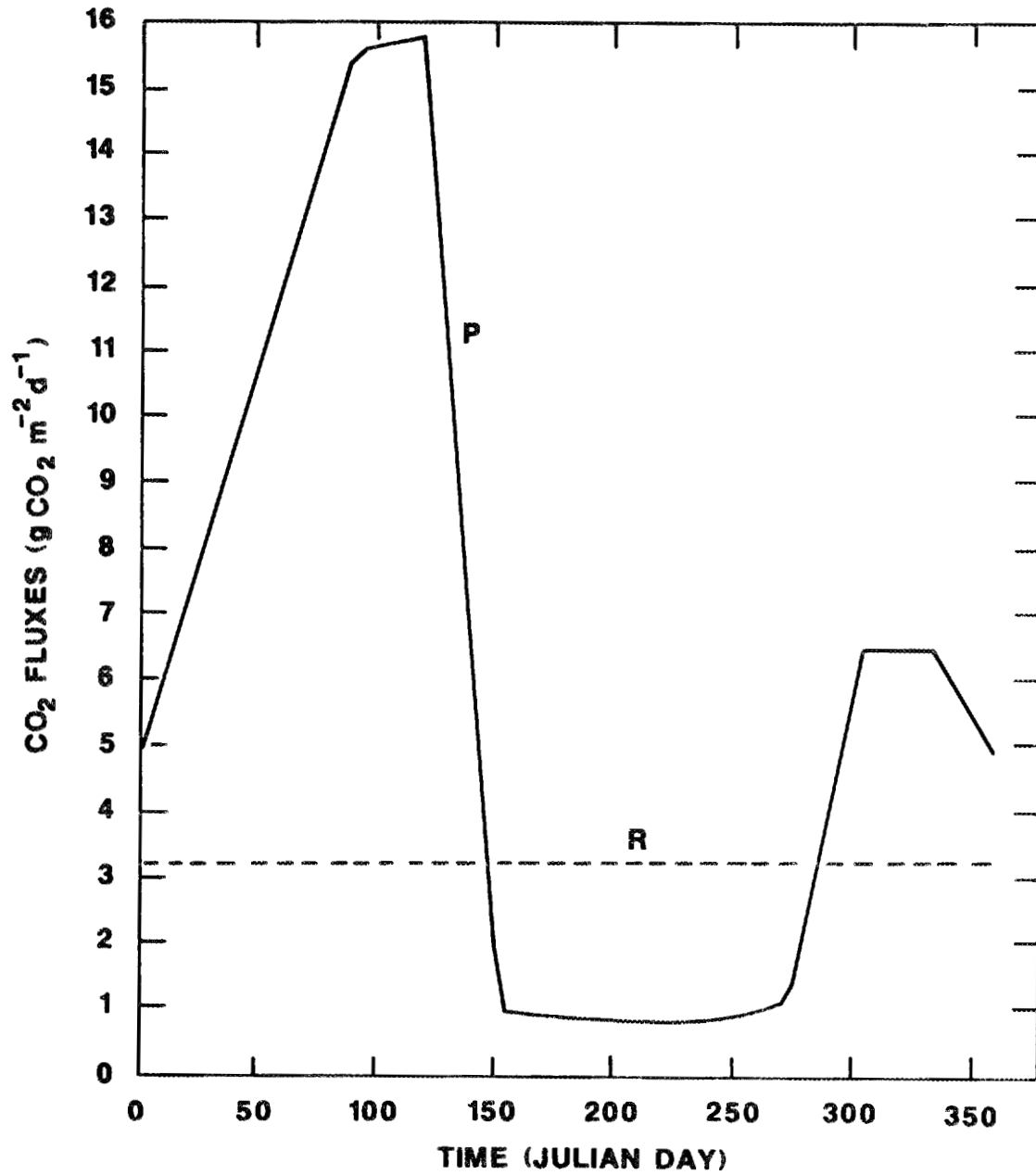


Figure 2.9. Seasonal total ecosystem photosynthesis (P) and respiration (R) for a temperate broadleaf evergreen forest stand. Flux units are g CO<sub>2</sub> m<sup>-2</sup> d<sup>-1</sup>.

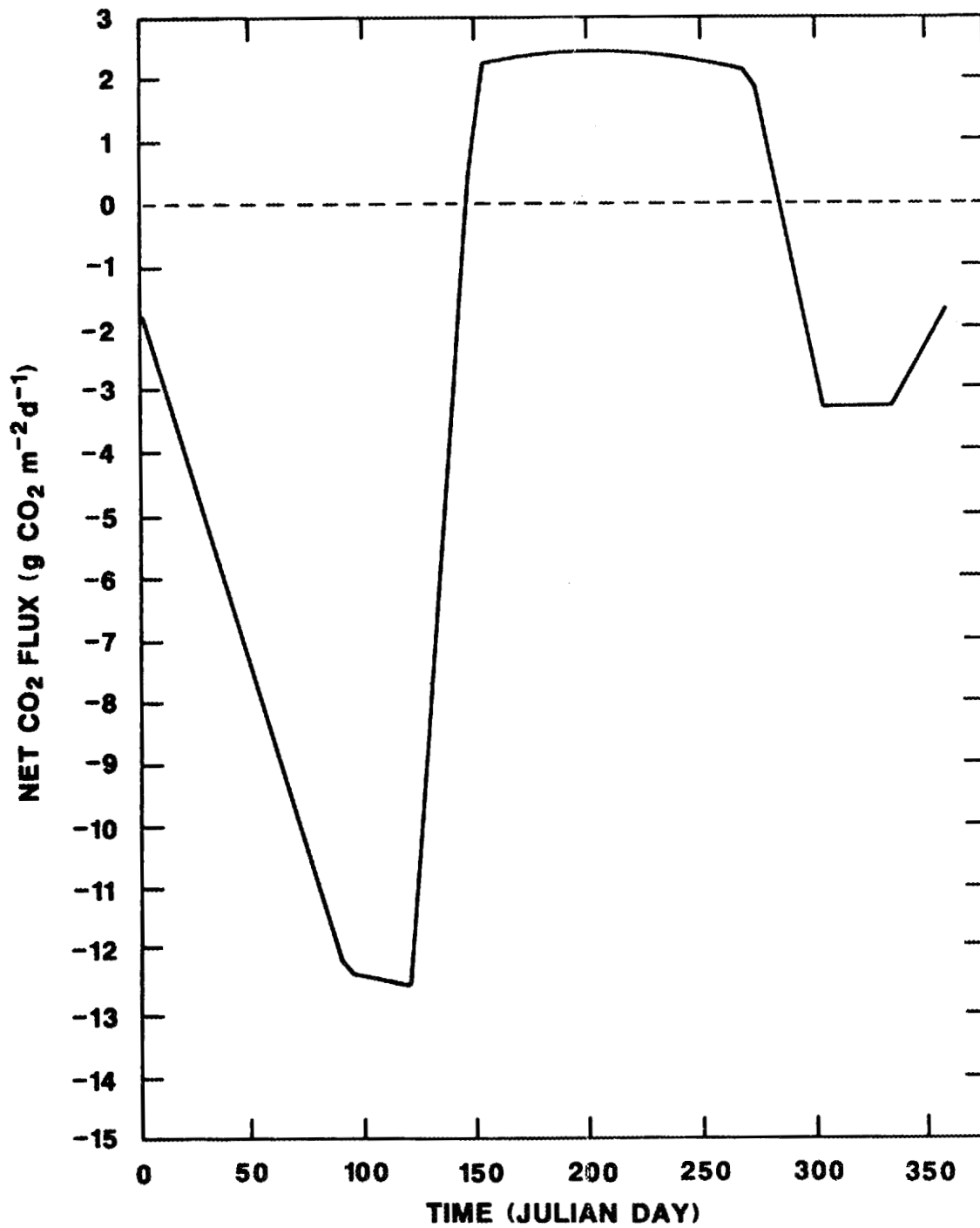


Figure 2.10. Seasonal net CO<sub>2</sub> exchange between the atmosphere and a temperate broadleaf evergreen forest stand. Net flux is respiration minus photosynthesis. Flux units are g CO<sub>2</sub> m<sup>-2</sup> d<sup>-1</sup>.

## 2.3 COOL CONIFEROUS FOREST MODEL

To model the seasonal carbon dynamics of cool coniferous forests, we use the model, CONIFER, developed for the Coniferous Forest Biome of the United States (Coniferous Forest Biome Modeling Group 1977). CONIFER is based on an old-growth (450 year old) Douglas-fir (*Pseudotsuga menziesii* [Mirb] Franco) stand in the H. J. Andrews Experimental Forest, Oregon (44°15'N, 122°20'W). Grier and Logan (1977) provide a description of this site. The model is described by difference equations with a time step of one day for water dynamics and one week for carbon dynamics.

### 2.3.1 Structure Of The Model

#### 2.3.1.1 Compartments

The compartmental structure of the model is shown in Figures 2.11 and 2.12. Note that the carbon and water dynamics constitute separate parts of the model. The arrows indicate intercompartmental transfers of carbon and water, respectively, in the two parts of the model. The complex pattern of effects other than material transfers that occur between compartments is not shown. These are discussed in the CONIFER documentation (Coniferous Forest Biome Modeling Group 1977).

The state variables corresponding to the compartments of Figures 2.11 and 2.12 and their units are listed in Table 2.7. The heat energy compartments of the model are defined (Table 2.7) although they are not depicted in either Figure.

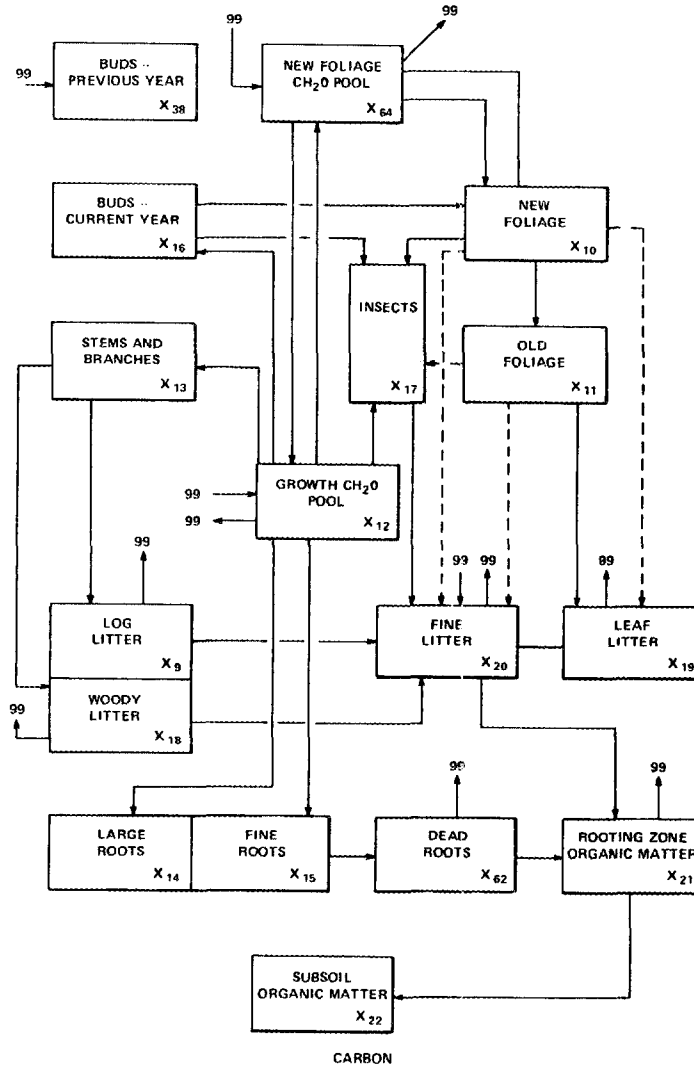


Figure 2.11. Compartmental structure of the cool coniferous forest model - carbon submodel. Arrows indicate the directional flow of carbon. Dashed lines indicate fluxes that occur only during perturbation. The 99's represent carbon sources and sinks. Adapted from Coniferous Forest Biome Modelling Group (1977).

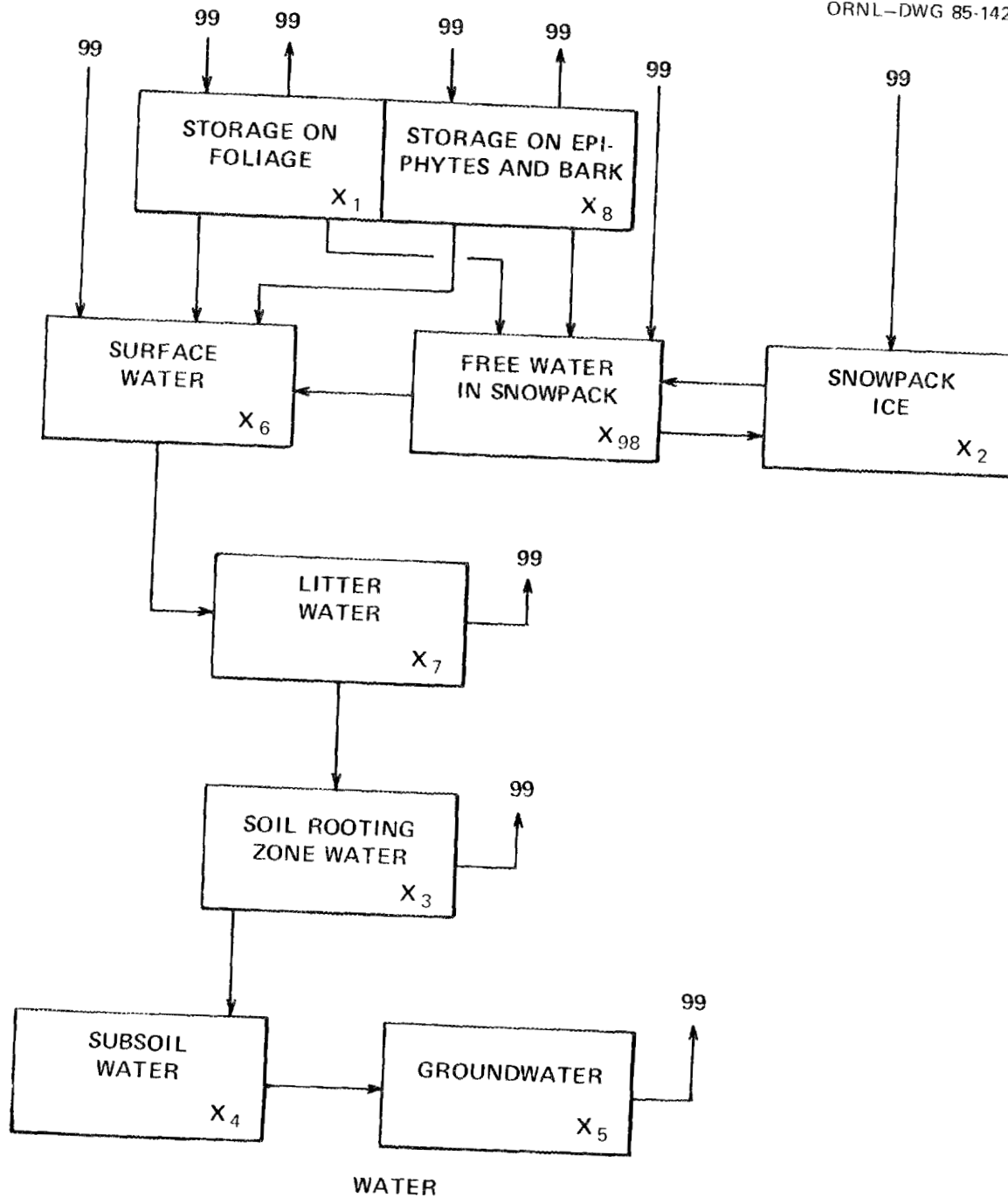


Figure 2.12. Compartmental structure of the cool coniferous forest model - water submodel. Arrows indicate the directional flow of water. The 99's represent water sources and sinks. Adapted from Coniferous Forest Biome Modelling Group (1977).

Table 2.7. State variables of the cool coniferous forest model.

State Variable	Description	Unit
X <sub>1</sub>	water storage on foliage	(m <sup>3</sup> ha <sup>-1</sup> )
X <sub>2</sub>	snowpack ice	(m <sup>3</sup> ha <sup>-1</sup> )
X <sub>3</sub>	soil rooting zone water	(m <sup>3</sup> ha <sup>-1</sup> )
X <sub>4</sub>	subsoil water	(m <sup>3</sup> ha <sup>-1</sup> )
X <sub>5</sub>	groundwater storage	(m <sup>3</sup> ha <sup>-1</sup> )
X <sub>6</sub>	water storage on litter surface	(m <sup>3</sup> ha <sup>-1</sup> )
X <sub>7</sub>	litter water	(m <sup>3</sup> ha <sup>-1</sup> )
X <sub>8</sub>	water storage on epiphytes and bark surfaces	(m <sup>3</sup> ha <sup>-1</sup> )
X <sub>9</sub>	log litter carbon	(t ha <sup>-1</sup> )
X <sub>10</sub>	new foliage carbon	(t ha <sup>-1</sup> )
X <sub>11</sub>	old foliage carbon	(t ha <sup>-1</sup> )
X <sub>12</sub>	carbon in growth CH <sub>2</sub> O pool	(t ha <sup>-1</sup> )
X <sub>13</sub>	stem plus branch carbon	(t ha <sup>-1</sup> )
X <sub>14</sub>	large root carbon	(t ha <sup>-1</sup> )
X <sub>15</sub>	fine root carbon	(t ha <sup>-1</sup> )
X <sub>16</sub>	bud carbon (current year)	(t ha <sup>-1</sup> )
X <sub>17</sub>	canopy insect carbon	(t ha <sup>-1</sup> )
X <sub>18</sub>	woody litter carbon	(t ha <sup>-1</sup> )
X <sub>19</sub>	foliage litter carbon	(t ha <sup>-1</sup> )
X <sub>20</sub>	fine litter carbon	(t ha <sup>-1</sup> )
X <sub>21</sub>	carbon in soil rooting zone organic matter	(t ha <sup>-1</sup> )
X <sub>22</sub>	carbon in subsoil organic matter	(t ha <sup>-1</sup> )
X <sub>25</sub>	litter temperature	(°C)
X <sub>26</sub>	soil rooting zone temperature	(°C)
X <sub>37</sub>	snowpack heat deficit	(°C)
X <sub>38</sub>	bud carbon (previous year)	(t ha <sup>-1</sup> )
X <sub>62</sub>	dead root carbon	(t ha <sup>-1</sup> )
X <sub>64</sub>	carbon in new foliage CH <sub>2</sub> O pool	(t ha <sup>-1</sup> )
X <sub>98</sub>	free water in snowpack	(m <sup>3</sup> ha <sup>-1</sup> )

### 2.3.1.2 Driving Variables

Model seasonality is determined by eight exogenous driving variables and five phenology parameters (Table 2.8). Daily empirical values for the exogenous variables ( $Z_1$  to  $Z_8$ ) and the constant values for the phenology parameters ( $Z_9$  to  $Z_{14}$ ) are read into the simulation program as input data.

### 2.3.1.3 Flows Or Rate Processes

The model includes flow functions which correspond to the arrows in Figures 2.11 and 2.12. They control the amounts of carbon or water being transferred from one compartment to another. The specific formulations for these often complicated functions can be found in the CONIFER documentation (Coniferous Forest Biome Modeling Group 1977). Here, we simply define the flows and indicate which of the driving variables (Table 2.8) influence a particular flow (Table 2.9). The notation  $F(i,j)$  indicates the flow of material from compartment  $i$  to compartment  $j$ . The number '99' refers to a compartment external to the system. All flows into the system are labelled  $F(99,j)$ , and all flows out of the system are labelled  $F(i,99)$ .

### 2.3.1.4 Photosynthesis And Respiration

Net daily photosynthesis is the sum of net new foliage photosynthesis (NNFP) and net old foliage photosynthesis (NOFP) where

$$NNFP = \frac{-B_{32}B_{33}G_{110}X_{10}G_{102}}{B_{35}G_{49}G_{61}} \ln \left( \frac{B_{34} + G_{109} \exp(-B_{35}G_{61})}{B_{34} + G_{109}} \right), \quad (2.17)$$

Table 2.8. Driving variables and phenology parameters of the cool coniferous forest model.

Driving Variable	Description
Z <sub>1</sub>	total precipitation (m <sup>3</sup> ha <sup>-1</sup> d <sup>-1</sup> )
Z <sub>2</sub>	average shortwave radiation (Langley min <sup>-1</sup> )
Z <sub>3</sub>	average 24-h air temperature (°C)
Z <sub>4</sub>	day length
Z <sub>5</sub>	average 24-h dew point temperature (°C)
Z <sub>6</sub>	average daytime temperature (°C)
Z <sub>7</sub>	average nighttime temperature (°C)
Z <sub>8</sub>	average wind speed (m s <sup>-1</sup> )
Z <sub>9</sub>	week on which bud break occurs
Z <sub>10</sub>	week on which growing season begins
Z <sub>11</sub>	week on which growing season ends
Z <sub>12</sub>	week on which new foliage becomes old foliage
Z <sub>13</sub>	week on which leaf fall is minimal

Table 2.9. The flows of carbon and water simulated by the cool coniferous forest model.

Flow <sup>a</sup>	Description <sup>b</sup>
F(99,1)	rain input to foliar surfaces: Z <sub>1</sub>
F(99,2)	precipitation as snow: Z <sub>1</sub>
F(99,6)	rainfall passing directly to litter surface water: Z <sub>1</sub>
F(99,8)	rain input to bark and epiphyte surfaces: Z <sub>1</sub>
F(99,12)	input from old foliage photosynthesis to growth CH <sub>2</sub> O pool: Z <sub>2</sub> , Z <sub>3</sub> , Z <sub>4</sub> , Z <sub>6</sub>
F(99,20)	input to fine litter from microparticulate matter and carbon dissolved in precipitation
F(99,25)	change in litter temperature: Z <sub>1</sub> , Z <sub>3</sub>
F(99,26)	change in soil temperature: Z <sub>1</sub>
F(99,37)	net increase in heat deficit of snowpack: Z <sub>1</sub> , Z <sub>2</sub> , Z <sub>3</sub> , Z <sub>4</sub>
F(99,38)	change in last year's buds: Z <sub>9</sub>
F(99,64)	input to new foliage CH <sub>2</sub> O pool due to net new foliage photosynthesis: Z <sub>2</sub> , Z <sub>3</sub> , Z <sub>4</sub> , Z <sub>6</sub>
F(99,98)	rainfall passing directly into free water in snowpack: Z <sub>1</sub>
F(1,99)	evaporation from foliage: Z <sub>1</sub> , Z <sub>2</sub> , Z <sub>3</sub> , Z <sub>4</sub> , Z <sub>5</sub> , Z <sub>8</sub>
F(1,6)	drip from foliage to litter surface: Z <sub>1</sub> , Z <sub>2</sub> , Z <sub>3</sub> , Z <sub>4</sub> , Z <sub>5</sub> , Z <sub>8</sub>
F(1,98)	drip from foliage to free water in snowpack: Z <sub>1</sub> , Z <sub>2</sub> , Z <sub>3</sub> , Z <sub>4</sub> , Z <sub>5</sub> , Z <sub>8</sub>
F(2,98)	transfer from ice to free water in snowpack: Z <sub>1</sub> , Z <sub>2</sub> , Z <sub>3</sub> , Z <sub>4</sub>
F(3,99)	transpiration rate: Z <sub>1</sub> , Z <sub>2</sub> , Z <sub>3</sub> , Z <sub>4</sub> , Z <sub>5</sub> , Z <sub>8</sub>
F(3,4)	water transfer from soil rooting zone to subsoil: Z <sub>3</sub> , Z <sub>5</sub>
F(4,5)	water transfer from subsoil to groundwater: Z <sub>3</sub> , Z <sub>5</sub>
F(5,99)	outflow from groundwater
F(6,7)	water flow from surface to litter layer
F(7,99)	evaporation from litter: Z <sub>1</sub> , Z <sub>3</sub> , Z <sub>5</sub>
F(7,3)	water transfer from litter to soil rooting zone: Z <sub>3</sub> , Z <sub>5</sub>
F(8,99)	evaporation from epiphyte and bark surfaces: Z <sub>1</sub> , Z <sub>2</sub> , Z <sub>3</sub> , Z <sub>4</sub> , Z <sub>6</sub>
F(8,6)	water drip from epiphyte and bark surfaces to storage on litter surface: Z <sub>1</sub> , Z <sub>2</sub> , Z <sub>3</sub> , Z <sub>4</sub> , Z <sub>5</sub> , Z <sub>8</sub>
F(8,98)	drip from epiphytes and bark surfaces to free water in snowpack: Z <sub>1</sub> , Z <sub>2</sub> , Z <sub>3</sub> , Z <sub>4</sub> , Z <sub>5</sub> , Z <sub>8</sub>
F(9,99)	carbon loss from logs due to decomposer respiration
F(9,20)	carbon loss from logs due to fragmentation
F(10,11)	carbon transfer with aging of new foliage: Z <sub>3</sub> , Z <sub>12</sub>

Table 2.9. (Continued)

Flow <sup>a</sup>	Description <sup>b</sup>
F(10,17)	new foliage consumption by insects: $Z_3$
F(10,19)	carbon transfer from new foliage to leaf litter due to acute defoliation
F(10,20)	carbon transfer from new foliage to fine litter due to acute defoliation
F(10,64)	carbon transfer from new foliage to new foliage $CH_2O$ pool
F(11,17)	old foliage consumption by insects: $Z_3$
F(11,19)	transfer from old foliage to leaf litter due to leaf fall and acute defoliation: $Z_{13}$
F(11,20)	transfer from old foliage to fine litter due to acute defoliation
F(12,99)	total respiration loss from growth $CH_2O$ pool: $Z_3, Z_4, Z_7$
F(12,13)	carbon transfer to stems plus branches from growth $CH_2O$ pool: $Z_3$
F(12,14)	carbon transfer to large roots from growth $CH_2O$ pool
F(12,15)	carbon transfer to fine roots from growth $CH_2O$ pool
F(12,16)	bud growth from growth $CH_2O$ pool: $Z_3, Z_{10}, Z_{11}$
F(12,17)	consumption of growth $CH_2O$ pool by insects: $Z_3$
F(12,64)	transfer of carbon from growth $CH_2O$ pool to new foliage $CH_2O$ pool to meet foliar respiration and growth demands
F(13,9)	carbon transfer from stems plus branches to log litter
F(13,18)	carbon transfer from stems plus branches to woody litter
F(14,62)	large root mortality
F(15,62)	fine root mortality
F(16,10)	carbon transfer from buds to new foliage: $Z_9$
F(16,17)	bud consumption by insects: $Z_3$
F(17,20)	insect frass input to fine litter
F(18,99)	carbon loss from woody litter due to decomposer respiration
F(18,20)	carbon loss from woody litter due to fragmentation
F(19,99)	carbon loss from foliage litter due to decomposer respiration
F(19,20)	carbon loss from foliage litter due to fragmentation
F(20,99)	carbon loss from fine litter due to decomposer respiration
F(20,21)	incorporation of fine litter into rooting zone organic matter
F(21,99)	carbon loss from rooting zone due to decomposer respiration
F(21,22)	carbon transfer from rooting zone to subsoil organic matter due to leaching
F(62,99)	carbon loss from dead roots due to decomposer respiration

Table 2.9. (Continued)

Flow <sup>a</sup>	Description <sup>b</sup>
F(62,21)	carbon loss from dead roots due to fragmentation
F(64,99)	new foliage nighttime respiration from CH <sub>2</sub> O pool: Z <sub>4</sub> , Z <sub>7</sub>
F(64,10)	transfer of carbon to new foliage from new foliage CH <sub>2</sub> O pool
F(64,12)	transfer of surplus carbon from new foliage CH <sub>2</sub> O pool to growth CH <sub>2</sub> O pool
F(98,2)	transfer from free water in snowpack to ice
F(98,6)	water draining from snowpack to litter surface

<sup>a</sup>Units of the flows are m<sup>3</sup> ha<sup>-1</sup> d<sup>-1</sup> for water and t ha<sup>-1</sup> week<sup>-1</sup> for carbon.

<sup>b</sup>Includes a list of those driving variables (if any) that influence the flow.

and where

$X_{10}$  = new foliage carbon,

$G_{49}$  = average weekly stomatal resistance of new foliage,

$G_{61}$  = total foliage carbon,

$G_{102}$  = effect of temperature on photosynthesis ,

$G_{109}$  = average weekly photosynthetically active solar radiation,

$G_{110}$  = average weekly day length,

$B_{32}$  = ratio of net new foliage photosynthesis based on carbon budget to amount extrapolated from cuvette experiments,

$B_{33}$  = rate constant for new foliage photosynthesis,

$B_{34}$  = light intensity at which new foliage photosynthesis is 1/2 maximum rate,

$B_{35}$  = coefficient of attenuation of shortwave radiation by foliage.

A similar expression holds for NOFP. Photosynthates derived from NNFP accumulate in the new foliage  $\text{CH}_2\text{O}$  pool; NOFP photosynthates accumulate in the growth  $\text{CH}_2\text{O}$  pool.

Net daily respiration (NDR) from the stand is given by

$$\begin{aligned} \text{NDR} = & G_{25} + G_{30} + G_{103} + G_{111} + G_{113} + G_{125} + G_{131} \\ & + G_{133} + G_{138} + G_{139} + G_{140} , \end{aligned} \quad (2.18)$$

where

$G_{25}$  = new foliage nighttime respiration,

$G_{30}$  = old foliage nighttime respiration,

$G_{103}$  = carbon loss from foliage litter due to decomposer respiration,

$G_{111}$  = carbon loss from woody litter due to decomposer respiration,

$G_{113}$  = carbon loss from log litter due to decomposer respiration,

$G_{125}$  = carbon loss from fine litter due to decomposer respiration,

$G_{131}$  = carbon loss from dead roots due to decomposer respiration,

$G_{133}$  = carbon loss from rooting zone due to decomposer respiration,

$G_{138}$  = stem and branch respiration,

$G_{139}$  = large root respiration,

$G_{140}$  = fine root respiration.

An example of the functional form of the individual respiration term is shown here for  $G_{25}$ , new foliage nighttime respiration,:

$$G_{25} = B_{26}(1 - G_{110})X_{10}\exp(B_{145}G_{108}) , \quad (2.19)$$

where

$X_{10}$  = new foliage carbon,

$G_{108}$  = average weekly nighttime air temperature,

$G_{110}$  = average weekly day length,

$B_{26}$  = foliar respiration rate constant,

$B_{145}$  = coefficient for temperature effect on foliar respiration.

### 2.3.1.5 Release Of Carbon Through Decomposition

The release of carbon in  $\text{CO}_2$  during microbial decomposition of litter contributes to total net daily respiration from the stand (see Equation 2.19). An example of the functional form describing these decomposer respiratory fluxes is shown for  $G_{103}$ , carbon loss from foliage litter due to decomposer respiration,

$$G_{103} = (1 - B_{149})G_{81} , \quad (2.20)$$

where  $B_{149}$  is the fraction of carbon loss from foliage litter due to fragmentation, and  $G_{81}$  is the foliage litter decomposition rate. The term  $G_{81}$  is given by

$$G_{81} = B_{62}G_{69}X_{19} , \quad (2.21)$$

where  $X_{19}$  is foliage litter carbon;  $G_{69}$  is the effect of moisture and temperature on litter processes, and  $B_{62}$  is a rate constant. The effect of temperature and water on decomposition is described in the CONIFER documentation (Coniferous Forest Biome Modeling Group 1977).

### 2.3.2 Seasonal Photosynthesis And Respiration

Seasonal input data for the forcing functions ( $Z_i$ 's) were obtained from the CONIFER report, and used to generate (from the model) total ecosystem photosynthesis and respiration values during the year. A plot of weekly values for a particular year is shown in Figure 2.13. The carbon fluxes generated by the model were converted to  $\text{CO}_2$  fluxes using the conversion factor of 1 g carbon = 3.66 g  $\text{CO}_2$

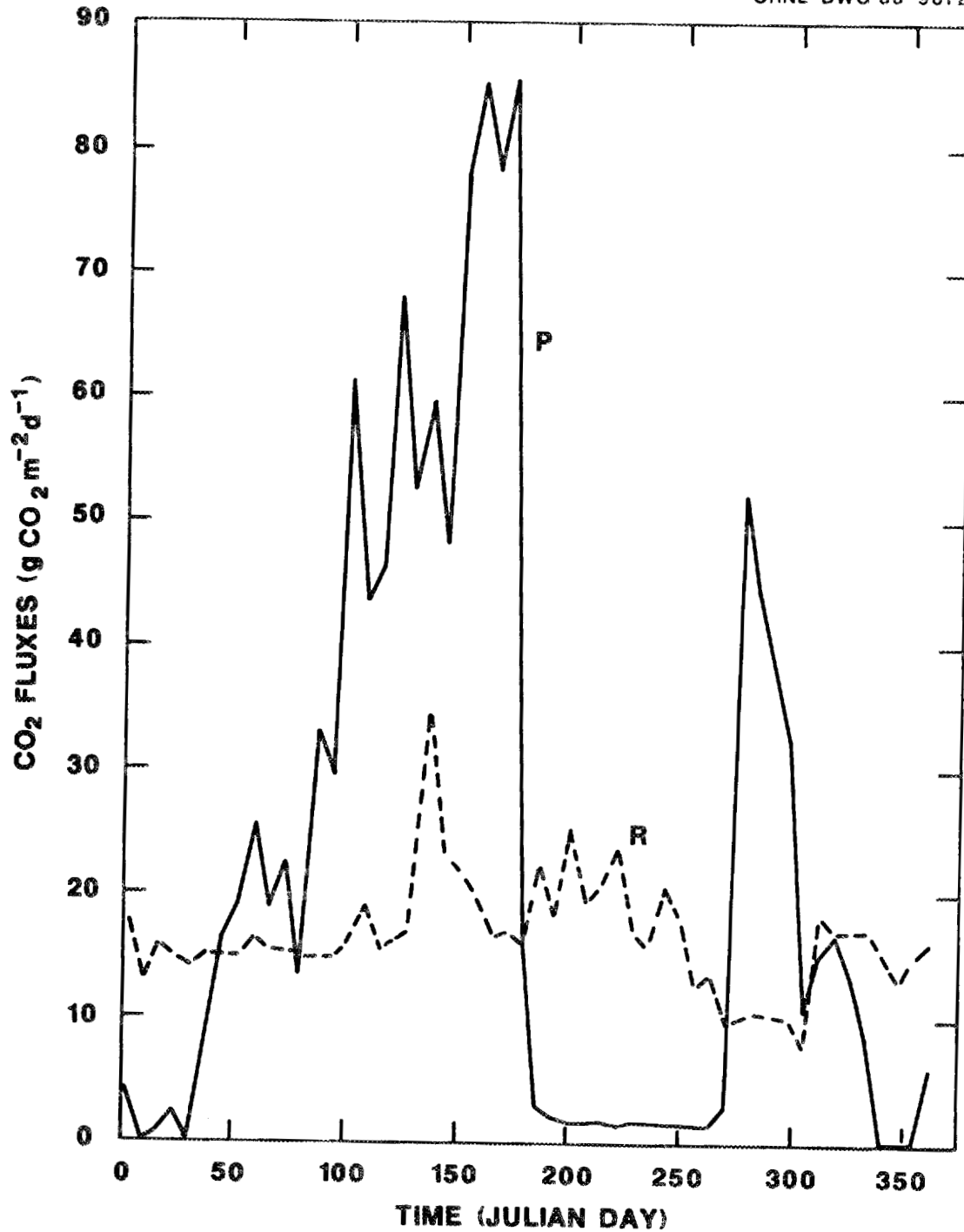


Figure 2.13. Seasonal total ecosystem photosynthesis (P) and respiration (R) for a cool coniferous forest stand. Flux units are g CO<sub>2</sub> m<sup>-2</sup> d<sup>-1</sup>.

(Brown and Trlica 1974). Figure 2.14 is a plot of net carbon dioxide exchange between the stand and the atmosphere.

## 2.4 WARM CONIFEROUS FOREST MODEL

A model of carbon, phosphorus, and water cycles in a pine flatwoods ecosystem in north central Florida (29°50'N, 82°10'W) was developed by Golkin (1981) and Golkin and Ewel (1984). The system is a 40-year-old slash pine (*Pinus elliotii* Engelm.) plantation and is typical of commercial forests that occupy 46% of the Florida landscape. The model should be representative of seasonal carbon dynamics for warm conifer forests such as the pine forests of the southeastern United States. The model is described by differential equations, and the solutions involve a time step of approximately one week (0.02 years).

### 2.4.1 Structure Of The Model

#### 2.4.1.1 Compartments

The model includes three submodels for carbon (Figure 2.15), phosphorus (Figure 2.16), and water (Figure 2.17). The three models are intricately coupled, as the availability of phosphorus controls the photosynthetic rates and phosphorus transport is regulated by soil water. The state variables corresponding to these compartments and their units are given in Table 2.10.

#### 2.4.1.2 Driving Variables

There are three exogenous driving variables in the model, seven forcing functions which control the timing of carbon and phosphorus

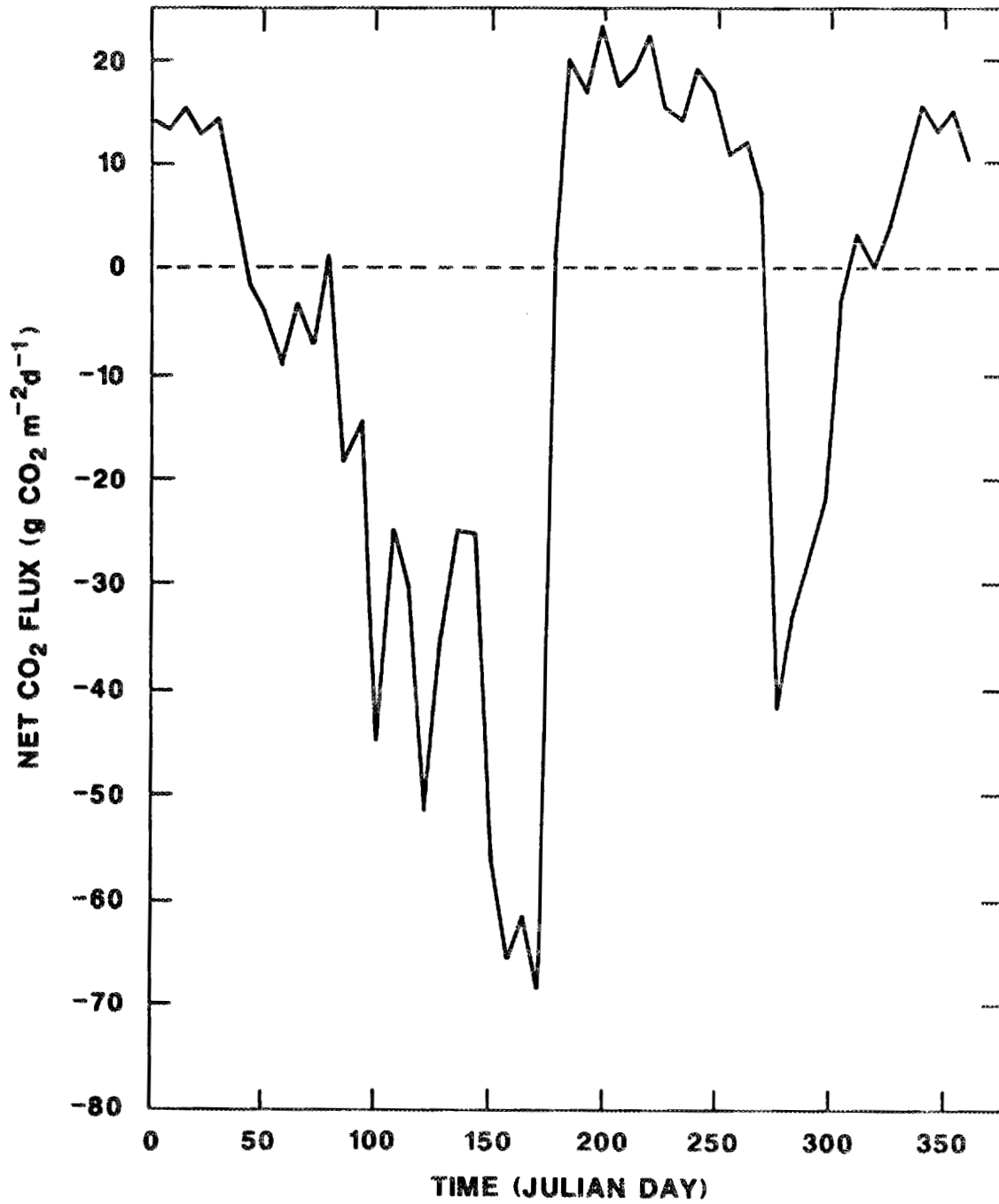


Figure 2.14. Seasonal net CO<sub>2</sub> exchange between the atmosphere and a cool coniferous forest stand. Net flux is respiration minus photosynthesis. Flux units are g CO<sub>2</sub> m<sup>-2</sup> d<sup>-1</sup>.

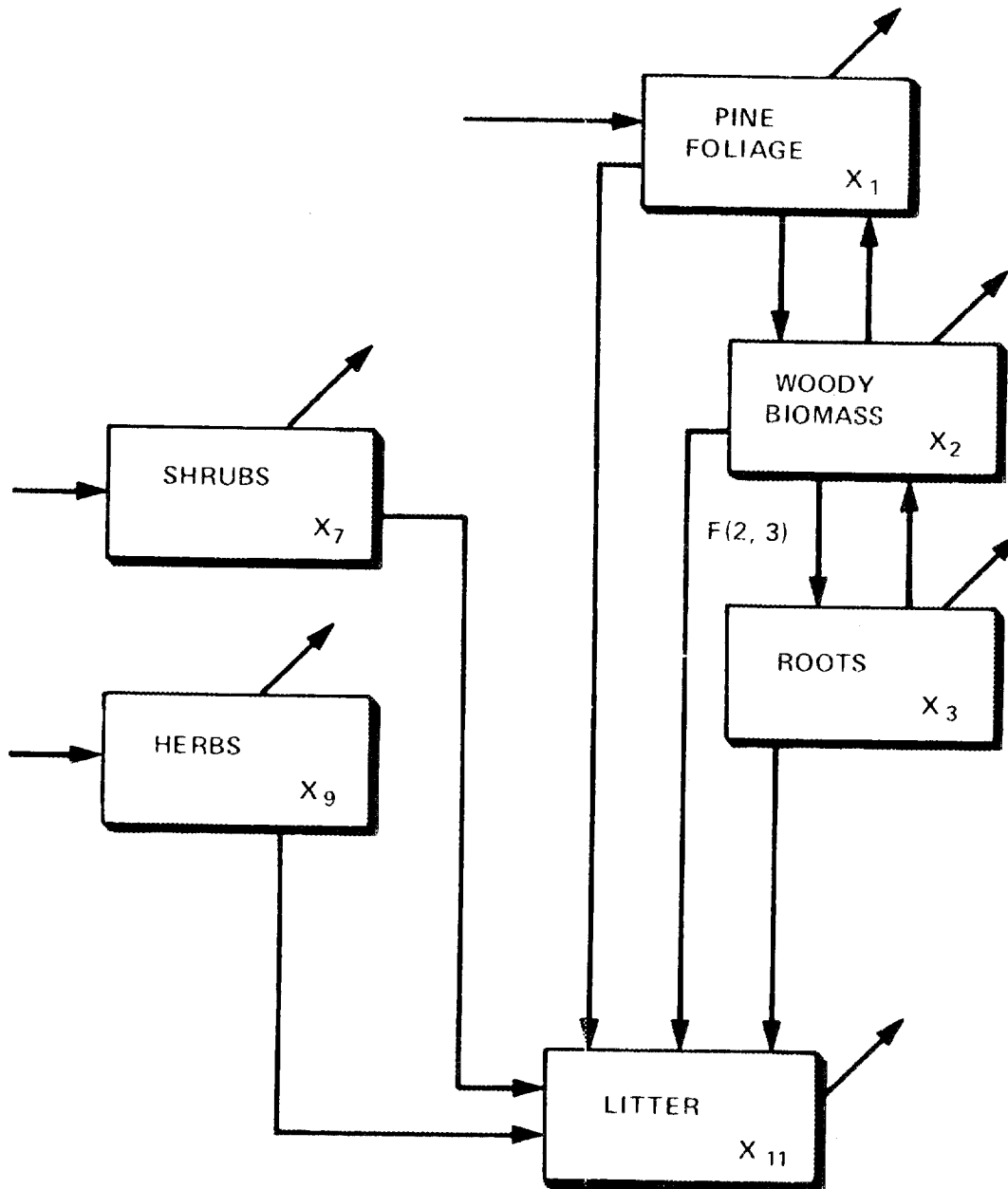


Figure 2.15. Compartmental structure of the warm coniferous forest model - carbon flow submodel.

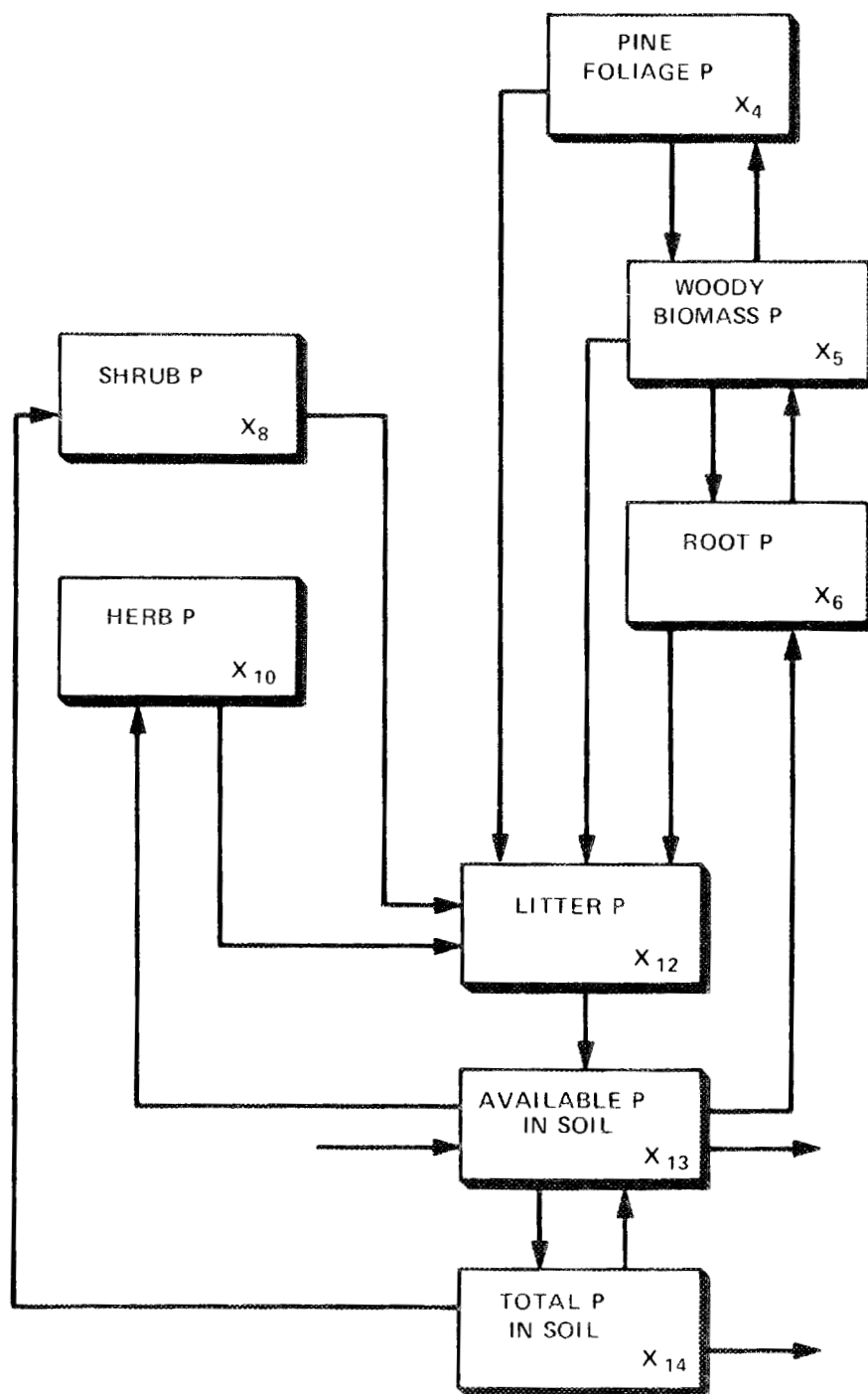


Figure 2.16. Compartmental structure of the warm coniferous forest model - phosphorus cycling submodel.

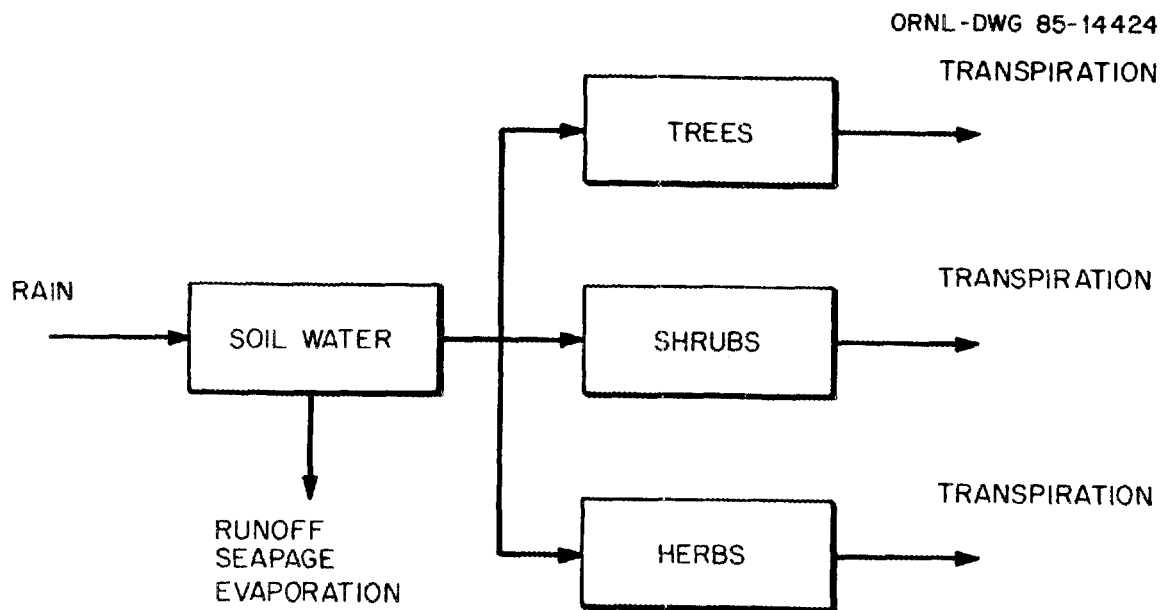


Figure 2.17. Compartmental structure of the warm coniferous forest model - water flow submodel.

Table 2.10. State variables of the warm coniferous forest model.

State Variable	Description	Units
$X_1$	pine foliage	(g C m <sup>-2</sup> )
$X_2$	pine stems and branches	(g C m <sup>-2</sup> )
$X_3$	pine roots	(g C m <sup>-2</sup> )
$X_4$	phosphorus in pine foliage	(g P m <sup>-2</sup> )
$X_5$	phosphorus in pine stems and branches	(g P m <sup>-2</sup> )
$X_6$	phosphorus in pine roots	(g P m <sup>-2</sup> )
$X_7$	shrubs	(g C m <sup>-2</sup> )
$X_8$	phosphorus in shrubs	(g P m <sup>-2</sup> )
$X_9$	herbs	(g C m <sup>-2</sup> )
$X_{10}$	phosphorus in herbs	(g P m <sup>-2</sup> )
$X_{11}$	carbon in litter and upper soil horizons	(g C m <sup>-2</sup> )
$X_{12}$	phosphorus in litter and associated with soil organic matter	(g P m <sup>-2</sup> )
$X_{13}$	available (acid-extractable) phosphorus in the soil	(g P m <sup>-2</sup> )
$X_{14}$	total phosphorus in the soil	(g P m <sup>-2</sup> )
$X_{15}$	soil water	(kg H <sub>2</sub> O m <sup>-2</sup> )
$X_{16}$	water in deep aquifer	(kg H <sub>2</sub> O m <sup>-2</sup> )
$X_{17}$	phosphorus in fertilizer	(g P m <sup>-2</sup> )

flows within a tree, and two phenology forcings (Table 2.11). Together they determine the seasonal CO<sub>2</sub> dynamics of the pine stand.

Daily values of temperature and insolation are interpreted from a seasonal series of empirical values. Daily values of rainfall are read into the simulation program as input data.

#### 2.4.1.3 Flows Or Rate Processes

The flows of carbon, phosphorus, and water correspond, respectively, to the arrows in Figures 2.15, 2.16, and 2.17. The assumptions underlying these flows and their functional representation are described in detail by Golkin and Ewel (1984). Here we only define the flows and indicate which, if any, of the driving variables influence a particular flow (Table 2.12). The model representation of photosynthesis and respiration is discussed further in Section 2.4.1.4. In Table 2.12, the number 99 refers to a compartment external to the system. All flows into the system are labelled F(99,j) and all flows out of the system are labelled F(i,99).

#### 2.4.1.4 Photosynthesis And Respiration

There are three photosynthesis functions: (1) pine foliage, A<sub>1</sub>; (2) shrubs, A<sub>2</sub>; and (3) herbs, A<sub>3</sub>. The formulations reflect light attenuation by the canopy, soil moisture limitations, and phosphorus limitations. These all have the same form, so we only show the photosynthesis of one gram of pine foliage, or

$$A_1 = K_4 L_1 W_1 X_4 / (K_9 X_1 + X_4) , \quad (2.22)$$

Table 2.11. Driving variables and seasonal forcings of the warm coniferous forest model.

Driving Variable	Description
Z <sub>1</sub>	temperature (°C)
Z <sub>2</sub>	rainfall (inches)
Z <sub>3</sub>	insolation (Langleys week <sup>-1</sup> )
Z <sub>4</sub>	forcing for nutrient uptake by roots
Z <sub>5</sub>	forcing for translocation of carbon in new photosynthate
Z <sub>6</sub>	forcing for translocation of carbon in root reserves
Z <sub>7</sub>	forcing for translocation of carbon from stems and branches to roots
Z <sub>8</sub>	forcing for translocation of phosphorus from stems and branches to foliage
Z <sub>9</sub>	forcing for translocation of phosphorus from foliage to stems and branches
Z <sub>10</sub>	forcing for translocation of phosphorus from stems and branches to roots
Z <sub>11</sub>	forcing for root sloughing
Z <sub>12</sub>	forcing for litterfall

Table 2.12. The flows of carbon, phosphorus, and water simulated by the warm coniferous forest model.

Flow <sup>a</sup>	Description <sup>b</sup>
F(99,1)	photosynthesis of pine foliage: Z <sub>3</sub>
F(99,7)	photosynthesis of shrubs: Z <sub>3</sub>
F(99,9)	photosynthesis of herbs: Z <sub>3</sub>
F(99,13)	phosphorus in rainfall: Z <sub>2</sub>
F(99,15)	rainfall input to soil water: Z <sub>2</sub>
F(1,2)	translocation of carbon from foliage to stem and branches: Z <sub>5</sub>
F(1,11)	litterfall of pine foliage: Z <sub>12</sub>
F(1,99)	respiration of pine foliage: Z <sub>1</sub> , Z <sub>3</sub>
F(2,3)	translocation of carbon from stem and branches to roots: Z <sub>7</sub>
F(2,11)	stem and branch litterfall
F(2,99)	respiration of stem and branches: Z <sub>1</sub>
F(3,1)	translocation of carbon from roots to foliage: Z <sub>6</sub>
F(3,11)	root sloughing: Z <sub>11</sub>
F(3,99)	root respiration
F(4,5)	phosphorus translocated from foliage to stem and branches: Z <sub>5</sub> , Z <sub>9</sub>
F(4,12)	phosphorus in litterfall: Z <sub>12</sub>
F(5,4)	phosphorus translocation from stem and branches to foliage: Z <sub>8</sub>
F(5,6)	phosphorus translocation from stem and branches to roots: Z <sub>7</sub> , Z <sub>10</sub>
F(5,12)	phosphorus in stem and branch litterfall
F(6,5)	phosphorus translocation from roots to stem and branches: Z <sub>8</sub>
F(6,12)	phosphorus in sloughed roots: Z <sub>11</sub>
F(7,11)	shrub litterfall: Z <sub>12</sub>
F(7,99)	shrub respiration: Z <sub>1</sub> , Z <sub>3</sub>
F(8,12)	phosphorus in shrub litterfall: Z <sub>12</sub>
F(9,11)	herb litterfall
F(9,99)	respiration of herbs
F(10,12)	phosphorus in herb litter
F(11,99) <sub>1</sub>	litter respiration: Z <sub>1</sub>
F(11,99) <sub>2</sub>	carbon lost in runoff
F(12,99) <sub>1</sub>	phosphorus mobilized from litter: Z <sub>1</sub>
F(12,99) <sub>2</sub>	litter phosphorus lost in runoff
F(13,6)	phosphorus uptake by roots
F(13,8)	phosphorus uptake by shrubs
F(13,10)	phosphorus uptake by herbs
F(13,14)	transfer of available to unavailable phosphorus
F(13,99) <sub>1</sub>	available phosphorus lost in lateral flow
F(13,99) <sub>2</sub>	available phosphorus lost in overland flow

Table 2.12. (Continued)

Flow <sup>a</sup>	Description <sup>b</sup>
F(13,99) <sub>3</sub>	available phosphorus lost in deep percolation
F(14,13)	transfer of unavailable to available phosphorus
F(14,99)	unavailable phosphorus lost in overland flow
F(17,13)	transfer of fertilizer to available phosphorus
F(17,99)	fertilizer lost in runoff

<sup>a</sup>Units for carbon and phosphorus flows are  $\text{g m}^{-2} \text{ year}^{-1}$ ; units for water flows are  $\text{kg m}^{-2} \text{ year}^{-1}$ .

<sup>b</sup>Includes a list of those driving variables (if any) that influence the flow.

where  $K_4$  is a pine productivity coefficient;  $K_9$  is a parameter expressing the effect of phosphorus availability on pine photosynthesis;  $W_1$  is the effect of soil water conditions on pine photosynthesis;  $X_1$  is foliage carbon;  $X_4$  is foliage phosphorus, and  $L_1$  is a light availability function. This latter function is given by

$$L_1 = K_1 Z_3(t) / (1 + K_1 X_1) , \quad (2.23)$$

where  $K_1$  is a light extinction coefficient for pine, and  $Z_3(t)$  is solar insolation at time  $t$ . The daily gross photosynthetic uptake of  $CO_2$  by the pine foliage is  $A_1$  (Equation 2.22) times the mass of pine foliage carbon ( $X_1$ ).

Photosynthesis for shrubs and herbs is represented by substituting their respective coefficients and carbon and phosphorus compartments into Equations 2.22 and 2.23.

The respiratory releases of  $CO_2$  from pine foliage, shrubs, and herbs are each modeled as the sum of temperature dependent maintenance respiration, growth respiration (proportional to photosynthesis), and a constant respiratory factor. For example, pine foliage respiration is given by

$$R_1 = (K_5 Z_1(t) + K_6 A_1 - K_7) X_1 , \quad (2.24)$$

where  $A_1$  is gross photosynthesis (see Equation 2.22),  $Z_1(t)$  is temperature at time  $t$ , and  $K_5$ ,  $K_6$ , and  $K_7$  are constants.

Shrub and herb respiration is described by substituting their respective constants, gross photosynthetic rates, and carbon masses into Equation 2.24.

Pine stem and branch respiration is the difference between a linearly dependent temperature term and a constant term, both proportional to carbon mass. Root respiration is proportional to the square of root mass; the rate coefficient is a constant.

#### 2.4.1.5 Release Of Carbon Through Decomposition

Respiratory losses of  $\text{CO}_2$  from litter is represented by the function

$$R_{11} = (K_{26}Z_1(t) + K_{27})X_{11} , \quad (2.25)$$

where  $Z_1(t)$  is temperature;  $K_{26}$  and  $K_{27}$  are constants, and  $X_{11}$  is litter carbon (i.e., carbon in the litter and soil organic matter).

#### 2.4.2 Seasonal Photosynthesis And Respiration

Data on the exogenous driving variables, temperature, rainfall, and insolation, were provided in Golkin (1981). Values of the forcing functions,  $F_1(t)$  through  $F_9(t)$ , as well as the initial values of the state variables, were obtained from the same source. These values were used to simulate  $\text{CO}_2$  fluxes over the course of a year. Daily fluxes at 5-day intervals are plotted in Figure 2.18. Carbon values generated by the model were converted to  $\text{CO}_2$  equivalents using a conversion factor of  $1 \text{ g C} = 3.66 \text{ g CO}_2$ . Seasonal net  $\text{CO}_2$  exchange between the forest stand and the atmosphere is plotted in Figure 2.19.

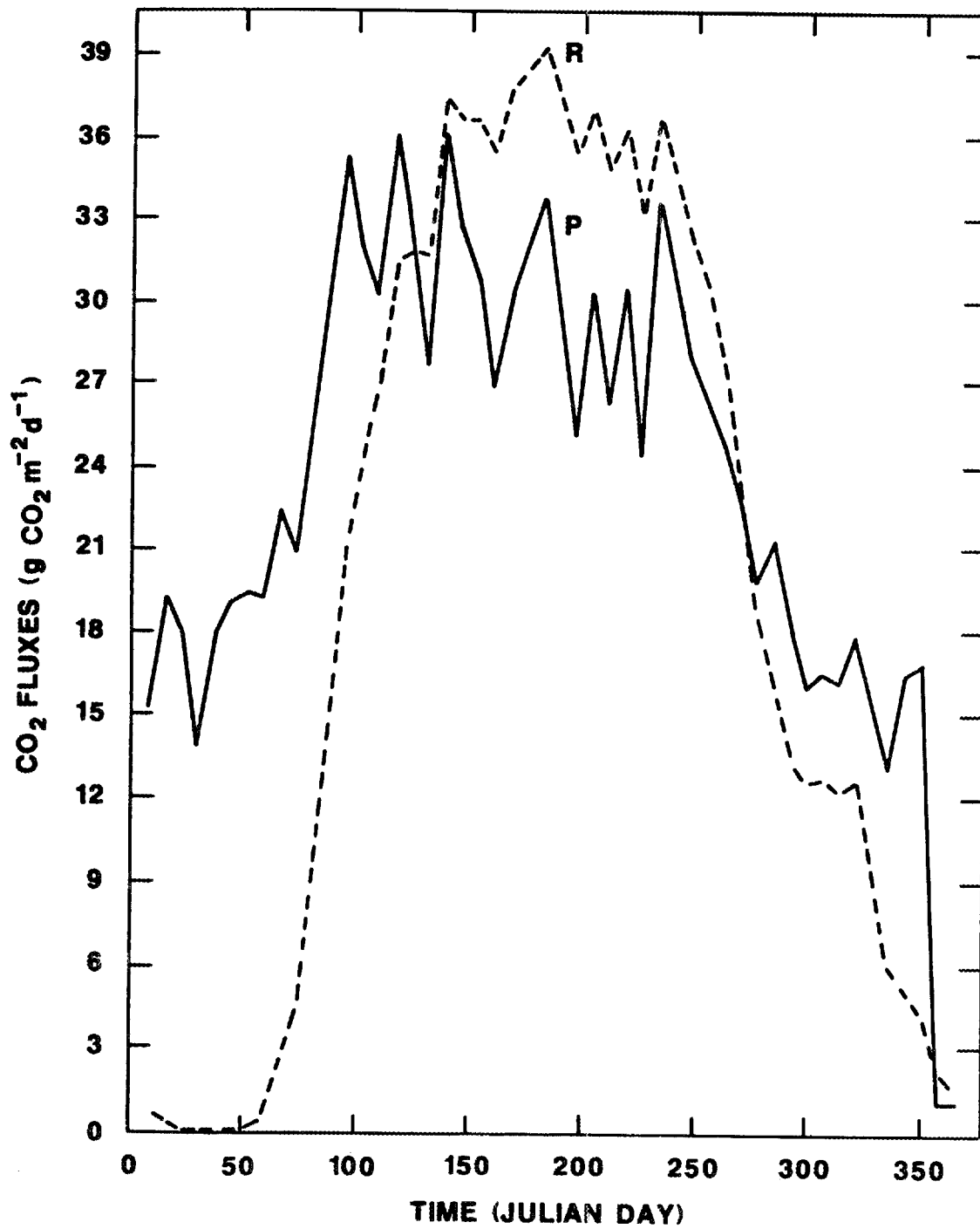


Figure 2.18. Seasonal total ecosystem photosynthesis (P) and respiration (R) for a warm coniferous forest stand. Flux units are g CO<sub>2</sub> m<sup>-2</sup> d<sup>-1</sup>.

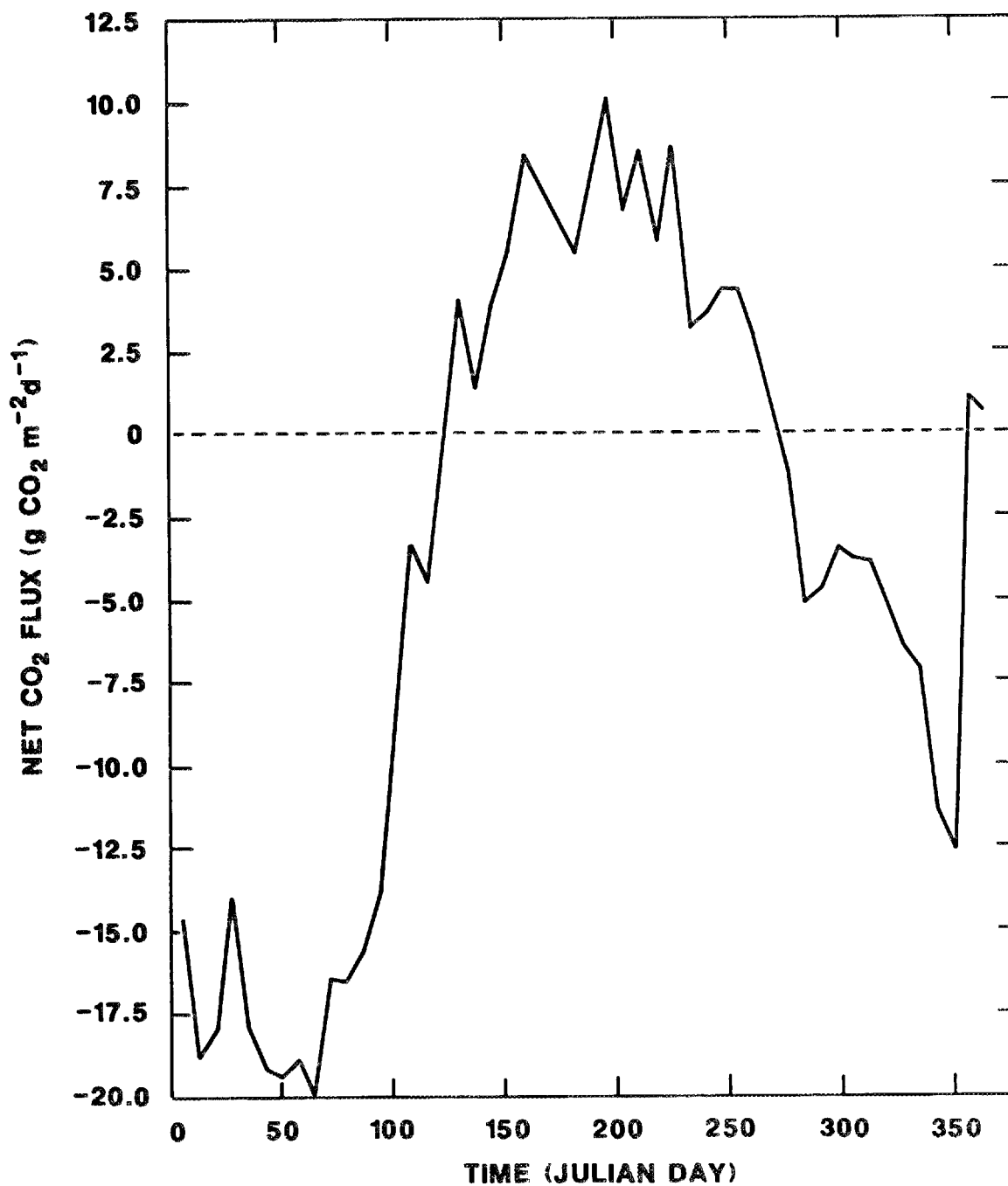


Figure 2.19. Seasonal net CO<sub>2</sub> exchange between the atmosphere and a warm coniferous forest stand. Net flux is respiration minus photosynthesis. Flux units are g CO<sub>2</sub> m<sup>-2</sup> d<sup>-1</sup>.

## 2.5 TROPICAL MOIST EVERGREEN FOREST MODEL

The model of seasonal carbon dynamics in a tropical moist evergreen forest is an adaptation of Bandhu et al.'s (1973) model of a Malaysian rain forest at Pasoh ( $2^{\circ}59'N, 102^{\circ}18'E$ ). The model was originally developed during the International Woodlands Workshop (Reichle, O'Neill, and Olson 1973) using data provided by John Bullock (see Bullock 1973 for a site description). The seasonal model was developed from an annual linear donor-controlled compartment model and retains much of the earlier model's structure and process. The model simulates biomass dynamics using first-order linear differential equations and a time step of five days.

### 2.5.1 Structure Of The Model

#### 2.5.1.1 Compartments

The compartmental structure of the model is depicted in Figure 2.20. Trees and groundcover are distinguished, and the trees are further subdivided by structural units. The state variables corresponding to the compartments are listed in Table 2.13.

#### 2.5.1.2 Driving Variables

The rain forest model includes only one seasonal driving variable. Seasonal phenomena are assumed to be related to monthly rainfall,  $Z(m)$  ( $m = 1, 12$ ), expressed in mm. Monthly rainfall amounts are input data for the simulation program.

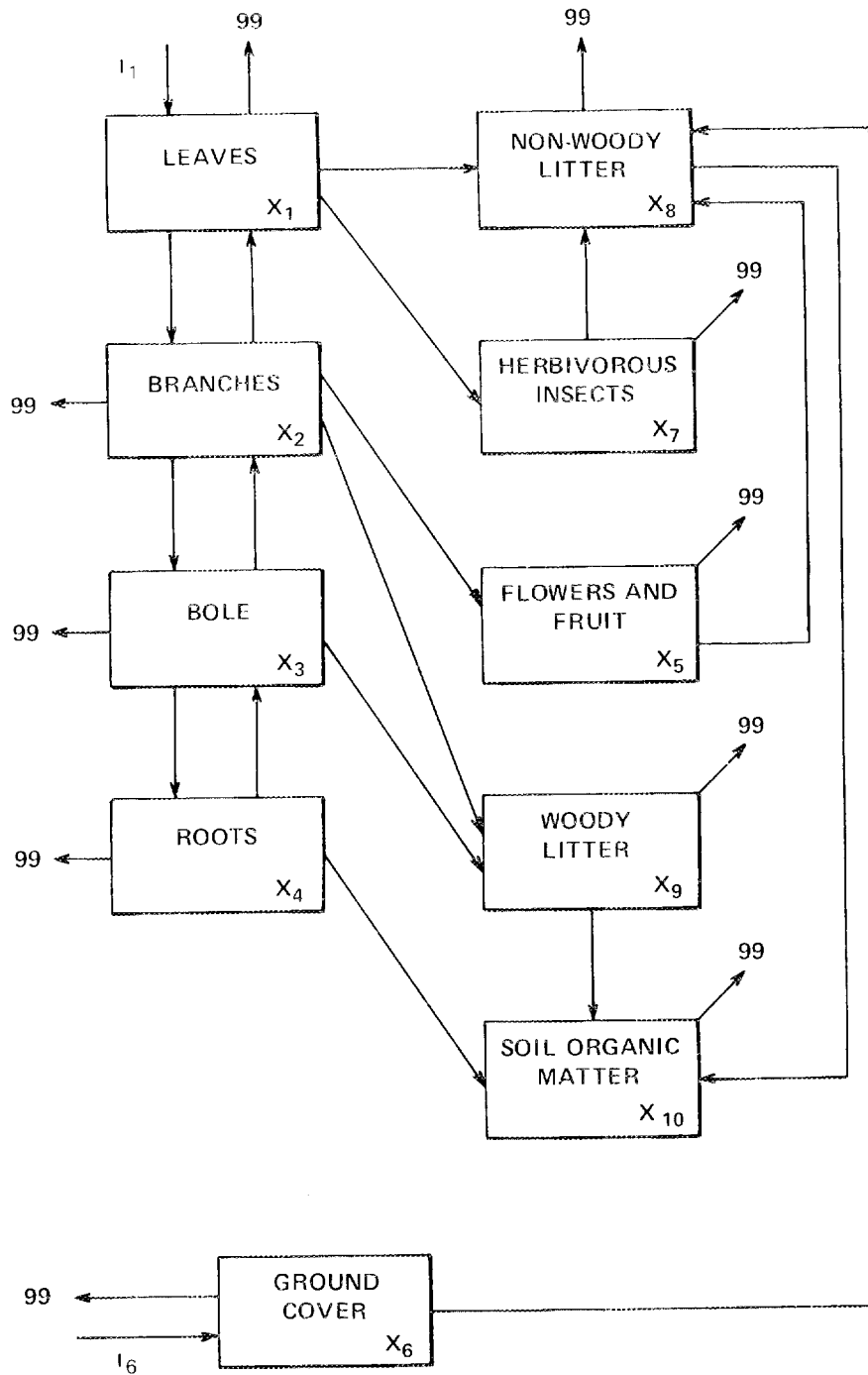


Figure 2.20. Compartmental structure of the tropical moist evergreen forest model. The arrows indicate the flux of biomass from compartment  $i$  to compartment  $j$ . The number 99 indicates a compartment external to the system.

Table 2.13. State variables of the tropical moist evergreen forest model.

State Variable*	Description
X <sub>1</sub>	tree leaves
X <sub>2</sub>	tree branches
X <sub>3</sub>	tree boles
X <sub>4</sub>	tree roots
X <sub>5</sub>	tree flowers and fruits
X <sub>6</sub>	groundcover vegetation
X <sub>7</sub>	herbivorous insects
X <sub>8</sub>	non-woody litter
X <sub>9</sub>	woody litter
X <sub>10</sub>	soil organic matter

\*Units are g biomass m<sup>-2</sup>.

### 2.5.1.3 Flows Or Rate Processes

Most intercompartmental flows are modeled as constant donor control processes. However, the photosynthetic forcings, the  $I_1$ 's, and leaf litterfall,  $F(1,8)$ , are functions of rainfall, the sole exogenous driving variable. Details can be found in Bandhu et al. (1973); here (Table 2.14) we define the flows indicated by the arrows in Figure 2.20. The notation  $F(i,j)$  indicates the flux of biomass from compartment  $i$  to compartment  $j$ . The number 99 represents a carbon sink, generally the atmosphere.

### 2.5.1.4 Photosynthesis And Respiration

The forcing,  $I_1$ , on the leaf compartment,  $X_1$ , is a function relating leaf primary production to rainfall. The forcing can be interpreted as net daytime photosynthesis or carbon assimilation. The equations used to calculate this forcing are:

$$I_1(1) = 12.0(7.51P(1)) , \quad (2.26)$$

and

$$I_1(m) = 12.0(3.755P(m) + 3.755P(m - 1)) , \quad (2.27)$$

for  $m = 2, \dots, 12$ . The term  $P(m)$  is given by:

$$P(m) = (10/12)Z(m) \quad m = 1, 2, \dots, 12 , \quad (2.28)$$

where  $Z(m)$  is monthly rainfall (mm).

The production forcing,  $I_6$ , on the groundcover compartment,  $X_6$ , is presumably of the same form (Bandhu et al. 1973). However,

Table 2.14. The flows of organic matter simulated by the tropical moist evergreen forest model.

Flow <sup>a</sup>	Description <sup>b</sup>
I <sub>1</sub>	tree leaf photosynthesis forcing: Z(m)
I <sub>6</sub>	groundcover photosynthesis forcing: Z(m)
F(1,99)	leaf dark respiration
F(1,2)	leaf to branch translocation
F(1,7)	herbivory
F(1,8)	leaf litterfall: Z(m)
F(2,99)	branch respiration
F(2,1)	branch to leaf translocation
F(2,3)	branch to bole translocation
F(2,5)	branch to flowers and fruit translocation
F(2,9)	fall of dead branches
F(3,99)	bole respiration
F(3,2)	bole to branch translocation
F(3,4)	bole to roots translocation
F(3,9)	fall of dead boles
F(4,99)	root respiration
F(4,10)	transfer of dead root to soil organic matter
F(5,99)	flower and fruit respiration
F(5,8)	fall of flower and fruit litter
F(6,99)	groundcover respiration
F(6,8)	fall of groundcover to litter
F(7,99)	herbivore respiration
F(7,8)	fall of dead herbivores and waste material
F(8,99)	decomposition of non-woody litter (CO <sub>2</sub> evolution)
F(8,10)	decomposition of non-woody litter (transfer to soil organic matter)
F(9,99)	decomposition of woody litter (CO <sub>2</sub> evolution)
F(9,10)	decomposition of woody litter (transfer to soil organic matter)
F(10,99)	decomposition of soil organic matter

<sup>a</sup>Units are g biomass m<sup>-2</sup> year<sup>-1</sup>.

<sup>b</sup>A Z(m) indicates that the flow is influenced by rainfall.

in our implementation  $I_6$  is set equal to zero. The Bandhu et al. (1973) paper is ambiguous about the original value used for  $I_6$ .

Respiration from living compartments  $X_1$  through  $X_7$  is modeled using constant rate coefficients in equations of the form:

$$F(i,0) = r_i X_i \quad i = 1,2,\dots,7, \quad (2.29)$$

where  $F(i,0)$  is the respiratory flux from compartment  $i$ , and  $r_i$  is the constant rate coefficient relating respiration to compartment size. The absence of seasonality in respiration, which might be modeled as function of seasonally varying temperature, is a result of Bandhu et al.'s assumption that all seasonal phenomena were related to precipitation. This implies an additional assumption that temperature is relatively constant in the Pasoh, Malaysia rain forest.

#### 2.5.1.5 Release Of Carbon Through Decomposition

Respiration losses from non-living compartments, representing the release of  $CO_2$  during microbial decomposition of organic matter, are modeled by applying Equation 2.29 to compartments  $X_8$ ,  $X_9$ , and  $X_{10}$ . The constant rate coefficients reflect the implicit assumption that litter/soil moisture and temperature remain relatively constant throughout the year.

#### 2.5.2 Seasonal Photosynthesis And Respiration

Data on seasonal rainfall in a Malaysian rain forest were provided by Bandhu et al. (1973). These data were used to drive the production forcing of the simulation model and generate seasonal

CO<sub>2</sub> assimilation (photosynthesis) and respiration values for the total ecosystem. Daily fluxes sampled at 5-day intervals are plotted in Figure 2.21. Biomass values generated by the model were converted to CO<sub>2</sub> equivalents using a conversion factor of 1 g dry matter = 1.65 g CO<sub>2</sub> (Lieth 1978). Seasonal net CO<sub>2</sub> exchange between the forest stand and the atmosphere is plotted in Figure 2.22.

## 2.6 TROPICAL DRY DECIDUOUS FOREST MODEL

The model of seasonal carbon dynamics in a tropical dry deciduous forest is based on a model of miombo forest at Lubumbashi, Zaire (11°29'S, 27°36'E) presented by Bandhu et al. (1973, see Malaisse 1973 for further site description). Their seasonal model evolved from an annual constant coefficient model during the International Woodlands Workshop (Reichle, O'Neill, and Olson 1973). The model simulates biomass dynamics in a compartmented system using first-order linear differential equations, and the solutions involve a time step of five days (0.014 year). The model is structured very similarly to the tropical rain forest model (see Section 2.5).

### 2.6.1 Structure Of The Model

#### 2.6.1.1 Compartments

Ten compartments representing biomass reservoirs are modeled (Figure 2.23). The state variables corresponding to these compartments are defined in Table 2.15.

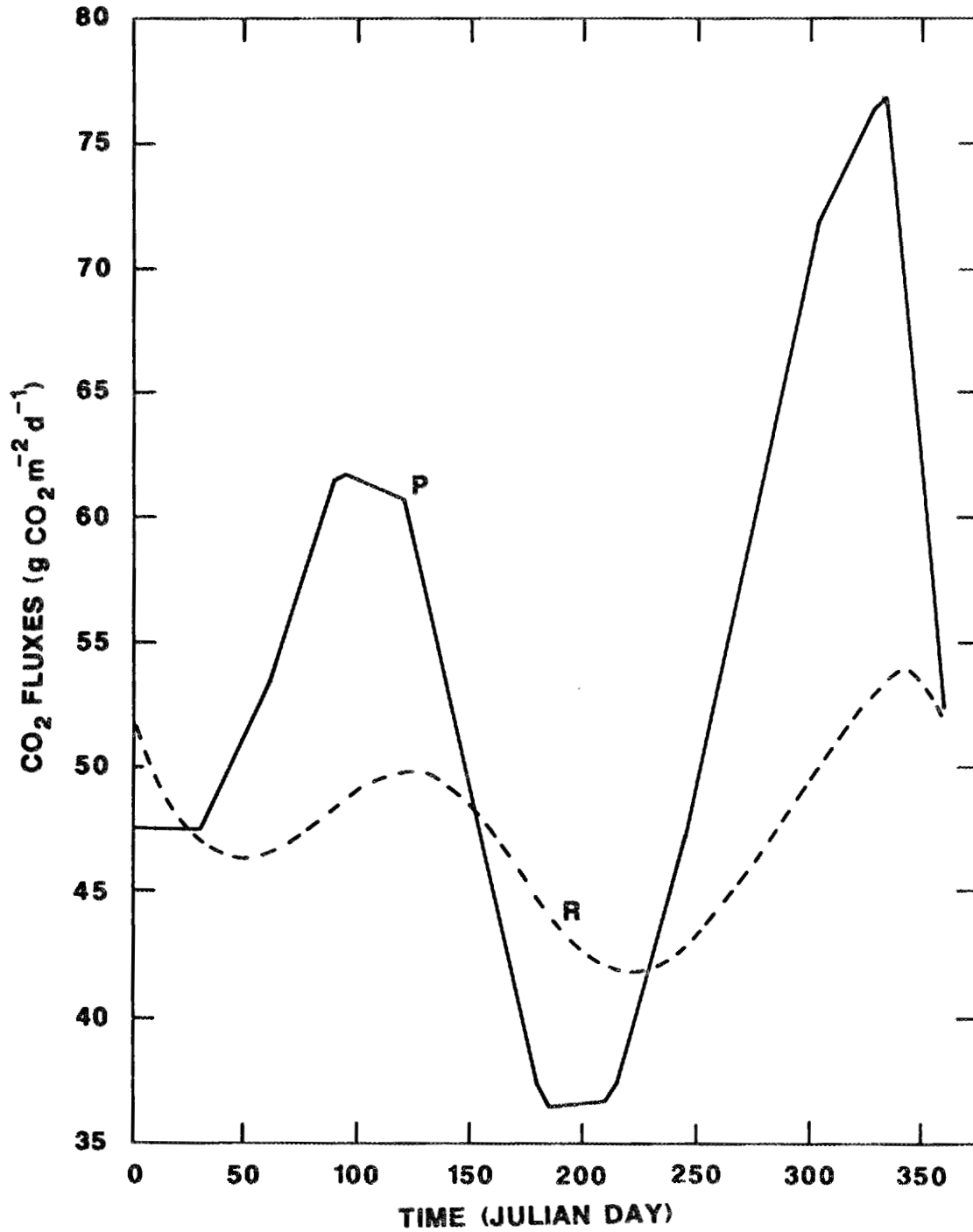


Figure 2.21. Seasonal total ecosystem photosynthesis (P) and respiration (R) for a tropical moist evergreen forest stand. Flux units are g CO<sub>2</sub> m<sup>-2</sup> d<sup>-1</sup>.

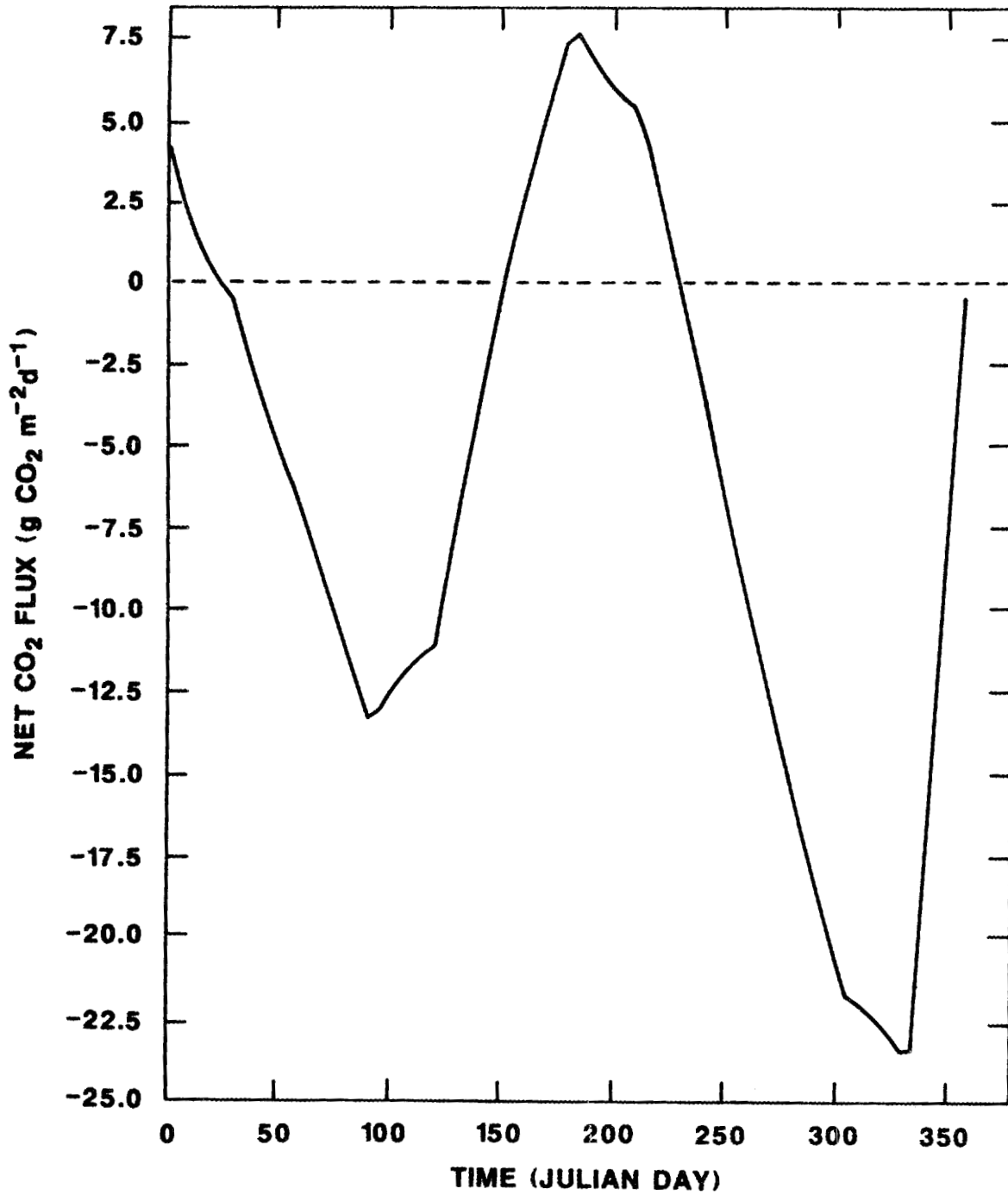


Figure 2.22. Seasonal net CO<sub>2</sub> exchange between the atmosphere and a tropical moist evergreen forest stand. Net flux is respiration minus photosynthesis. Flux units are g CO<sub>2</sub> m<sup>-2</sup> d<sup>-1</sup>.

ORNL-DWG 85-14260

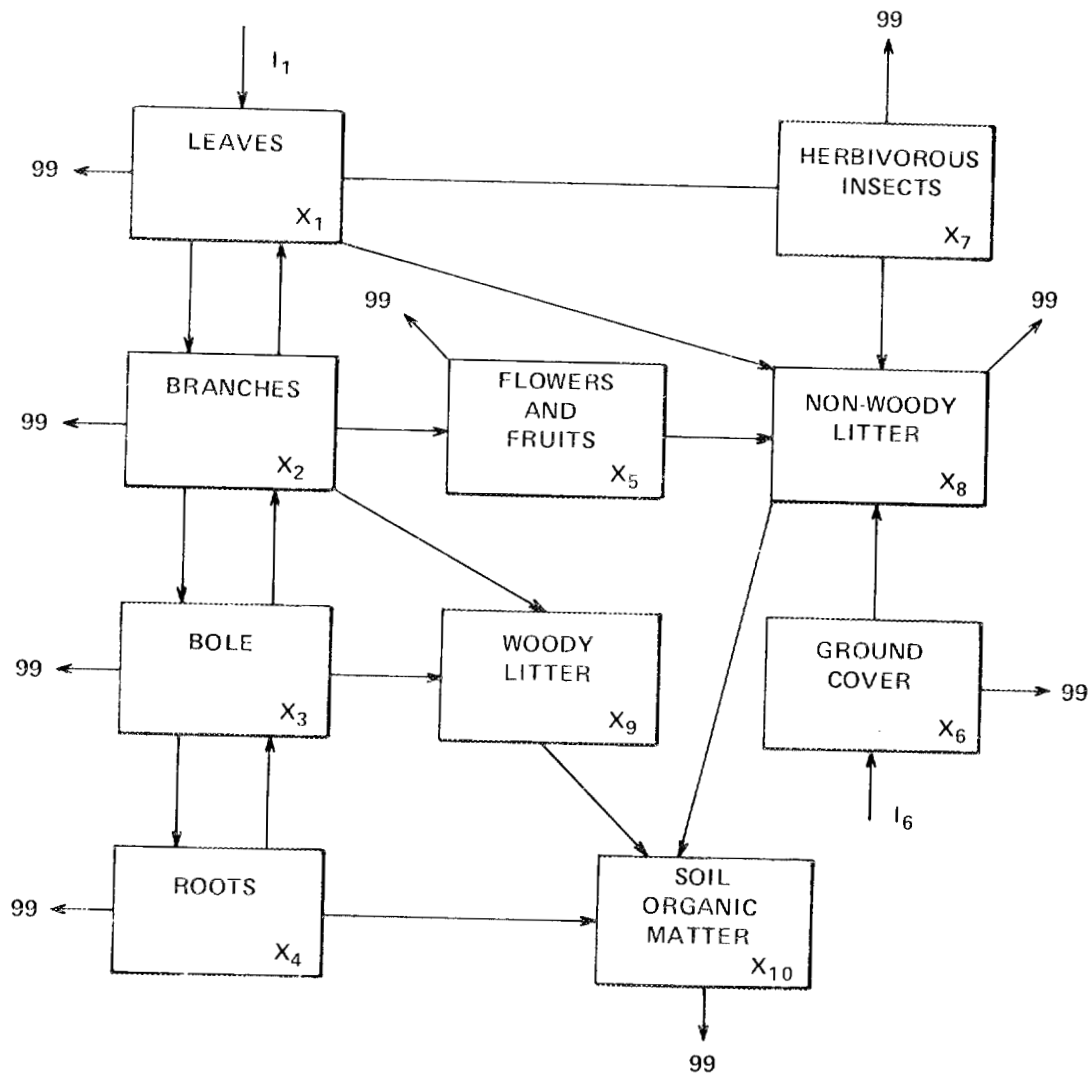


Figure 2.23. Compartmental structure of the tropical dry deciduous forest model. The arrows indicate the flux of biomass from compartment  $i$  to compartment  $j$ . The number 99 indicates a compartment external to the system.

Table 2.15. State variables of the tropical dry deciduous forest model.

State Variable*	Description
$x_1$	tree leaves
$x_2$	tree branches
$x_3$	tree boles
$x_4$	tree roots
$x_5$	tree flowers and fruits
$x_6$	groundcover vegetation
$x_7$	herbivorous insects
$x_8$	non-woody litter
$x_9$	woody litter
$x_{10}$	soil organic matter

\*Units are kg biomass ha<sup>-1</sup>.

### 2.6.1.2 Driving Variables

Seasonal dynamics of the miombo forest are assumed to be dependent on moisture (Bandhu et al. 1973). However, the model, as described by Bandhu et al. (1973) and in this implementation, does not involve any exogenous driving variables. Time varying forcings and rate coefficients (Table 2.16) are in principle related to variations in rainfall or moisture.

### 2.6.1.3 Flows Or Rate Processes

Most intercompartmental fluxes are represented as constant donor control processes. A few flows (e.g., photosynthesis, litterfall, and litter to soil transfer) involve time-varying rate coefficients. The flows indicated by arrows in Figure 2.23 are defined in Table 2.17. The notation  $F(i,j)$  indicates the flow of biomass from compartment  $i$  to compartment  $j$ . The number 99 represents a carbon sink, generally the atmosphere.

### 2.6.1.4 Photosynthesis And Respiration

Seasonal variations in photosynthesis are incorporated as monthly forcings,  $I_7(m)$  and  $I_6(m)$  ( $m = 1, \dots, 12$ ), on tree leaves,  $X_7$ , and groundcover,  $X_6$ , respectively. The monthly forcing values are input data to the simulation program.

Respiration from live compartments is given by:

$$F(i,0) = r_i X_i \quad i = 1, \dots, 7, \quad (2.30)$$

where  $X_i$  is the biomass of compartment  $i$ , and  $r_i$  is a constant rate coefficient specific to that compartment.

Table 2.16. Time-varying rate coefficients of the tropical dry deciduous forest model.

---

Rate Coefficient	Description
$a_{18}(t)$	controls the fall of leaf litter
$a_{58}(t)$	controls the fall of flowers and fruit
$a_{68}(t)$	controls the fall of groundcover litter
$a_{810}(t)$	controls the transfer of non-woody litter to soil organic matter
$a_{910}(t)$	controls the transfer of woody litter to soil organic matter

---

Table 2.17. The flows of organic matter simulated by the tropical dry deciduous forest model.

Flow <sup>a</sup>	Description <sup>b</sup>
I <sub>1</sub>	tree leaf photosynthesis forcing
I <sub>6</sub>	groundcover photosynthesis forcing
F(1,99)	leaf dark respiration
F(1,2)	leaf to branch translocation
F(1,7)	herbivory
F(1,8)	leaf litterfall: $a_{18}(t)$
F(2,99)	branch respiration
F(2,1)	branch to leaf translocation
F(2,3)	branch to bole translocation
F(2,5)	branch to flowers and fruit translocation
F(2,9)	fall of dead branches
F(3,99)	bole respiration
F(3,2)	bole to branch translocation
F(3,4)	bole to root translocation
F(3,9)	fall of dead boles
F(4,99)	root respiration
F(4,3)	root to bole translocation
F(4,10)	transfer of dead roots to soil organic matter
F(5,99)	flowers and fruits respiration
F(5,8)	flowers and fruit litterfall: $a_{58}(t)$
F(6,99)	groundcover respiration
F(6,8)	groundcover litterfall: $a_{68}(t)$
F(7,99)	herbivore respiration
F(7,8)	fall of dead herbivores and waste material
F(8,99)	decomposition of non woody litter (CO <sub>2</sub> evolution)
F(8,10)	decomposition of non woody litter (transfer to soil organic matter): $a_{810}(t)$
F(9,99)	decomposition of woody litter (CO <sub>2</sub> evolution)
F(9,10)	decomposition of woody litter (transfer to soil organic matter): $a_{910}(t)$
F(10,99)	decomposition of soil organic matter

<sup>a</sup>Units are kg biomass ha<sup>-1</sup> year<sup>-1</sup>.

<sup>b</sup>Includes a list of those time-varying coefficients (if any) that influence the flow.

#### 2.6.1.5 Release Of Carbon Through Decomposition

The evolution of  $\text{CO}_2$  during microbial decomposition of dead organic matter is modeled by applying Equation 2.27 to the litter compartments,  $X_8$  and  $X_9$ , and the soil organic matter compartment,  $X_{10}$ . Obviously, the model does not consider seasonal variation in the rate of  $\text{CO}_2$  release during decomposition. Decomposition does exhibit seasonality, however, through time-varying rates of transfer from litter to soil organic matter. These variations are assumed to be related to soil and litter moisture (Bandhu et al. 1973), although the model does not include any functional representation of this relationship.

#### 2.6.2 Seasonal Photosynthesis And Respiration

The time-varying coefficients and forcings which drive the seasonal dynamics of the miombo forest model were provided by Bandhu et al. (1973). These were used to derive seasonal total ecosystem photosynthesis and respiration values. Figure 2.24 is a plot of daily fluxes sampled at 5-day intervals. Model generated biomass fluxes were converted to  $\text{CO}_2$  fluxes (1 g dry weight = 1.65 g  $\text{CO}_2$ ; Lieth 1978). Seasonal net  $\text{CO}_2$  exchange (respiration minus photosynthesis) between the forest stand and the atmosphere is plotted in Figure 2.25.

### 2.7 TUNDRA MODEL

A general model of biomass decomposition, ABISK0, was developed by Bunnell and Dowding (1974) to compare tundra sites during the IBP

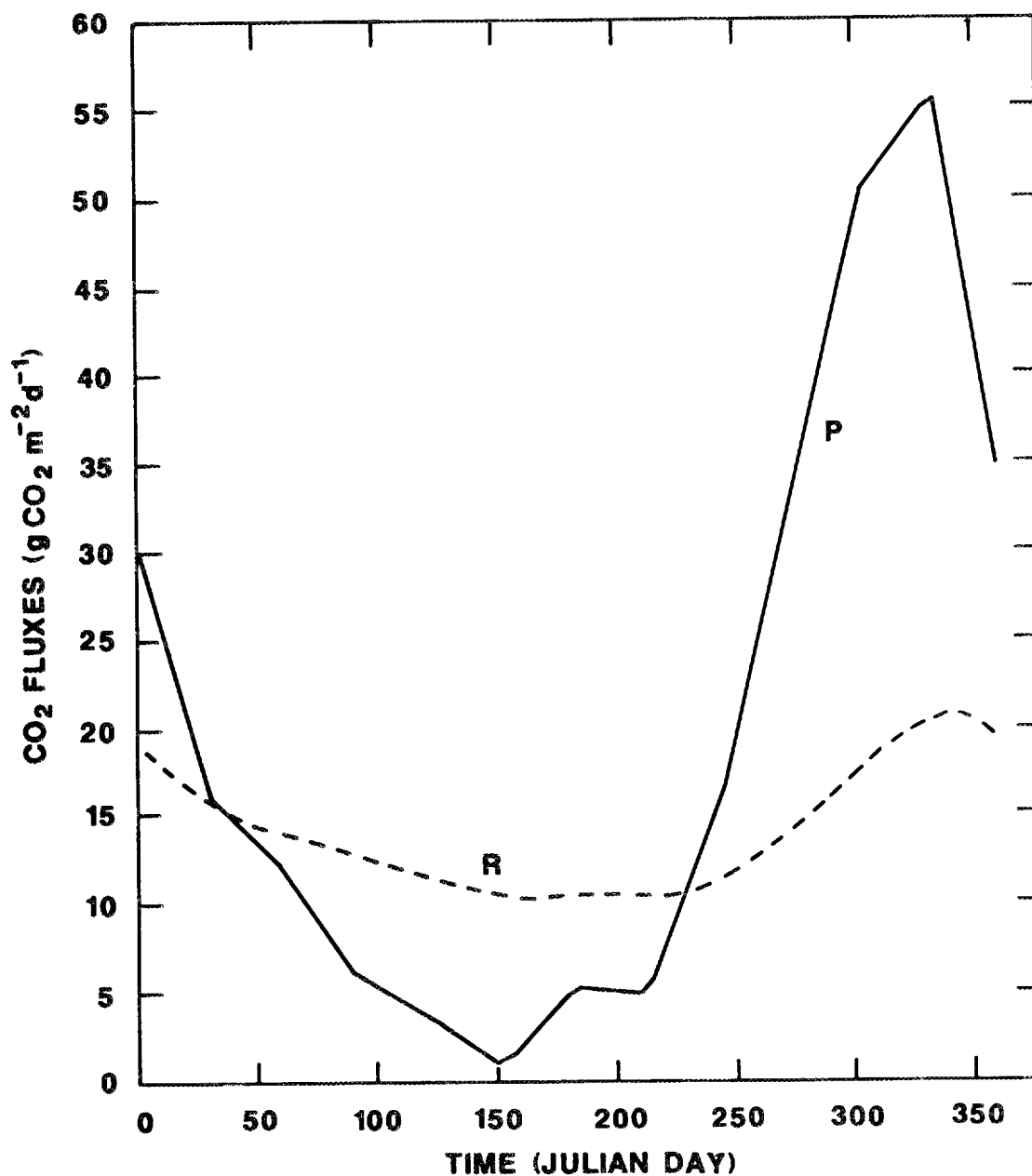


Figure 2.24. Seasonal total ecosystem photosynthesis (P) and respiration (R) for a tropical dry deciduous forest stand. Flux units are g CO<sub>2</sub> m<sup>-2</sup> d<sup>-1</sup>.

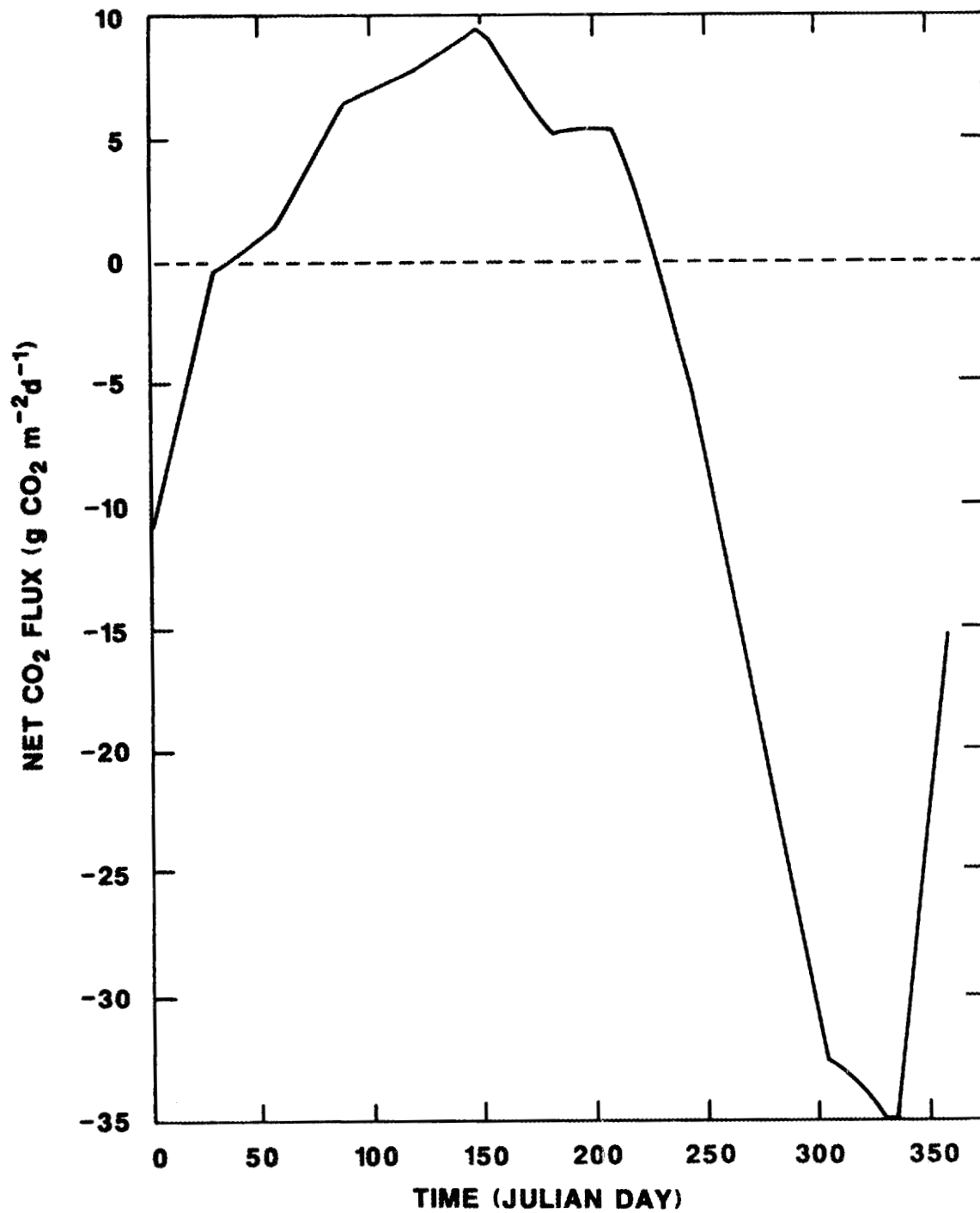


Figure 2.25. Seasonal net CO<sub>2</sub> exchange between the atmosphere and a tropical dry deciduous forest stand. Net flux is respiration minus photosynthesis. Flux units are g CO<sub>2</sub> m<sup>-2</sup> d<sup>-1</sup>.

Tundra Program. Later the model was extended by Bunnell and Scoullar (1975) to provide a fairly complete description of tundra biomass dynamics, and was renamed ABISKO II. In its details (e.g., parameters), the model describes a pure stand of DuPontia fischeri R. Br. at Point Barrow, Alaska (71°18'N, 156°40'W; see Brown et al. 1980 for a site description). The model is described by difference equations with a time step of one day.

## 2.7.1 Structure Of The Model

### 2.7.1.1 Compartments

The compartmental structure of the model is shown in Figure 2.26. The state variables corresponding to these compartments are defined in Table 2.18.

### 2.7.1.2 Driving Variables

There are seven exogenous driving variables in the model (Table 2.19). Daily values for these variables are interpolated from monthly means read into the simulation program as input data. In addition to these driving variables, the timing of snowmelt ( $Z_8$ ) and snowfall ( $Z_9$ ) influences the phenology and seasonality of the simulated tundra.

### 2.7.1.3 Flows Or Rate Processes

The flows of organic matter correspond to the arrows between compartments in Figure 2.26. The detailed functional representations of these flows and the assumptions involved are described in Bunnell and Scoullar (1975). In Table 2.20 we define these fluxes and

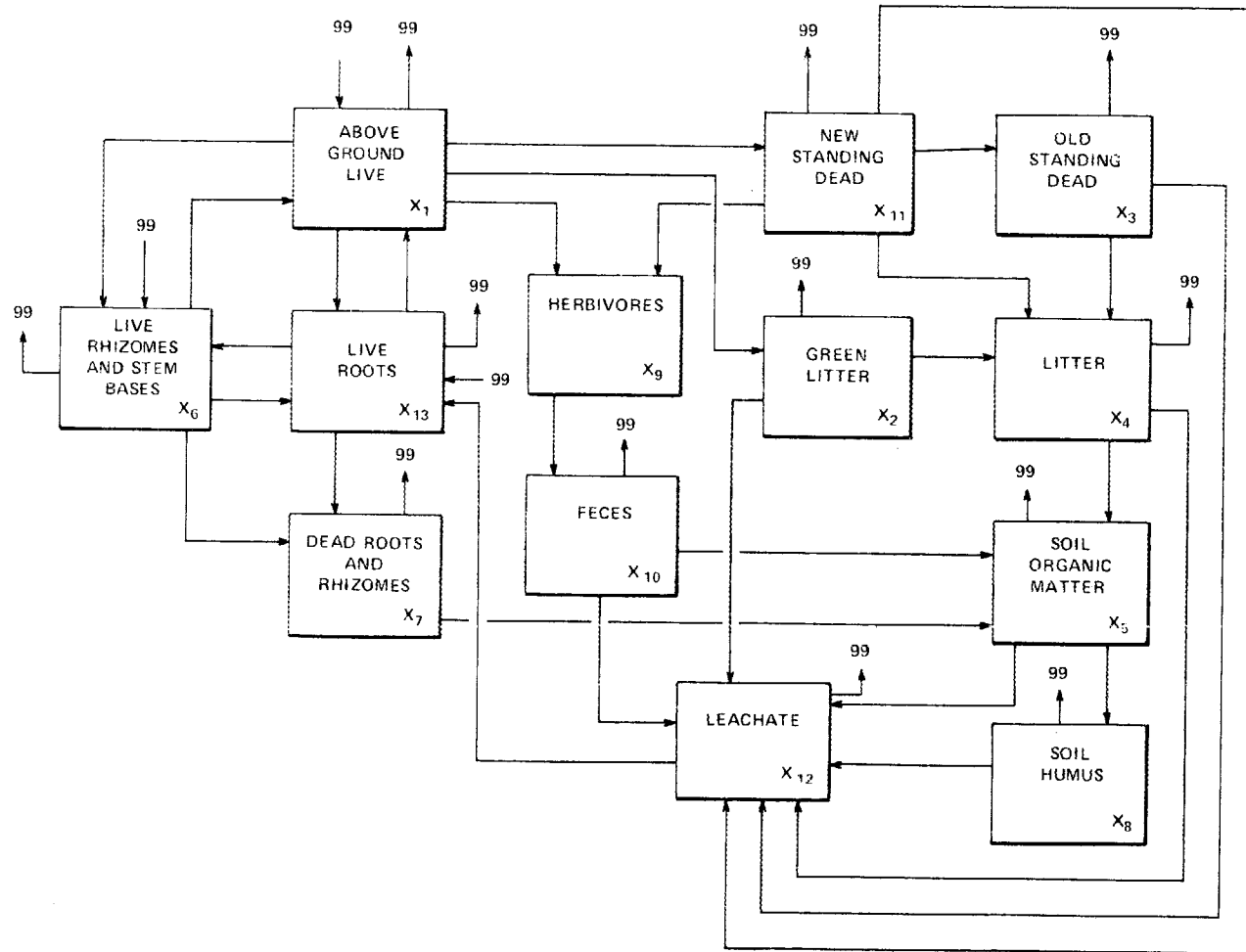


Figure 2.26. Compartmental structure of the tundra model. Modified from Bunnell and Scoullar (1975).

Table 2.18. State variables of the tundra model.

State Variable*	Description
$X_1$	aboveground live biomass
$X_2$	green litter
$X_3$	old standing dead biomass
$X_4$	litter
$X_5$	soil organic matter
$X_6$	live rhizomes and stem bases
$X_7$	dead roots and rhizomes
$X_8$	soil humus
$X_9$	herbivores
$X_{10}$	feces
$X_{11}$	new standing dead biomass
$X_{12}$	leachate
$X_{13}$	live roots

\*Units are g biomass  $m^{-2}$ .

Table 2.19. Driving variables of the tundra model.

Driving Variable	Description
Z <sub>1</sub>	relative sunlight intensity (as a fraction of the annual maximum)
Z <sub>2</sub>	air temperature (°C)
Z <sub>3</sub>	litter temperature (°C)
Z <sub>4</sub>	soil temperature (°C)
Z <sub>5</sub>	moisture level of the standing dead (g H <sub>2</sub> O g <sup>-1</sup> substrate)
Z <sub>6</sub>	moisture level of the litter (g H <sub>2</sub> O g <sup>-1</sup> substrate)
Z <sub>7</sub>	moisture level of the soil (g H <sub>2</sub> O g <sup>-1</sup> substrate)
Z <sub>8</sub>	day of snowmelt
Z <sub>9</sub>	day of snowfall

Table 2.20. Flows of organic matter simulated by the tundra model.

Flow <sup>a</sup>	Description <sup>b</sup>
F(99,1)	photosynthetic input to aboveground live biomass: Z <sub>1</sub> , Z <sub>2</sub>
F(1,2)	transfer from aboveground living biomass to green litter
F(1,6)	translocation to live rhizomes
F(1,11)	transfer from aboveground living biomass to new standing dead biomass
F(1,13)	translocation to live roots
F(1,99)	respiration of above ground live: Z <sub>2</sub>
F(2,4)	transfer of green litter to litter: Z <sub>3</sub> , Z <sub>6</sub>
F(2,12)	leaching of green litter: Z <sub>3</sub> , Z <sub>6</sub>
F(2,99)	respiration of green litter decomposers: Z <sub>3</sub> , Z <sub>6</sub>
F(3,12)	leaching of old standing dead biomass: Z <sub>3</sub> , Z <sub>6</sub>
F(3,99)	respiration of old standing dead decomposers: Z <sub>2</sub> , Z <sub>5</sub>
F(4,5)	transfer from litter to soil organic matter: Z <sub>3</sub> , Z <sub>6</sub>
F(4,12)	leaching of litter: Z <sub>3</sub> , Z <sub>6</sub>
F(4,99)	respiration of litter decomposers: Z <sub>3</sub> , Z <sub>6</sub>
F(5,8)	transfer from soil organic matter to soil biomass: Z <sub>4</sub> , Z <sub>7</sub>
F(5,12)	leaching of soil organic matter: Z <sub>4</sub> , Z <sub>7</sub>
F(5,99)	respiration of soil organic matter decomposers: Z <sub>4</sub> , Z <sub>7</sub>
F(6,7)	death of rhizomes
F(6,13)	transfer from rhizomes to roots
F(6,99)	respiration of rhizomes and stem bases: Z <sub>4</sub>
F(7,99)	respiration of dead root decomposers: Z <sub>4</sub> , Z <sub>7</sub>
F(8,12)	leaching of soil humus: Z <sub>4</sub> , Z <sub>7</sub>
F(8,99)	respiration of soil humus decomposers: Z <sub>4</sub> , Z <sub>7</sub>
F(10,99)	respiration of feces decomposers: Z <sub>3</sub> , Z <sub>6</sub>
F(11,3)	transfer of new standing dead to old standing dead: Z <sub>2</sub> , Z <sub>5</sub>
F(11,12)	leaching of new standing dead biomass: Z <sub>2</sub> , Z <sub>5</sub>
F(11,99)	respiration of new standing dead decomposers: Z <sub>2</sub> , Z <sub>5</sub>
F(12,99)	respiration of leachate decomposers: Z <sub>4</sub> , Z <sub>7</sub>
F(13,6)	translocation from live root to rhizomes
F(13,7)	transfer of live root biomass to dead root biomass
F(13,99)	respiration of live roots: Z <sub>4</sub>

<sup>a</sup>Units are g biomass m<sup>-2</sup> d<sup>-1</sup>.

<sup>b</sup>Includes a list of those driving variables (if any) that influence the flow.

indicate which, if any, of the driving variables influence a particular flow. Photosynthesis and respiration are discussed more fully in the next section. The units of the fluxes are g biomass  $m^{-2} d^{-1}$ . The notation  $F(i,j)$  indicates the flow of material from compartment  $i$  to compartment  $j$ . The number 99 refers to a compartment external to the system. All flows into the system are labelled  $F(99,j)$ , and all flows out of the system are labelled  $F(i,99)$ .

#### 2.7.1.4 Photosynthesis And Respiration

Photosynthetic growth is expressed as

$$PHOTOS = (CO1PHT)(Z_1)(TEMPO)(SUNLIT)X_1, \quad (2.31)$$

where  $CO1PHT$  is a constant (i.e., maximum photosynthetic rate);  $Z_1$  is irradiance (Langleys), and  $TEMPO$  represents the temperature effect on photosynthesis.  $TEMPO$  is given by:

$$TEMPO = \begin{cases} 0.0 & Z_2 < TP_{MIN} \\ & \text{or } Z_2 > TP_{MAX} \\ \frac{(CO1HPT - TP_{MIN} + TPOPT)(Z_2 - TP_{MIN})}{(CO1HPT - TP_{MIN} + TP_{MAX} - Z_2)TPOPT} & TP_{MIN} < Z_2 \\ & \text{and } Z_2 \leq TPOPT \\ \frac{(CO1HPT - TP_{MIN} + TPOPT)(TP_{MAX} - Z_2)}{(CO1HPT - TP_{MIN} + TP_{MAX} - Z_2)TPOPT} & TPOPT < Z_2 \\ & \text{and } Z_2 < TP_{MAX}. \end{cases} \quad (2.32)$$

where  $TP_{MIN}$  is the minimum and  $TP_{MAX}$  is the maximum temperature for photosynthesis. The term  $TPOPT$  defines the optimum temperature for photosynthesis, and  $CO1HPT$  is a constant describing the maximum

photosynthetic rate. In Equation 2.31, SUNLIT is the proportion of green biomass capable of photosynthesis, or,

$$\text{SUNLIT} = 1.0 - (1.0 - (X_1/\text{BTOT}))(X_1/\text{BMX}) , \quad (2.33)$$

where

$$\text{BTOT} = X_1 + X_2 + X_3,$$

BMX = live biomass necessary for 100% interception of incoming radiation.

Respiration from live plant compartments is modeled as a temperature dependant process. Respiration per unit live biomass, RES<sub>i</sub>, is given by

$$\text{RES}_i = a_{3i} a_{4i}^{((T - 10)/10)} \quad i = 1, 6, 13 , \quad (2.34)$$

where  $a_{3i}$  is the respiration rate at 10°C;  $a_{4i}$  is the  $Q_{10}$  coefficient, and T is the appropriate temperature (i.e., air, litter, or soil).

#### 2.7.1.5 Release Of Carbon Through Decomposition

Respiratory losses of carbon from dead plant, litter, and soil organic matter compartments, generate by microbial decomposers utilizing the substrate as an energy source, is simulated with an explicit model of microbial respiration (Bunnell and Tait 1974). The respiration rate per unit biomass of the dead organic matter compartments, RES<sub>i</sub>, is a function of both temperature, T, and substrate moisture, M, and is given by

$$R(T,M) = \frac{M}{a_1 + M} \left( \frac{a_2}{a_2 + M} \right) a_3 a_4^{((T - 10)/10)}, \quad (2.35)$$

where

$a_1$  = % moisture content at which the substrate is half-saturated with water,

$a_2$  = % moisture content at which half the channels are saturated and blocked with water,

$a_3$  = the respiration rate at 10°C when neither oxygen or moisture are limiting,

$a_4$  = the  $Q_{10}$  coefficient.

Equation 2.35 is applied to compartments  $X_2$  to  $X_5$ ,  $X_7$ ,  $X_8$ , and  $X_{10}$  to  $X_{12}$ . The parameters  $a_1$ ,  $a_2$ ,  $a_3$ , and  $a_4$  are compartment specific.

### 2.7.2 Seasonal Photosynthesis And Respiration

Monthly values for the tundra model's driving variables (F. L. Bunnell, pers. comm.) were used to interpolate the daily values required by the flux equations. A plot of total ecosystem photosynthesis and respiration values over a year is shown in Figure 2.27. Biomass fluxes generated by the model ( $\text{g biomass m}^{-2} \text{d}^{-1}$ ) were corrected to  $\text{CO}_2$  fluxes ( $\text{kg CO}_2 \text{ m}^{-2} \text{d}^{-1}$ ) by multiplication by  $(1.65)(0.001)$ . Seasonal net  $\text{CO}_2$  exchange (respiration minus photosynthesis) between the tundra ecosystem and the atmosphere is shown in Figure 2.28.

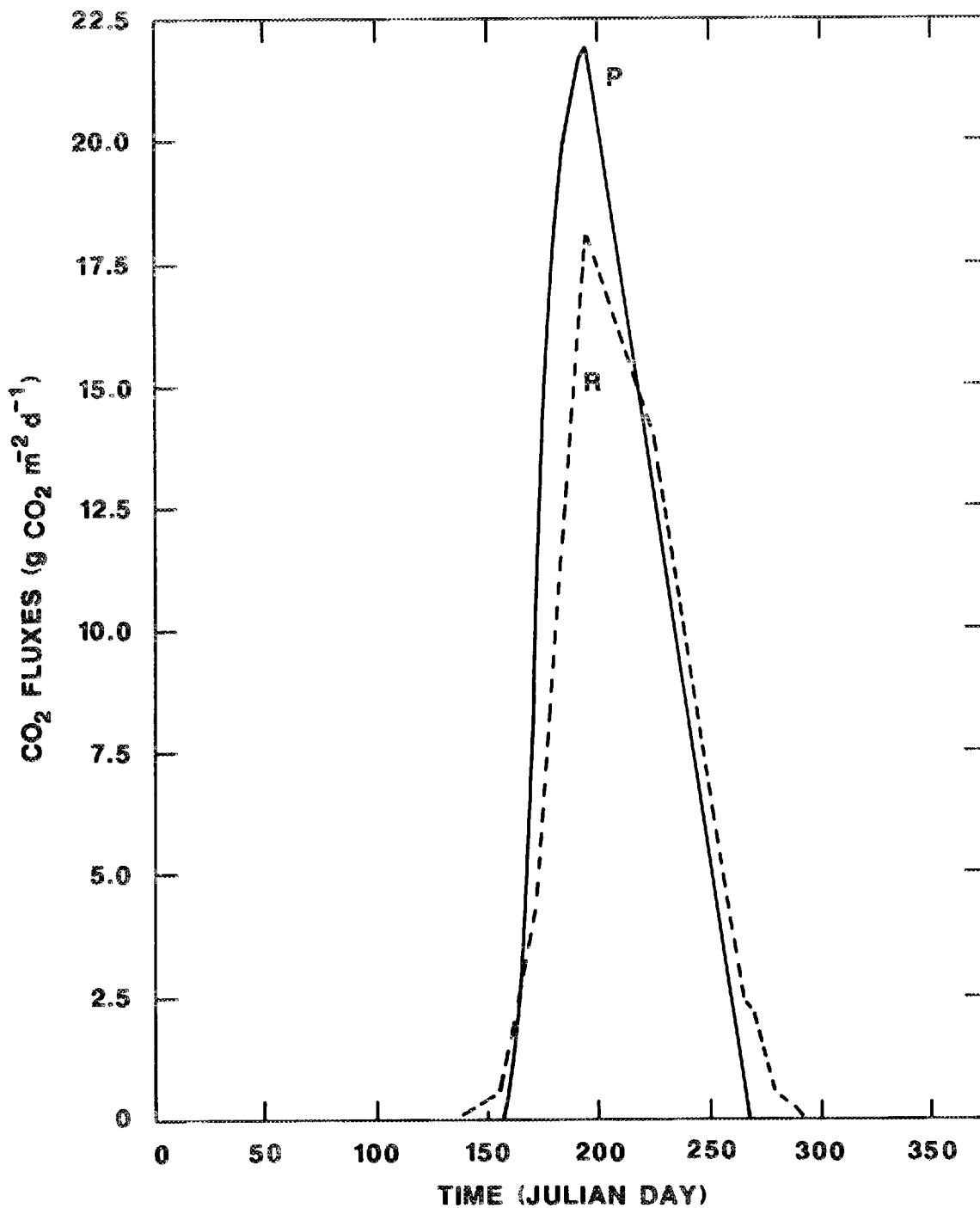


Figure 2.27. Seasonal total ecosystem photosynthesis (P) and respiration (R) for a tundra ecosystem. Flux units are g CO<sub>2</sub> m<sup>-2</sup> d<sup>-1</sup>.

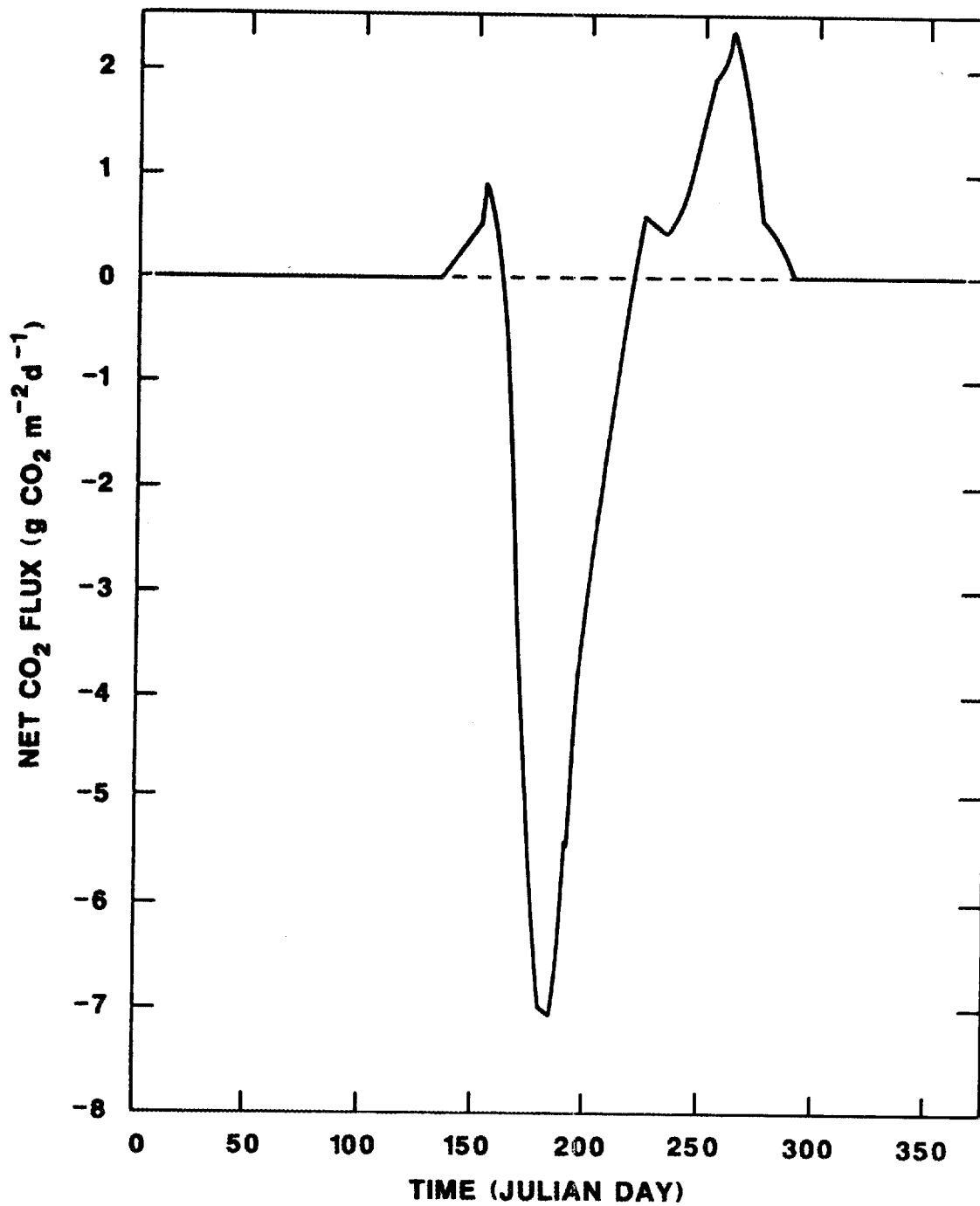


Figure 2.28. Seasonal net CO<sub>2</sub> exchange between the atmosphere and a tundra ecosystem. Net flux is respiration minus photosynthesis. Flux units are g CO<sub>2</sub> m<sup>-2</sup> d<sup>-1</sup>.

## 2.8 GRASSLAND MODEL

The grassland model is adapted from the shortgrass prairie producer model described by Parton, Singh, and Coleman (1978) and Parton and Singh (1976). Plant biomass, both aboveground and belowground, is described by a compartmental model using difference equations and a time step of one day. The model was originally constructed for the shortgrass prairie at the US/IBP Grassland Biome Pawnee Site (40°49'N, 104°46'W) dominated by blue grama (Bouteloua gracilis (H.B.K.) Lag.) (Parton and Singh 1976; Parton, Singh, and Coleman 1978). The model has also been applied to the tallgrass prairie at the Osage Site, dominated by little bluestem (Andropogon scoparius Michx.), by Parton and Singh (1976). We have implemented the Pawnee version of the model.

### 2.8.1 Structure Of The Model

#### 2.8.1.1 Compartments

Forty-one compartments or state variables are modeled (Figure 2.29). Conceptually, the model considers a single species of grass and does not consider other grass species, plant types, or age classes (except for three root age classes). In practice the model was parameterized with data for the dominant species at the site (i.e., blue grama at Pawnee). The state variables corresponding to the compartments of Figure 2.29 are defined in Table 2.21.

ORNL DWG 85-14262

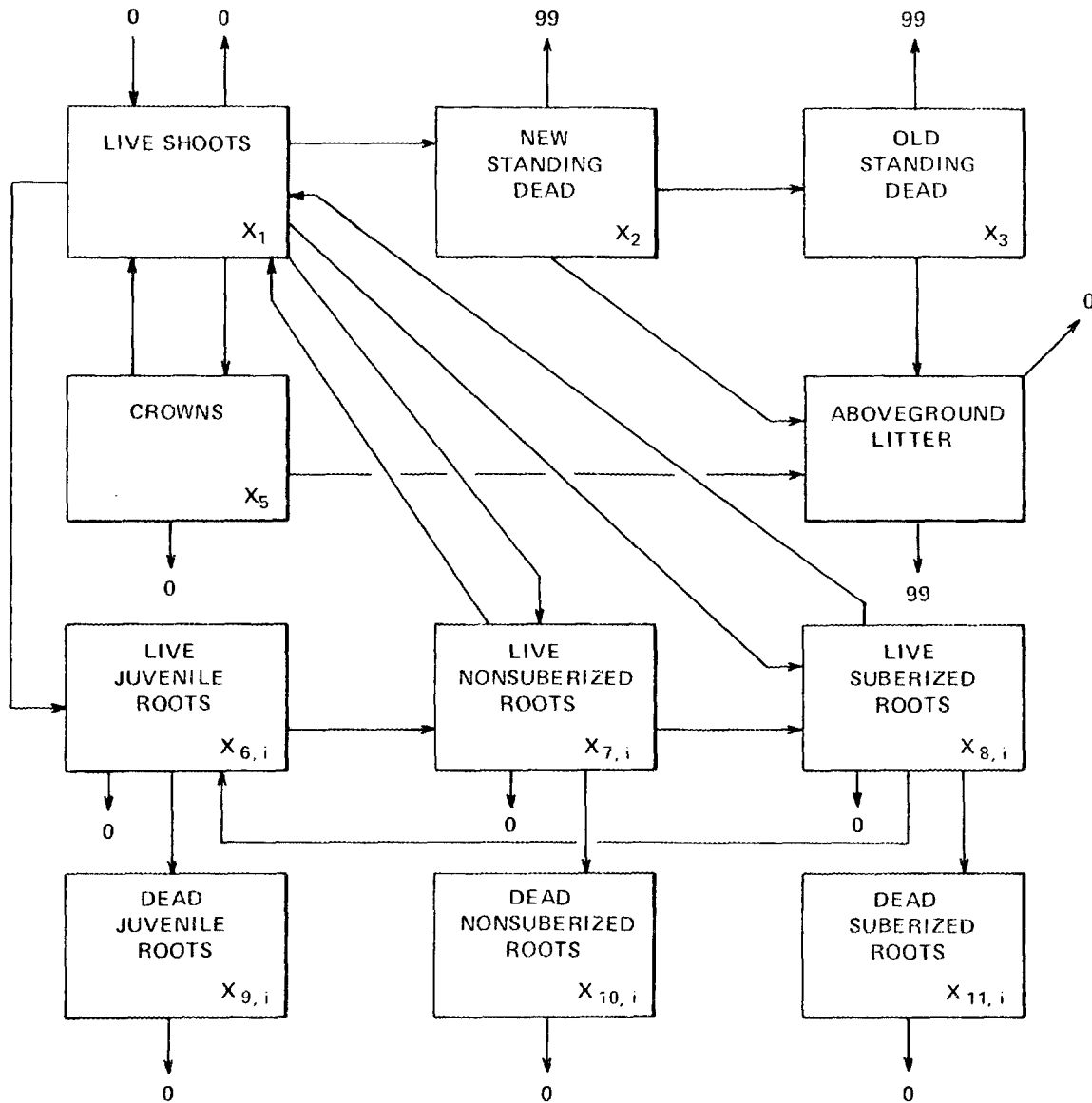


Figure 2.29. Compartmental structure of the temperate grassland model. The arrows indicate the flux of biomass from compartment  $i$  to compartment  $j$ . The numbers 99 and 0 indicate compartments external to the system.

Table 2.21. State variables of the grassland model.

State Variable*	Description
$X_1$	live shoots
$X_2$	new standing dead (standing dead of current year)
$X_3$	old standing dead
$X_4$	aboveground litter
$X_5$	crowns
$X_{6,i}$	live juvenile roots in the $i$ th soil layer, Six soil layers are considered (0-5, 5-15, 15-30, 30-45, 45-60, and 60-75 cm).
$X_{7,i}$	live non suberized roots in the $i$ th soil layer
$X_{8,i}$	live suberized roots in the $i$ th soil layer
$X_{9,i}$	dead juvenile roots in the $i$ th soil layer
$X_{10,i}$	dead non suberized roots in the $i$ th soil layer
$X_{11,i}$	dead suberized roots in the $i$ th soil layer

\*Units are g biomass  $m^{-2}$ .

### 2.8.1.2 Driving Variables

The model involves a number of driving variables. The original model was coupled with an abiotic submodel (Parton 1976) which calculated most of these variables, many of which responded to changes in the state variables (i.e., there was feedback between the biota and the abiotic environment). Other variables were strictly exogenous driving variables. The submodel we used to derive and incorporate the driving variables is a minor modification of Parton (1976). Table 2.22 describes the driving variables used in the model.

### 2.8.1.3 Flows Or Rate Processes

Fluxes between compartments are modeled mechanistically, and the equations describing them can be quite complex. Details of the functional forms can be found in Parton and Singh (1976), Parton, Singh, and Coleman (1978), and Detling, Parton, and Hunt (1978). Here (Table 2.23) we simply define the fluxes indicated by arrows in Figure 2.29 and indicate which, if any, of the driving variables influence a particular flow. The notation  $F(i,j)$  indicates the flow of biomass from compartment  $i$  to compartment  $j$ . The number 0 represents the atmosphere; the number 99 represents a carbon/biomass sink external to the modeled system.

### 2.8.1.4 Photosynthesis And Respiration

Net photosynthesis is the difference between net daytime photosynthesis,  $F(0,1)$ , and night respiration  $F(1,0)$ . Net daytime photosynthesis is calculated as a function of canopy air temperature,

Table 2.22. Driving variables of the grassland model.

Driving Variable	Description
$Z_1(i)$	soil water potential in the $i$ th soil layer (-bars)
$Z_2$	weighted average soil water potential (-bars)
$Z_3(i)$	soil temperature in the $i$ th soil layer ( $^{\circ}\text{C}$ )
$Z_4$	soil surface temperature ( $^{\circ}\text{C}$ )
$Z_5$	14-day running average soil temperature in the top two soil layers ( $^{\circ}\text{C}$ )
$Z_6$	solar irradiance ( $\text{W m}^{-2}$ )
$Z_7(j)$	daytime air temperature for the $j$ th ( $j = 1, \dots, 4$ ) daytime interval ( $^{\circ}\text{C}$ )
$Z_8(j)$	nighttime air temperature for the $j$ th ( $j = 1, \dots, 4$ ) nighttime interval ( $^{\circ}\text{C}$ )
$Z_9$	minimum daily air temperature ( $^{\circ}\text{C}$ )
$Z_{10}$	maximum daily air temperature ( $^{\circ}\text{C}$ )
$Z_{11}$	average daily air temperature ( $^{\circ}\text{C}$ )
$Z_{12}$	daily rainfall (cm)
$Z_{13}$	wind speed ( $\text{km h}^{-1}$ )
$Z_{14}$	phenological stage (dimensionless)

Table 2.23. The flows of organic matter simulated by the grassland model.

Flow <sup>a</sup>	Description <sup>b</sup>
F(0,1)	net daytime photosynthesis: $Z_2, Z_6, Z_7, Z_{14}$
F(1,0)	night respiration: $Z_2, Z_8$
F(1,2)	shoot mortality: $Z_2, Z_9, Z_{14}$
F(1,5)	shoot to crown translocation: $Z_2, Z_{14}$
F(1,6 <sub>i</sub> )	shoot to juvenile roots translocation: $Z_1(i), Z_2, Z_{14}$
F(1,7 <sub>i</sub> )	shoot to non-suberized roots translocation: $Z_1(i), Z_2, Z_{14}$
F(1,8 <sub>i</sub> )	shoot to suberized roots translocation: $Z_1(i),$ $Z_2, Z_{14}$
F(2,3)	transfer of recent standing dead to old standing dead (g dw biomass m <sup>-2</sup> year <sup>-1</sup> )
F(2,4)	fall of new standing dead: $Z_{12}, Z_{13}$
F(2,99)	leaching of recent standing dead: $Z_{12}$
F(3,4)	fall of old standing dead: $Z_{12}, Z_{13}$
F(3,99)	leaching of old standing dead: $Z_{12}$
F(4,0)	litter decomposition: $Z_1(1), Z_2$
F(4,99)	leaching and mechanical mixing of litter: $Z_{12}$
F(5,0)	crown respiration: $Z_1(1), Z_4$
F(5,1)	transfer of stored carbohydrates to shoots: $Z_1(1)$
F(5,4)	crown death: $Z_1(1), Z_2$
F(6 <sub>i</sub> ,0)	juvenile root respiration: $Z_1(i), Z_3(i)$
F(6 <sub>i</sub> ,7 <sub>i</sub> )	aging of juvenile roots in the <i>i</i> th soil layer
F(6 <sub>i</sub> ,9 <sub>i</sub> )	death of juvenile roots in the <i>i</i> th soil layer: $Z_1(i), Z_3(i)$
F(7 <sub>i</sub> ,0)	non-suberized root respiration: $Z_1(i), Z_3(i)$
F(7,1)	transfer of carbohydrates stored in non-suberized roots: $Z_1(i)$
F(7 <sub>i</sub> ,8 <sub>i</sub> )	aging of non-suberized roots in the <i>i</i> th soil layer: $Z_3(1)$
F(7 <sub>i</sub> ,10 <sub>i</sub> )	death of non-suberized roots in the <i>i</i> th soil layer: $Z_1(i), Z_3(i)$
F(8 <sub>i</sub> ,0)	suberized root respiration: $Z_1(i), Z_3(i)$
F(8,1)	transfer of carbohydrates stored in suberized roots: $Z_1(i)$
F(8 <sub>i</sub> ,6 <sub>i</sub> )	spring initiation of juvenile root growth: $Z_1(i)$
F(8 <sub>i</sub> ,11 <sub>i</sub> )	death of suberized roots in the <i>i</i> th soil layer: $Z_1(i), Z_3(i)$
F(9 <sub>i</sub> ,0)	decomposition of dead juvenile roots in the <i>i</i> th soil layer: $Z_1(i), Z_3(i)$
F(10 <sub>i</sub> ,0)	decomposition of dead non-suberized roots in the <i>i</i> th soil layer: $Z_1(i), Z_3(i)$

Table 2.23. (Continued)

Flow <sup>a</sup>	Description <sup>b</sup>
F(11 <sub>j</sub> ,0)	decomposition of dead suberized roots in the <i>i</i> th soil layer: Z <sub>1</sub> ( <i>i</i> ), Z <sub>3</sub> ( <i>i</i> )

<sup>a</sup>Unless otherwise indicated, all flows are in units of g dw biomass m<sup>-2</sup> d<sup>-1</sup>.

<sup>b</sup>Includes a list of those driving variables (if any) that influence the flow.

$Z_7(j)$ , soil water potential,  $Z_2$ , total shortwave solar radiation,  $Z_6$ , and phenology,  $Z_{14}$ , using the equation

$$F(0,1) = \sum_{j=1}^4 C_j L M_x P \Delta t_d / 4 , \quad (2.36)$$

where

$C_j$  = the combined effect of daily weighted average soil water potential and air temperature,

$L$  = leaf area index,

$M_x$  = net photosynthesis rate for a given irradiance under conditions of optimal temperature and soil water potential,

$P$  = phenology control parameter,

$\Delta t_d / 4$  = length of daytime period  $j$ .

The term  $M_x$  is given by a piecewise linear approximation of the functional relationship presented by Parton, Singh, and Coleman (1978). The leaf area index and phenology control parameter (a function of  $Z_{14}$ , Table 2.22) are calculated according to Parton, Singh, and Coleman (1978). The term  $C_j$  is determined for each  $j$ th daylight time period using the equation presented by Detling, Parton, and Hunt (1978).

Shoot dark respiration,  $F(1,0)$ , is a function of nighttime air temperature,  $Z_8(j)$ , and the weighted average soil water potential.

The flux is described by

$$F(1,0) = \sum_{j=1}^4 C_j L \Delta t_n / 4 , \quad (2.37)$$

where  $C_j$  is dark respiration as a function of nighttime air temperature and soil water potential;  $L$  is leaf area index, and  $\Delta t_n/4$  is the length of nighttime period  $j$ . The equation used to obtain  $C_j$  is described by Detling, Parton, and Hunt (1978).

Root respiration in the  $i$ th soil layer is calculated as a function of soil water potential,  $Z_1(i)$ , and temperature,  $Z_3(i)$ , using the equations

$$F(6_i,0) = M_r T_r R_1 X_{6,i} \quad (2.38a)$$

$$F(7_i,0) = M_r T_r R_2 X_{7,i} \quad (2.38b)$$

$$F(8_i,0) = M_r T_r R_3 X_{8,i} \quad (2.38c)$$

where

$M_r$  = control parameter for the effect of soil water potential,

$T_r$  = control parameter for the effect of soil temperature,

$R_j$  = maximum fraction of root biomass of type  $j$  respired per day at 0 bars soil water potential,

$X_{j,i}$  = live root biomass of type  $j$  in the  $i$ th soil layer.

The control parameters  $M_r$  and  $T_r$  are given by equations described in Parton, Singh, and Coleman (1978).

Crown respiration is calculated using Equation 2.38b with the following modifications: crown biomass,  $X_5$ , replaces root biomass; soil surface temperature,  $Z_4$ , is used to determine  $T$ ; and soil water potential in the top 5 cm,  $Z_1(1)$ , is used to determine  $M_r$ . Also, the maximum respiration rate for non-suberized roots,  $R_2$ , is assumed to approximate that for crowns.

### 2.8.1.5 Release Of Carbon Through Decomposition

The release of  $\text{CO}_2$  during the decomposition of dead roots is described by

$$F(9_i, 0) = D_i^D \min(M_i^D, T_i^D) X_{9,i} d_i, \quad (2.39a)$$

$$F(10_i, 0) = D_i^D \min(M_i^D, T_i^D) X_{10,i} d_i, \quad (2.39b)$$

$$F(11_i^D, 0) = D_i^D \min(M_i^D, T_i^D) X_{11,i} d_i \quad (2.39c)$$

where

$D_j^D$  = maximum turnover rate for dead roots of type  $j$ ,

$X_{j,i}$  = dead root biomass of type  $j$  in the  $i$ th layer,

$d_i$  = depth control parameter for decomposition in the  $i$ th soil layer,

$M_i^D$  = soil water control parameter for decomposition in  $i$ th soil layer,

$T_i^D$  = soil temperature control parameter for decomposition in the  $i$ th soil layer.

The control parameters  $M_i^D$  and  $T_i^D$  are implemented as piecewise linear approximations of the functional relationships presented by Parton, Singh, and Coleman (1978). The formulation  $\min(M_i^D, T_i^D)$  indicates that only the most limiting factor, the minimum control parameter, is used to depress the maximum root turnover rate,  $D_j^D$ .

The release of  $\text{CO}_2$  in the decomposition of aboveground litter,  $F(4,0)$ , is a function of litter biomass,  $X_4$ , soil water potential in the top soil layer,  $Z_7(1)$ , and soil surface temperature,  $Z_4$ .

Equation 2.39b is used with the assumption that maximum litter

turnover due to decomposition is 75% of that for non-suberized roots. We decompose dead crowns and litter mixed into the top soil layer with the same equation used for aboveground litter, with the appropriate biomass substitutions. This may be a slight deviation from Parton, Singh, and Coleman (1978), who did not explicitly describe the fate of these components.

### 2.8.2 Seasonal Photosynthesis And Respiration

An only slightly modified version of Parton's (1976) abiotic model was used to generate driving variables for the simulation model. Parameters for the abiotic model were taken from Parton (1976), Parton and Singh (1976), and Parton (1978). Input data for the abiotic model were extracted from various US/IBP Grassland Biome Technical Reports and a climatic atlas of the United States (U.S. Department of Commerce 1968). When daily input values were called for, they were interpolated from monthly means using a piecewise-linear spline function. Daily rainfall was an exception and was obtained by dividing the appropriate mean monthly rainfall by the number of days in the month. The input data were generally long-term averages, and they permitted simulation of seasonal total stand photosynthesis and respiration values for an "average" year. A plot of daily fluxes sampled at weekly intervals is shown in Figure 2.30. Biomass fluxes generated by the model were converted to CO<sub>2</sub> fluxes using a conversion factor of 1 g dry matter = 1.467 g CO<sub>2</sub> (Brown and Trlica 1974). Seasonal net CO<sub>2</sub> exchange between the grassland stand and the atmosphere is plotted in Figure 2.31.

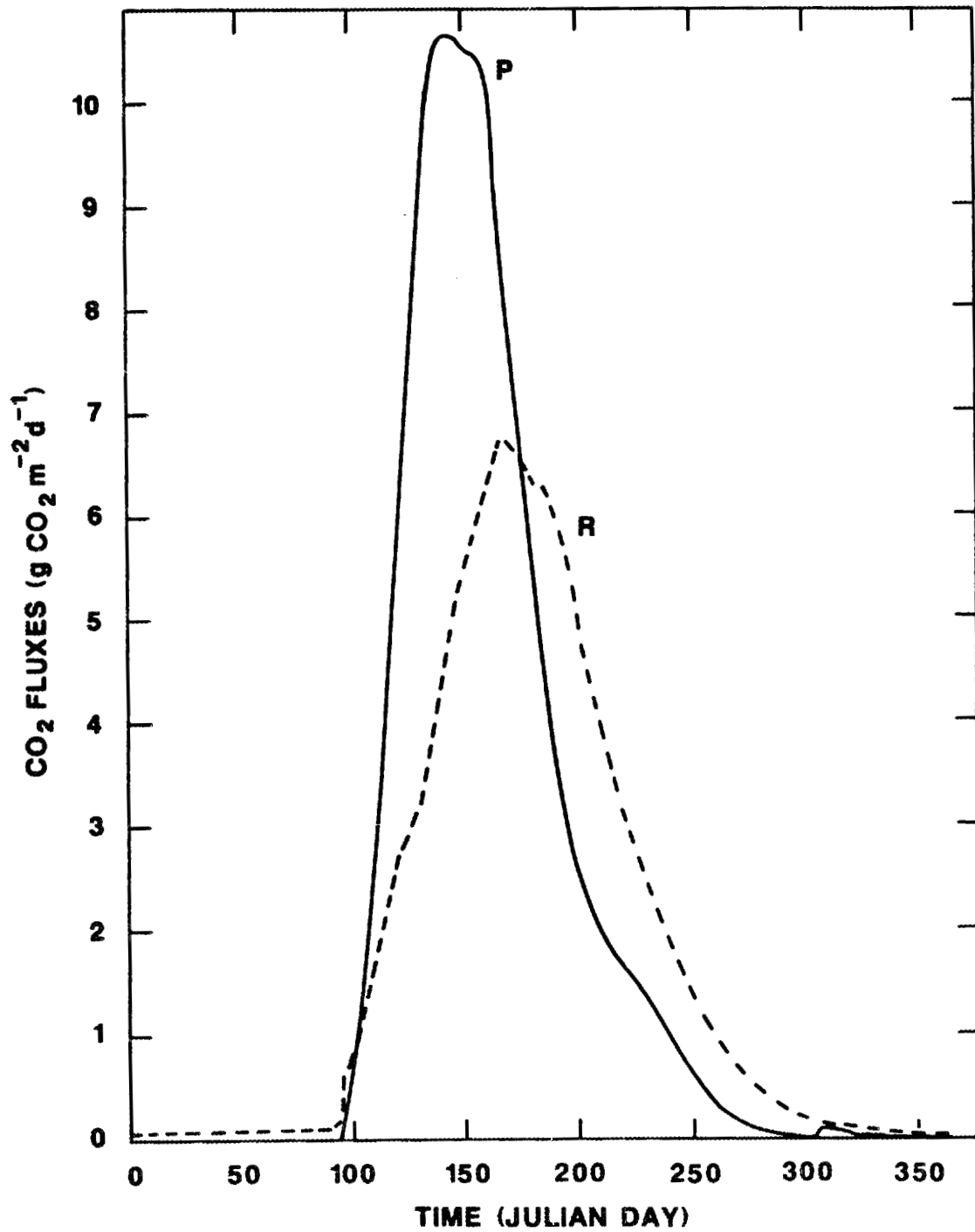


Figure 2.30. Seasonal total ecosystem photosynthesis (P) and respiration (R) for a temperate grassland plot. Flux units are  $\text{g CO}_2 \text{ m}^{-2} \text{ d}^{-1}$ .

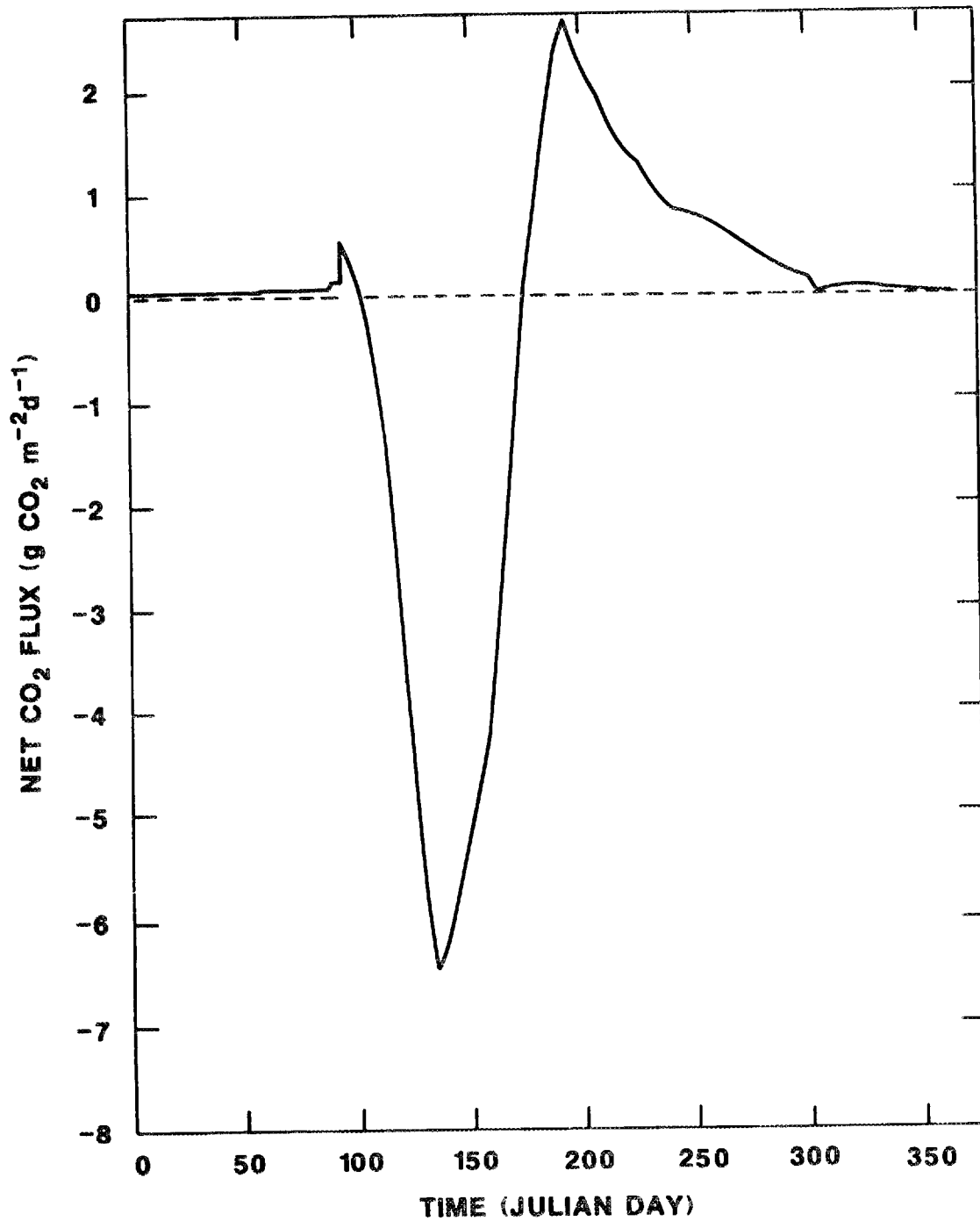


Figure 2.31. Seasonal net CO<sub>2</sub> exchange between the atmosphere and a temperate grassland plot. Net flux is respiration minus photosynthesis. Flux units are g CO<sub>2</sub> m<sup>-2</sup> d<sup>-1</sup>.

## 2.9 DESERT AND ARID SHRUBLAND MODEL

The model of seasonal carbon dynamics in arid lands is an adaptation of models developed as part of the US/IBP Desert Biome Program (see Goodall 1981). The models were designed as general models for the North American deserts; our implementation targets the Mohave Desert site at Rock Valley, Nye County, Nevada (approximately 37°N, 116°30'W). The site is a perennial shrub desert dominated by ragweed (Ambrosia dumosa (Gray) Payne) and squawberry (Lycium andersoni Gray) (see Turner and McBrayer 1974 for further site description). Production or carbon assimilation is modeled with an adaptation of Valentine's (1974) plant processes submodel; decomposition is modeled with an adaptation of Parnas and Radford's (1974) decomposition submodel. These mechanistic process oriented models are described by difference equations with a time step of one day. In the original Desert Biome implementation difference equations with time steps variable by submodel were used to approximate the differential equations (Goodall and Gist 1973).

### 2.9.1 Structure Of The Model

#### 2.9.1.1 Compartments

The compartmental structure of the arid lands model is illustrated in Figures 2.32 and 2.33. Figure 2.32 depicts the plant production portion of the model; Figure 2.33 shows the structure of the decomposition submodel. The compartments of Figure 2.32 are repeated for three functional plant groups (i.e., annuals, perennial

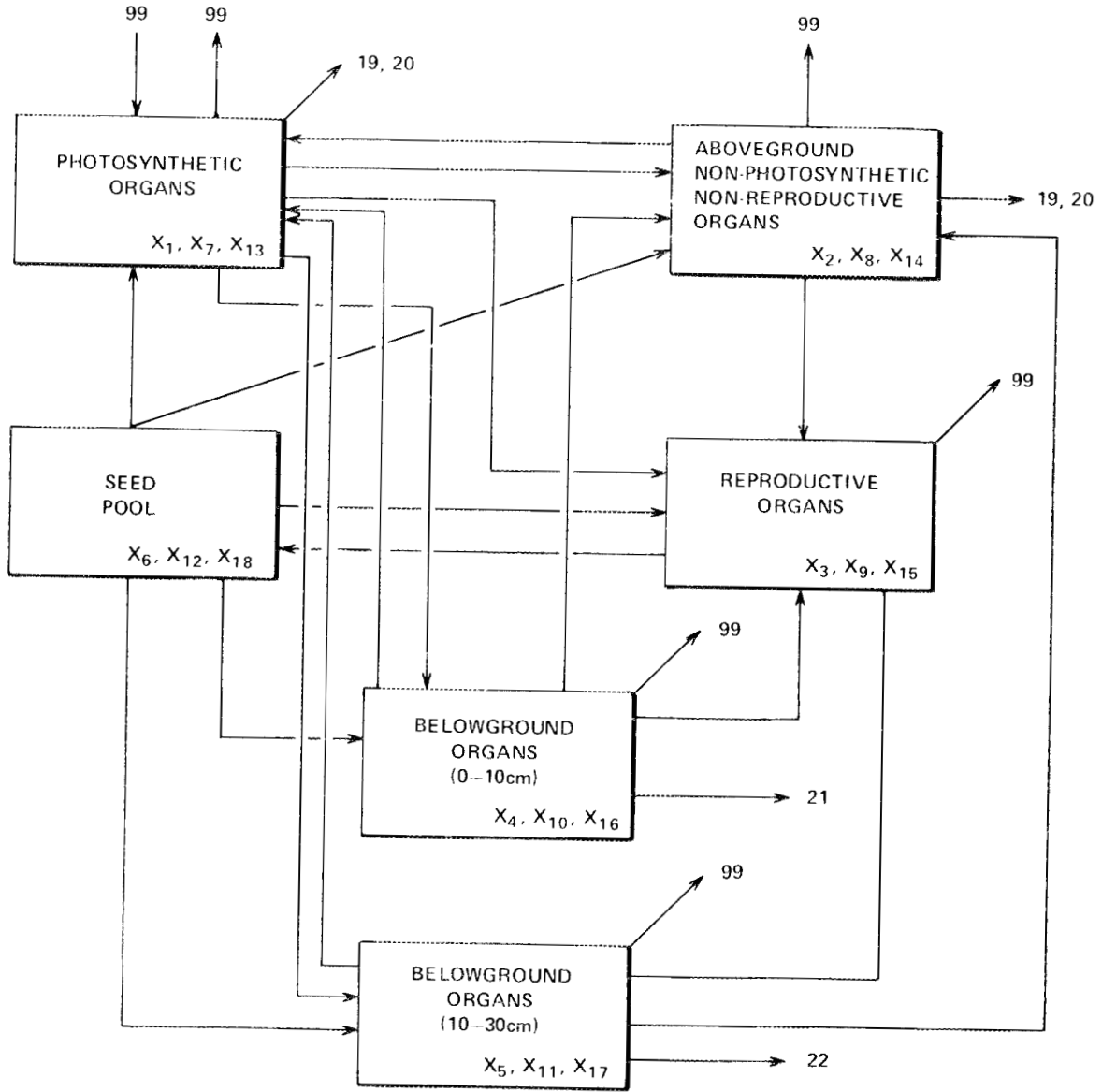


Figure 2.32. Compartmental structure of the desert and arid shrubland model - production submodel. The number 99 refers to a compartment external to the system. The numbers 19, 20, 21, and 22 refer to compartments in Figure 2.33.

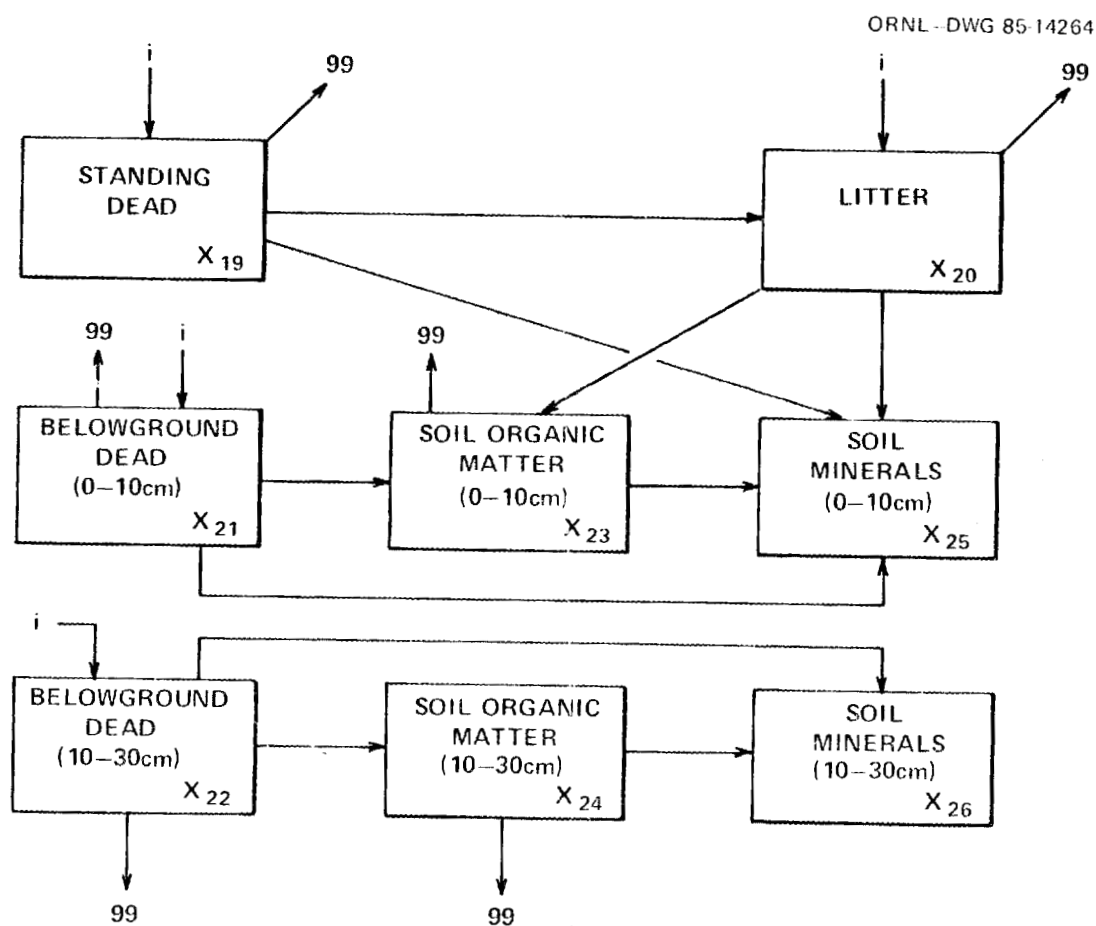


Figure 2.33. Compartmental structure of the desert and arid shrubland model - decomposition submodel. The arrows indicate the flux of biomass from compartment  $i$  to compartment  $j$ . The number 99 indicates a compartment external to the system; the letter  $i$  refers to source compartments in Figure 2.32.

herbs, and woody shrubs), and dry matter within each compartment is divided into nitrogen, ash, protein carbon, reserve carbon, and structural carbon. Similarly, the dead organic material of Figure 2.33 is divided into these five constituents. The biomass of  $n$  decomposer groups is modeled, where  $n$  is equal to the number of dead material types.

The state variables corresponding to the compartments of Figures 2.32 and 2.33 are described in Table 2.24. Recall that each organic matter state variable is subdivided into five constituents: protein carbon, reserve carbon, structural carbon, nitrogen, and ash. The soil mineral compartments contain nitrogen and ash.

Not depicted in Figure 2.33, for the sake of clarity, are compartments or state variables representing decomposer biomass. There is a specific decomposer group associated with each soil horizon, the standing dead, and the litter. These state variables are also given in Table 2.24.

#### 2.9.1.2 Driving Variables

Most processes in the model are described mechanistically and involve a number of exogenous driving variables and driving variables calculated within the model. These variables are defined in Table 2.25.

Driving variables  $Z_3$  to  $Z_7$  are incorporated as daily inputs to the simulation program. Variables  $Z_8$  and  $Z_9(i)$  are calculated within the model.

Table 2.24. State variables of the desert and arid shrubland model.

State Variable*	Description
annuals	
X <sub>1</sub>	photosynthetic organs
X <sub>2</sub>	aboveground structural organs
X <sub>3</sub>	reproductive organs
X <sub>4</sub>	belowground organs (0-10 cm)
X <sub>5</sub>	belowground organs (10-30 cm)
X <sub>6</sub>	seed pool
perennial herbs	
X <sub>7</sub>	photosynthetic organs
X <sub>8</sub>	aboveground structural organs
X <sub>9</sub>	reproductive organs
X <sub>10</sub>	belowground organs (0-10 cm)
X <sub>11</sub>	belowground organs (10-30 cm)
X <sub>12</sub>	seed pool
woody shrubs	
X <sub>13</sub>	photosynthetic organs
X <sub>14</sub>	aboveground structural organs
X <sub>15</sub>	reproductive organs
X <sub>16</sub>	belowground organs (0-10 cm)
X <sub>17</sub>	belowground organs (10-30 cm)
X <sub>18</sub>	seed pool
dead organic material	
X <sub>19</sub>	standing dead
X <sub>20</sub>	litter
X <sub>21</sub>	belowground dead (0-10 cm)
X <sub>22</sub>	belowground dead (10-30 cm)
X <sub>23</sub>	soil organic matter (0-10 cm)
X <sub>24</sub>	soil organic matter (10-30 cm)
X <sub>25</sub>	soil minerals (0-10 cm)
X <sub>26</sub>	soil minerals (10-30 cm)

Table 2.24. (Continued)

---

State Variable*	Description
decomposers	
X <sub>27</sub>	decomposers of standing dead
X <sub>28</sub>	decomposers of litter
X <sub>29</sub>	decomposers of the upper soil horizon
X <sub>30</sub>	decomposers of the lower soil horizon

---

\*Units are g C (or N or ash) ha<sup>-1</sup>.

Table 2.25. Driving variables of the desert and arid shrubland model.

Driving Variable	Description
Z <sub>1</sub> (i)	soil temperature in the ith soil horizon (°C)
Z <sub>2</sub> (i)	soil water potential in the ith soil horizon (bars)
Z <sub>3</sub>	mean daytime air temperature (°C)
Z <sub>4</sub>	mean nighttime air temperature (°C)
Z <sub>5</sub>	photoperiod (hours)
Z <sub>6</sub>	precipitation (mm)
Z <sub>7</sub>	solar radiation (cal cm <sup>-2</sup> d <sup>-1</sup> )
Z <sub>8</sub>	current phenological stage (nondimensional)
Z <sub>9</sub> (i)	soil nitrogen concentration in the ith soil horizon (g ha <sup>-1</sup> mm <sup>-1</sup> )

### 2.9.1.3 Flows Or Rate Processes

The arrows in Figures 2.32 and 2.33 represent the flux of chemical constituents between components of the model. Many of these fluxes are described by equations relating a flux rate to various combinations of driving variables and carbon concentrations. These functions are for the most part too complex to be adequately described in the limited scope of this synopsis. In Table 2.26 we only define the model fluxes and indicate which, if any, of the driving variables influence a particular flow. Full details can be found in Valentine (1974) and Parnas and Radford (1974). The notation  $F(i,j)$  indicates the flow of constituent material from compartment  $i$  to compartment  $j$ . The number 99 indicates a source/sink external to the system. All flows into the system are labelled  $F(99,j)$ ; all flows out of the system are labelled  $F(i,99)$ . Some flows involve all four of the motile constituents (storage carbon is not transferred), others involve only  $\text{CO}_2$  carbon or reserve carbon. The fluxes labelled  $F(i,j)^*$  involve only  $\text{CO}_2$  carbon; those labelled  $F(i,j)^{**}$  involve only reserve carbon. Those flows without asterisks involve all four motile constituents (i.e., nitrogen, ash, protein carbon, and reserve carbon).

Within each plant organ compartment there are three carbon subcompartments. These subcompartments are illustrated in Figure 2.34. The possible fluxes between carbon fractions are indicated by arrows in Figure 2.34 and are defined below:

$f(p,r)$  - allocation of carbon to reserve pool after protein synthesis is provided for,

Table 2.26. The flows of carbon, nitrogen, and ash simulated by the desert and arid shrubland model.

Flow <sup>a,b</sup>	Description <sup>c</sup>
Production Sub-system (Figure 2.32)	
annuals	
F(99,1)*	net daytime photosynthesis: Z <sub>2</sub> , Z <sub>3</sub> , Z <sub>5</sub> , Z <sub>7</sub>
F(1,2)**	translocation from leaves to structural organs: Z <sub>2</sub> , Z <sub>3</sub> , Z <sub>4</sub> , Z <sub>8</sub>
F(1,3)**	translocation from leaves to reproductive organs: Z <sub>2</sub> , Z <sub>3</sub> , Z <sub>4</sub> , Z <sub>8</sub>
F(1,4)**	translocation from leaves to belowground organs in the upper soil horizon: Z <sub>2</sub> , Z <sub>3</sub> , Z <sub>4</sub> , Z <sub>8</sub>
F(1,5)**	translocation from leaves to belowground organs in the lower soil horizon: Z <sub>2</sub> , Z <sub>3</sub> , Z <sub>4</sub> , Z <sub>8</sub>
F(1,19)	transfer of dead leaves to standing dead: Z <sub>1</sub> , Z <sub>2</sub> , Z <sub>8</sub>
F(1,20)	transfer of dead leaves to litter: Z <sub>1</sub> , Z <sub>2</sub> , Z <sub>8</sub>
F(1,99)*	leaf respiration: Z <sub>2</sub> , Z <sub>4</sub>
F(2,19)	transfer of dead structural parts to standing dead: Z <sub>1</sub> , Z <sub>2</sub> , Z <sub>8</sub>
F(2,20)	transfer of dead structural parts to litter: Z <sub>1</sub> , Z <sub>2</sub> , Z <sub>8</sub>
F(2,99)*	structural organ respiration: Z <sub>2</sub> , Z <sub>3</sub> , Z <sub>4</sub>
F(3,6)	seed shedding: Z <sub>1</sub> , Z <sub>2</sub> , Z <sub>8</sub>
F(3,99)*	reproductive organ respiration: Z <sub>2</sub> , Z <sub>3</sub> , Z <sub>4</sub>
F(4,21)	root mortality in the upper soil horizon: Z <sub>1</sub> (i), Z <sub>2</sub> (i)
F(4,99)*	root respiration from the upper soil horizon: Z <sub>1</sub> (i), Z <sub>2</sub> (i)
F(5,22)	root mortality in the lower soil horizon: Z <sub>1</sub> (i), Z <sub>2</sub> (i)
F(5,99)*	root respiration from the lower soil horizon: Z <sub>1</sub> (i), Z <sub>2</sub> (i)
F(6,1)	seed germination: Z <sub>1</sub> (1), Z <sub>2</sub> (1)
F(6,2)	seed germination: Z <sub>1</sub> (1), Z <sub>2</sub> (1)
F(6,3)	seed germination: Z <sub>1</sub> (1), Z <sub>2</sub> (1)
F(6,4)	seed germination: Z <sub>1</sub> (1), Z <sub>2</sub> (1)
F(6,5)	seed germination: Z <sub>1</sub> (1), Z <sub>2</sub> (1)
perennial herbs	
F(99,7)*	net daytime photosynthesis: Z <sub>2</sub> , Z <sub>3</sub> , Z <sub>5</sub> , Z <sub>7</sub>
F(7,8)**	translocation from leaves to structural organs: Z <sub>2</sub> , Z <sub>3</sub> , Z <sub>4</sub> , Z <sub>8</sub>
F(7,9)**	translocation from leaves to reproductive organs: Z <sub>2</sub> , Z <sub>3</sub> , Z <sub>4</sub> , Z <sub>8</sub>
F(7,10)**	translocation from leaves to belowground organs in the upper soil horizon: Z <sub>2</sub> , Z <sub>3</sub> , Z <sub>4</sub> , Z <sub>8</sub>

Table 2.26. (Continued)

Flow <sup>a,b</sup>	Description <sup>c</sup>
F(7,11)**	translocation from leaves to belowground organs in the lower soil horizon: Z <sub>2</sub> , Z <sub>3</sub> , Z <sub>4</sub> , Z <sub>8</sub>
F(7,19)	transfer of dead leaves to standing dead: Z <sub>1</sub> , Z <sub>2</sub> , Z <sub>8</sub>
F(7,20)	transfer of dead leaves to litter: Z <sub>1</sub> , Z <sub>2</sub> , Z <sub>8</sub>
F(7,99)*	leaf respiration: Z <sub>2</sub> , Z <sub>4</sub>
F(8,19)	transfer of dead structural parts to standing dead: Z <sub>1</sub> , Z <sub>2</sub> , Z <sub>8</sub>
F(8,20)	transfer of dead structural parts to litter: Z <sub>1</sub> , Z <sub>2</sub> , Z <sub>8</sub>
F(8,99)*	structural organ respiration: Z <sub>2</sub> , Z <sub>3</sub> , Z <sub>4</sub>
F(9,12)	seed shedding: Z <sub>1</sub> , Z <sub>2</sub> , Z <sub>8</sub>
F(9,99)*	reproductive organ respiration: Z <sub>2</sub> , Z <sub>3</sub> , Z <sub>4</sub>
F(10,7)	translocation during leafing out: Z <sub>1</sub> (1), Z <sub>2</sub> (1), Z <sub>8</sub>
F(10,8)	translocation during leafing out: Z <sub>1</sub> (1), Z <sub>2</sub> (1), Z <sub>8</sub>
F(10,9)	translocation during leafing out: Z <sub>1</sub> (1), Z <sub>2</sub> (1), Z <sub>8</sub>
F(10,21)	root mortality in the upper soil horizon: Z <sub>1</sub> (1), Z <sub>2</sub> (1)
F(10,99)*	root respiration from the upper soil horizon: Z <sub>1</sub> (1), Z <sub>2</sub> (1)
F(11,7)	translocation during leafing out: Z <sub>1</sub> (2), Z <sub>2</sub> (2), Z <sub>8</sub>
F(11,8)	translocation during leafing out: Z <sub>1</sub> (2), Z <sub>2</sub> (2), Z <sub>8</sub>
F(11,9)	translocation during leafing out: Z <sub>1</sub> (2), Z <sub>2</sub> (2), Z <sub>8</sub>
F(11,22)	root mortality in the lower soil horizon: Z <sub>1</sub> (2), Z <sub>2</sub> (2)
F(11,99)*	root respiration from the lower soil horizon: Z <sub>1</sub> (2), Z <sub>2</sub> (2)
F(12,7)	seed germination: Z <sub>1</sub> (1), Z <sub>2</sub> (1)
F(12,8)	seed germination: Z <sub>1</sub> (1), Z <sub>2</sub> (1)
F(12,9)	seed germination: Z <sub>1</sub> (1), Z <sub>2</sub> (1)
F(12,10)	seed germination: Z <sub>1</sub> (1), Z <sub>2</sub> (1)
F(12,11)	seed germination: Z <sub>1</sub> (1), Z <sub>2</sub> (1)
woody shrubs <sup>d</sup>	
F(99,13)*	net daytime photosynthesis
F(13,14)**	translocation from leaves to structural organs
F(13,15)**	translocation from leaves to reproductive organs
F(13,16)**	translocation from leaves to belowground organs in the upper soil horizon

Table 2.26. (Continued)

Flow <sup>a,b</sup>	Description <sup>c</sup>
F(13,17)**	translocation from leaves to belowground organs in the lower soil horizon
F(13,19)**	transfer of dead leaves to standing dead
F(13,20)	transfer of dead leaves to litter
F(13,99)	leaf respiration
F(14,13)	translocation during leafing out
F(14,15)	translocation during leafing out
F(14,19)	transfer of dead structural parts to standing dead
F(14,20)	transfer of dead structural parts to litter
F(14,99)*	structural organ respiration
F(15,18)	seed shedding
F(15,99)*	reproductive organ respiration
F(16,13)	translocation during leafing out
F(16,15)	translocation during leafing out
F(16,21)	root mortality in the upper soil horizon
F(16,99)*	root respiration from the upper soil horizon
F(17,13)	translocation during leafing out
F(17,15)	translocation during leafing out
F(17,22)	root mortality in the lower soil horizon
F(17,99)*	root respiration from the lower soil horizon
F(18,13)	seed germination
F(18,14)	seed germination
F(18,15)	seed germination
F(18,16)	seed germination
F(18,17)	seed germination
Decomposition Sub-system (Figure 2.33) <sup>e</sup>	
F(i,19)	input of dead organic matter to standing dead
F(19,25)	mineralization of nitrogen from standing dead
F(19,25)	mineralization of ash from standing dead
F(19,99)*	decomposer respiration from standing dead
F(i,20)	input of dead organic matter to litter
F(20,23)	external breakdown of litter
F(20,25)	mineralization of nitrogen from litter
F(20,25)	mineralization of ash from litter
F(20,99)*	decomposer respiration from litter
F(i,21)	input of dead organic matter to belowground dead in the upper soil horizon
F(21,23)	external breakdown of belowground dead in the upper soil horizon
F(21,25)	mineralization of nitrogen from belowground dead in the upper soil horizon

Table 2.26. (Continued)

Flow <sup>a,b</sup>	Description <sup>c</sup>
F(21,25)	mineralization of ash from belowground dead in the upper soil horizon
F(21,99)*	decomposer respiration from belowground dead in the upper soil horizon
F(i,22)	input of dead organic matter to belowground dead in the lower soil horizon
F(22,24)	external breakdown of belowground dead in the lower soil horizon
F(22,26)	mineralization of nitrogen from belowground in the lower soil horizon
F(22,26)	mineralization of ash from belowground dead in the lower soil horizon
F(22,99)*	decomposer respiration from belowground dead in the lower soil horizon
F(23,25)	mineralization of nitrogen from the soil organic matter of the upper soil horizon
F(23,25)	mineralization of ash from the soil organic matter of the upper soil horizon
F(23,99)	decomposer respiration from the soil organic matter of the upper soil horizon
F(24,26)	mineralization of nitrogen from the soil organic matter of the lower soil horizon
F(24,26)	mineralization of ash from the soil organic matter of the lower soil horizon
F(24,99)*	decomposer respiration from the soil organic matter of the lower soil horizon

<sup>a</sup>Units are g C (or N or ash) ha<sup>-1</sup> d<sup>-1</sup>.

<sup>b</sup>See text for significance of asterisks.

<sup>c</sup>Includes a list of those driving variables (if any) that influence the flow.

<sup>d</sup>The influence of driving variables is identical to that for perennial herbs.

<sup>e</sup>All respiratory fluxes and external breakdown are influenced by the temperature ( $Z_1$ ) and water potential ( $Z_2$ ) of the appropriate horizon. Litter and standing dead decay are driven by air temperature ( $Z_3$ ,  $Z_4$ ) and soil water potential in the upper horizon ( $Z_2(1)$ ). Mineralization is also influenced by soil nitrogen concentration.

ORNL-DWG 85-14265

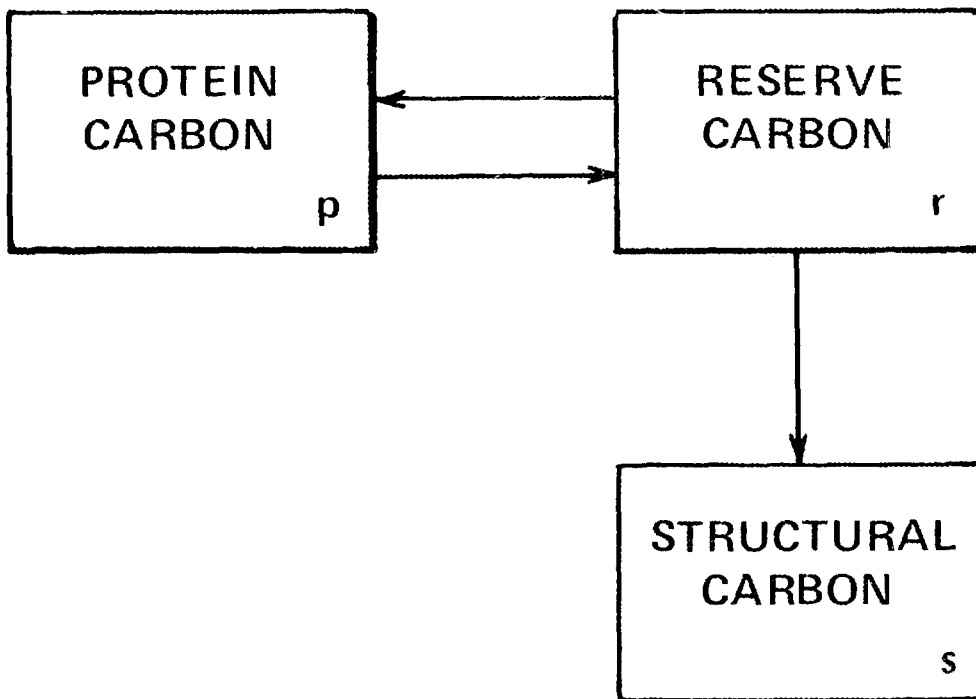


Figure 2.34. Compartmental representation of carbon components in living plant compartments of the desert and arid shrubland model. The arrows represent the transformation of carbon from one form to another.

$f(r,p)$  - allocation of reserve carbon to protein carbon for protein synthesis,

$f(r,s)$  - allocation of reserve carbon to structural carbon.

Decomposers are associated with the standing dead, litter, belowground dead, and soil organic matter compartments of Figure 2.33. These are not depicted in the figure for the sake of clarity. The flows between decomposers, substrate, and material sink not included in Figure 2.33 are defined in Table 2.27.

#### 2.9.1.4 Photosynthesis And Respiration

The model computes a mean hourly rate of net daytime carbon fixation. This net daytime photosynthesis is a function of mean daytime air temperature ( $Z_3$ ), mean hourly irradiance for the day ( $Z_7'$ ), and mean weighted soil water potential ( $Z_2'$ ), or

$$P_H = P_{HMAX} f_1(Z_3) f_2(Z_7') f_3(Z_2'), \quad (2.40)$$

where

$P_H$  = realized hourly rate of net photosynthesis,

$P_{HMAX}$  = optimal hourly rate of net photosynthesis,

$f_1(Z_3)$  = effect of air temperature,

$f_2(Z_7')$  = effect of irradiance,

$f_3(Z_2')$  = effect of soil water.

The functional forms for  $f_1$ ,  $f_2$ , and  $f_3$  can be found in Valentine (1974) and Goodall (1981). The model allows for changes in  $P_{HMAX}$  and optimal temperature ( $Z_3$  where  $f_1(Z_3) = 1.0$ ) as a result of acclimatization (see Valentine 1974).

Table 2.27. The flows of carbon and nitrogen simulated by the desert and arid shrubland model that are not depicted in Figure 2.33.

Flow <sup>a</sup>	Description
F(19,27)	assimilation of standing dead material by the standing dead decomposers
F(20,28)	assimilation of litter material by litter decomposers
F(21,29)	assimilation of upper soil horizon belowground dead by decomposers of the upper soil horizon
F(22,23)	assimilation of lower soil horizon belowground dead by decomposers of the lower soil horizon
F(23,29)	assimilation of upper soil horizon soil organic matter by decomposers of the upper soil horizon
F(24,30)	assimilation of lower soil horizon soil organic matter by decomposers of the lower soil horizon
F(25,28)	nitrogen immobilization by litter decomposers
F(25,29)	nitrogen immobilization by decomposers of the upper soil horizon
F(26,30)	nitrogen immobilization by decomposers of the lower soil horizon
F(27,19)	death of standing dead decomposers
F(28,20)	death of litter decomposers
F(29,23)	death of upper soil horizon decomposers
F(30,24)	death of lower soil horizon decomposers

<sup>a</sup>Units are g C or g N ha<sup>-1</sup> d<sup>-1</sup>.

The daily net photosynthesis rate is given by

$$P_D = P_H Z_5 , \quad (2.41)$$

where  $Z_5$  is the photoperiod. The amount of carbon actually fixed per day ( $P_N$ ) is

$$P_N = P_D X_{Ip} , \quad (2.42)$$

where  $X_{Ip}$  is the amount of protein carbon in the photosynthetic organs. Equations 2.40, 2.41, and 2.42 are applied to annuals, perennial herbs, and woody shrubs. Constants such as PHMAX may vary with plant type, and  $X_{Ip}$  is replaced by  $X_{1p}$ ,  $X_{7p}$ , and  $X_{13p}$ .

Hourly rates of respiration for photosynthetic organs are averages over dark hours. Hourly rates of respiration for non-photosynthetic organs are averages over a 24-hour period. Respiration rates for the organs of each plant type are calculated as functions of air temperature (soil temperature for roots) and soil water potential using equations of the form

$$R_H(j) = a_1(j) + a_2(j) \exp(a_3(j)T) f_4(W) , \quad (2.43)$$

where

$R_H(j)$  = hourly respiration rate of the jth organ,

$a_1(j)$ - $a_3(j)$  = rate parameters,

$T$  = temperature (air temperature for aboveground organs, soil temperature for belowground organs, adjusted for acclimation,

$f_4(W)$  = the effect of soil water potential,

$W$  = soil water potential of the horizon  
appropriate for organ  $j$ .

The functional form of  $f_4(W)$  is described in Valentine (1974) and Goodall (1981). Daily rates and amounts of carbon respired are obtained by the appropriate transformations.

#### 2.9.1.5 Release Of Carbon Through Decomposition

Carbon dioxide is released during decomposition through decomposer respiration. The rate of carbon release via microbial decomposition is

$$R_m = \sum_c (\sum_i r_{ic}) , \quad (2.44)$$

where

$R_m$  = rate of carbon release,

$\sum_c$  = summation over all carbon types,

$\sum_i$  = summation over all dead organic matter compartments,

$r_{ic}$  = rate of respiration of carbon type  $c$  from decomposition of dead organic matter type  $i$ .

The rate  $r_{ic}$  is given by

$$r_{ic} = (1 - e)D_{ic} , \quad (2.45)$$

where  $e$  is the efficiency of microbial assimilation, and  $D_{ic}$  is the rate of decomposition of carbon type  $c$  in dead organic matter type  $i$ .

#### 2.9.2 Seasonal Photosynthesis And Respiration

Input data for the driving variables were generated by a subroutine provided by Valentine (1974) that involved empirically

derived parameters, data tables, and sinusoidal variations with time. The driving variables permitted simulation of seasonal total ecosystem (less live plant consumers) photosynthesis and respiration. A plot of daily fluxes, sampled weekly, is shown in Figure 2.35. Carbon fluxes were converted to CO<sub>2</sub> fluxes using a conversion factor of 1 g C = 3.66 g CO<sub>2</sub> (Brown and Trlica 1974). Seasonal net CO<sub>2</sub> exchange (respiration minus photosynthesis) between the vegetation and the atmosphere is plotted in Figure 2.36.

## 2.10 CROPLAND MODEL

Seasonal carbon dynamics in a cropland ecosystem are modeled with the BACROS model of de Wit et al. (1978). The model simulates the vegetative growth phase of a corn (Zea mays L.) crop in Flevoland, The Netherlands (approximately 52°30'N, 5°30'E). The model is described by differential equations, and the solutions involve a time step of one hour.

### 2.10.1 Structure Of The Model

#### 2.10.1.1 Compartments

There are four compartments in the model; three biomass compartments and a plant water compartment (Figure 2.37). The state variables corresponding to these compartments are defined in Table 2.28.

#### 2.10.1.2 Driving Variables

Seasonal CO<sub>2</sub> dynamics are driven by micro-weather. A complex weather submodel calculates the daily course of micro-weather

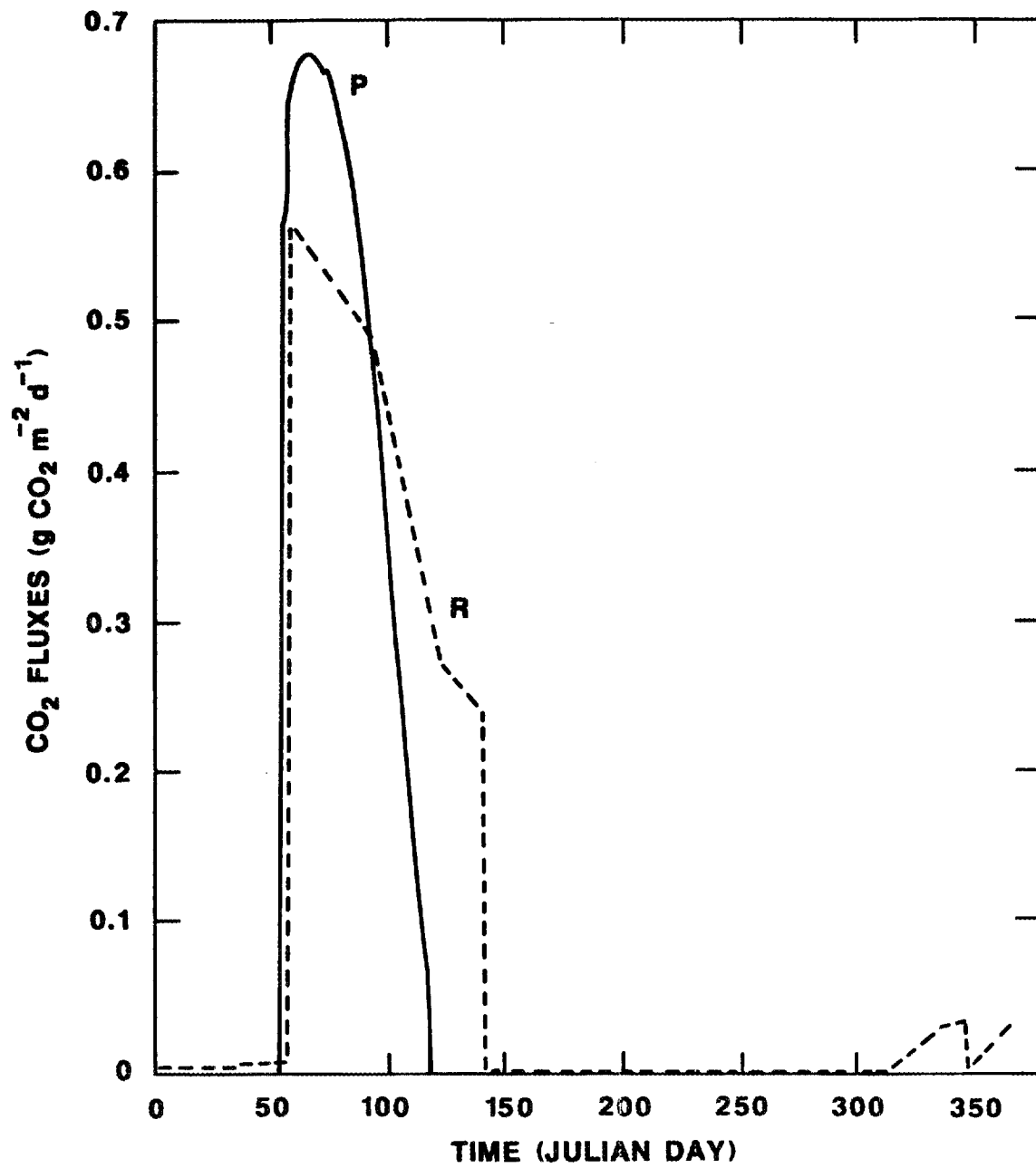


Figure 2.35. Seasonal total ecosystem photosynthesis (P) and respiration (R) for a stand of arid land vegetation. Flux units are g CO<sub>2</sub> m<sup>-2</sup> d<sup>-1</sup>.

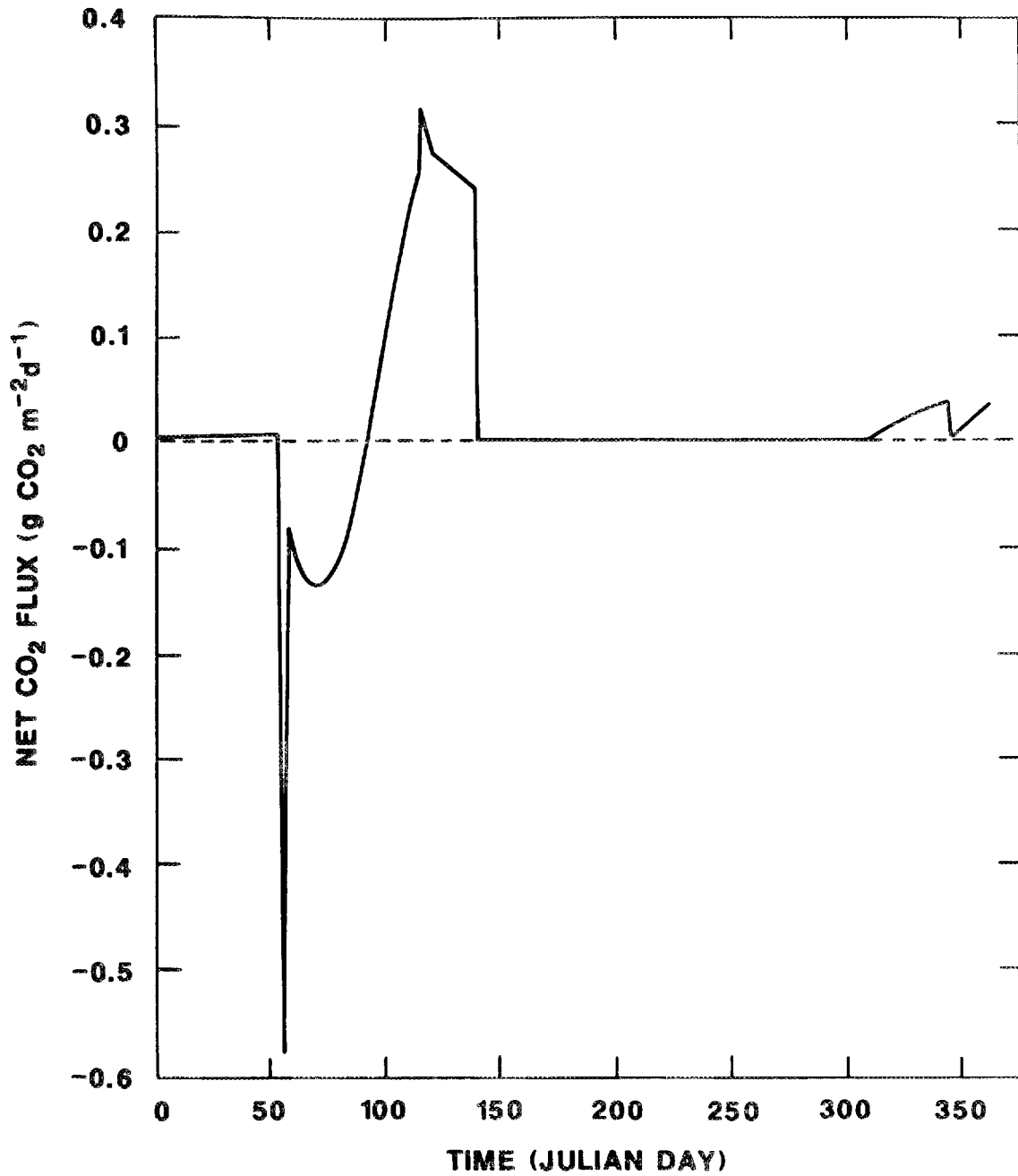


Figure 2.36. Seasonal net CO<sub>2</sub> exchange between the atmosphere and a stand of arid land vegetation. Net flux is respiration minus photosynthesis. Flux units are g CO<sub>2</sub> m<sup>-2</sup> d<sup>-1</sup>.

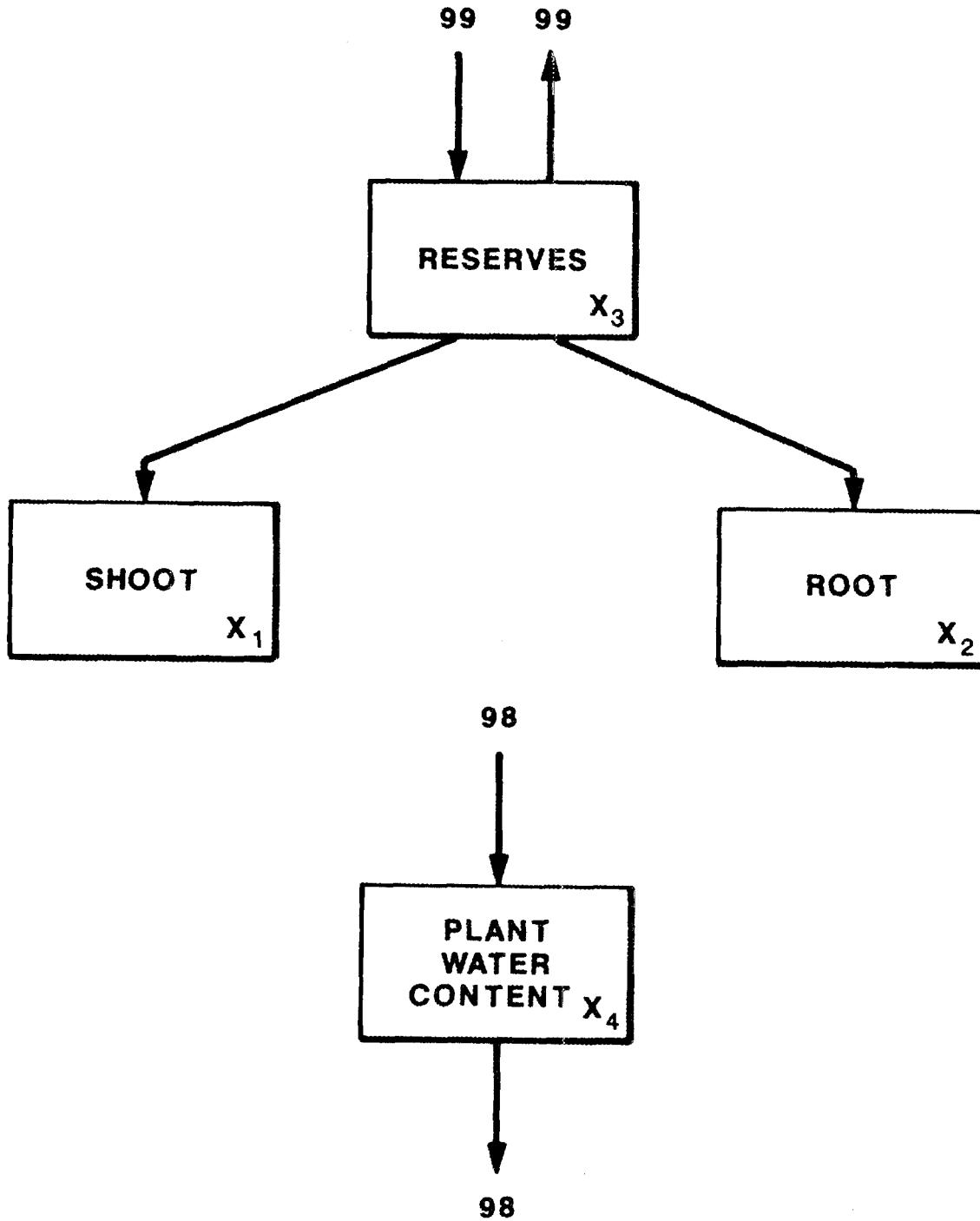


Figure 2.37. Compartmental structure of the cropland model. The arrows indicate the flux of organic matter or water from compartment  $i$  to compartment  $j$ . The number 99 indicates a carbon source or sink, and the number 98 indicates a water source or sink.

Table 2.28. State variables of the cropland model.

Variable	Description	Unit
$X_1$	shoot weight	(kg dry matter ha <sup>-1</sup> )
$X_2$	root weight	(kg dry matter ha <sup>-1</sup> )
$X_3$	weight of reserve starches	(kg dry matter ha <sup>-1</sup> )
$X_4$	plant water content	(kg H <sub>2</sub> O ha <sup>-1</sup> )

parameters within the crop and soil from standard meteorological data (see de Wit et al. 1978 for details). Daily values of five weather parameters are input data for this weather submodel. These driving variables are described in Table 2.29. In addition to these exogenous driving variables, a number of time-varying parameters (e.g., chemical composition of tissue) are used in forcing functions.

#### 2.10.1.3 Flows Or Rate Processes

The arrows between compartments in Figure 2.37 represent the flows of organic matter. The detailed functional representations of these flows and the assumptions involved are described by de Wit et al. (1978). In Table 2.30 we define these fluxes and indicate which, if any, of the driving variables influence a particular flow. Figure 2.37 and Table 2.30 do not show the complex interactions between state variables, fluxes, and auxiliary variables (see de Wit et al. 1978). Photosynthesis and respiration are discussed more fully in the next section. The units of the fluxes are kg dry matter  $\text{ha}^{-1} \text{h}^{-1}$ . The notation  $F(i,j)$  represents the flow of material from compartment  $i$  to compartment  $j$ . The numbers 99 and 98 refer to carbon and water compartments (respectively) external to the system. All flows into the system are labelled  $F(99,j)$  or  $F(98,j)$ , and all flows out of the system are labelled  $F(i,99)$  or  $F(i,98)$ .

#### 2.10.1.4 Photosynthesis And Respiration

Photosynthetic assimilation of  $\text{CO}_2$  is described by:

$$F_n = (F_m - F_d)(1 - \exp(-eR_v/F_m)) + F_d , \quad (2.46)$$

Table 2.29. Driving variables of the cropland model.

Driving Variable	Description
Z <sub>1</sub>	wind speed (m s <sup>-1</sup> )
Z <sub>2</sub>	dew point temperature (°C)
Z <sub>3</sub>	daily minimum temperature (°C)
Z <sub>4</sub>	daily maximum temperature (°C)
Z <sub>5</sub>	solar radiation (J m <sup>-2</sup> d <sup>-1</sup> )

Table 2.30. The flows of carbon and water simulated by the cropland model.

Flow <sup>a</sup>	Description <sup>b</sup>
F(99,1)	photosynthesis: Z <sub>3</sub> , Z <sub>4</sub> , Z <sub>5</sub>
F(3,1)	conversion and translocation from reserves to shoots
F(3,2)	conversion and translocation from reserves to roots
F(3,99)	respiration
F(98,4)	water uptake by plant: Z <sub>3</sub> , Z <sub>4</sub>
F(4,98)	transpiration: Z <sub>1</sub> , Z <sub>2</sub> , Z <sub>3</sub> , Z <sub>4</sub> , Z <sub>5</sub>

<sup>a</sup>Units of the flows are  $\text{g m}^{-2} \text{h}^{-1}$  for water and  $\text{kg ha}^{-1} \text{h}^{-1}$  for carbon.

<sup>b</sup>Includes a list of those driving variables (if any) that influence the flow.

where  $F_n$  is net assimilation,  $R_v$  is absorbed radiant flux in the photosynthetically active range,  $F_m$  is the maximum rate of net assimilation at high light intensities,  $e$  is efficiency at the light compensation point, and  $F_d$  is net assimilation in the dark (i.e., dark respiration). Dark respiration is a constant proportion of positive  $CO_2$  assimilation.

The maximum rate of net assimilation ( $F_m$ ) is dependent on leaf temperature and a limiting feedback from the level of reserve photosynthate. Stomatal control is reflected in the dependence of the net assimilation rate on intercellular  $CO_2$ -concentration. When leaf water is limiting, net assimilation is also governed by the stomatal resistance for transpiration. Details of these functional representations and the complex calculation of energy and water balances used in the simulation of photosynthesis can be found in de Wit et al. (1978).

Total plant respiration is the sum of growth and maintenance respiration of the shoots and roots,  $CO_2$  evolution resulting from mineral uptake, and  $CO_2$  evolution resulting from the decarboxylation of organic anions. Respiration associated with mineral uptake is a constant times the starch required for mineral uptake (an auxiliary variable in the model), and respiration due to decarboxylation is a constant times the rate of transport of organic anions to the root. Maintenance respiration is proportional to the starch requirements for maintenance of the shoots and roots. These starch requirements are mobilized from the reserve compartment.

Although the respective costs of maintaining the roots and shoots may differ, the proportionality constant is the same for the two compartments. Growth respiration is the sum of the respiration costs associated with the growth rates of proteins, carbohydrates, fats, lignins, minerals, and the starch requirements for the transport of organic ions in the roots and shoots. These costs are a constant proportion of the associated growth rates. The simulation of these growth rates and the conversions from photosynthate to the various constituents is described in detail by de Wit et al. (1978).

#### 2.10.1.5 Release Of Carbon Through Decomposition

The BACROS model of de Wit et al. (1978) does not consider respiratory losses from dead plant material and soil organic matter. In fact, the model does not even provide for plant mortality or the production of litter during or after the growing season. BACROS is not unique among crop models in this regard (see King and DeAngelis 1986).

Litter production and, consequently,  $\text{CO}_2$  evolution due to decomposition are heavily dependent upon culture practices. The production and fate of crop residues depend on whether the corn is grown for grain or silage, on whether stems left after the harvest of the grain (the stover) are left standing, mulched, or removed from the field, and whether there is conventional tillage, stubble mulch farming, or no tillage. de Wit et al. (1978) do not describe the culture practices of the crop they simulate.

Given that BACROS does not consider litter production or decomposition, and given the lack of any decomposition model that can be readily coupled with BACROS (see King and DeAngelis 1987), we are forced to make some very simplifying assumptions about the CO<sub>2</sub> evolution associated with decomposition in the corn field. We assume that the crop is grown for grain production, and that 37% of net primary production is harvested with the grain. We base this percentage on an assumed harvest index (yield/aboveground net production) of 0.43 (Mitchell 1984). We further assume that all crop residues decay at a constant rate during the non-growing season when photosynthesis is zero), and there is no net litter accumulation (i.e., all residues are gone by the beginning of the following growing season). Under the assumption that litter production is minimal during crop growth, there is no litter decay during the growing season. Alternative, more realistic, treatments are possible, but they are too involved to be implemented within the scope of this report. This limitation can be alleviated with the development of agroecosystem models that consider both production and decomposition processes over an entire year. Current model development is moving in this direction (Basil Acock, pers. comm.).

#### 2.10.2 Seasonal Photosynthesis And Respiration

The daily values of the cropland model's driving variables for a field in Flevoland, The Netherlands, provided by de Wit et al. (1978) were used as model input. A plot of simulated photosynthesis and live plant respiration is shown in Figure 2.38. Remember that

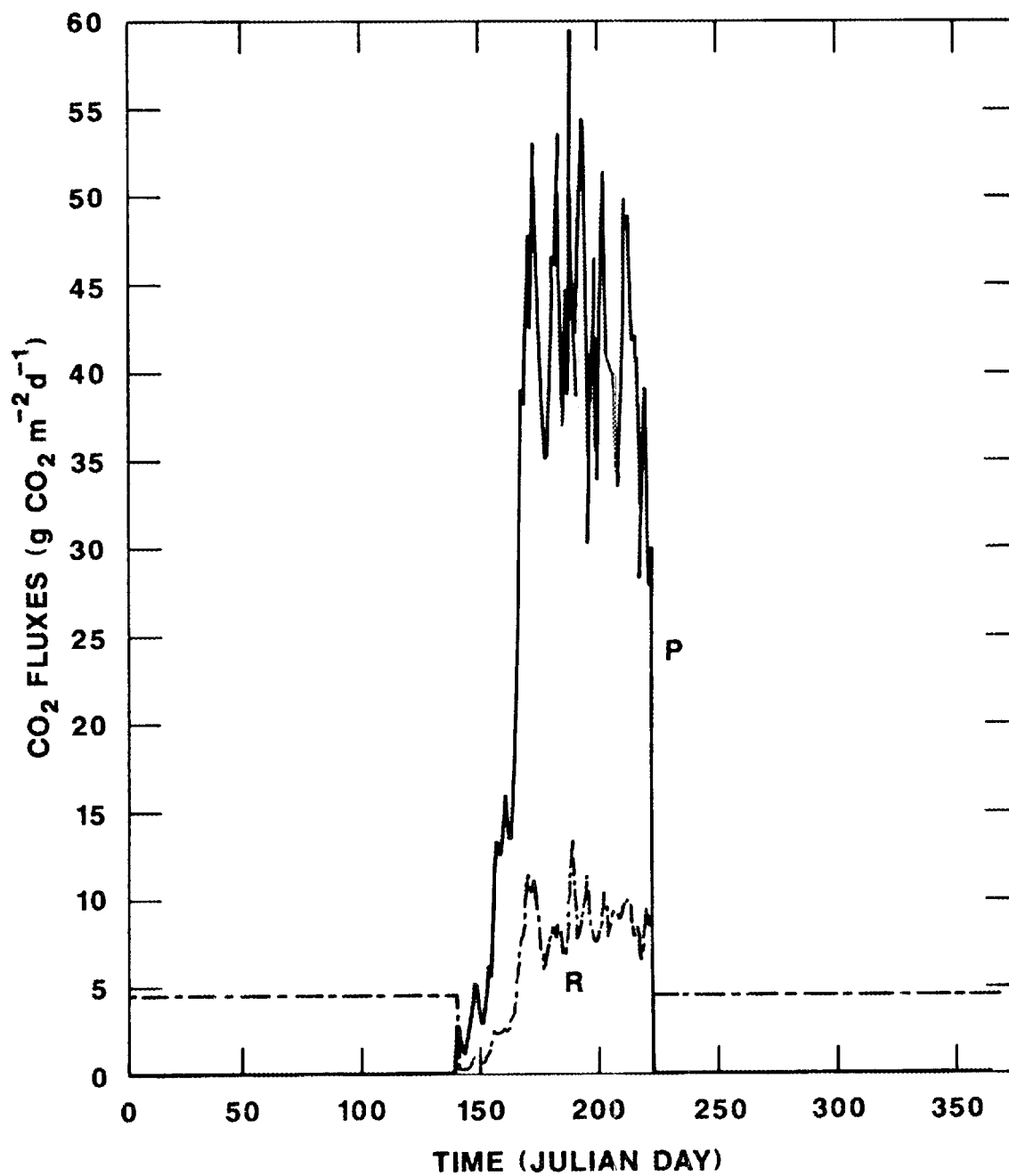


Figure 2.38. Seasonal photosynthesis (P) and respiration (R) for a corn crop. Flux units are g CO<sub>2</sub> m<sup>-2</sup> d<sup>-1</sup>.

the constant respiratory fluxes during the non-growing season are the result of simplifying model assumptions. Similarly, respiration during the growing season is only autotrophic respiration. Carbon dioxide fluxes generated by the model ( $\text{kg CO}_2 \text{ ha}^{-1} \text{ h}^{-1}$ ) were converted to  $\text{g CO}_2 \text{ m}^{-2} \text{ d}^{-1}$  by summing hourly fluxes for each day and using a conversion factor of 0.1. Seasonal net  $\text{CO}_2$  exchange (respiration minus photosynthesis) between the cropland and the atmosphere is plotted in Figure 2.39.

Together, the cropland model and the nine models of natural ecosystems (Sections 2.1 to 2.9) are an appropriate set of site-specific ecosystem models. They are good representative models of their ecosystem types, they simulate the  $\text{CO}_2$  dynamics necessary for incorporation into a seasonal  $\text{CO}_2$  exchange function, and they meet the criteria set forth at the beginning of this chapter. The set of models is not unique; other models could be substituted as ecosystem representatives. However, the problem of extrapolation, of how to extend site-specific models of  $\text{CO}_2$  exchange across larger heterogeneous regions, is characteristic of any set of site-specific models, regardless of the identity of individual members. In the following chapters we investigate this central problem of extrapolation using the set of ten site-specific models described in this chapter.

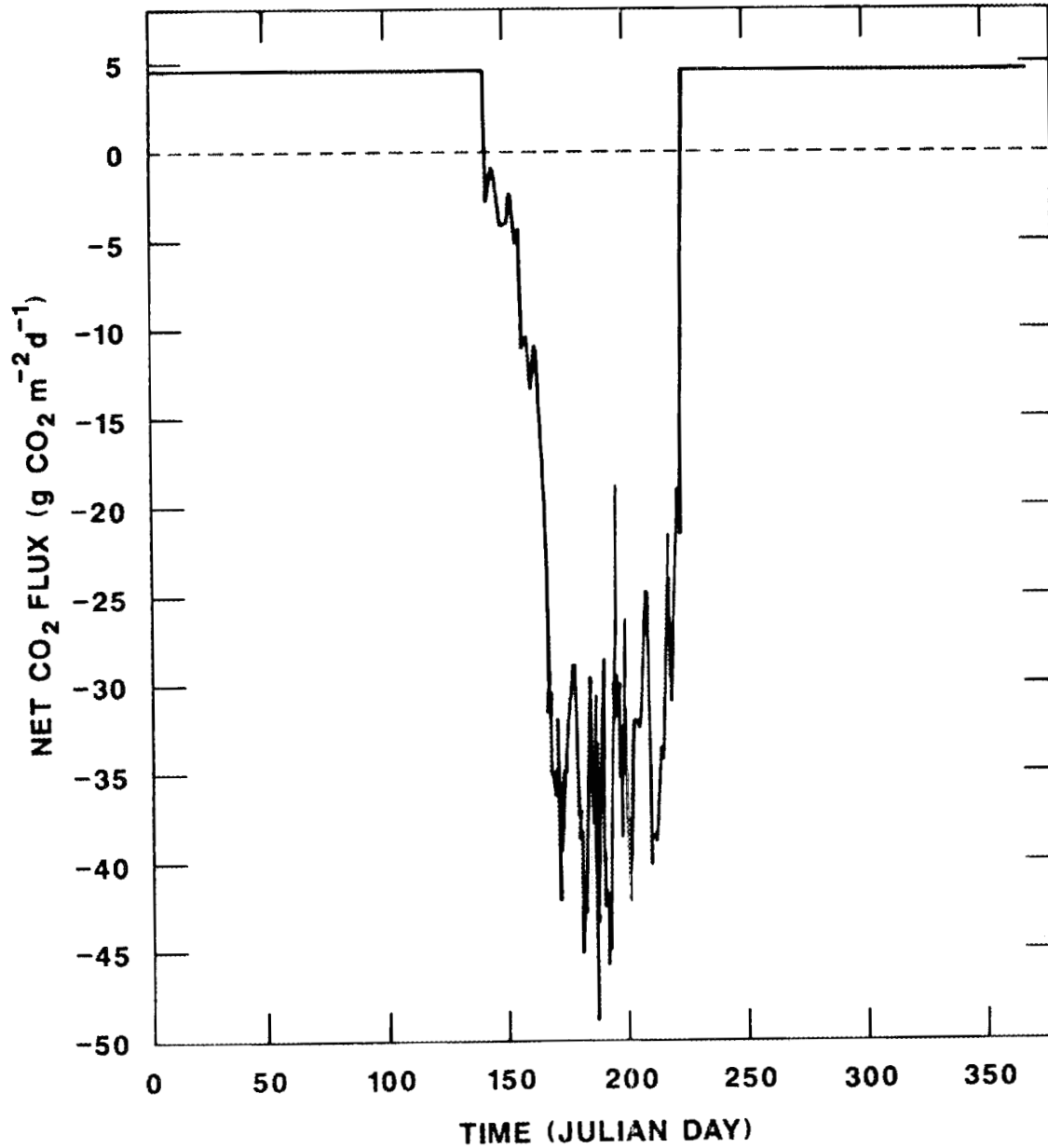


Figure 2.39. Seasonal net CO<sub>2</sub> exchange between the atmosphere and a corn crop. Net flux is respiration minus photosynthesis. Flux units are g CO<sub>2</sub> m<sup>-2</sup> d<sup>-1</sup>.

## CHAPTER 3

A GLOBAL CO<sub>2</sub> EXCHANGE FUNCTION FOR THE TERRESTRIAL BIOSPHERE

Generating a global CO<sub>2</sub> exchange function from the site-specific models of Chapter 2 is an extrapolation problem. The models must be extended to cover areas larger than the particular sites for which they were originally designed. Phase one of the extrapolation process is the identification of the geographical extent of the biome or ecosystem type over which each of the site-specific models can be taken as representative. Phase two is the simulation of regional CO<sub>2</sub> exchanges at the resolution of the tracer transport model involved. This chapter describes a simple extrapolation (presented as a first approximation), generates a set of CO<sub>2</sub> exchange functions that differ in their geographic resolution, and compares these exchange functions with existing functions of the same resolution.

## 3.1 BIOME IDENTIFICATION AND GEOGRAPHICAL EXTENT

## 3.1.1 Model Biome Identification

Any classification of ecosystems or plant formations is to some degree subjective (Lieth 1975a). The classification scheme, and mapping of geographical distribution, is dependent on the criteria for similarity (e.g., biotic or climatic) and the purpose behind the classification. No matter how classified, a biome will have a considerable amount of internal heterogeneity in vegetative, climatic, and edaphic characteristics, as well as land use and

successional stages. We dealt with this problem of biome identification and heterogeneity by combining the site-specific models with the classification and mapping of major world ecosystems described by Olson, Watts, and Allison (1983). In essence we allowed the models of Chapter 2 to define the biomes.

The ten site-specific models encompass at some coarse level much of the variation in global biome types; they include tropical and temperate sites, forest and grassland, and deciduous and evergreen vegetation. The land cover classification of Olson, Watts, and Allison (1983), hereafter referred to as the Olson classification, involves a much finer dissection of vegetation. Each cell of  $0.5^\circ$  latitude by  $0.5^\circ$  longitude is assigned to one of over 50 ecosystem types. Our problem was one of aggregation. We had to assign each of the Olson ecosystem complexes to the most appropriate site-specific model, on average, a five to one aggregation.

The assignments were largely based on obvious structural characteristics and general type similarities. For example, forest types within the Olson classification were assigned to one of the forest models, and not to the grassland model. Forest types dominated by conifers were assigned to one of the two conifer models, rather than one of the broadleaf models. These assignment decisions, as well as more subtle decisions, were guided by the descriptions of the ecosystem complexes provided by Olson, Watts, and Allison (1983) and their global map of ecosystem complexes. Problematic assignments were, on occasion, influenced by the classifications and mappings of global vegetation and land use

provided by Haden-Guest, Wright, and Tecliff (1956), Walter (1985), Espenshade and Morrison (1983), Matthews (1983), and Wilson and Henderson-Sellers (1985). Throughout the process, we made subjective judgments on the appropriateness of particular assignments. These judgments were influenced by the general "intuition" that developed from working with the site-specific models, the Olson classification, the supplementary references, and several iterations of the assignment process. We present the final assignments (Table 3.1) and briefly describe our reasoning behind a couple of the more problematic assignments. A description of Olson's land cover categories or ecosystem complexes can be found in Olson, Watts, and Allison (1983).

For the most part, a particular assignment did not vary with geographic location. An exception is Olson's forest/field complex. None of the site-specific models reflect the heterogeneous mixture of woodlands and open fields or disturbed areas described by this type (see Olson, Watts, and Allison 1983). Consequently, we decided that those areas designated as forest/field would be assigned to the site-specific forest model that best fit the surrounding intact forest. We reasoned that in many cases these forest/field mosaics were the result of incomplete land clearing, and hence the forest elements of the complex would be similar to the forests surrounding that area. We assigned each area of forest/field to the site-specific model specified by Olson's classification of the neighboring intact forest using our derived correspondence between Olson's classification and the site-specific models (Table 3.1).

Table 3.1. The correspondence between the site-specific models and Olson's land cover categories.

Site-specific model <sup>a</sup>	Olson ecosystem complex
Temperate Broadleaf Deciduous Forest (11)	Cool hardwood-conifer Deciduous warm woods with conifers Deciduous (summergreen forest) Forest/field complex <sup>b</sup>
Temperate Broadleaf Evergreen Forest (15)	Broad-leaved evergreen or partly deciduous forest Evergreen broad-leaved and/or conifer forest Broad-leaved south temperate forest Tropical montane complex Mediterranean type Forest/field complex <sup>b</sup>
Cool Coniferous Forest (22)	Cool conifer forest Main taiga Southern continental taiga Northern or maritime taiga Forest/field complex <sup>b</sup>
Warm Coniferous Forest (25)	Warm or hot conifer forest Partly evergreen broad-leaved and/or subtropical conifer forest Other dry or highland tree or shrub types <sup>b</sup> Forest/field complex <sup>b</sup>
Tropical Moist Evergreen Forest (33)	Evergreen equatorial forest Tropical seasonal forest Forest/field complex <sup>b</sup>
Tropical Dry Deciduous Forest (35)	Tropical dry forest and woodland Forest/field complex <sup>b</sup>
Tundra (44)	Tundra Wooded tundra Bog/mire of cool or cold climates
Grassland (45)	Cool grassland/scrub Warm or hot shrub and grassland Siberian parklands Tibetan meadows Heath and moorland Tropical savanna and woodlands Succulent and thorn woods and scrub Semiarid woodland
Desert and Arid Shrubland (55)	Desert and semidesert Semidesert scrub Other dry or highland tree or shrub types <sup>b</sup>
Cropland (66)	Cool or cold farms, town, etc. Warm or hot farms, towns, etc. Cold irrigated dryland row crops Cool irrigated dryland row crops Warm-hot irrigated dryland row crops Paddyland Field/woods complex

<sup>a</sup>The number in parentheses is the model's classification code (see Section 3.1.2).

<sup>b</sup>In part, depending on the geographic location of the ecosystem complex (see Section 3.1.1).

The neighboring forests can differ, of course, from one geographic location to another; therefore, we used Olson's map of ecosystem complexes (Olson, Watts, and Allison 1983) to determine the neighboring forest type. Thus, for example, forest/field complexes of the extreme southeastern United States were assigned to the warm coniferous forest model (Section 2.4), and forest/field complexes of Indonesia were assigned to the tropical moist evergreen forest model (Section 2.5). Occasionally, the appropriate forest type could not be determined from the Olson, Watts, and Allison (1983) map. In these cases, decisions based on Kuchler's natural vegetation maps (Espenshade and Morrison 1983) and forest information provided by Haden-Guest, Wright, and Tecliff (1956) were used to make the assignment.

The assignment of forest/field complexes to forest biomes (models) may overestimate the present-day areal extent of those forest types. However, the reciprocal assignment of field/woods complexes (Olson, Watts, and Allison 1983) to the agroecosystem model (reflecting the predominance of fields over woods in these areas) may swing the balance of areal estimation back the other way.

The treatment of Olson's Tropical Savanna and Woodland was also problematic. Faced with an absence of tropical savanna ecosystem models that represent both grasses and trees (see King and DeAngelis 1985), we had to decide which of the available models best represented this ecosystem complex. We assumed that the grassy undercover of savanna systems, by virtue of its dominant role in ground cover and metabolically active biomass, determines the

seasonal exchange of atmospheric CO<sub>2</sub> in areas occupied by tropical savanna (despite the characteristic presence of scattered trees). Our decision to assign these ecosystems to the grassland model developed for a temperate grassland site rather than one developed for a tropical site was influenced by:

1. the failure of available tropical grassland models to meet our model selection criteria (outlined in Chapter 2), and
2. the demonstration by Parton and Singh (1984) that a temperate grassland model could simulate biomass dynamics for a tropical grassland site without structural changes in the model.

According to the supplementary land cover references, the areas classified by Olson, Watts, and Allison (1983) as Succulent and Thorn Woods and Scrub are generally covered with tropical savanna. Consequently, we assigned this ecosystem complex to the grassland model.

### 3.1.2 Geographical Distribution And Areal Extent

The final assignments were used with Olson's digitized map of major world ecosystem complexes (provided by Jerry S. Olson and William R. Emanuel of Oak Ridge National Laboratory) to determine the global distribution of the model biomes. We assigned each of Olson's 0.5° latitude by 0.5° longitude cells to one of 14 classification codes. Ten of these codes represent the ten site-specific models (Table 3.1). Oceans, lakes, and small islands are represented by another code (0), wetlands (swamps, marshes, and mangrove systems) account for another code (77), and the remaining two codes represent

Olson's shore and hinterland complexes (88) and ice, sand desert, and polar or rock desert (99). The Olson data base covers the earth's surface from 80°N to 56°S. Since the land surface beyond the extent of the data base is largely covered by ice or polar desert, we assigned all land area north of 80°N and south of 56°S to the ice and polar desert category (99). The code numbers have no special significance; the particular numbers were chosen only to facilitate "bookkeeping" and to improve the appearance of digitized maps of the data base.

We designed a simple algorithm to convert Olson's data base to one that reflected our model assignments and new coding. Figure 3.1 illustrates this transformation for one area of the earth's surface (40°–30°N by 85°–75°W). Plate 3.1 (see Appendix) is a world map of the resulting model biomes.

The area occupied by each model biome, or synonymously, the areal extent over which each of the site-specific models can be taken as representative, was determined by summing the areas of each 0.5° by 0.5° grid cell of each type or classification. The area of each grid cell was calculated using the equation presented by Esser (1984):

$$A = 510,108,933.5 \times B \times \cos(L) \times (\sin(B/2)/360) , \quad (3.1)$$

where A is the area of each grid cell in km<sup>2</sup>; B is the width of each grid cell in degrees, and L is the latitude of the midpoint of the grid cell. By this formula, the area of a 0.5° by 0.5° grid cell adjacent to the equator is 3091.31 km<sup>2</sup>, approximately 2176.38 km<sup>2</sup>



for cells in the mid-latitudes, and  $550.15 \text{ km}^2$  for cells near  $80^\circ$  latitude. The total area occupied by each model biome is presented in Table 3.2.

### 3.2 SIMULATION OF GLOBAL $\text{CO}_2$ EXCHANGES

#### 3.2.1 Extrapolation From Site-specific To Regional $\text{CO}_2$ Fluxes: An Hypothesis

In the initial extrapolations, the net exchange of  $\text{CO}_2$  between the atmosphere and the terrestrial biosphere of some prescribed region of the earth's surface is the area-weighted sum of the site-specific fluxes characteristic of the vegetation complexes found within that region. In practice, we determined the areal extent of each model biome or land cover category encompassed by the region and multiplied this area by the site-specific  $\text{CO}_2$  flux simulated by the site-specific model assigned to that land cover category. Fluxes from oceans, lakes and small islands, wetlands, shores and hinterlands, and ice, sand, rock and polar deserts were zero. The site-specific fluxes used for each model biome are those presented in Chapter 2.

This initial extrapolation attempt is an expression of the working hypothesis that perceived within-biome heterogeneity in vegetation, climate, and soil does not significantly influence the seasonal exchange of  $\text{CO}_2$  between the atmosphere and the terrestrial biosphere. The hypothesis implies the model biomes can be considered strictly homogeneous with respect to properties that influence seasonal dynamics of  $\text{CO}_2$  exchange. This hypothesis

Table 3.2. Area of the terrestrial biosphere represented by each of the land cover categories, by hemisphere and globally, from 80°N to 60°S.

Land Cover Category	Northern Hemisphere		Southern Hemisphere		Global	
	Area (km <sup>2</sup> )	%	Area (km <sup>2</sup> )	%	Area (km <sup>2</sup> )	%
Temperate Broadleaf Deciduous Forest	6,460,066	6.49	97,154	0.28	6,557,220	4.89
Temperate Broadleaf Evergreen Forest	1,927,556	1.94	1,569,034	4.54	3,496,590	2.61
Cool Coniferous Forest	14,725,325	14.79	0	0.00	14,725,325	10.97
Warm Coniferous Forest	2,213,298	2.22	45,842	0.13	2,259,140	1.68
Tropical Moist Evergreen Forest	4,944,456	4.96	6,482,035	18.74	11,426,491	8.51
Tropical Dry Deciduous Forest	1,571,612	1.58	3,454,712	9.99	5,026,324	3.75
Tundra	11,955,477	12.00	360,154	1.04	12,315,631	9.18
Grassland	21,578,453	21.67	12,315,458	35.61	33,893,911	25.26
Desert and Arid Shrubland	10,771,419	10.82	3,922,190	11.34	14,693,609	10.95
Cropland	15,848,412	15.91	4,009,959	11.59	19,858,371	14.80
Wetland	719,060	0.72	868,441	2.51	1,587,501	1.18
Shore and Hinterland	703,312	0.71	303,284	0.88	1,006,596	0.75
Ice, Sand, and Rock	6,174,682	6.20	1,153,040	3.33	7,327,722	5.46

could be characterized as naive. However, the extrapolation is a logical first approximation and one that should be evaluated in its own right, not simply dismissed a priori. If regional CO<sub>2</sub> exchanges simulated by the extrapolation fail to match observations or, in conjunction with a tracer transport model, fail to generate the seasonal pattern of atmospheric CO<sub>2</sub> concentrations recorded at the monitoring stations, the hypothesis will be rejected. In the following sections we present several CO<sub>2</sub> exchange functions generated by the simple extrapolation and evaluate them within this framework. In the absence of either large-scale observations or tracer transport simulations, we evaluate the hypothesis by comparing calculated CO<sub>2</sub> exchange functions with those published for the various tracer transport models.

### 3.2.2 Global CO<sub>2</sub> Exchange Functions: A Test Of The Hypothesis

Tracer transport models differ in their spatial resolution of the Earth's surface. As introduced in Chapter 1, the one and two dimensional models use circumglobal latitude belts; the three dimensional models use grid cells. To facilitate comparisons with existing source functions and to promote compatibility with the available tracer transport models, we generated four CO<sub>2</sub> source functions with horizontal resolutions of 10° latitude belts (Figure 3.2), 20° belts (Figure 3.3), approximately equal area belts (Figure 3.4), and 8° by 10° grid cells (Figure 3.5), respectively.

The source functions were generated by extrapolation of the site-specific models. We determined the areal extent of each model

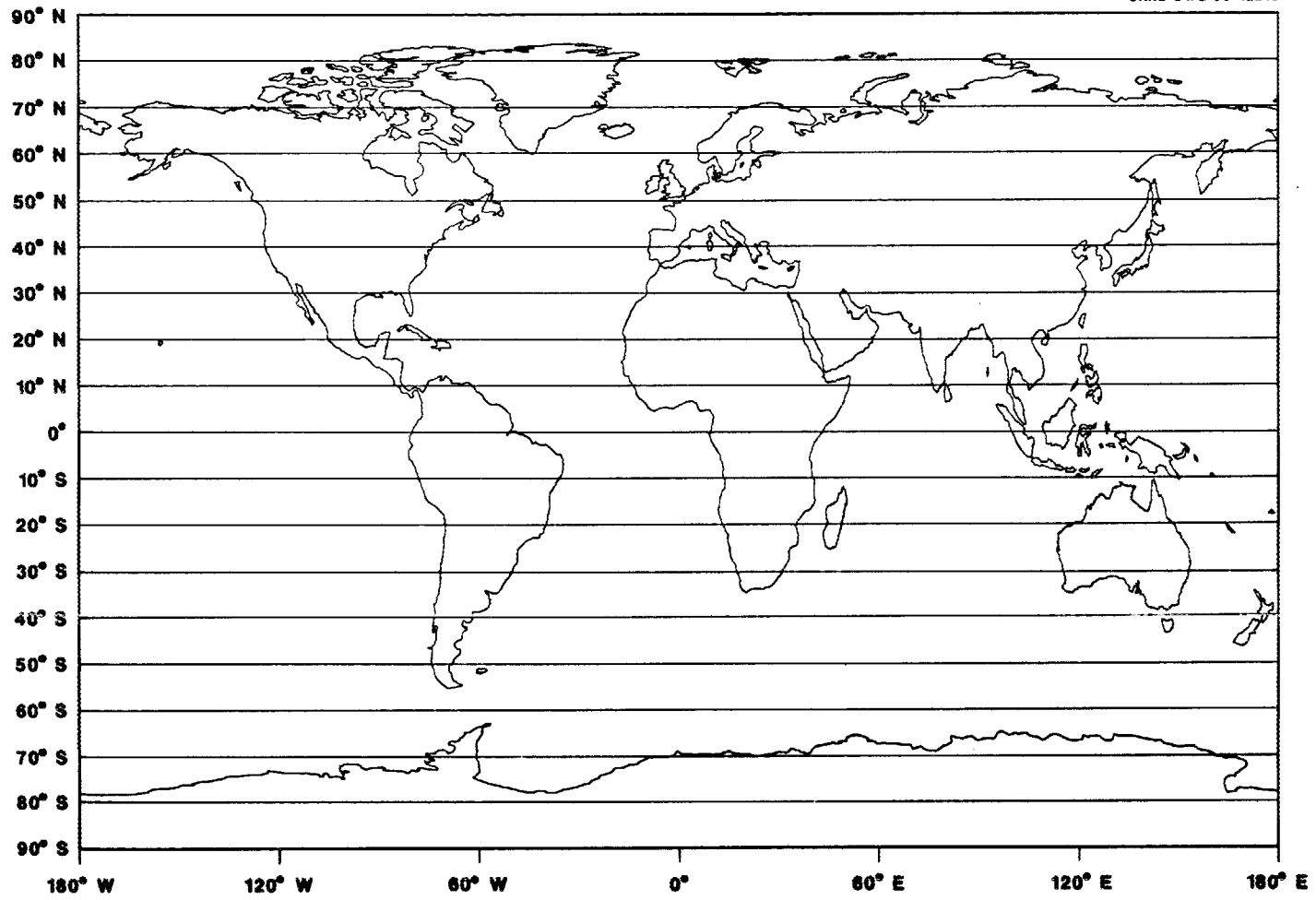


Figure 3.2. World map of 10° latitude belts.

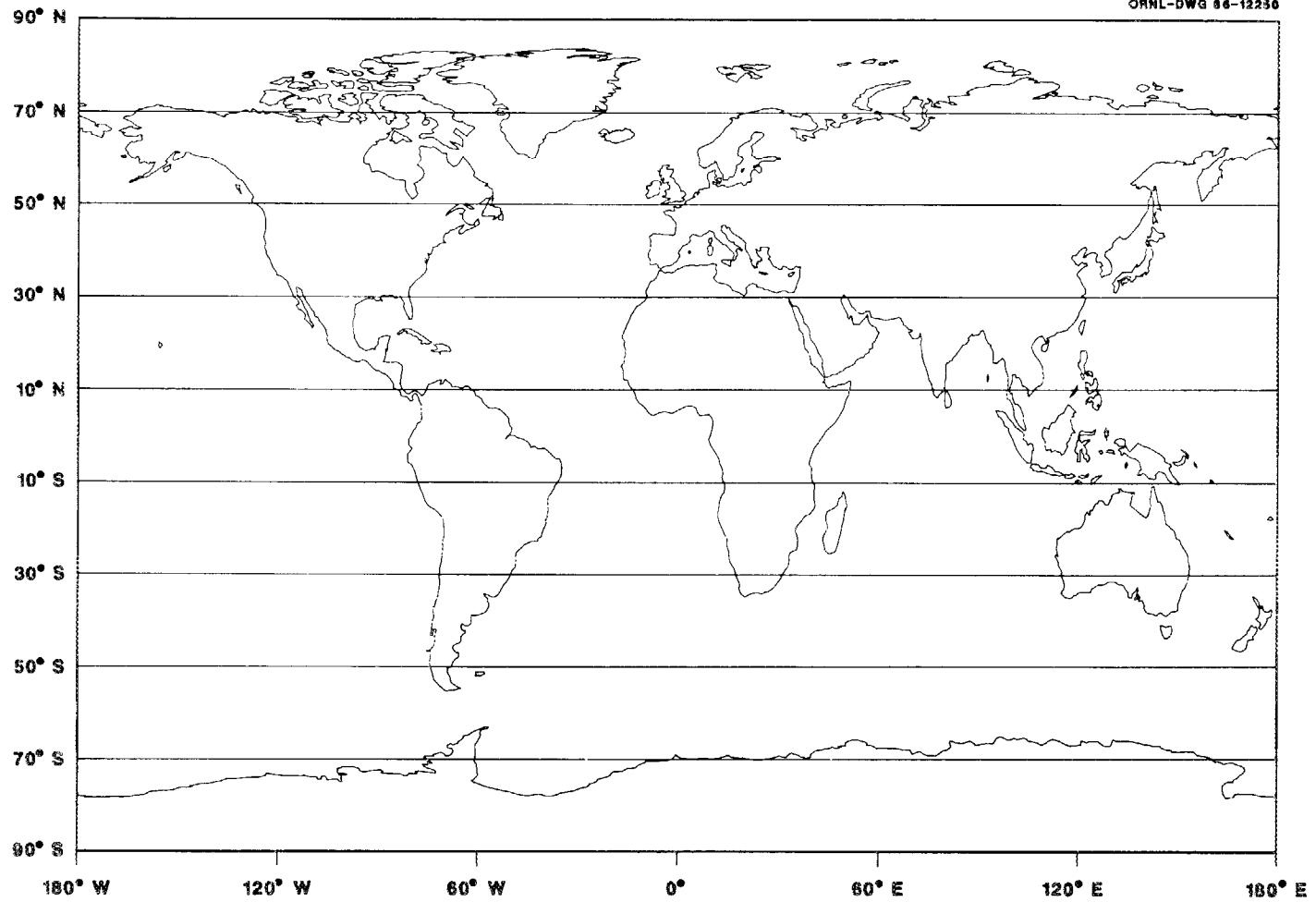


Figure 3.3. World map of 20° latitude belts.

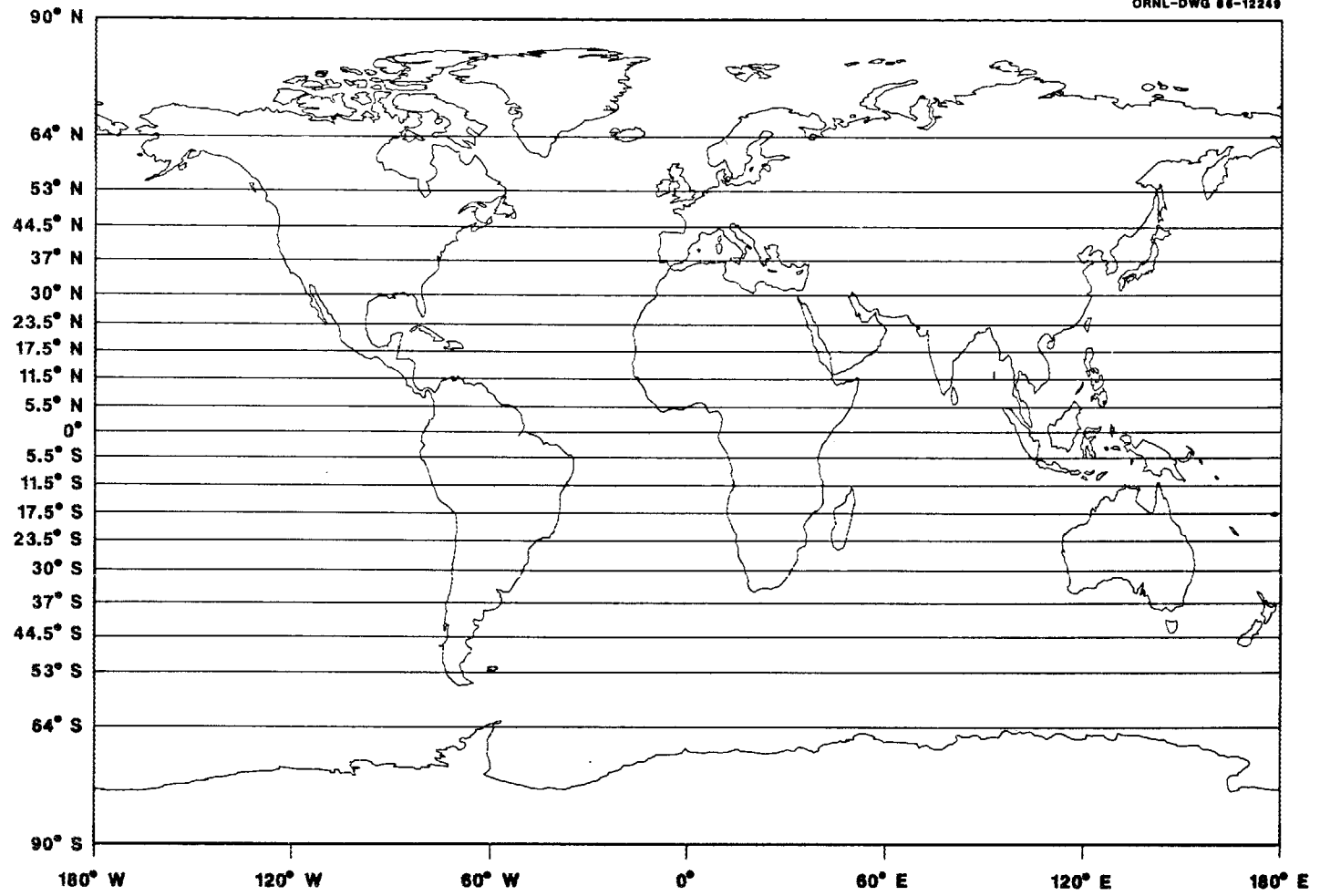


Figure 3.4. World map of equal-area latitude belts.

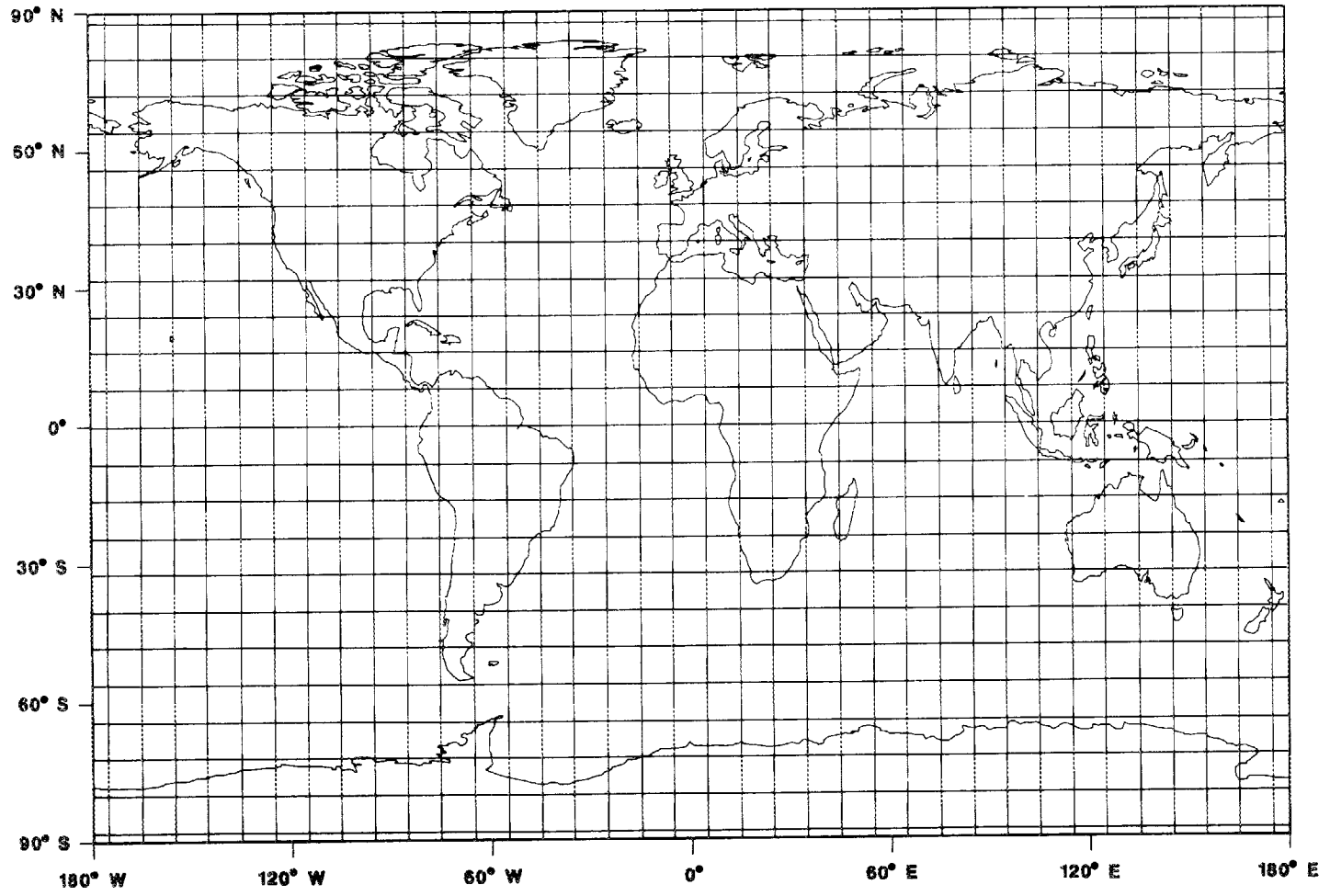


Figure 3.5. World map of 8° by 10° grid cells.

biome or land cover category within each latitude belt or grid cell. The monthly net CO<sub>2</sub> exchange between the atmosphere and terrestrial biosphere for a given belt or grid cell is

$$Q_m = \sum_{i=1}^{13} a_i f_{i,m} \quad m = (1, \dots, 12) , \quad (3.2)$$

where  $Q_m$  is the monthly exchange per unit of spatial resolution (in units of  $10^{15}$  g CO<sub>2</sub> month<sup>-1</sup>),  $a_i$  is the area (km<sup>2</sup>) of the  $i$ th land cover category, and  $f_{i,m}$  is the monthly site-specific net CO<sub>2</sub> flux ( $10^{15}$  g CO<sub>2</sub> km<sup>-2</sup> month<sup>-1</sup>) associated with the  $i$ th land cover category (see Table 3.2). Net monthly site-specific CO<sub>2</sub> flux ( $f_{i,m}$ ) is the sum of the site's daily net fluxes for each month (from Chapter 2).

The CO<sub>2</sub> exchange functions generated in this manner are presented in Tables 3.3 to 3.5. The source function with 10° latitude belt resolution (Table 3.3) can be compared with Azevedo's (1982) source function (Table 1.5, p. 33). The source function with 20° latitude belt resolution (Table 3.4) can be compared with Machta's (1972) source function (Table 1.3, p. 28), and the source function with equal-area latitude belts (Table 3.5) can be compared with Pearman and Hyson's (1981b) source function (Table 1.4, p. 30). The latitude belts of the Pearman and Hyson function do not exactly coincide with mine. To simplify area calculations, we adjusted the span of their equal-area belts. The difference should not influence comparisons. A cell by cell tabulation of CO<sub>2</sub> exchanges for a three-dimensional model

Table 3.3. Estimates of seasonal CO<sub>2</sub> exchange (10<sup>15</sup> g CO<sub>2</sub> month<sup>-1</sup>) derived from the simple extrapolation of the site-specific models for 10° latitude belts.<sup>a</sup>

Latitude Belt	Jan	Feb	Mar	Apr	May	Jun	Jul	Aug	Sep	Oct	Nov	Dec
80°-90°N	0.00	0.00	0.00	0.00	0.00	0.00	0.00	0.00	0.00	0.00	0.00	0.00
70°-80°N	0.02	0.00	-0.01	-0.04	-0.06	-0.22	-0.27	0.04	0.13	-0.03	0.01	0.02
60°-70°N	3.15	-0.34	-1.24	-5.24	-8.88	-9.34	2.66	4.01	2.32	-5.58	0.69	2.48
50°-60°N	3.49	0.10	-0.73	-5.05	-8.96	-11.06	-0.12	3.12	1.99	-4.90	1.26	2.89
40°-50°N	1.52	0.53	0.35	-1.42	-3.37	-6.08	-3.79	0.04	0.44	-0.85	1.02	1.43
30°-40°N	0.23	-0.02	0.04	-0.37	-1.17	-3.33	-3.68	-0.52	0.11	0.06	0.47	0.53
20°-30°N	0.30	0.06	-0.15	-0.49	-1.04	-2.26	-2.35	-0.32	0.06	-0.01	0.09	0.25
10°-20°N	0.31	-0.01	-0.52	-0.91	-1.68	-1.99	-1.48	-0.02	0.18	-0.13	-0.25	0.04
0°-10°N	0.42	-0.19	-1.21	-1.52	-1.59	-0.98	-0.43	-0.01	-0.72	-1.66	-2.11	-0.90
0°-10°S	0.00	0.03	-1.16	-2.54	-3.28	-1.50	0.53	-0.38	-1.95	-2.34	-1.87	-0.70
10°-20°S	-0.96	0.06	0.26	0.14	0.11	0.33	0.56	0.07	-1.00	-2.11	-3.22	-2.54
20°-30°S	-0.94	0.00	0.20	0.10	0.06	0.15	0.25	0.12	-0.09	-0.37	-1.09	-1.31
30°-40°S	-1.17	-0.25	-0.14	-0.16	0.03	0.21	0.21	0.20	0.21	0.11	-0.22	-0.90
40°-50°S	-0.13	-0.05	-0.06	-0.06	-0.01	0.03	0.03	0.03	0.03	0.01	-0.04	-0.10
50°-60°S	-0.02	-0.02	-0.03	0.00	0.01	0.01	0.01	0.01	0.01	-0.01	-0.02	-0.02
60°-70°S	0.00	0.00	0.00	0.00	0.00	0.00	0.00	0.00	0.00	0.00	0.00	0.00
70°-80°S	0.00	0.00	0.00	0.00	0.00	0.00	0.00	0.00	0.00	0.00	0.00	0.00
80°-90°S	0.00	0.00	0.00	0.00	0.00	0.00	0.00	0.00	0.00	0.00	0.00	0.00

<sup>a</sup>Positive values indicate release to the atmosphere; negative values indicate uptake by the terrestrial biosphere.

Table 3.4. Estimates of seasonal CO<sub>2</sub> exchange (10<sup>15</sup> g CO<sub>2</sub> month<sup>-1</sup>) derived from the simple extrapolation of the site specific models for 20° latitude belts.<sup>a</sup>

Latitude Belt	Jan	Feb	Mar	Apr	May	Jun	Jul	Aug	Sep	Oct	Nov	Dec
70°-90°N	0.02	0.00	-0.01	-0.04	-0.06	-0.22	-0.27	0.04	0.13	-0.02	0.01	0.02
50°-70°N	6.64	-0.24	-1.97	-10.29	-17.84	-20.40	2.54	7.13	4.31	-10.47	1.95	5.36
30°-50°N	1.74	0.51	0.39	-1.79	-4.54	-9.41	-7.47	-0.48	0.55	-0.79	1.49	1.97
10°-30°N	0.59	0.04	-0.62	-1.28	-2.55	-4.13	-3.81	-0.34	0.22	-0.17	-0.20	0.26
10°N-10°S	0.42	-0.16	-2.37	-4.06	-4.87	-2.48	0.10	-0.39	-2.67	-4.00	-3.98	-1.60
10°-30°S	-1.90	0.06	0.46	0.24	0.17	0.48	0.81	0.19	-1.10	-2.48	-4.31	-3.85
30°-50°S	-1.30	-0.30	-0.20	-0.22	0.02	0.24	0.24	0.22	0.23	0.11	-0.26	-1.00
50°-70°S	-0.02	-0.02	-0.03	0.00	0.01	0.01	0.01	0.01	-0.01	-0.01	-0.02	-0.02
70°-90°S	0.00	0.00	0.00	0.00	0.00	0.00	0.00	0.00	0.00	0.00	0.00	0.00

<sup>a</sup>Positive values indicate release to the atmosphere; negative values indicate uptake by the terrestrial biosphere.

Table 3.5. Estimates of seasonal CO<sub>2</sub> exchange (10<sup>15</sup> g CO<sub>2</sub> month<sup>-1</sup>) derived from the simple extrapolation of the site-specific models for latitude belts of equal area (ca. 2.55 x 10<sup>7</sup> km<sup>2</sup>).<sup>a</sup>

Latitude Belt	Jan	Feb	Mar	Apr	May	Jun	Jul	Aug	Sep	Oct	Nov	Dec
64.0°-90.0°N	1.52	-0.18	-0.62	-2.52	-4.27	-4.73	0.88	1.99	1.35	-2.69	0.31	1.19
53.0°-64.0°N	4.04	-0.17	-1.24	-6.47	-11.07	-12.20	2.11	4.32	2.37	-6.46	1.20	3.26
44.5°-53.0°N	2.22	0.41	-0.01	-2.45	-5.05	-7.74	-2.60	1.17	1.13	-2.18	1.09	1.93
37.0°-44.5°N	0.60	0.30	0.30	-0.35	-1.20	-3.20	-3.18	-0.43	0.09	-0.03	0.55	0.67
30.0°-37.0°N	0.03	-0.12	-0.06	-0.28	-0.73	-2.25	-2.68	-0.37	0.14	0.10	0.30	0.30
23.5°-30.0°N	0.23	0.10	0.05	-0.24	-0.69	-1.53	-1.57	-0.25	0.00	0.05	0.18	0.23
17.5°-23.5°N	0.16	-0.05	-0.34	-0.48	-0.68	-1.24	-1.26	-0.10	0.09	-0.11	-0.16	0.03
11.5°-17.5°N	0.16	-0.03	-0.32	-0.54	-1.03	-1.16	-0.82	0.02	0.11	-0.10	-0.19	-0.01
5.5°-11.5°N	0.24	0.03	-0.33	-0.64	-1.20	-1.14	-0.67	0.00	0.00	-0.21	-0.28	-0.01
0.0°- 5.5°N	0.24	-0.20	-0.93	-1.02	-0.70	-0.16	0.05	0.00	-0.69	-1.43	-1.82	-0.85
0.0°- 5.5°S	0.06	-0.01	-0.85	-1.79	-2.30	-1.08	0.31	-0.26	-1.22	-1.33	-0.82	-0.16
5.5°-11.5°S	-0.12	0.05	-0.33	-0.84	-1.11	-0.45	0.31	-0.13	-0.96	-1.38	-1.51	-0.84
11.5°-17.5°S	-0.71	0.03	0.21	0.19	0.20	0.31	0.40	0.06	-0.70	-1.52	-2.28	-1.82
17.5°-23.5°S	-0.55	0.04	0.16	0.10	0.07	0.12	0.18	0.07	-0.15	-0.42	-1.01	-0.99
23.5°-30.0°S	-0.57	-0.01	0.11	0.05	0.03	0.08	0.14	0.08	-0.02	-0.15	-0.56	-0.74
30.0°-37.0°S	-0.99	-0.20	-0.09	-0.11	0.03	0.18	0.18	0.16	0.17	0.10	-0.19	-0.76
37.0°-44.5°S	-0.27	-0.08	-0.08	-0.08	-0.01	0.05	0.05	0.05	0.05	0.02	-0.05	-0.20
44.5°-53.0°S	-0.04	-0.03	-0.05	-0.03	-0.01	0.01	0.01	0.01	0.01	-0.01	-0.03	-0.04
53.0°-64.0°S	-0.01	-0.01	-0.01	0.00	0.01	0.00	0.00	0.00	0.00	-0.01	-0.01	-0.01
64.0°-90.0°S	0.00	0.00	0.00	0.00	0.00	0.00	0.00	0.00	0.00	0.00	0.00	0.00

<sup>a</sup>Positive values indicate release to the atmosphere; negative values indicate uptake by the terrestrial biosphere.

(i.e., a source function with longitudinal resolution) was not available for comparisons; consequently, we have not included the large table (over 4000 entries) that describes the source function with  $8^\circ$  by  $10^\circ$  resolution. This  $\text{CO}_2$  source function is, however, available from the authors on request.

The  $\text{CO}_2$  source functions generated by simple extrapolation of the site-specific models do not compare favorably with existing source functions. In general, exchanges in the northern hemisphere are overestimated, and the period of uptake by the biosphere is shifted toward the spring. The differences are not so extreme in the southern hemisphere, but discrepancies exist, particularly in the period of net uptake. The  $\text{CO}_2$  source functions extrapolated from the site-specific models indicate a seasonality in the tropics not found in the other source functions.

These results led us to reject the working hypothesis that within-biome heterogeneity does not significantly influence the exchange of  $\text{CO}_2$  between the atmosphere and the terrestrial biosphere. This suggests that any successful extrapolation procedure must explicitly incorporate within-biome heterogeneity.

## CHAPTER 4

## EXTRAPOLATION FROM SITE-SPECIFIC MODELS TO REGIONAL MODELS

How can local, site-specific models be extrapolated across larger heterogeneous regions? The results of Chapter 3 reinforce the intuition that a simple extrapolation that assumes relative homogeneity will be unsuccessful. An alternative that comes to mind, the idea of using mean values for the region as input variables to the site-specific model, is also unlikely to succeed. From the definition of mathematical expectation (Feller 1971), in general

$$E[f(X)] \neq f(E[X]) , \quad (4.1a)$$

or

$$E[f(X)] \neq f(\bar{X}) . \quad (4.1b)$$

That is, whenever  $f(X)$  is a non-linear function, the expected value of the function is not equal to the function evaluated at the expected value, or mean, of the variable  $X$ . Non-linear functions can be contrived that are exceptions to this general rule, but the relationship expressed in Equations 4.1a and 4.1b is characteristic of many, if not most, non-linear functions. In the special case where  $f(X)$  is linear, the right and left terms of Equation 4.1a are equal. However, the solution of a system of linear differential equations will in general be non-linear; thus, the equality does not necessarily hold even for linear systems. Consequently, it seems

unlikely that site-specific models with relevant ecological structure can be successfully extrapolated by the use of mean inputs.

However, the very definition of an expected value that proscribes the use of mean inputs is also the key to a correct method of extrapolation. In this chapter we develop this method and test its effectiveness with a relevant, albeit limited, application.

#### 4.1 EXTRAPOLATION AND THE EXPECTED VALUE OF A RANDOM VARIABLE

Consider an area,  $A$ , that is spatially heterogeneous, or patchy, with respect to some discrete-valued random variable,  $X$ . At any location  $z$  in  $A$ ,  $X$  is equal to  $X(z)$ . Within patch-type  $i$  all  $X(z) = X_i$ , where  $X_i$  is a constant value. In other words a patch-type is homogeneous with respect to  $X$ , and different patch-types in  $A$  take on different values of  $X$ . The random variable  $X$  is a determinant of a local, site-specific process, a flux for example. The total flux,  $F_A$ , from area  $A$  is given by

$$F_A = \sum_{i=1}^k f(x_i) a_i , \quad (4.2)$$

where  $f(x_i)$  is the site-specific model evaluated at  $x_i$ ,  $a_i$  is the area of patch-type; and  $k$  is the number of patch-types within the total area  $A$ . Equivalently,  $k$  is the number of possible values of  $X$  in the area  $A$ .

The area of patch-type  $i$ ; ( $a_i$  in Equation 4.2) can be estimated by uniform sampling of  $A$ . Thus,

$$a_i = (m_i/n)A , \quad (4.3)$$

where  $n$  is the number of independent sample points or quadrats in  $A$ , and  $m_i$  is the number of occurrences of  $X_i$  in the sample. The more complete the coverage of all possible locations in area  $A$ , the better the estimate. Substituting the right side of Equation 4.3 for  $a_i$  in Equation 4.2 results in

$$F_A = \sum_{i=1}^k f(x_i)(m_i/n)A , \quad (4.4a)$$

or

$$F_A = A \sum_{i=1}^k f(x_i)(m_i/n) , \quad (4.4b)$$

Since  $m_i/n$  is an empirical estimate of the probability that, at any point  $z$  in  $A$ ,  $X$  is equal to  $x_i$  (i.e.,  $P(X=x_i) = p(x_i)$ ), Equation 4.4b can be rewritten as

$$F_A = A \sum_{i=1}^k f(x_i)p(x_i) , \quad (4.5)$$

The summation term in Equation 4.5 defines the mathematical expectation of the random variable  $Y=f(X)$ , or  $E[Y]$ . Consequently the total flux for the heterogeneous region is

$$F_A = AE[Y] . \quad (4.6)$$

The equivalence of Equations 4.2 and 4.6 is the key to a solution of the extrapolation problem. Before proceeding further, however, a simple example will be useful in reinforcing these points.

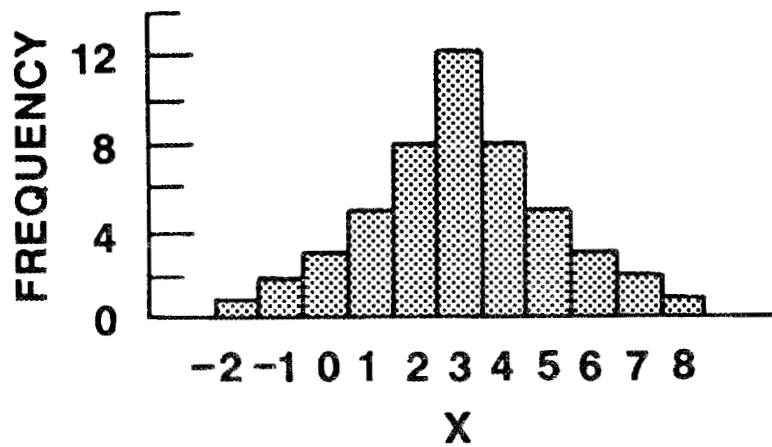
Figure 4.1 depicts a heterogeneous area  $A$  of  $1 \text{ km}_2$  and illustrates the frequency distribution of the random variable  $X$ . Let the site-specific phenomenon (for example,  $\text{CO}_2$  flux) be modeled by  $Y=f(X)=\exp(X)$ . The units of  $Y$  are, for purposes of the example,  $\text{Gt CO}_2 \text{ km}^{-2} \text{ d}^{-1}$ . In any given cell, or patch, within  $A$  (Figure 4.1) all  $X(z)$  have the same value of  $X$ . All cells (or patches) where  $X = x_i$  belong to patch-type  $i$ . The cells need not be contiguous. Hence, for example, the area ( $a_i$ ) of patch-type 7 (where all  $X(z) = 7$  is  $40,000 \text{ m}^2$  (i.e., two cells of  $20,000 \text{ m}^2$  each). From Equation 4.2 the total flux from the area is  $157.619 \text{ Gt CO}_2 \text{ d}^{-1}$ . This value can be taken as the "truth" or the reference point for model evaluation. The expected value,  $E[Y]$ , of the random variable  $Y=f(X)$  is  $157.619 \text{ Gt CO}_2 \text{ km}^{-2} \text{ d}^{-1}$ . With an area of  $1 \text{ km}^2$ , Equation 4.6 predicts a total flux of  $157.619 \text{ Gt CO}_2 \text{ km}^{-2} \text{ d}^{-1}$  (i.e., the actual flux from the area). The alternative extrapolation, using the mean value of  $X$  ( $X=3$ ) as input to the site-specific model, predicts a total flux from  $A$  of  $\exp(3) = 20.086 \text{ Gt CO}_2 \text{ km}^{-2} \text{ d}^{-1}$ , an estimate with a relative error of 87.26%. The simple extrapolation of Chapter 3, with the lower left cell randomly chosen as the initial site, predicts a total flux of  $54.598 \text{ Gt CO}_2 \text{ km}^{-2} \text{ d}^{-1}$  (relative error = 65.36%).

The choice between the three extrapolation models is obvious. The extrapolation by expected value provides the only accurate estimate of regional flux; the other methods are incorrect. The extreme differences are due in part to the behavior of the exponential function and in part to the contrived nature of the

ORNL-DWG 86-12493

3	1	8	0	2	3	0	3	2	1
5	2	7	6	4	4	5	0	3	2
5	-2	4	1	4	-1	4	2	6	5
3	-1	3	5	3	2	4	6	3	7
4	3	1	2	3	3	1	3	4	2

### HETEROGENEOUS AREA



### FREQUENCY DISTRIBUTION

Figure 4.1. An abstract area, heterogeneous in  $X$ , and the frequency distribution of the random variable  $X$ .

example. In practice, the magnitude of the error will vary with the mathematical form of the model and the degree of variability in  $X$  (O'Neill 1979a, O'Neill, Elwood, and Hildebrand 1979). Nevertheless, the example illustrates the potential for error in spatial extrapolations that do not correctly account for spatial heterogeneity.

This example, at the risk of belaboring the point for those familiar with probability theory, supports the appropriateness of using the mathematical expectation of a random variable as a means of extrapolating site-specific models across heterogeneous regions. The potential for error associated with the assumption of spatial homogeneity or the use of spatial averages in non-linear models has been recognized for crop simulation models (McCree and Loomis 1969; Dugas, Arkin, and Jackson 1983; Leduc and Holt 1987) and for ecosystem models (O'Neill, Elwood, and Hildebrand 1979; Gardner, O'Neill, and Carney 1981; Gardner and O'Neill 1983), and there is a large literature dealing with the influence of spatial variability on the dynamics and stability of populations and communities (e.g., see Levin 1976, Ziegler 1978, Chesson 1978, Smith 1980, Chesson 1985, and Lefkovitch and Fahrig 1985). There are studies that simulate spatially distributed systems by first simulating each spatial subsystem and then summing or averaging these results to describe the areas overall properties (e.g., Duncan et al. 1967; vollenvieder 1970; Curry, Shapiro, and Vanderlip 1977; O'Neill, Elwood, and Hildebrand 1979; Bolla and Kutas 1984). These studies are making correct use of an expected value to investigate spatially

heterogeneous systems. However, they are generally not presented as an extrapolation problem. They seldom consider explicitly the frequency distribution of model input (see Gardner, O'Neill, and Carney 1981 as an exception), and the areas involved are smaller than the scales appropriate to global studies. To our knowledge there are no ecological studies that use mathematical expectation to extrapolate ecosystem models across large regional and continental areas, and there are none that deal with  $\text{CO}_2$  and the carbon cycle. In the next section we present a procedure for actually implementing this site-to-region extrapolation.

#### 4.2 A RECIPE FOR EXTRAPOLATION OF THE SITE-SPECIFIC MODELS

Using mathematical expectation as a means of extrapolating site-specific models across heterogeneous regions requires four main ingredients: (1) the local site-specific model, (2) designation of the larger region of interest, (3) the frequency distribution of model parameters or variables that vary across that region (and which in fact define the heterogeneity of that region), and 4) a procedure for calculating the expected value of the model. For purposes of example and theoretical development these ingredients are defined and manufactured as needed. In this section we outline the assembly of these ingredients for the problem at hand, the extrapolation from site-specific models to biome-level models of seasonal  $\text{CO}_2$  exchange between the atmosphere and the terrestrial biosphere.

#### 4.2.1 Ingredient 1: The Site-specific Models

The objective is to extrapolate each of the site-specific models of Chapter 2 across an entire biome. We assume that each model is an accurate structural representation of any stand or site within the associated model biome defined in Chapter 3. In other words, model structure (state variables, rate processes, etc.) does not change from site-to-site within the model biome. However, the biomes are heterogeneous; sites may differ in either biotic or abiotic factors or both. Biome heterogeneity is reflected in site-to-site changes in the values of the model's parameters and driving variables.

Within-biome (between-site) variability in the seasonal exchange of  $\text{CO}_2$  between the atmosphere and the vegetation is the result of between-site variability in endogenous, biotic factors (e.g., variability in maximum photosynthetic rate) and between-site variability in exogenous, abiotic factors (e.g., variability in temperature). We assume that biotic variability is highly correlated with variability in model parameters, and abiotic variability is highly correlated with variability in model driving variables (model parameters may in fact represent both biotic factors and abiotic factors that are not included explicitly in the model structure, but this crude dichotomy is more useful for our present purpose).

We assume that most within-biome variability in  $\text{CO}_2$  dynamics is explained by within-biome variability in model driving variables. Why this particular assumption? For one reason, we suspect that between-site variability in model driving variables

(abiotic factors) is greater than between-site variability in model parameters (biotic factors), and, given equal model sensitivity, greater variability in model forcings or parameters means greater variability in model output. Furthermore, it is much easier to describe empirically the within-biome variability of driving variables (frequently climate variables) than the corresponding variability in model parameters. Consequently, the extrapolation is more readily applied to a region with significant between-site variability in model driving variables than to a region with comparable variability in model parameters. Hereafter, we consider only the biome heterogeneity reflected in the models' driving variables.

#### 4.2.2 Ingredient 2: The Region Of Extrapolation

The latitude belts of the existing CO<sub>2</sub> source functions are a convenient way of defining the region over which a site-specific model is extrapolated. The site-specific model is extrapolated across that portion of the associated model biome occurring within a defined latitude belt (e.g., temperate broadleaf deciduous forest between 30°N and 40°N). Defining the region of extrapolation in this way facilitates comparison of the regional CO<sub>2</sub> flux estimated by mathematical expectation with published fluxes predicted by other means (i.e., from the source functions of Chapter 1). As in Chapter 3, these comparisons are tests of the effectiveness of the extrapolation procedure.

#### 4.2.3 Ingredient 3: The Frequency Distributions

Model biome heterogeneity is defined by within-biome variability in model driving variables (see Section 4.2.1). The driving variables of the site-specific models (Chapter 2) are treated as random variables. Simulated CO<sub>2</sub> flux, as a function of the driving variables, is also a random variable, and the regional flux is determined by the mathematical expectation of this random variable. Equations 4.1 and 4.6 are easily generalized to functions of two or more variables (see Rozanov 1969, Spiegel 1975).

The frequency distributions of the model's driving variables characterize the spatial heterogeneity of driving variables across the model biome, within the prescribed latitude belt. Each driving variable of the model is described by its own frequency distribution. Data used to build these distributions may come from a variety of sources, including research sites where the variable was measured and, in the case of climate variables, from a network of climate stations. These data are also used to calculate a correlation matrix for the driving variables.

#### 4.2.4 Ingredient 4: Calculation Of The Expected Value

We calculate the expected value of site-specific model output by Monte Carlo simulation using PRISM, a program designed for the analysis of model sensitivity and uncertainty (see Gardner, Rojder, and Bergstrom 1983; and Gardner and Trabalka 1985). PRISM uses Latin Hypercube sampling (see Gardner and Trabalka 1985) to select parameters (driving variables in this application) from frequency

distributions specified in model input. Each of the empirical frequency distributions for the model driving variables is described by the approximate probability distribution (normal, triangular, uniform, log normal, or constant), central tendency (mean or mode), standard deviation, maximum value, and minimum value. Spearman rank correlations between driving variables are also specified in model input (see Iman and Conover 1983). These rank order correlations, the Latin Hypercube sampling, a large sample size ( $n \geq 200$ ), and the specified frequency distributions generate, during the course of the Monte Carlo simulation, an approximation of the joint frequency distribution for the driving variables (Iman and Helton 1985, Robert H. Gardner, pers. comm.). A full set of driving variables is drawn from this distribution, and the model simulation of seasonal  $\text{CO}_2$  flux is executed. This process is repeated a specified number of times, and the results are saved for calculation of the moments of the output distribution (e.g., the mean and variance of the Monte Carlo runs). The expected value times the area of extrapolation is the predicted  $\text{CO}_2$  flux for the region.

#### 4.3 AN APPLICATION OF EXTRAPOLATION BY EXPECTED VALUE

To recapitulate, the objective of this report is to describe the derivation of a  $\text{CO}_2$  exchange function based on site-specific models of ecosystem carbon metabolism. If such a source function is feasible, investigations of changes in atmospheric  $\text{CO}_2$  (e.g., the increase in the amplitude of the seasonal cycle) can take advantage of the mechanistic description of ecosystem-atmosphere  $\text{CO}_2$

exchange expressed in the site-specific models. This approach suffers, however, from the disadvantage that existing ecosystem models are local, generally developed for a particular site and relatively small-scale. The models must be extended to represent areas larger than the particular sites for which they were originally designed. Thus, the objective becomes to find a suitable extrapolation technique. Towards this objective, we must demonstrate that the extrapolation generates reasonable values of monthly net biosphere-atmosphere  $\text{CO}_2$  exchange at a regional scale. The extrapolation of Chapter 3 failed to provide these values, leaving the question of whether or not a more sophisticated extrapolation would permit the use of site-specific models in a  $\text{CO}_2$  exchange function.

The extrapolation by expected value described in Section 4.1 of this Chapter is the theoretically correct way to extrapolate across a heterogeneous region. However, it must still be shown that the technique is applicable to the simulation of regional  $\text{CO}_2$  exchange, given the nature of the site-specific models and the available description of within-biome heterogeneity. We must also show that the recipe we have proposed for implementation of the technique is appropriate and useful.

We evaluated the extrapolation by simulating the seasonal exchange of  $\text{CO}_2$  between the atmosphere and the terrestrial biosphere of the 64°N-90°N latitude belt (see Figure 3.4, page 185). We chose this latitude belt because few site-specific models are involved, and because Pearman and Hyson (1981b) have published an

estimate of CO<sub>2</sub> exchange for approximately the same region (64.2°N-90°N, Table 1.4, p. 30). Their estimate is the CO<sub>2</sub> exchange necessary for the best fit between observed and simulated atmospheric CO<sub>2</sub> cycles, given their tracer transport model. This estimate is a reference point for evaluating the extrapolation.

#### 4.3.1 The Tundra Between 64°N And 90°N Latitude

Tundra, as defined in Chapter 3, occupies 6,129,716 km<sup>2</sup> (approximately 54%) of the land area between 64°N and 90°N. In this section we describe the extrapolation of the associated site-specific tundra model (see Section 2.7).

##### 4.3.1.1 Driving Variables And Their Frequency Distributions

The tundra model has nine driving variables ( $Z_1$  to  $Z_9$ ; Table 2.19, p. 121). Daily values for seven of these variables ( $Z_1$  to  $Z_7$ ) are interpolated (linearly) from monthly means read into the simulation program as input data. Day of snowmelt ( $Z_8$ ) and day of snowfall ( $Z_9$ ) are also inputs to the program. For the calculation of the expected value, we determined the frequency distributions of mean monthly solar radiation ( $Z_1$ ), air temperature ( $Z_2$ ), and soil moisture ( $Z_7$ ), and of day of snowmelt ( $Z_8$ ) and day of snowfall ( $Z_9$ ). The data for solar radiation, temperature, snowfall, and snowmelt came from climate stations within the tundra model biome (Plate 3.1, see Appendix) lying between 64°N and 90°N (from Johannessen 1970, Hare and Hay 1974, Lydolph 1977, and Muller 1982), and from IBP Tundra Biome sites (Barry, Courtin, and Labine 1981). These stations and sites are identified in Table 4.1 and

Table 4.1. Climate stations and IBP Tundra Biome sites used in describing the spatial heterogeneity of the tundra model's driving variables.

Station	Location
Kevo, Finland*	69°45'N, 27°01'E
Abisko, Sweden*	68°22'N, 19°03'E
Devon Island, Canada*	75°33'N, 84°40'W
Point Barrow, U.S.A.*	71°18'N, 156°41'W
Kresty Village, U.S.S.R.*	70°N, 89°E
Agapa, U.S.S.R.*	71°25'N, 88°53'E
Disko Island, Greenland	69°15'N, 53°30'W
Cokurdach, U.S.S.R.	70°37'N, 147°53'E
Dudinka, U.S.S.R.	69°24'N, 86°10'E
Chatanga, U.S.S.R.	71°50'N, 102°28'E
Malyje-Karmakuly, U.S.S.R.	72°23'N, 52°44'E
Mys Smidta, U.S.S.R.	68°55'N, 179°29'W
Mys Celuskin, U.S.S.R.	77°43'N, 104°17'E
Narjan-Mar, U.S.S.R.	67°39'N, 53°01'E
Dikson, U.S.S.R.	73°30'N, 80°14'E
Ostrov Kotelnyi, U.S.S.R.	76°00'N, 137°54'E
Salecard, U.S.S.R.	66°32'N, 66°32'E
Velen, U.S.S.R.	66°10'N, 169°50'W
Anadyr, U.S.S.R.	64°47'N, 177°34'E
Ostrov Domashniy, U.S.S.R.	79°30'N, 91°08'E
Ostrov Vrangel'a, U.S.S.R.	70°58'N, 178°32'W
Bulun, U.S.S.R.	70°45'N, 127°47'E
Barter Island, U.S.A.	70°07'N, 143°40'W
Nome, U.S.A.	64°30'N, 165°20'W
Resolute, Canada	74°41'N, 95°54'W
Sachs Harbour, Canada	71°57'N, 122°44'W
Baker Lake, Canada	64°18'N, 96°00'W
Coral Harbour, Canada	64°12'N, 83°22'W

\*Indicates an IBP Tundra Biome site.

mapped in Figure 4.2. Radiation and temperature data were climatic means; day of snowfall and day of snowmelt were estimated from monthly snowcover data. Not all stations and sites provided data on all variables, nor were all the climate means based on the same record length. The histograms we used to describe the frequency distributions were built from a composite of available data.

We could not obtain monthly values of soil moisture directly from the stations and sites. However, seasonal highs and lows were available for the IBP Tundra Biome sites (French 1981, Heal et al. 1981). We assumed that the seasonal pattern in the data from Point Barrow, Alaska (F. L. Bunnell, pers. comm.) was typical of all the tundra sites (discussions by Rydin (1981) support this assumption), and we interpolated the monthly values for the other sites from their seasonal highs and lows using the seasonal pattern for Point Barrow (e.g., the seasonal high always occurred in June and the low in September).

From these data, we obtained estimates of minimum values, maximum values, and central tendencies for each of the driving variables. Frequency histograms suggested the appropriate shape for the probability distributions. PRISM, the program used to perform the Monte Carlo simulations (Section 4.2.4), treats each of the monthly values of the driving variables as a separate variable; as a result, there were 38 input variables (twelve monthly values each for solar radiation, air temperature, and soil moisture plus day of snowfall and day of snowmelt), each described by its own frequency

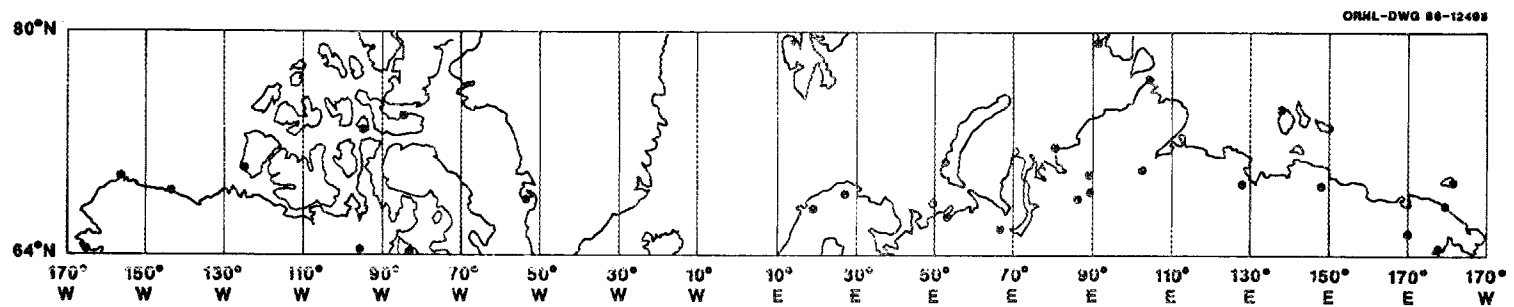


Figure 4.2. Map of the climate stations and IBP Tundra Biome sites used in describing the spatial heterogeneity of the tundra model's driving variables.

distribution. Table 4.2 shows the input to PRISM. Remember that these distributions describe the spatial variability (between-site or within-biome variability) of the driving variables (e.g., the variability in mean January air temperature across the tundra between 64°N and 90°N).

Data on soil and litter temperature and standing dead and litter moisture for sites across the tundra were not available. We used the monthly values of air temperature and soil moisture drawn during Monte Carlo simulation to calculate monthly litter and soil temperature, and standing dead and litter moisture, respectively; we used the monthly relationships (proportions) between these variables specified by the data from Point Barrow to make these calculations.

Calculation of the expected value of a function of multiple random variables (e.g., the site-specific models and the driving variables) requires the joint probability distribution for the random variables (Rozanov 1969, Spiegel 1975). The structure of PRISM can accommodate this requirement (see Section 4.2.4). From another perspective, a realistic climate (i.e., set of driving variables) should be involved in each iteration (each site-specific model run) of the Monte Carlo simulation. The seasonal pattern of monthly climate and the between variable correlations experienced by the vegetation of an individual site should be retained. Rank order correlations for the driving variables (both serial and between-variable correlations) insure that this is indeed the case.

PRISM allows for pair-wise specification of first-order correlations between driving variables; however, it is easy

Table 4.2. Input to PRISM used to describe frequency distributions of the tundra model's driving variables for the 64°N to 90°N latitude belt.

Variable <sup>a</sup>	Distribution <sup>b</sup>	Central Tendency <sup>c</sup>	Minimum Value	Maximum Value
Z <sub>1</sub> (1)	T	0.00	0.00	6.00
Z <sub>1</sub> (2)	U	34.00	4.00	64.00
Z <sub>1</sub> (3)	U	132.00	84.00	181.00
Z <sub>1</sub> (4)	U	334.00	267.00	400.00
Z <sub>1</sub> (5)	U	504.00	352.00	657.00
Z <sub>1</sub> (6)	U	526.00	420.00	633.00
Z <sub>1</sub> (7)	U	436.00	355.00	516.00
Z <sub>1</sub> (8)	U	288.00	210.00	336.00
Z <sub>1</sub> (9)	U	148.00	57.00	238.00
Z <sub>1</sub> (10)	U	54.00	13.00	95.00
Z <sub>1</sub> (11)	T	0.00	0.00	23.00
Z <sub>1</sub> (12)	T	0.00	0.00	10.00
Z <sub>2</sub> (1)	T	-30.00	-41.00	-5.00
Z <sub>2</sub> (2)	T	-30.00	-40.00	-10.00
Z <sub>2</sub> (3)	T	-25.00	-35.00	-7.00
Z <sub>2</sub> (4)	T	-18.00	-26.00	-1.00
Z <sub>2</sub> (5)	T	-8.00	-12.00	4.00
Z <sub>2</sub> (6)	T	1.00	-3.00	10.00
Z <sub>2</sub> (7)	U	8.00	1.00	14.00
Z <sub>2</sub> (8)	U	6.00	0.00	11.00
Z <sub>2</sub> (9)	U	1.00	-5.00	6.00
Z <sub>2</sub> (10)	T	-8.00	-15.00	1.00
Z <sub>2</sub> (11)	T	-17.00	-30.00	-5.00
Z <sub>2</sub> (12)	T	-24.00	-37.00	-9.00
Z <sub>7</sub> (1)	U	6.02	0.14	11.90
Z <sub>7</sub> (2)	U	5.02	0.12	9.92
Z <sub>7</sub> (3)	U	2.47	0.08	4.85
Z <sub>7</sub> (4)	U	3.18	0.09	6.26
Z <sub>7</sub> (5)	U	4.46	0.71	8.80
Z <sub>7</sub> (6)	U	7.58	0.16	15.00
Z <sub>7</sub> (7)	U	3.82	0.10	7.53
Z <sub>7</sub> (8)	U	2.10	0.07	4.13
Z <sub>7</sub> (9)	U	1.62	0.04	3.21
Z <sub>7</sub> (10)	U	1.97	0.06	3.88
Z <sub>7</sub> (11)	U	2.89	0.09	5.69
Z <sub>7</sub> (12)	U	5.23	0.12	10.34

Table 4.2. (Continued)

Variable <sup>a</sup>	Distribution <sup>b</sup>	Central Tendency <sup>c</sup>	Minimum Value	Maximum Value
Z <sub>8</sub>	T	152.00	130.00	175.00
Z <sub>9</sub>	T	276.00	252.00	300.00

<sup>a</sup>Numbers in parentheses indicate the month (1=January, 2=February, etc.). Units are given in Table 2.19, p. 121.

<sup>b</sup>T specifies a triangular distribution, U a uniform distribution. The triangular distributions can be non-symmetric or right-triangular (i.e., linear).

<sup>c</sup>Mode for a triangular distribution, mean for a uniform distribution.

to specify correlations that are computationally impossible (Robert H. Gardner, pers. comm.). With highly correlated data like the climatic driving variable data, partial specification of the correlation structure (i.e., leaving out non-zero pair-wise correlations) results in a fatal error and termination of the program during numerical manipulation of the correlation matrix. For example, if variables A and B are correlated and variables B and C are correlated, specification of the correlation coefficients for A and B and B and C, without specifying the correlation between A and C, can result in program termination.

This problem could be eliminated by specifying as input all pair-wise rank order correlation (703 entries for the tundra model; i.e., the upper (or lower) triangle of the correlation matrix minus the principal diagonal). However, because of the number, pattern, and magnitude of the correlations in the driving variable data for the tundra between 64°N and 90°N, complete specification of the correlations (Spearman rank correlations calculated using procedures from SAS (SAS Institute Inc. 1982), results in a fatal numerical precision problem. Solution of this latter problem will require recoding those elements of PRISM involved in manipulation of the correlation matrix and further significant program development. Consequently, we only present results from simulations where no correlations are specified. These results are the first estimate of regional CO<sub>2</sub> flux predicted by using the expected value of site-specific fluxes. They permit an initial evaluation of the extrapolation, and they represent a baseline for comparisons with

extrapolations that will follow. These future extrapolations are dependent upon modifications of the Monte Carlo program or implementation of alternative recipes for calculating the expected value.

#### 4.3.1.2 Monte Carlo Simulation

Monte Carlo simulation of the tundra between 64°N and 90°N involved 200 iterations. Experience with PRISM indicates that 200 samples from the frequency distributions, using Latin Hypercube sampling, are adequate to approximate the specified distributions (Robert H. Gardner, pers. comm.). For each of the 200 iterations, a full set of driving variables was established (by direct draws from the frequency distributions and subsequent derivations), and the carbon dynamics of the tundra were simulated for 10 years. Daily values of net CO<sub>2</sub> flux (total ecosystem respiration minus total ecosystem photosynthesis) during the tenth year were saved for calculation of the expected value. Values for the driving variables did not change from one year to the next during the tundra simulation; climate was constant. The ten year runs were chosen to allow time for the standing crops, the state variables, to come to some sort of quasi-equilibrium with the climate. Earlier explorations with the site-specific models indicated that the initial values of the state variables could significantly influence simulations if only one year was simulated. Experience with the models suggested that ten years was sufficient to allow the climate to condition the state variables.

#### 4.3.1.3 Expected Net Seasonal CO<sub>2</sub> Exchange

Figure 4.3 compares the mean (expected) seasonal net CO<sub>2</sub> exchange for 200 Monte Carlo iterations of the tundra model with that simulated for Point Barrow, Alaska (Section 2.7). The shift in peak uptake from early July in the Point Barrow simulation to mid-June in the mean Monte Carlo simulation is a direct consequence of including within-biome heterogeneity in the simulations. The June temperature in the Point Barrow site-specific simulation is 0.3°C. June temperatures across the tundra (characterized by the distribution of Z<sub>2</sub>(6), Table 4.2) tend to be warmer and closer to the site-specific model's optimum temperature for photosynthesis (15°C); the result is earlier photosynthesis and net uptake in the mean site flux. Some of the general smoothing and broadening of response expected when natural variability is included in functional responses (O'Neill 1979a, 1979b) can be seen, particularly in early summer, but an increased CO<sub>2</sub> release in the mean simulation dominates the comparison of late summer exchange. Part of this release is due to autotroph respiration associated with the earlier accumulation of live biomass; however, most of the difference is due to reduced late summer photosynthesis in the mean Monte Carlo simulation. Autotrophic and heterotrophic respiratory fluxes are relatively similar in the two simulations; therefore the differences in net exchange are primarily the result of reductions in photosynthesis.

The driving variables do not appear to be responsible for this reduced photosynthesis, at least in any simple way. For example,

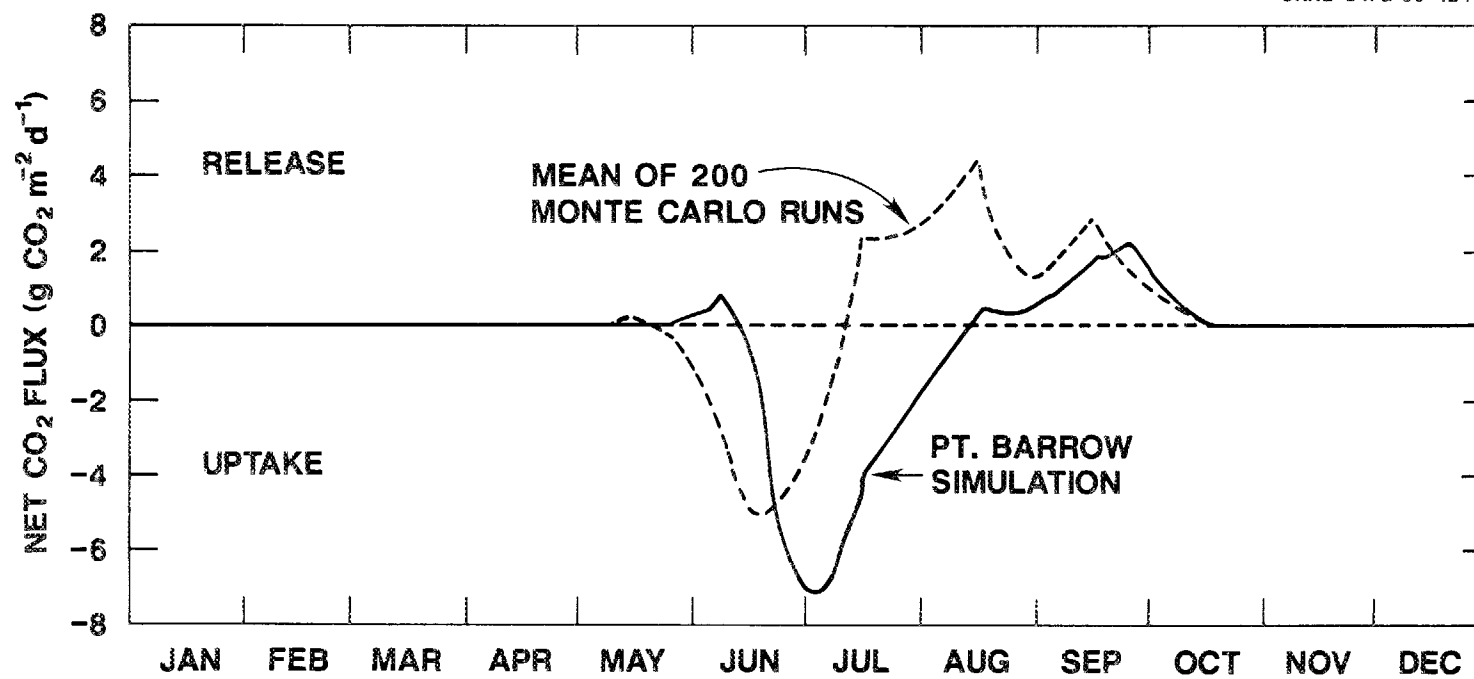


Figure 4.3. Seasonal net biosphere-atmosphere CO<sub>2</sub> exchange from the site-specific tundra model and the mean of the Monte Carlo simulation of that model.

summer temperatures across the tundra should support net photosynthesis. Mean summer temperatures are slightly above Point Barrow temperatures and tend to be closer to the temperature optimum. The solar radiation values are scaled such that optimum light conditions are equated with the highest monthly light intensity for that particular model run; hence, runs simulating sites with suboptimal light conditions are unlikely. This raises the suspicion that the reduced summer photosynthesis is either the result of complex interactions within the site-specific model (e.g., photosynthate allocation), interactions between driving variables and model parameters (which are not changed from the Point Barrow simulation), or error introduced by not including driving variable correlations. Perhaps the late summer decline from optimum solar radiation is more precipitous than it should be because of chance draws from the lower ends of the distributions for radiation. This situation might be avoided with the inclusion of serial correlations. A definitive response to these speculations will require an expanded evaluation of the tundra model (e.g., a formal uncertainty analysis) and the ability to include correlation in the simulations. Fortunately, a full understanding of the differences between the site-specific simulation and the Monte Carlo expected value is not necessary before continuing this initial evaluation of the extrapolation.

We calculated the expected monthly net CO<sub>2</sub> flux by summing daily fluxes for each month. The extrapolated monthly net CO<sub>2</sub> fluxes for the tundra biome between 64°N and 90°N are the expected

monthly net CO<sub>2</sub> fluxes times the area of the tundra within the latitude belt (see Equation 4.6). Table 4.3 compares this regional level CO<sub>2</sub> exchange between the tundra and the atmosphere with that predicted by the simple extrapolation (Chapter 3) of the site-specific Point Barrow exchange. The reduced and spring-shifted net uptake and the increased late summer net release seen in the mean of the Monte Carlo runs (Figure 4.3) is also expressed in the monthly estimates of regional CO<sub>2</sub> exchange obtained with the extrapolation by expected value (Table 4.3).

#### 4.3.2 The Cool Coniferous Forest Between 64°N And 90°N Latitude

Cool coniferous forest, as defined in Chapter 3, occupies 3,137,733 km<sup>2</sup> (approximately 28%) of the land area between 64°N and 90°N. In this section we describe the extrapolation of the associated site-specific model (see Section 2.3).

##### 4.3.2.1 Driving Variables And Their Frequency Distributions

The cool coniferous forest model has thirteen driving variables (Table 2.8, p. 79), eight exogenous climate variables ( $Z_1$  to  $Z_8$ ) and five phenology parameters ( $Z_9$  to  $Z_{13}$ ). In the site-specific model, daily values of the climate variables are read into the simulation program as input data. The constant values for the phenology parameters are also input data. Daily values for the climate variables are not readily available for sites across the cool coniferous forest of the 64°N-90°N latitude belt, but mean monthly values are. We calculated the monthly means of the actual input data for the site-specific model and ran the model using daily

Table 4.3. Predicted net CO<sub>2</sub> exchange between the atmosphere and the tundra of the 64°N to 90°N latitude belt.

Month	Net CO <sub>2</sub> Exchange (10 <sup>15</sup> g CO <sub>2</sub> month <sup>-1</sup> ) <sup>a</sup>	
	Simple Extrapolation	Extrapolation by Expected Value
January	0.00	0.00
February	0.00	0.00
March	0.00	0.00
April	0.00	0.00
May	0.02	-0.02
June	-0.40	-0.69
July	-0.81	0.16
August	0.01	0.56
September	0.31	0.37
October	0.06	0.05
November	0.00	0.00
December	0.00	0.00

<sup>a</sup>Positive values indicate release to the atmosphere; negative values indicate uptake by the tundra.

values interpolated (linearly) from these monthly values. This simulation resulted in a smoother seasonal pattern of CO<sub>2</sub> flux, but otherwise the results closely matched the simulations using actual daily measurements. From this we concluded that we could use the slightly modified site-specific model for the extrapolation.

Data for the climate driving variables came from climate stations within the cool coniferous forest model biome (Plate 3.1, see Appendix) lying between 64°N and 90°N (from Johannessen 1970, Hare and Hay 1974, Lydolph 1977, and Muller 1982). These stations are identified in Table 4.4 and mapped in Figure 4.4. The monthly values were climatic means. Not all stations and sites provided data on all variables, nor were all the climate means based on the same record length. The histograms we used to describe the frequency distributions were built from a composite of available data.

Dew point temperature is one of the cool coniferous forest model's driving variables ( $Z_5$ ). Data for this variable was not available from the climate stations. Therefore, we calculated monthly dew point temperature from monthly relative humidity and monthly low temperature (both available from the station data) using the formula derived by J. Gentilli (referenced in Stringer 1972). Mean daily maximum temperature and mean daily minimum temperature (Muller 1982) were used as estimates of average daytime temperature ( $Z_6$ ) and average nighttime temperature ( $Z_7$ ), respectively. The daily maximum and minimum probably overestimate the daytime and nighttime averages, resulting in a diurnal variation wider than that actually experienced by the forest. However, they are useful first

Table 4.4. Climate stations used in describing the spatial heterogeneity of the cool coniferous forest model's driving variables.

Station	Location
Kotzebue, U.S.A.	66°52'N, 160°38'W
Fairbanks, U.S.A.	64°49'N, 147°52'W
Aklavik, Canada	68°14'N, 134°50'W
Norman Wells, Canada	65°17'N, 126°48'W
Haparanda, Sweden	65°50'N, 24°09'E
Stensele, Sweden	65°04'N, 17°10'E
Sodankyla, Finland	67°22'N, 26°36'E
Oulu, Finland	65°01'N, 25°29'E
Kajaani, Finland	64°17'N, 27°41'E
Murmansk, U.S.S.R.	68°58'N, 33°03'E
Louchi, U.S.S.R.	66°05'N, 32°59'E
Kem', U.S.S.R.	65°00'N, 34°48'E
Turuchansk, U.S.S.R.	65°47'N, 87°57'E
Tura, U.S.S.R.	64°10'N, 100°04'E
Olen'ok, U.S.S.R.	68°30'N, 112°36'E
Verchojansk, U.S.S.R.	67°33'N, 133°23'E
Zyr'anka, U.S.S.R.	65°44'N, 150°54'E
Archangel'sk, U.S.S.R.	64°30'N, 40°30'E

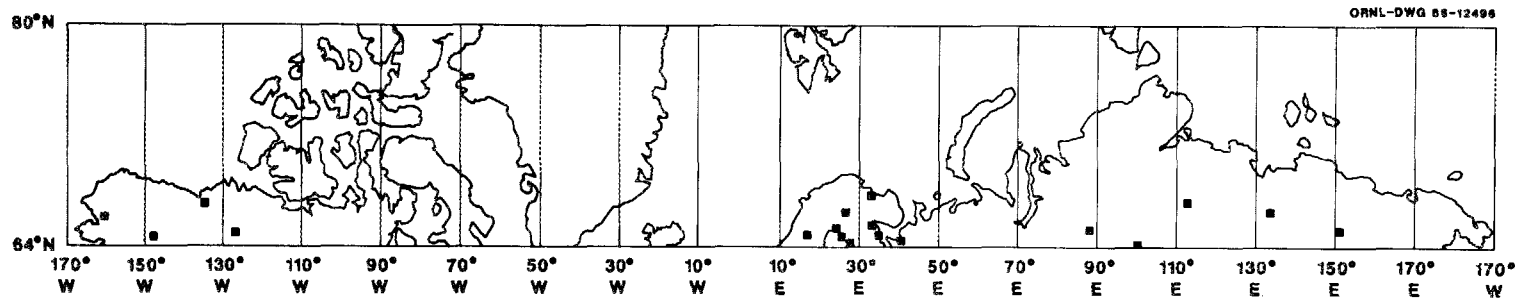


Figure 4.4. Map of the climate stations used in describing the spatial heterogeneity of the cool coniferous forest model's driving variables.

approximations that are obtainable directly from the climate station data. We calculated day length ( $Z_4$ ) from data on mean duration of sunshine (Muller 1982).

From these data we obtained estimates of minimum values, maximum values, and central tendencies for each of the climate variables. Frequency histograms suggested the appropriate shape for the probability distributions. The Scandinavian stations were overrepresented in the data (see Figure 4.4). Their number and proximity resulted in a clustering of driving variable values around those characteristic of the Scandinavian climate. Concerned that this artifact of station distribution would bias the desired description of climate heterogeneity for the entire coniferous forest region, we discounted the Scandinavian influence on the shape of the distribution by not counting multiple occurrences of driving variable values from these stations. As a result, all distributions were specified as uniform. Input for the Monte Carlo (PRISM) program is given in Table 4.5. Remember that these distributions describe the spatial variability (between-site or within-biome variability) of the model's driving variables (e.g., the variability in mean January temperature across the cool coniferous forest between 64°N and 90°N).

The phenology parameters ( $Z_9$  to  $Z_{13}$ ) are almost certainly correlated with climate, and, consequently, they likely vary from site to site across the biome. However, independent data on these parameters is not available. Therefore, we derived values for these

Table 4.5. Input to PRISM used to describe frequency distributions of the cool coniferous forest model's driving variables for the 64°N to 90°N latitude belt.

Variable <sup>a</sup>	Distribution <sup>b</sup>	Minimum Value	Maximum Value
Z <sub>1</sub> (1)	U	7.00	40.00
Z <sub>1</sub> (2)	U	5.00	37.00
Z <sub>1</sub> (3)	U	5.00	28.00
Z <sub>1</sub> (4)	U	4.00	35.00
Z <sub>1</sub> (5)	U	5.00	39.00
Z <sub>1</sub> (6)	U	12.00	67.00
Z <sub>1</sub> (7)	U	33.00	80.00
Z <sub>1</sub> (8)	U	30.00	74.00
Z <sub>1</sub> (9)	U	13.00	67.00
Z <sub>1</sub> (10)	U	11.00	56.00
Z <sub>1</sub> (11)	U	9.00	58.00
Z <sub>1</sub> (12)	U	7.00	46.00
Z <sub>2</sub> (1)	U	0.00	25.00
Z <sub>2</sub> (2)	U	20.00	71.00
Z <sub>2</sub> (3)	U	149.00	215.00
Z <sub>2</sub> (4)	U	234.00	352.00
Z <sub>2</sub> (5)	U	372.00	465.00
Z <sub>2</sub> (6)	U	420.00	483.00
Z <sub>2</sub> (7)	U	397.00	508.00
Z <sub>2</sub> (8)	U	267.00	319.00
Z <sub>2</sub> (9)	U	102.00	187.00
Z <sub>2</sub> (10)	U	50.00	91.00
Z <sub>2</sub> (11)	U	10.00	27.00
Z <sub>2</sub> (12)	U	0.00	3.00
Z <sub>3</sub> (1)	U	-48.90	-9.80
Z <sub>3</sub> (2)	U	-43.70	-9.90
Z <sub>3</sub> (3)	U	-29.90	-6.70
Z <sub>3</sub> (4)	U	-13.00	0.30
Z <sub>3</sub> (5)	U	-0.90	8.40
Z <sub>3</sub> (6)	U	6.60	14.70
Z <sub>3</sub> (7)	U	11.50	16.50
Z <sub>3</sub> (8)	U	9.70	14.60
Z <sub>3</sub> (9)	U	2.50	9.00
Z <sub>3</sub> (10)	U	-14.10	2.80
Z <sub>3</sub> (11)	U	-36.10	-2.30
Z <sub>3</sub> (12)	U	-45.60	-6.20
Z <sub>4</sub> (1)	U	0.000	0.083
Z <sub>4</sub> (2)	U	0.048	0.179
Z <sub>4</sub> (3)	U	0.163	0.301
Z <sub>4</sub> (4)	U	0.232	0.419
Z <sub>4</sub> (5)	U	0.265	0.469

Table 4.5. (Continued)

Variable <sup>a</sup>	Distribution <sup>b</sup>	Minimum Value	Maximum Value
Z <sub>4</sub> (6)	U	0.342	0.557
Z <sub>4</sub> (7)	U	0.258	0.434
Z <sub>4</sub> (8)	U	0.155	0.324
Z <sub>4</sub> (9)	U	0.101	0.236
Z <sub>4</sub> (10)	U	0.056	0.132
Z <sub>4</sub> (11)	U	0.004	0.099
Z <sub>4</sub> (12)	U	0.000	0.048
Z <sub>5</sub> (1)	U	69.00	91.00
Z <sub>5</sub> (2)	U	68.00	89.00
Z <sub>5</sub> (3)	U	66.00	91.00
Z <sub>5</sub> (4)	U	61.00	93.00
Z <sub>5</sub> (5)	U	58.00	93.00
Z <sub>5</sub> (6)	U	66.00	89.00
Z <sub>5</sub> (7)	U	62.00	87.00
Z <sub>5</sub> (8)	U	70.00	91.00
Z <sub>5</sub> (9)	U	74.00	93.00
Z <sub>5</sub> (10)	U	79.00	92.00
Z <sub>5</sub> (11)	U	73.00	94.00
Z <sub>5</sub> (12)	U	71.00	94.00
Z <sub>6</sub> (1)	U	-47.80	-6.30
Z <sub>6</sub> (2)	U	-40.60	-6.30
Z <sub>6</sub> (3)	U	-25.00	-0.90
Z <sub>6</sub> (4)	U	-7.20	5.60
Z <sub>6</sub> (5)	U	1.70	15.00
Z <sub>6</sub> (6)	U	9.40	21.70
Z <sub>6</sub> (7)	U	15.00	22.20
Z <sub>6</sub> (8)	U	12.20	18.90
Z <sub>6</sub> (9)	U	6.10	12.50
Z <sub>6</sub> (10)	U	-11.10	5.20
Z <sub>6</sub> (11)	U	-35.00	0.60
Z <sub>6</sub> (12)	U	-46.70	-3.30
Z <sub>7</sub> (1)	U	-52.80	-13.30
Z <sub>7</sub> (2)	U	-48.90	-13.60
Z <sub>7</sub> (3)	U	-39.40	-11.20
Z <sub>7</sub> (4)	U	-43.00	-3.80
Z <sub>7</sub> (5)	U	-5.60	2.10
Z <sub>7</sub> (6)	U	2.80	8.90
Z <sub>7</sub> (7)	U	8.10	11.80
Z <sub>7</sub> (8)	U	4.40	10.20
Z <sub>7</sub> (9)	U	-2.80	5.60
Z <sub>7</sub> (10)	U	-19.40	0.90
Z <sub>7</sub> (11)	U	-40.00	-4.60
Z <sub>7</sub> (12)	U	-48.90	-9.10

Table 4.5. (Continued)

Variable <sup>a</sup>	Distribution <sup>b</sup>	Minimum Value	Maximum Value
Z <sub>g</sub> (1)	U	0.70	6.80
Z <sub>g</sub> (2)	U	0.80	6.40
Z <sub>g</sub> (3)	U	1.00	5.90
Z <sub>g</sub> (4)	U	1.80	6.00
Z <sub>g</sub> (5)	U	2.70	4.80
Z <sub>g</sub> (6)	U	2.40	5.50
Z <sub>g</sub> (7)	U	2.00	5.80
Z <sub>g</sub> (8)	U	2.00	6.20
Z <sub>g</sub> (9)	U	1.80	5.80
Z <sub>g</sub> (10)	U	1.40	6.10
Z <sub>g</sub> (11)	U	0.80	6.20
Z <sub>g</sub> (12)	U	0.70	5.80

<sup>a</sup>Numbers in parentheses indicate the month (1 = January, 2 = February, etc.). Units are given in Table 2.8, p. 79, except for Z<sub>5</sub>. In the extrapolation, the dew point temperature (Z<sub>5</sub> in Table 2.8) of the site-specific model is replaced by percent relative humidity (Z<sub>5</sub> in this table).

<sup>b</sup>U specifies a uniform distribution.

parameters with a simple algorithm. After examining the data from the Andrews Experimental Forest site (the site of the site-specific simulation), we defined the week on which the growing season begins ( $Z_{10}$ ) as the first week of the first month (beginning with January) with a mean temperature greater than  $10^{\circ}\text{C}$ . We defined the week on which the growing season ends ( $Z_{11}$ ) as the first week of the first subsequent month where mean temperature again falls below  $10^{\circ}\text{C}$ . Following the pattern in the Andrews Experimental Forest data, we set the week of bud break ( $Z_9$ ) equal to the week on which the growing season begins ( $Z_{10}$ ), and we set the week on which new foliage becomes old foliage ( $Z_{12}$ ) equal to the week on which the growing season ends ( $Z_{11}$ ). We defined the week of minimum leaf fall ( $Z_{13}$ ) as the week on which the growing season ends minus five weeks. In this way, the phenology parameters were determined by the values of daily temperature drawn from the specified frequency distributions during Monte Carlo simulation.

We encountered the same correlation problem with the coniferous forest model as we experienced with the tundra model (see Section 4.3.1.1). Consequently, we again present only those simulations where no correlations were specified.

#### 4.3.2.2 Monte Carlo Simulation

Monte Carlo simulation of the cool coniferous forest model proceeded exactly as described for the tundra model (see Section 4.3.1.2).

#### 4.3.2.3 Expected Net Seasonal CO<sub>2</sub> Exchange

Figure 4.5 compares the mean (expected) seasonal net CO<sub>2</sub> exchange for the 200 Monte Carlo iterations of the cool coniferous forest model with that simulated for the Andrews Experimental Forest site (Section 2.3). The climate in the Cascades Mountains of Oregon, the location of the site-specific simulation, is quite different from the climate of the 64°N–90°N latitude belt; monthly values of the driving variables for the Andrews Experimental Forest site almost always exceeded the limits on the distributions of driving variables used in the extrapolation. The coniferous forests of the high latitudes are much cooler (particularly during the winter), the days are shorter, and solar irradiance is reduced. These forests do not experience the summer drought seen in the Oregon mountains, and they receive much less precipitation during the rest of the year. All of these factors working together are responsible for the mean coniferous forest site's general reduction in magnitude of exchange (Figure 4.5). They are also responsible for the three month shift in the spring transition from source (net release) to sink (net uptake) and the change from a sink during autumn (Andrews Experimental Forest) to a source (the mean of the Monte Carlo runs). The absence of summer drought is a major factor in the change from mid-summer source to mid-summer sink. Because of the greater introduced variability, the general smoothing and reduction in magnitude often seen when natural variability is considered (O'Neill 1979a, 1979b) is more obvious for the coniferous forest model than for the tundra model (compare Figures 4.3, p. 214, and 4.5).

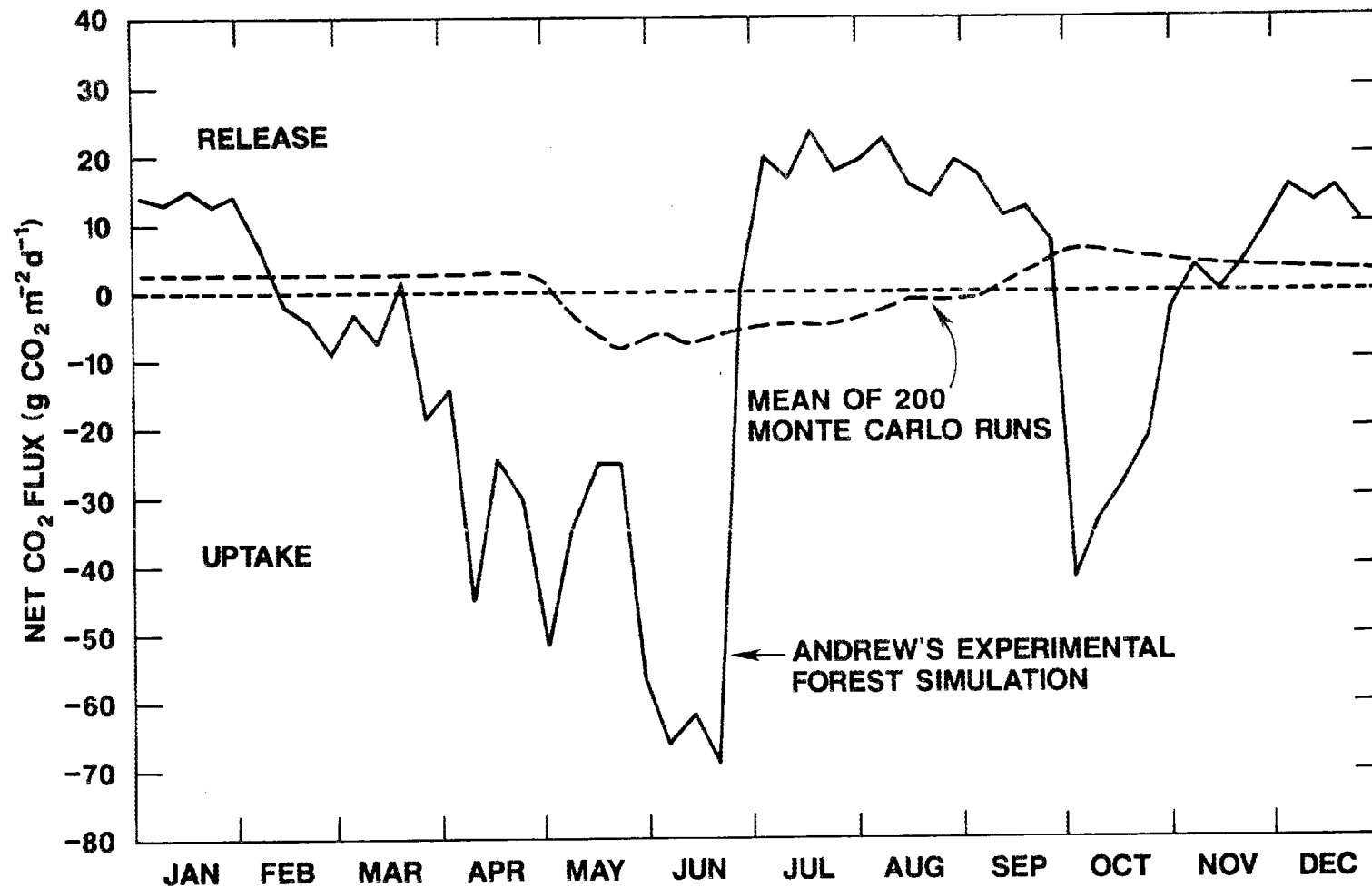


Figure 4.5. Seasonal net biosphere-atmosphere CO<sub>2</sub> exchange from the site-specific cool coniferous forest model and the mean of the Monte Carlo simulation of that model.

We calculated the expected monthly net CO<sub>2</sub> flux by summing daily fluxes for each month. The extrapolated monthly net CO<sub>2</sub> fluxes for the cool coniferous forest biome between 64°N and 90°N are the expected monthly net CO<sub>2</sub> fluxes times the area of the cool coniferous forest within the latitude belt (see Equation 4.6). Table 4.6 compares this regional-level exchange of CO<sub>2</sub> between the cool coniferous forest and the atmosphere with that predicted by the simple extrapolation (Chapter 3) of the Andrews Experimental Forest exchange. The prediction from extrapolation by expected value is much more reasonable than the prediction from the simple extrapolation. The magnitudes of the monthly exchanges are more reasonable (i.e., they are more in-line with estimates from other CO<sub>2</sub> source functions, see Chapter 1), and the restriction of net uptake to the summer is a more realistic description of production dynamics in the high northern latitudes.

#### 4.3.3 NET SEASONAL BIOSPHERE-ATMOSPHERE CO<sub>2</sub> EXCHANGE FOR 64°N TO 90°N

Together tundra and cool coniferous forest cover nearly 82% of the land area between 64°N and 90°N, and they represent nearly 99% of that area with potentially non-zero biosphere-atmosphere CO<sub>2</sub> exchanges. The rest of the latitude belt is covered by Siberian grassland (0.8%), cropland (0.2%), wetland (0.2%), shore and hinterland (0.08%), and ice, polar desert, sand, and rock (17%). Enough of the latitude belt is represented by the extrapolated tundra and cool coniferous forest models to justify a comparison (Table 4.7) of the biosphere-atmosphere CO<sub>2</sub> exchange predicted by

Table 4.6. Predicted net CO<sub>2</sub> exchange between the atmosphere and the cool coniferous forest of the 64°N to 90°N latitude belt.

Month	Net CO <sub>2</sub> Exchange (10 <sup>15</sup> g CO <sub>2</sub> month <sup>-1</sup> ) <sup>a</sup>	
	Simple Extrapolation	Extrapolation by Expected Value
January	1.52	0.29
February	-0.18	0.22
March	-0.62	0.22
April	-2.52	0.25
May	-4.27	-0.50
June	-4.31	-0.58
July	1.70	-0.44
August	1.98	-0.23
September	1.03	0.15
October	-2.76	0.48
November	0.31	0.42
December	1.19	0.27

<sup>a</sup>Positive values indicate release to the atmosphere; negative values indicate uptake by the cool coniferous forest.

Table 4.7. Predicted net CO<sub>2</sub> exchange between the atmosphere and the terrestrial biosphere of the 64°N to 90°N latitude belt.

Month	Net CO <sub>2</sub> Exchange (10 <sup>15</sup> g CO <sub>2</sub> month <sup>-1</sup> ) <sup>a</sup>	
	Estimate from Pearman and Hyson's tracer transport model	Estimate from the Extrapolation by Expected Value
January	0.27	0.30
February	0.27	0.22
March	0.34	0.23
April	0.36	0.25
May	0.14	-0.54
June	-0.89	-1.30
July	-1.30	-0.29
August	-1.20	0.33
September	0.53	0.52
October	0.66	0.53
November	0.48	0.43
December	0.33	0.27

<sup>a</sup>Positive values indicate release to the atmosphere; negative values indicate uptake by the terrestrial biosphere of the latitude belt.

the extrapolation and the exchange predicted by Pearman and Hyson's (1981b) tracer transport model. Figure 4.6 illustrates this comparison. The predictions do show some similarity, especially with respect to magnitude. Relative errors (the ratio of the difference between the two estimates to the Pearman and Hyson estimate) are less than one for all months except May and August, and these exceptions are due to reversals in the direction of exchange. Also, both estimates show an extended period of net release (positive values) and a contracted period of net uptake (negative values). Certainly, the CO<sub>2</sub> exchange for the 64°–90°N latitude belt predicted by extrapolation using mathematical expectation comes much closer to the Pearman and Hyson estimate than the exchange predicted by simple extrapolation (compare Table 3.5, p. 190, with Table 4.7).

There are, however, notable differences. With the a priori constraint of a balanced latitude belt (i.e., no net annual exchange), Pearman and Hyson's estimate predicts a small net annual uptake for the latitude belt of  $0.01 \times 10^{15} \text{ g CO}_2 \text{ month}^{-1}$  (possibly due to round-off errors). Without this constraint, the extrapolation predicts a net biospheric release of  $0.92 \times 10^{15} \text{ g CO}_2 \text{ month}^{-1}$  for the latitude belt. If this annual release of nearly one Gigaton is too large, and it probably is, either the extrapolated uptake is underestimated or the extrapolated release is overestimated.

Net exchange over the period of vegetative dormancy (January to April and September to December) is  $3.38 \times 10^{15} \text{ g CO}_2$  for the

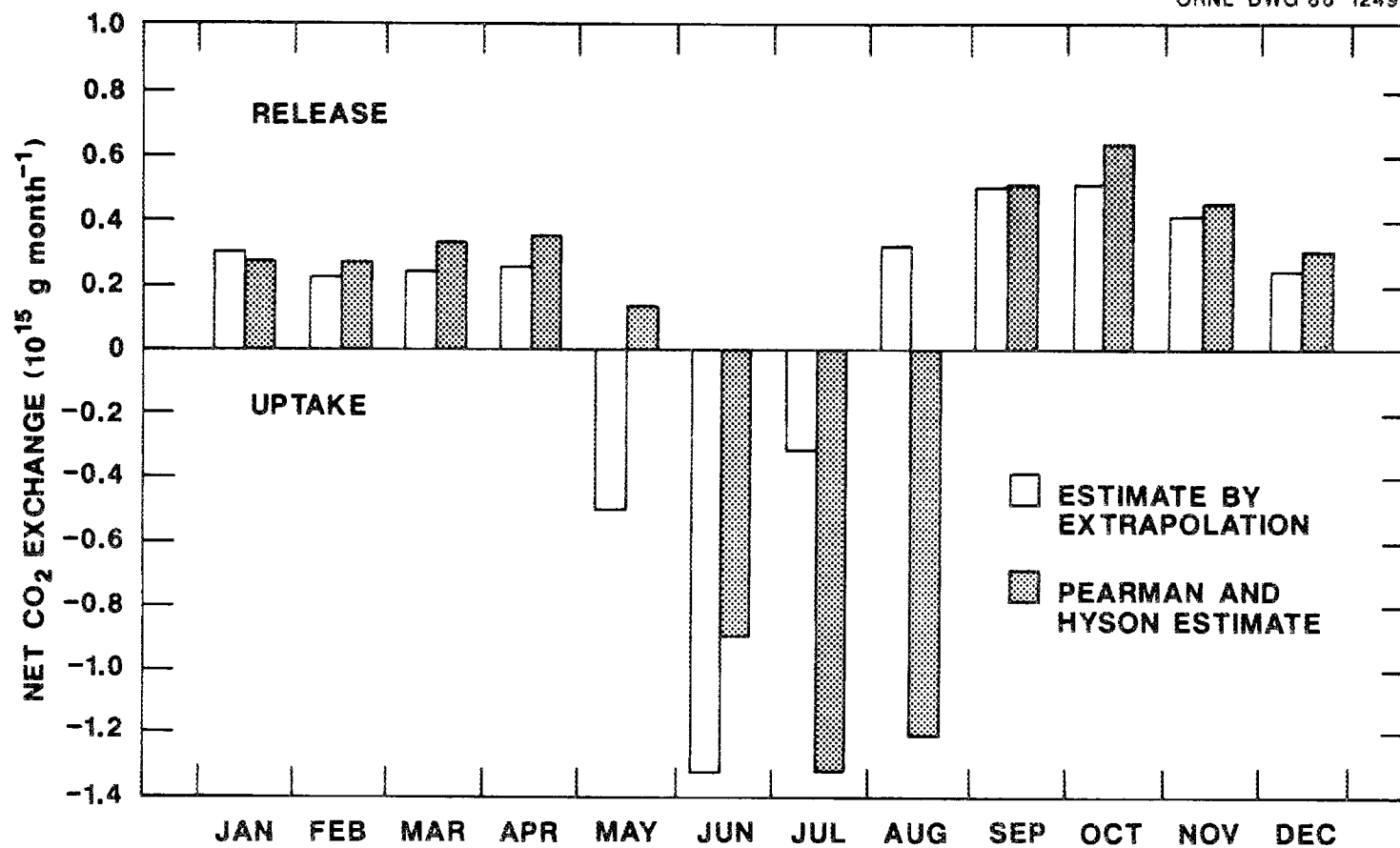


Figure 4.6. Net CO<sub>2</sub> exchange between the atmosphere and the terrestrial biosphere of the 64°N to 90°N latitude belt. The solid bars represent the exchange predicted from Pearnan and Hyson's (1981b) tracer transport model; the open bars represent the exchange predicted from the extrapolation by expected value of site-specific model simulations.

Pearman and Hyson estimate and  $3.08 \times 10^{15}$  g CO<sub>2</sub> for the estimate by extrapolation, a difference of less than 10% (relative error = 0.089). For the growing season (May through August), total net exchange is  $-3.39 \times 10^{15}$  g CO<sub>2</sub> for the Pearman and Hyson estimate and  $-2.13 \times 10^{15}$  g CO<sub>2</sub> for the estimate by extrapolation (a relative error of 0.372). This comparison suggests that the extrapolation underestimates net biospheric uptake during the growing season. Since net exchange is respiration minus photosynthesis, an underestimate of net uptake could be the result of either an overestimate of respiration or an underestimate of photosynthesis.

There is little independent data available to help distinguish between these alternatives, but estimates of annual net primary production (NPP; see Woodwell and Whittaker 1978) can provide some clues; an underestimate of photosynthesis could manifest itself as reduced NPP. Based on our calculation of the expected value of seasonal CO<sub>2</sub> flux, mean annual NPP for the tundra of the 64°N to 90°N latitude belt is 132 g dry matter (dm) m<sup>-2</sup> year<sup>-1</sup>. Lieth (1975b), Whittaker and Likens (1975), and Ajtay, Ketner, and Duvigneaud (1979) estimated a mean tundra NPP of 140 g dm m<sup>-2</sup> year<sup>-1</sup>. Olson's (1975) estimates of NPP for tundra and tundra-like ecosystems (which are treated as tundra in my aggregation; see Table 3.1, p. 175) ranged from 4 g dm m<sup>-1</sup> year<sup>-1</sup> to 1000 g dm m<sup>-2</sup> year<sup>-1</sup>. Our prediction of mean NPP for the coniferous forest of the region is 379 g dm m<sup>-2</sup> year<sup>-1</sup>. Whittaker and Likens (1975) and Ajtay, Ketner, and Duvigneaud (1979) estimated the range of NPP for boreal forest (which includes high

latitude coniferous forests) at 400 to 2000 g dm m<sup>-2</sup> year<sup>-1</sup>. Lieth (1975) placed the lower end of the range at 200 g dm m<sup>-2</sup> year<sup>-1</sup>. Most of what we consider as cool coniferous forest in the 64°N to 90°N latitude belt belongs to Olson's (1975) northern taiga and middle taiga. His estimates of NPP for these ecosystems range from 500 to 700 g dm m<sup>-2</sup> year<sup>-1</sup>. Finally, the NPP values predicted by the extrapolation are within the range of NPP (<100 to 500 g dm m<sup>-2</sup> year<sup>-1</sup>) predicted for these latitudes by the "Miami Model" from annual averages for temperature and precipitation (Lieth 1975b). Thus, the extrapolation results in reasonable estimates of mean NPP; the estimates might be low, but they are not dramatically low.

Considering both the tundra and coniferous forest biomes (plus the minor land cover categories), the extrapolation predicts an area weighted mean zonal NPP of 179 g dm m<sup>-2</sup> year<sup>-1</sup> for the 64°N to 90°N latitude belt. Pearman and Hyson (1980) used Whittaker and Likens' (1973) data to estimate a zonal NPP for the latitude belt of 309 g dm m<sup>-2</sup> year<sup>-1</sup>. Fung et al. (1983) estimated a zonal NPP of 305 g dm m<sup>-2</sup> year<sup>-1</sup> for the comparable, but slightly smaller, 66.5°N to 90°N latitude belt. Both of these latter estimates are based on tabulated estimates of NPP; they are not derived from the CO<sub>2</sub> source functions. The Fung et al. source function is constrained to reproduce their estimate of NPP, but, unfortunately for comparisons, the Pearman and Hyson (1980, 1981b) source function cannot be used to estimate NPP because it cannot separate gross primary production, autotroph respiration, and heterotroph

respiration. The Pearman and Hyson source function is not constrained by NPP, and the compatibility of their predicted biosphere-atmosphere exchanges and their estimate of NPP is unknown. Nevertheless, the extrapolation's prediction of zonal NPP, given the available numbers, is well below either the Pearman and Hyson estimate or the Fung et al. estimate (relative errors are 0.42 and 0.41, respectively).

We believe that the extrapolation's prediction of lower zonal NPP is supported in part by our larger estimate of low-productivity tundra land area (36% by Pearman and Hyson versus our 54%), and by the fact that the NPP of boreal forests at these latitudes probably falls at or below the lower end of Whittaker and Likens (1973) production estimates (i.e.,  $\leq 400 \text{ g dm m}^{-2} \text{ year}^{-1}$ ) and not at the  $800 \text{ g dm m}^{-2} \text{ year}^{-1}$  used by Pearman and Hyson. Indeed, if Pearman and Hyson had used the lower value, their estimate of zonal NPP would have been  $189 \text{ g dm m}^{-2} \text{ year}^{-1}$ ; their published estimate was  $309 \text{ g dm m}^{-2} \text{ year}^{-1}$  and our estimate is  $179 \text{ g dm m}^{-2} \text{ year}^{-1}$ . The revised estimate is much closer to our own. Nevertheless, these NPP comparisons, combined with the apparent tendency of the extrapolated tundra model to underestimate late-summer photosynthesis, lead us to conclude that the imbalance in our estimate of regional exchange (i.e., a net annual release of  $0.95 \times 10^{15} \text{ g CO}_2$ ) is probably the result of an underestimate of photosynthetic production during the latter part of the growing season. We cannot, however, rule out the possibility of contributions from heterotrophic respiration by decomposers;

estimates of respiration comparable to those for NPP are not available (but see Gillette and Box (1986) for a move in this direction).

An obvious difference between the Pearman and Hyson estimate and the exchange predicted by extrapolation using mathematical expectation (Table 4.7 and Figure 4.6) is the timing and magnitude of biospheric CO<sub>2</sub> uptake during the growing season. The discrepancy in total growing season net uptake (most notable in July and August) is related to the extrapolation's prediction of a substantial annual release. If the net annual exchange predicted by extrapolation is balanced (ad hoc) by subtracting the annual release of  $0.95 \times 10^{15}$  g CO<sub>2</sub> from the late-summer (July-August) exchange (simulating an increase in production), the difference between total growing season uptake predicted by Pearman and Hyson and the uptake predicted by our extrapolation is reduced from 37.2% to 9.1%. Remember that the difference in predicted exchange over the non-growing season was 8.9%. This coarse manipulation suggests that, if the source of the annual imbalance could be eliminated, the extrapolation would generate a quite acceptable CO<sub>2</sub> exchange function for the 64°N to 90°N latitude belt with a relative error of less than 10%.

The extrapolation's prediction of net biosphere uptake in May (in comparison with net May release in the Pearman and Hyson estimate, Table 4.7 and Figure 4.6) is largely a consequence of the extrapolated conifer model's behavior (see Table 4.6). This behavior is probably a response to spring temperature across the

biome. Conifers in central Sweden (at 50° 48'N latitude) begin net photosynthetic activity in April as soon as the soil thaws (Linder and Troeng 1980, Agren et al. 1980), which suggests that coniferous forests of slightly higher latitudes (i.e., within the 64°N to 90°N latitude belt) could be a net CO<sub>2</sub> sink in May. Interestingly, Pearman and Hyson (1981b; see their Figure 2) underestimate the spring concentration and changes in concentration of atmospheric CO<sub>2</sub> at Point Barrow, Alaska, where the influence of the terrestrial biosphere between 64°N and 90°N might be most visible. Perhaps the earlier growing season predicted by the extrapolation would result in closer agreement with the concentrations of atmospheric CO<sub>2</sub> observed at Point Barrow.

The preceding examination suggests that with the important exception of underestimated net CO<sub>2</sub> uptake in late-summer, possibly due to an underestimate of photosynthetic production, the extrapolation of the site-specific models by calculation of the expected value of site-specific fluxes generates a reasonable CO<sub>2</sub> exchange function for the 64°N to 90°N latitude belt. We now turn to a brief consideration of why the two estimates fail to match more closely than they do. Possible sources of error include:

1. Errors in the Pearman and Hyson estimate. Remember that the Pearman and Hyson estimate is the tuned model boundary condition required for the best fit between simulated and observed annual cycles of CO<sub>2</sub> concentration; it is not the result of direct observations. Some of the exchange predicted by Pearman and Hyson could be, and probably is, the result of atmospheric circulation

between the 64°N to 90°N latitude belt and surrounding air masses rather than biosphere uptake and release within the belt. Thus, some of the differences between our source function and the Pearman and Hyson could be due to atmospheric circulation not modeled by Pearman and Hyson.

2. Within-biome biotic heterogeneity. The extrapolation only considered spatial variability in abiotic factors described by model driving variables. We assumed that model parameters, which frequently describe biotic factors (e.g., maximum photosynthetic rate) were constant across the region. In fact, model parameters, or biotic factors, probably do vary from site-to-site, and the site-specific models could be sensitive to this variability. The influence of this probable, but unknown, variability is not considered in our estimate of regional CO<sub>2</sub> exchange.

3. Exchanges by the other biomes in the latitude belt. CO<sub>2</sub> exchange for 0.98% of the latitude belt's land area (0.82% in grassland and 0.16% in cropland) was estimated by simple extrapolation (area times site-specific flux); variability within these biome-types was ignored. Furthermore, because we did not implement a wetlands model, we assumed that CO<sub>2</sub> exchange for wetlands (0.17% of the belt's land area) was inconsequential and set those fluxes to zero. Prediction of CO<sub>2</sub> fluxes to and from these areas using extrapolation by expected value could alter the estimate of regional CO<sub>2</sub> exchange.

4. Failure to include driving variable correlations. As discussed earlier (Section 4.3.1.1) it is currently impossible to include driving variable correlations in the recipe for extrapolation that we have implemented. These serial and between-variable correlations are important, and they might strongly influence the estimate of regional CO<sub>2</sub> exchange. Indeed, the extrapolation's prediction of net annual release might be the result of not including correlations (see Section 4.3.1.3).

5. Uncertainties in estimating driving variables. The climate stations and IBP sites did not always provide the needed driving variable data. We frequently had to use surrogates (e.g., using daily maximum temperature for average daytime temperature in the coniferous forest model) or derive values indirectly (e.g., the derivation of monthly soil moisture in the tundra model and phenology variables in the coniferous forest model). Uncertainties in these approximations could easily introduce error into the extrapolation.

6. Uncertainties in estimating the within-biome variability in driving variables. Even when driving variable data could be obtained directly from the climate stations, the number and distribution of these stations introduced uncertainty into the estimate of regional variability (i.e., the frequency distributions describing the spatial variability of the driving variables). We elected to use the distributions of least bias, the uniform and triangular (Tiwari and Hobbie 1976, Gardner and O'Neill 1983) described by the best available information (Morgan et al. 1978). Different distributions could generate different results, although

O'Neill, Gardner, and Carney (1982) concluded that the shape of the distribution had little effect on the prediction uncertainty of a stream ecosystem model. Estimates of maxima and minima might have more influence than shape, but there is less uncertainty associated with these estimates. The potential error involved in the specification of distributions is probably increased by the difficulty of estimating some variables (see 5 above).

7. Failure to specify additional constraints. Site-specific  $\text{CO}_2$  flux may be constrained by abiotic or biotic variables not included in the formulation of a site-specific model developed at one particular location. For example, if nutrients are not important at the model site, they will probably not be included in the model. They may, however, be an important constraint at other sites. If these neglected constraints are important enough, and if the situation occurs frequently across the region, an extrapolation by expected value could result in an erroneous estimate of regional  $\text{CO}_2$  flux. Could the extrapolation's prediction of net annual release be due to neglected constraints? Possibly, but the constraint in question does not immediately come to mind.

8. Uncertainties in estimating the areal extent of biome-types. The regional flux,  $F_R$ , predicted by extrapolation is given by

$$F_R = \sum_{i=1}^n A_i E[Y_i] , \quad (4.7)$$

where  $E[Y]_i$  is the expected value of site-specific flux for biome-type  $i$  (e.g., tundra) in region  $R$ ,  $A_i$  is the area of biome-type  $i$  in  $R$ , and  $n$  is the number of biome-types in  $R$ . Obviously, different estimates of biome-type areal extent will result in different estimates of regional flux; consequently, uncertainties in estimating  $A_i$  are a potential source of error in the prediction of regional exchange. Our estimates of areal extent were based on Olson, Watts, and Allison's (1983) estimates of land-use and our adopted correspondence between Olson's land cover types and the site-specific models. Uncertainties in both could produce errors in the estimate of regional flux.

9. Errors in the site-specific models. The site-specific models we chose to work with are good representative models of their ecosystem types, and the assembled set is an appropriate one. The models do, however, as all models do, have error associated with them. This error could persist or propagate through the extrapolation and introduce error into the estimate of regional exchange. For many of the reasons just cited, running the site-specific models under conditions for which they were not explicitly designed could increase the chances of significant error in the prediction of site-specific  $CO_2$  flux.

10. Failure to equilibrate climate and state variables. In the Monte Carlo simulations, we allowed ten years for the climate (i.e., driving variables) to condition the initial values of the state variables, that is, to bring them into equilibrium with the prevailing climate. For some state variables (e.g., deciduous

leaves and annually incremented non-woody biomass) this conditioning is not important because the initial values are always zero. However, for others (e.g., litter, soil organic matter, tree trunks, and old evergreen foliage) this conditioning could be important in the erroneous prediction of regional exchange. We believe ten years is sufficient to account for most of the potential error, but it is possible that more time is required, and that the choice of ten years contributes to errors in the regional estimate. It is also possible that the state variables might never equilibrate. It might be impossible, for example, to produce the stunted taiga conifers of the tundra-coniferous forest ecotone from the large Douglas-firs of the coniferous forest's site-specific model.

All of these factors, working alone and in concert, contribute to the potential for error in the extrapolation's estimate of regional CO<sub>2</sub> exchange. Some undoubtedly contribute more than others, and some will be easier to eliminate than others. The next round of extrapolation should be directed at evaluating the relative contribution of each potential source of error, and at eliminating or minimizing those that are important and can be eliminated or minimized most effectively.

We believe that the absence of driving variable correlations is the most important of these targets. The correlations can be introduced either by changes in PRISM (see Section 4.3.1.1) or by using an alternative calculation of the expected value. For example, it might be possible to calculate an acceptable expected value by running the site-specific models at each of the climate

stations (and only at these stations), thereby retaining the driving variable correlations inherent at each site. This approach eliminates the problem of specifying correlations, which is a direct result of the assumption of variable independence implicit in PRISM's input requirements. The trade-off may lie in the ability to include within-biome variability not seen at the climate stations. In either case, solution of the correlation problem is possible with time. The correlations will improve the description of regional variability in driving variables, insuring that each simulation during the Monte Carlo runs involves a realistic climate. The introduction of correlations will almost certainly improve, rather than detract from, what are already very promising results.

The extrapolation by expected value meets the objectives we set forth in Chapter 1 and in Section 4.3 of this chapter. We have collected a set of site-specific models of ecosystem carbon metabolism (Chapter 2). We have shown how these models can be interpreted as components of a seasonal  $\text{CO}_2$  exchange function, and I have demonstrated the assignment of these models to larger regional and global areas (Chapter 3). In this chapter we have presented the calculation of the expected value as the correct way to extrapolate site-specific models across larger heterogeneous regions, and we have applied the technique to a test region in order to evaluate whether the methodology can be successfully applied to the specific problem of simulating regional  $\text{CO}_2$  exchange. The resulting values of monthly net biosphere-atmosphere  $\text{CO}_2$  exchange for the 64°N to 90°N latitude belt are, admittedly, not as

corroborative as they could be, but they are reasonable enough to justify the conditional acceptance of the technique as a method of incorporating mechanistic ecosystem models into a global CO<sub>2</sub> exchange function.

Whether the extrapolation's estimate of regional CO<sub>2</sub> exchange is an accurate representation of actual biosphere-atmosphere exchange cannot be determined until these results are combined with estimates of regional exchange for the rest of the biosphere and with a tracer transport model. Nevertheless, the extrapolation's prediction of a net annual release from the belt of nearly one gigaton CO<sub>2</sub> is probably sufficient reason to reject the specific results of the extrapolation as a prediction of the regions CO<sub>2</sub> exchange. Rejection of the specific monthly values of net exchange is not, however, sufficient reason to reject the extrapolation outright as a feasible procedure for predicting regional CO<sub>2</sub> exchange.

First, the investigation identifies the calculation of an expected value as the correct way to extrapolate site-specific models across heterogeneous regions. This approach may be limited by the ability to calculate this expected value correctly, but mathematical expectation is theoretically the most correct way to predict regional CO<sub>2</sub> from site-specific models. This was not obvious at the outset of the study.

Second, the extrapolation has several positive results. Throughout much of the year, the agreement between the extrapolation's estimate of regional CO<sub>2</sub> exchange and the

reference estimate by Pearman and Hyson (1980, 1981b) was good; the relative error was less than 10%. Most of the differences between the estimates were limited to the growing season, especially the late summer. The extrapolation's estimates of NPP were somewhat low, but were generally reasonable. In at least one respect, the prediction of net uptake in May, the extrapolation seemed to be a better estimate of regional exchange than the Pearman and Hyson estimate.

Third, the level of agreement with the Pearman and Hyson estimate is good despite the many possible sources of error. This result supports the acceptance of the general technique and the recipe for its implementation, even if refinements are needed to eventually permit precise predictions.

Finally, this is the first application of the methodology to regional CO<sub>2</sub> exchange. Too critical an evaluation could unnecessarily deter further development of a potentially very useful methodology.

Further tests and extensions are necessary (e.g., incorporation of driving variable correlations and further consideration of balanced CO<sub>2</sub> exchange) before the conditional acceptance can be upgraded, but extrapolation by mathematical expectation is a promising technique for extrapolating from site-specific models to regional and biome-level models.

## CHAPTER 5

## SUMMARY, SYNTHESIS, AND CONCLUSION

Our motivation for the research presented in this report was the recognized need for ecological models of the seasonal exchange of  $\text{CO}_2$  between the atmosphere and the terrestrial biosphere. These ecological models of the terrestrial biosphere are models derived from ecological data, independently of the requirements of any particular model of atmospheric  $\text{CO}_2$  transport, that can be used as  $\text{CO}_2$  source functions in models describing changes in atmospheric  $\text{CO}_2$ . Ecological  $\text{CO}_2$  source functions are needed in the study of the seasonal cycle of atmospheric  $\text{CO}_2$  concentrations, especially in models of the observed changes in the amplitude of the seasonal cycle. An increased understanding of the seasonal cycle and its changes contributes to an understanding of the biosphere's role in the entire global carbon cycle, a role which is a continuing point of controversy (e.g., the biosphere's part in the secular increase of atmospheric  $\text{CO}_2$ ).

In Chapter 1 we introduced one particular approach to the problem of modeling seasonal  $\text{CO}_2$  exchange between the atmosphere and the biosphere, i.e., the idea of using existing site-specific ecosystem models as a basis for a model of larger-scale regional and global  $\text{CO}_2$  exchanges. Site-specific models like those described in Chapter 2 possess many characteristics that recommend them as a base for constructing biosphere models. However, their use is also hampered by a major disadvantage; the models are all local,

site-specific, and relatively small-scale models. Consequently, the use of site-specific models in a global  $\text{CO}_2$  source function becomes a problem in translating information from local scales to regional and global scales. The proper procedure for translation or extrapolation from site-specific simulations to regional and global simulations is uncertain, if indeed such translation is even obtainable. This problem is not unique to  $\text{CO}_2$  source functions. As ecologists deal more and more with larger scale problems in both landscape ecology and global ecology, the problem of extrapolation from small local scales to larger regional scales is increasingly recognized and increasingly important. This broader relevance of extrapolation from site-specific models to biome-level models reinforced our motivation to use the site-specific ecosystem models in a global  $\text{CO}_2$  exchange function.

In Chapter 3 we tested a very simple extrapolation. An area-weighted summation of site-specific fluxes, under the assumption of relative homogeneity within biomes, generated  $\text{CO}_2$  source functions that differed dramatically from published estimates of  $\text{CO}_2$  exchange. The differences were so great that we rejected the simple extrapolation as a means of incorporating site-specific models in a global  $\text{CO}_2$  source function. The principal conclusion drawn from Chapter 3 is the suggestion that within-biome, between-site heterogeneity is significant enough to influence extrapolation from local fluxes to regional fluxes, which further suggests that successful extrapolation procedures must explicitly incorporate within-biome heterogeneity.

In addition, the simple extrapolation of Chapter 3, although rejected as a general procedure, suggests a possible deficiency in the existing CO<sub>2</sub> source functions. All these source functions assume that monthly net CO<sub>2</sub> exchange is zero in the tropical latitudes. Tropical ecosystems are not strictly aseasonal; they often experience seasonal rainfall and moisture conditions (Walter 1985). If CO<sub>2</sub> flux is influenced by the site's moisture regime, which seems likely (see Sections 2.5 and 2.6), then some seasonality in regional CO<sub>2</sub> flux is probable. The quantitative predictions of tropical CO<sub>2</sub> flux made by the simple extrapolation may be in error, but the qualitative prediction of seasonality may be more reasonable than the aseasonality expressed by the other source functions. The assumed aseasonality of tropical zones is an a priori constraint, this constraint should be reevaluated.

In Chapter 4 we tested an extrapolation that explicitly considers within-biome heterogeneity, that is, spatial variation in those factors that influence CO<sub>2</sub> exchange between the ecosystem and the atmosphere. The extrapolation procedure is based on the mathematical expectation of a random variable. The estimate of regional CO<sub>2</sub> flux is a simple function of the expected value of the simulated site-specific fluxes, integrating across the frequency distributions describing the spatial heterogeneity of model driving variables for that region. Regional CO<sub>2</sub> flux is thus equal to the expected value times the area of the region. We used the 64°N to 90°N latitude belt as a test case for the extrapolation by expected value. Comparisons between the CO<sub>2</sub> fluxes estimated by the

extrapolation of the tundra model and the cool coniferous forest model and those estimated by Pearman and Hyson (1981b) support the appropriateness of extrapolation by expected value. Accurate predictions of net primary productivity provide further support for the extrapolation. The results of Chapter 4 indicate that extrapolation by mathematical expectation is theoretically sound and a promising technique for extrapolating from site-specific models to regional and biome-level models.

Obviously, the extrapolation must be extended to other latitude belts and, as a consequence, other site-specific models. These extensions are necessary in order to produce a global  $\text{CO}_2$  source function, and each one will serve as a test (comparable to the test described in Chapter 4) of the extrapolation procedure. The latitude belts or horizontal grid cells involved will depend upon the tracer transport model for which the  $\text{CO}_2$  source function is designed. Existing estimates of whole-belt or whole-grid cell  $\text{CO}_2$  exchange will serve as intermediate tests of the extrapolations (as described in Chapter 4), but ultimately the global  $\text{CO}_2$  source function generated by the extrapolation of site-specific models must be coupled with a tracer transport model. The ability of this coupled model to simulate the seasonal pattern of atmospheric  $\text{CO}_2$  concentrations, as observed at the various  $\text{CO}_2$  recording stations, is a critical test of the extrapolation of site-specific  $\text{CO}_2$  fluxes by mathematical expectation. In particular, if the tracer transport model simulates observed concentrations more accurately

with the extrapolated source function than with a source function estimated by some other means, then confidence in the extrapolation procedure will be increased.

These extensions expose a potential drawback in using the extrapolation of site-specific models to generate the source function for a global tracer transport model, i.e., the difficulties involved in a global implementation of the extrapolation. For each unit of spatial resolution (belt or grid cell), frequency distributions describing the spatial variation of all model driving variables (12 times the number of driving variables if each variable enters the program as monthly input) must be specified. This must be done for each site-specific model associated with the biome-types encompassed by the spatial unit. Up to 2000 computer simulations (200 Monte Carlo iterations of ten annual simulations) must be performed for each model. While the cost of the Monte Carlo simulation is not absolutely prohibitive, it is a consideration. A grid cell or latitude belt with 10 model biomes could require 20,000 model runs. Any simulation experiment (e.g., a doubled atmospheric CO<sub>2</sub> perturbation) would require two sets of runs, the reference simulations and the perturbed simulations. Climatic perturbations or simulations over several years with variable climate might require respecification of the driving variable frequency distributions.

Another difficulty arises in actually specifying the frequency distributions of the driving variables. If model driving variables are standard climate station measurements, or can be derived from

these measurements, the frequency distributions can be constructed fairly easily. However, if driving variables are not standard climate measurements, then the construction of frequency distributions is more problematic. Some non-climate variables (e.g., soil moisture) may be standard ecological measurements and can be obtained from various data sources (e.g., IBP research sites), although these sources may be geographically sparse. The task of constructing the frequency distributions becomes more difficult as the driving variables become more unusual or non-standard. For example, a model that requires daily leaf microclimate as input would be very difficult to handle. Even with standard climatic data, the spatial distribution of stations could hinder the construction of reliable frequency distributions. Available stations might be too few and too scattered to adequately describe regional variations in climate. This problem will increase with increased spatial resolution by the tracer transport model. Some method of interpolating between stations might become necessary.

These difficulties should not be construed as a condemnation of the extrapolated site-specific models. Depending upon objectives, the advantages gained in using site-specific models (see Chapter 1) might outweigh the operational disadvantages. Indeed, we plan to complete the extrapolation of the site-specific models for the entire terrestrial biosphere. Furthermore, the operational difficulties do not detract from the more general result of a method by which local small scale models may be extrapolated to model

larger scales. Should the extrapolation by expected value prove to be corroborated by additional tests, we will have gained a useful tool.

In this light we think it useful to address two additional applications or tests of the extrapolation. One of these is directly applicable to the problem of devising ecologically sound global CO<sub>2</sub> source functions; the other to the more general problem of modeling ecosystem processes at landscape and regional scales.

The site-specific models need not be as complex or detailed as many of those in Chapter 2. These models are structured as they are because of objectives in place during their original development (e.g., simulation of biomass dynamics during the IBP). For the purpose of modeling CO<sub>2</sub> exchange with the atmosphere, simpler models could be constructed for each major vegetation type. By simpler we mean, in particular, models that use standard climate station data as driving variable input, or which derive necessary microclimate variables from standard station data. This constraint on model structure would reduce the problems associated with constructing frequency distributions for the driving variables. A general reduction in the number of state variables, rate processes, and other details could also reduce the operational difficulties involved in building a global CO<sub>2</sub> source function from site-specific models. The resulting set of simpler site-specific models, one model for each major vegetation complex or biome, would substitute for the site-specific models of Chapter 2.

A single generalized site model, a model that with the proper parameterization could represent  $\text{CO}_2$  exchange between the atmosphere and any stand of vegetation, would be even more advantageous than a set of simpler site-specific models. This model would likely be much more abstract than the site-specific ecosystem models of Chapter 2, but the principles of ecosystem  $\text{CO}_2$  dynamics built into those models could be incorporated into the single general model without compromising the objective of an ecologically sound  $\text{CO}_2$  source function. In particular, seasonality could be driven by functional responses to climate rather than the forcing functions of other simple biosphere models (e.g., Junge and Czeplak 1968, Azevedo 1982, Fung et al. 1983). The climate data might come from climate stations or remote sensing platforms. This model structure would allow for realistic simulation of geographical variations in  $\text{CO}_2$  exchange. The more recent modeling efforts of Inez Fung (pers. comm.), Katharine Prentice (Prentice 1986), Elgene Box (Gillette and Box 1986), and Richard Houghton (pers. comm.) are progressing in this direction. A model of this type is also being developed by King (in preparation (a)). These models will lose some of the advantages gained in using existing site-specific ecosystem models, but gain something in operational tractability and focused objective.

These proposed single models must still contend with biosphere heterogeneity (both biotic and abiotic). Functional representation of  $\text{CO}_2$  exchange will almost certainly be based on information gained at a smaller scale than the desired prediction of

atmosphere-biosphere exchange. Translating or moving across scales remains a problem, though one that can be addressed with further tests of the extrapolation by expected value.

Extrapolation by expected value is theoretically sound. This is demonstrated in the simple example at the beginning of Chapter 4, and a more detailed theoretical development based on a theory of spatial hierarchies is being developed elsewhere (King, in preparation (b)). However, it must be demonstrated that this theory of extrapolation can be successfully applied to actual problems. The test described in Chapter 4 is one such demonstration, and the extensions will provide further tests. The persuasiveness of these tests is, however, limited somewhat by the fact that the references against which the performance of the extrapolation is judged are themselves estimates and model predictions. There are no empirical measurements of large scale regional or biome-level atmosphere-biosphere CO<sub>2</sub> exchanges. Even a failure to match the observed atmospheric CO<sub>2</sub> concentrations with the extrapolated source function and a tracer transport model is equivocal since the transport model could be flawed. Consequently, a critical test of the extrapolation procedure will probably come at a smaller scale where the relatively larger scale integrated flux (not necessarily CO<sub>2</sub>) is measured directly. Watershed or small landscape scale tests of the extrapolation by expected value are desirable. If the procedure fails these tests, revisions of the procedure are called for. If, on the other hand, the procedure passes these tests and the regional CO<sub>2</sub> exchange tests outlined earlier, the predictions of global

scale biosphere-atmosphere CO<sub>2</sub> exchanges derived from the extrapolation of site-specific ecosystem models can be accepted with confidence.

In conclusion, an ecologically based model of the seasonal exchange of CO<sub>2</sub> between the atmosphere and the terrestrial biosphere can be derived, independently of any particular tracer transport model, using the understanding of ecosystem-atmosphere CO<sub>2</sub> exchanges reflected in models of ecosystem-level carbon dynamics. This objective can be realized with existing site-specific ecosystem models, but progress may be expedited by using simpler, generalized site-specific models designed specifically to simulate ecosystem-atmosphere CO<sub>2</sub> exchange. In either case, the derived CO<sub>2</sub> source function requires the non-trivial extrapolation from site-specific models to regional or biome-level models. The correct extrapolation requires the calculation of the expected value of variable site specific CO<sub>2</sub> exchange. Further applications and refinements are required, but extrapolation by expected value is a promising technique for extrapolating from site-specific models to regional and global models of seasonal biosphere-atmosphere CO<sub>2</sub> exchange.

## LIST OF REFERENCES

- Agren, G. I., B. Axelsson, J. G. K. Flower-Ellis, S. Linder, H. Persson, H. Staaf, and E. Troeng. 1980. Annual carbon budget for a young Scots pine. pp. 307-313. IN T. Persson (ed.), Structure and Function of Northern Coniferous Forests - An Ecosystem Study. Ecological Bulletin 32. Swedish Natural Resource Council, Stockholm.
- Armentano, T. V., and C. W. Ralston. 1980. The role of temperate zone forests in the world carbon cycle. Can. J. Forest Res. 10:53-60.
- Ajtay, G. L., P. Ketner, and P. Duvigneaud. 1979. Terrestrial primary production and phytomass. pp. 129-181. IN B. Bolin, E. T. Degens, S. Kempe, and P. Ketner (eds.), The Global Carbon Cycle, SCOPE 13. John Wiley and Sons, New York.
- Attiwill, P. M. 1973. Studies of productivity and nutrient cycling in Eucalyptus obliqua (L'Herit.). pp. 27-38. IN D. E. Reichle, R. V. O'Neill, and J. S. Olson (eds.), Modeling Forest Ecosystems. EDFB-IBP-73-7. Oak Ridge National Laboratory, Oak Ridge, Tennessee.
- Attiwill, P., R. S. Booth, F. Eckardt, P. Lossaint, J. B. Mankin, T. Shidei, H. H. Shugart, and B. Ulrich. 1973. Seasonal model of the broadleaved evergreen forest. pp. 313-319. IN D. E. Reichle, R. V. O'Neill, and J. S. Olson (eds.), Modeling Forest Ecosystems. EDFB-IBP-73-7. Oak Ridge National Laboratory, Oak Ridge, Tennessee.
- Azevedo, A. E. 1982. Atmospheric distribution of carbon dioxide and its exchanges with the biosphere and the oceans. Ph.D. dissertation, Columbia University.
- Bacastow, R. B., and C. D. Keeling. 1981. Atmospheric carbon dioxide concentration and the observed airborne fraction. pp. 103-112. IN B. Bolin (ed.), Carbon Cycle Modelling - SCOPE 16. John Wiley and Sons, New York.
- Bacastow, R. B., C. D. Keeling, and T. P. Whorf. 1981. Seasonal amplitude in atmospheric CO<sub>2</sub> concentration at Mauna Loa, Hawaii, 1959-1980. pp. 169-176. IN WMO/ICSU/UNEP Conference on Analysis and Interpretation of Atmospheric CO<sub>2</sub> Data. World Meteorol. Organ., Geneva.
- Bacastow, R. B., C. D. Keeling, and T. P. Whorf. 1985. Seasonal amplitude increase in atmospheric CO<sub>2</sub> concentration at Mauna Loa, Hawaii, 1959-1982. J. Geophys. Res. 90:10,529-10,540.

- Bacastow, R. B., C. D. Keeling, T. P. Whorf, and C. S. Wong. 1981. Seasonal amplitude in atmospheric CO<sub>2</sub> concentration at Canadian Weather Station P, 1970-1980. pp. 163-168. IN WMO/ICSU/UNEP Conference on Analysis and Interpretation of Atmospheric CO<sub>2</sub> Data. World Meteorol. Organ., Geneva.
- Bandhu, D., J. Bullock, C. S. Gist, F. Malaisse, H. Ogawa, B. Rust, and M. A. Strand. 1973. Seasonal model of the tropical forests. pp. 285-295. IN D. E. Reichle, R. V. O'Neill, and J. S. Olson (eds.), Modeling Forest Ecosystems. EDFB-73-7. Oak Ridge National Laboratory Oak Ridge, Tennessee.
- Barry, R. G., G. M. Courtin, and C. Labine. 1981. Tundra climate. pp. 81-114. IN L. S. Bliss, O. W. Heal, and J. J. Moore (eds.), Tundra Ecosystems: A Comparative Analysis. Cambridge University Press, Cambridge, United Kingdom.
- Bischoff, W. 1981. The CO<sub>2</sub> content of the upper polar troposphere between 1963-1979. pp. 113-116. IN B. Bolin (ed.), Carbon Cycle Modelling. SCOPE 16. John Wiley and Sons, New York.
- Bliss, L. S., O. W. Heal, and J. J. Moore (eds.). 1981. Tundra Ecosystems: A Comparative Analysis. Cambridge University Press, Cambridge, United Kingdom.
- Bolin, B., and W. Bischoff. 1970. Variations of the carbon dioxide content of the atmosphere in the Northern Hemisphere. Tellus 22:431-442.
- Bolin, B., and C. D. Keeling. 1963. Large-scale atmospheric mixing as deduced from seasonal and meridional variation of carbon dioxide. J. Geophys. Res. 68:3899-3920.
- Bolla, M., and T. Kutas. 1984. Submodels for the nutrient loading estimation on River Zala. Ecol. Modelling 26:115-143.
- Bremeyer, A. I., and G. M. Van Dyne. 1980. Grasslands, Systems, Analysis, and Man. Cambridge University Press, Cambridge, United Kingdom.
- Brown, J., P. C. Miller, L. L. Tieszen, and F. L. Bunnell (eds.). 1980. An Arctic Ecosystem: The Coastal Tundra at Barrow, Alaska. Dowden, Hutchinson, and Ross, Inc., Stroudsburg, Pennsylvania.
- Brown, L. F., and M. J. Trlica. 1974. Photosynthesis of two important grasses of the shortgrass prairie as affected by several ecological variables. US/IBP Grassland Biome Tech. Rep. No. 244. Colorado State University, Fort Collins.

- Bullock, J. A. 1973. Equatorial rain forest study - Malaysia. pp. 64-70. IN D. E. Reichle, R. V. O'Neill, and J. S. Olson (eds.), Modeling Forest Ecosystems. EDFB-IBP-73-7. Oak Ridge National Laboratory, Oak Ridge, Tennessee.
- Bunnell, F. L., and P. Dowding. 1974. ABISKO - A generalized decomposition model for comparisons between tundra sites. pp. 227-247. IN A. J. Holding, O. W. Heal, S. F. MacLean, Jr., and P. W. Flanagan (eds.), Soil Organisms and Decomposition in Tundra. Tundra Biome Steering Committee, Stockholm.
- Bunnell, F. L., and K. A. Scoullar. 1975. ABISKO II. A computer simulation model of carbon flux in tundra ecosystems. pp. 425-448. IN T. Rosswall and O. W. Heal (eds.), Structure and Function of Tundra Ecosystems. Ecol. Bull. 20. Swedish Natural Science Research Council, Stockholm.
- Bunnell, F. L., and D. E. N. Tait. 1974. Mathematical simulation models of decomposition processes. pp. 207-225. IN A. J. Holding, O. W. Heal, S. F. MacLean, Jr., and P. W. Flanagan (eds.), Soil Organisms and Decomposition in Tundra. Tundra Biome Steering Committee, Stockholm.
- Burgess, R. L. 1981. Physiognomy and phytosociology of the international woodlands research sites. pp. 1-35. IN D. E. Reichle (ed.), Dynamic Properties of Forest Ecosystems. Cambridge University Press, Cambridge, United Kingdom.
- Chesson, P. L. 1978. Predator-prey theory and variability. Annu. Rev. Ecol. Syst. 9:323-347.
- Chesson, P. L. 1985. Coexistence of competitors in spatially and temporally varying environments: A look at the combined effects of different sorts of variability. Theor. Pop. Biol. 28:263-287.
- Cleveland, W. S., A. E. Freeny, and T. E. Graedel. 1983. The seasonal component of atmospheric CO<sub>2</sub>: Information from new approaches to the decomposition of seasonal time series. J. Geophys. Res. 88:10934-10946.
- Coniferous Forest Biome Modeling Group. 1977. CONIFER: A model of carbon and water flow through a coniferous forest. Documentation. Coniferous Forest Biome Bull. 8. University of Washington, Seattle.
- Curry, J. W., Jr., L. G. Shapiro, and R. L. Vanderlip. 1977. A population simulation model for field crops. IN Proc. 8th Annual Pittsburg Conference on Modeling and Simulation. April 21-22, 1977.

- Dahlman, R. C. 1984. Carbon Cycle Research Plan. DOE/ER-0188. National Technical Information Service, Springfield, Virginia.
- DeAngelis, D. L., R. L. Gardner, and H. H. Shugart. 1981. Productivity of forest ecosystems studied during the IBP: The woodlands data set. pp. 567-672. IN D. E. Reichle (ed.), Dynamic Properties of Forest Ecosystems. Cambridge University Press, Cambridge, United Kingdom.
- Delcourt, H. R., and W. F. Harris. 1980. Carbon budget of the southeastern U.S. biota: Analysis of historical change in trend from source to sink. Science 201:321-322.
- Detling, J. K., W. J. Parton, and H. W. Hunt. 1978. An empirical model for estimating CO<sub>2</sub> exchange of Bouteloua gracilis (H. B. K.) Lag. in the shortgrass prairie. Oecologia (Berl.) 33:137-147.
- Detling, J. K., W. J. Parton, and H. W. Hunt. 1979. A simulation model of Bouteloua gracilis biomass dynamics on the North American shortgrass prairie. Oecologia (Berl.) 38:167-191.
- Detwiler, R. P., C. A. S. Hall, P. Bogdonoff. 1985. Land use change and carbon exchange in the tropics: II. Estimates for the entire region. Environmental Management 9:335-344.
- de Wit, C. T., J. Goudriann, H. H. van Laar, F. W. T. Penning de Vries, R. Rabbinge, H. van Keulen, W. Louwense, L. Simba, and C. de Jonge. 1978. Simulation of Assimilation, Respiration, and Transpiration of Crops. Pudoc, Wageningen, The Netherlands.
- Dugas, W. A., G. F. Arkin, and B. S. Jackson. 1983. Factors affecting simulated crop yield spatial extrapolation. TRANSACTIONS of the ASAE 26:1440-1444.
- Duncan, W. G., R. S. Loomis, W. A. Williams, and R. Hanau. 1967. A model for simulating photosynthesis in plant communities. Hilgardia 38:181-205.
- Eliassen, A. 1980. A review of long-range transport modeling. J. Appl. Meteorol. 19:231-240.
- Emanuel, W. R., and R. V. O'Neill. 1985. Terrestrial ecosystems and global element cycles. A renewal proposal to the National Science Foundation.
- Emanuel, W. R., G. E. G. Killough, and J. S. Olson. 1981. Modeling the circulation of carbon in the world's terrestrial ecosystems. pp. 335-353. IN B. Bolin (ed.), Carbon Cycle Modelling - SCOPE 16. John Wiley and Sons, New York.

- Espenshade, E. B., Jr., and J. L. Morrison (eds.). 1983. Goode's World Atlas. 16th Edition. Rand McNally and Company, Chicago.
- Esser, G. 1984. The significance of biospheric carbon pools and fluxes for the atmospheric CO<sub>2</sub>: A proposed model structure. Progress in Biometeorology 3:253-294.
- Feller, W. 1971. An Introduction to Probability Theory and Its Applications. Vol. II. Second Edition. John Wiley and Sons, Inc., New York.
- Fraser, P. J., G. I. Pearman, and P. Hyson. 1983. The global distribution of atmospheric carbon dioxide. 2. A review of provisional background observations, 1978-1980. J. Geophys. Res. 88:3591-3598.
- French, D. D. 1981. Multivariate comparisons of IBP tundra biome site characteristics. pp. 47-75. IN L. S. Bliss, O. W. Heal, and J. J. Moore (eds.), Tundra Ecosystems: A Comparative Analysis. Cambridge University Press, Cambridge, United Kingdom.
- Fung, I., K. Prentice, E. Matthews, J. Lerner, and G. Russel. 1983. Three-dimensional tracer model study of atmospheric CO<sub>2</sub>: Response to seasonal exchanges with the terrestrial biosphere. J. Geophys. Res. 88:1281-1294.
- Gardner, R. H., and R. V. O'Neill. 1983. Parameter uncertainty and model predictions: A review of Monte Carlo results. pp. 245-257. IN M. B. Beck and G. van Straten (eds.), Uncertainty and Forecasting of Water Quality. Springer-Verlag, Berlin.
- Gardner, R. H., and J. R. Trabalka. 1985. Methods of Uncertainty Analysis for a Global Carbon Dioxide Model. DOE/OR/21400-4. TR024. National Technical Information Service, Springfield, Virginia.
- Gardner, R. H., R. V. O'Neill, and J. H. Carney. 1981. Spatial patterning and error propagation in a stream ecosystem model. pp. 391-395. IN Proc. Summer Computer Simulation Conference. Simulation Council, La Jolla, California.
- Gardner, R. H., B. Rojder, and U. Bergstrom. 1983. PRISM: A systematic method for determining the effect of parameter uncertainties on model predictions. Report/NW-83/555. Studsvik Energiteknik AB, Nykoping Sweden.
- Gillette, D. A. 1982. Decomposition of annual patterns of atmospheric carbon dioxide concentrations: A preliminary interpretation of one year of data at 13 globally distributed locations. Atmospheric Environment 16:2537-2542.

- Gillette, D. A., and E. O. Box. 1986. Modeling seasonal changes of atmospheric carbon dioxide and carbon 13. *J. Geophys. Res.* 91:5287-5304.
- Golkin, K. R. 1981. A computer simulation of the carbon, phosphorus, and hydrological cycles of a pine flatwoods ecosystem. M. S. Thesis, University of Florida, Gainesville, Florida.
- Golkin, K. R., and K. C. Ewel. 1984. A computer simulation of the carbon, phosphorus, and hydrologic cycles of a pine flatwoods ecosystem. *Ecol. Modelling* 24:113-136.
- Goodall, D. W. 1981. The modeling of arid ecosystem dynamics. pp. 385-410. IN D. W. Goodall, R. A. Perry, and K. M. W. Howes (eds.), *Arid-land Ecosystems: Structure, Functioning, and Management*. Vol. 2. Cambridge University Press, Cambridge, United Kingdom.
- Goodall, D. W., and C. S. Gist. 1973. Terrestrial models: Calling programs and input/output subroutines. pp. 2.1.3.1-9 - 2.1.3.1-146. IN *US/IBP Desert Biome Reports of 1972 Progress*. Vol. 1. Utah State University, Logan.
- Goodall, D. W., and R. A. Perry (eds.). 1979. *Arid-land Ecosystems: Structure, Functioning, and Management*. Vol. I. Cambridge University Press, Cambridge, United Kingdom.
- Grier, C. C., and R. S. Logan. 1977. Old-growth *Pseudotsuga menziesii* communities of a western Oregon watershed: Biomass distribution and production budgets. *Ecol. Monogr.* 47:373-400.
- Haden-Guest, S., J. K. Wright, and E. M. Teclaff (eds.). 1956. *A World Geography of Forest Resources*. American Geographical Society Special Publication No. 33. The Ronald Press Company, New York.
- Hall, C. A. S., C. A. Ekdahl, and D. E. Wartenburg. 1975. A fifteen-year record of biotic metabolism in the Northern Hemisphere. *Nature* 255:136-138.
- Hanna, S. R., G. A. Briggs, and R. P. Hosker, Jr. 1982. *Handbook on Atmospheric Diffusion*. DOE/TIC-11223. Technical Information Center, Oak Ridge, Tennessee.
- Hansen, J., G. Russell, D. Rind, P. Stone, A. Lacis, S. Lebedeff, R. Ruedy, and L. Travis. 1983. Efficient three-dimensional global models for climate studies: Models I and II. *Monthly Weather Review* 111:609-662.

- Hare, F. K., and J. E. Hay. 1974. The climate of Canada and Alaska. pp. 49-192. IN R. A. Bryson and F. K. Hare (eds.), *Climates of North America*. World Survey Climatology, Vol. 11. Elsevier Publishing Company, Amsterdam.
- Heal, O. W., P. W. Flanagan, D. D. French, and S. F. MacLean, Jr. 1981. Decomposition and accumulation of organic matter. pp. 587-633. IN L. S. Bliss, O. W. Heal, and J. J. Moore (eds.), *Tundra Ecosystems: A Comparative Analysis*. Cambridge University Press, Cambridge, United Kingdom.
- Heimann, M., C. D. Keeling, and W. G. Mook. 1985. A three dimensional model of atmospheric CO<sub>2</sub> transport based on observed winds. 1. Observational data and model. Paper presented at Symposium on Atmospheric Carbon Dioxide: Its Sources, Sinks, and Global Transport. Kandersteg, Switzerland, September 1985.
- Heimann, M., C. D. Keeling, and C. J. Tucker. 1985. A three dimensional model of atmospheric CO<sub>2</sub> transport based on observed winds. 2. Analysis of the seasonal cycle of CO<sub>2</sub>. Paper presented at Symposium on Atmospheric Carbon Dioxide: Its Sources, Sinks, and Global Transport. Kandersteg, Switzerland, September 1985.
- Holdridge, L. 1980. A new look at atmospheric carbon dioxide. pp. 19-29. IN S. Brown, A. E. Lugo, and B. Liegel (eds.), *The Role of Tropical Forests in the World Carbon Cycle*. CONF-800350. National Technical Information Service, Springfield, Virginia.
- Houghton, R. A. 1982. An integration of Northern Hemispheric metabolism. pp. 14-15. IN *The Ecosystems Center Annual Report 1982*. Marine Biological Laboratory, Woods Hole, Massachusetts.
- Houghton, R. A., J. E. Hobbie, J. M. Melillo, B. Moore, B. J. Peterson, G. R. Shaver, and G. M. Woodwell. 1983. Changes in the carbon content of terrestrial biota and soils between 1860 and 1980: A net release of CO<sub>2</sub> to the atmosphere. *Ecol. Monogr.* 53:235-262.
- Hyson, P., P. J. Fraser, and G. I. Pearman. 1980. A two dimensional tracer-transport simulation model for trace atmospheric constituents. *J. Geophys. Res.* 85:4443-4455.
- Iman, R. L., and W. J. Conover. 1983. *A Modern Approach to Statistics*. John Wiley and Sons, New York.

- Iman, R. L., and J. C. Helton. 1985. Comparison of uncertainty and sensitivity analysis techniques for computer models. NUREG/CR-3904, SAND84-1461. Sandia National Laboratories, Albuquerque, New Mexico.
- Johannessen, T. W. 1970. The climate of Scandinavia. pp. 23-79. IN C. C. Wallem (ed.), *Climates of Northern and Western Europe*. World Survey of Climatology, Vol. 5. Elsevier Publishing Company, Amsterdam.
- Junge, C. E., and G. Czeplak. 1968. Some aspects of the seasonal variation of carbon dioxide and ozone. *Tellus* 20:422-434.
- Keeling, C. D. 1983. The global carbon cycle: What we know and could know from atmospheric, biospheric, and oceanic observations. pp. II.3-II.62. IN *Proceedings Carbon Dioxide Research Conference: Carbon Dioxide, Science, and Consensus*. CONF-820970. National Technical Information Service, Springfield, Virginia.
- Keeling, C. D., A. F. Carter, and W. G. Mook. 1984. Seasonal, latitudinal, and secular variations in the abundance and isotopic ratios of atmospheric CO<sub>2</sub>. 2. Results from oceanographic cruises in the tropical Pacific Ocean. *J. Geophys. Res.* 89:4615-4628.
- Keeling, C. D., J. A. Adams, Jr., C. A. Ekdahl, Jr., P. R. Guenther. 1976. Atmospheric carbon dioxide variations at the South Pole. *Tellus* 28:552-564.
- Keeling, C. D., T. P. Whorf, C. S. Wong, and R. D. Bellagay. 1985. The concentration of atmospheric carbon dioxide at Ocean Weather Station P from 1969-1981. *J. Geophys. Res.* 90:10511-10528.
- Keeling, C. D., R. B. Bacastow, A. E. Bainbridge, C. A. Ekdahl, Jr., P. R. Guenther, and L. S. Waterman. 1976. Atmospheric carbon dioxide variations at Mauna Loa Observatory, Hawaii. *Tellus* 28:538-551.
- King, A. W. A model of seasonal CO<sub>2</sub> exchange between the terrestrial biosphere and the atmosphere (in preparation, (a)).
- King, A. W. Linking levels in a spatial hierarchy: A theory of extrapolation (in preparation (b)).
- King, A. W., and D. L. DeAngelis. 1985. Information for seasonal models of carbon fluxes in terrestrial biomes. ORNL/TM-9404. Oak Ridge National Laboratory, Oak Ridge, Tennessee.

- King, A. W., and D. L. DeAngelis. 1986. Information for seasonal models of carbon fluxes in agroecosystems. ORNL/TM-9935. Oak Ridge National Laboratory, Oak Ridge, Tennessee (in press).
- Komhyr, W. D., R. H. Gammon, T. B. Harris, L. S. Waterman, T. J. Conway, W. R. Taylor, and K. W. Thoning. 1985. Global atmospheric CO<sub>2</sub> distribution and variations from 1968-1982 NOAA/GMCC CO<sub>2</sub> flask sample data. *J. Geophys. Res.* 90:5567-5596.
- Kumar, M., and J. L. Monteith. 1981. Remote sensing of crop growth. pp. 133-144. IN H. Smith (ed.), *Plants and the Daylight Spectrum*. Academic Press, London.
- Leduc, S. K., and D. A. Holt. 1987. Chapter 6. The scale problem: Modeling plant yield over time and space. IN K. Wisiol and J. Hesketh (eds.), *Plant Growth Modeling for Resource Management*. CRC Press, Boca Raton, Florida.
- Lefkovitch, L. P., and L. Fahrig. 1985. Spatial characteristics of habitat patches and population survival. *Ecol. Modelling* 30:297-308.
- Levin, S. A. 1976. Population dynamic models in heterogeneous environments. *Annu. Rev. Ecol. Syst.* 7:287-310.
- Lieth, H. 1965. Versuch einer Kartographischen Darstellung der Produktivität der Pflanzendecke auf der Erde. pp. 72-79. IN *Geographisches Taschenbuch*, Franz Steiner Verlag GmbH, Wiesbaden.
- Lieth, H. 1975a. Primary production of the major vegetation units of the world. pp. 203-215. IN H. Lieth and R. H. Whittaker (eds.), *Primary Productivity of the Biosphere*. Springer-Verlag, Berlin.
- Lieth, H. 1975b. Modeling the primary productivity of the world. pp. 237-263. IN H. Lieth and R. H. Whittaker (eds.), *Primary productivity of the Biosphere*. Springer-Verlag, New York.
- Lieth, H. 1978. Vegetation and CO<sub>2</sub> changes. pp. 103-109. IN J. Williams (ed.), *Carbon Dioxide, Climate, and Society*. Pergamon Press, Oxford.
- Linder, S., and E. Troeng. 1980. Photosynthesis and transpiration of 20-year-old Scots pine. pp. 165-181. IN T. Persson (ed.), *Structure and Function of Northern Coniferous Forests - An Ecosystem Study*. Ecological Bulletin 32. Swedish Natural Resource Council, Stockholm.

- Lowe, D. C., P. R. Guenther, and C. D. Keeling. 1979. The concentration of atmospheric carbon dioxide at Baring Head, New Zealand. *Tellus* 31:58-67.
- Lugo, A. E., and S. Brown. 1980. Ecological issues associated with the interpretation of atmospheric CO<sub>2</sub> data. pp. 30-43. IN S. Brown, A. E. Lugo, and B. Liegel (eds.), *The Role of Tropical Forests in the World Carbon Cycle*. CONF-800350. National Technical Information Service, Springfield, Virginia.
- Lydolph, P. E. 1977. *Climates of the Soviet Union*. World Survey of Climatology, Vol. 7. Elsevier Publishing Company, Amsterdam.
- Machta, L. 1972. Mauna Loa and global trends in air quality. *Bull. Am. Meteorol. Soc.* 53:402-420.
- Machta, L. 1974. Global scale atmospheric mixing. *Advan. Geophys.* 18B:33-56.
- Machta, L., K. Hanson, and C. D. Keeling. 1977. Atmospheric carbon dioxide and some interpretations. pp. 131-144. IN N. R. Anderson and A. Malahoff (eds.), *The Fate Fossil Fuel CO<sub>2</sub> in the Oceans*. Marine Science 6. Plenum Press, New York.
- Malaisse, F. 1973. Miombo project. pp. 139-143. IN D. E. Reichle, R. V. O'Neill, and J. S. Olson (eds.), *Modeling Forest Ecosystems*. EDFB-IBP-73-7. Oak Ridge National Laboratory, Oak Ridge, Tennessee.
- Matthews, E. 1983. Global vegetation and land use: New high resolution data bases for climate studies. *J. Climate and Applied Meterology* 22:474-487.
- McCree, K. J., and R. S. Loomis. 1969. Photosynthesis in fluctuating light. *Ecology* 50:422-428.
- Mitchell, R. 1984. The ecological basis for comparative primary production. pp. 13-53. IN R. Lowrance, B. R. Stinner, and G. J. House (eds.), *Agricultural Ecosystems: Unifying Concepts*. John Wiley and Sons, Inc., New York.
- Mook, W. G., M. Koopmans, A. F. Carter, and C. D. Keeling. 1983. Seasonal, latitudinal, and secular variations in the abundance and isotopic ratios of atmospheric carbon dioxide. 1. Results from land stations. *J. Geophys. Res.* 88:10915-10933.
- Morgan, M. G., S. C. Morris, A. K. Meier, and D. L. Shank. 1978. A probabilistic methodology for estimating air pollution health effects from coal-fired power plants. *Energy Systems Policy* 2:287-310.

- Muller, M. J. 1982. Selected Climatic Data for a Global Set of Standard Stations for Vegetative Science. Dr. W. Junk Publishers, The Hague.
- Olson, J. S. 1975. Productivity of forest ecosystems. pp. 33-43. IN D. E. Reichle, J. F. Franklin, and D. W. Goodall (eds.), Productivity of World Ecosystems. National Academy of Sciences, Washington, D.C.
- Olson, J. S., J. A. Watts, and L. J. Allison. 1983. Carbon in live vegetation of major world ecosystems. Environmental Sciences Division Publ. No. 1997, ORNL-5862. Oak Ridge National Laboratory, Oak Ridge, Tennessee.
- O'Neill, R. V. 1979a. Natural variability as a source of error in model predictions. pp. 23-32. IN G. S. Innis and R. V. O'Neill (eds.), Systems Analysis of Ecosystems. International Co-Operative Publishing House, Fairfield, Maryland.
- O'Neill, R. V. 1979b. Transmutations across hierarchical levels. pp. 59-78. In G. S. Innis and R. V. O'Neill (eds.), Systems Analysis of Ecosystems. International Cooperative Publishing House, Fairfield, Maryland.
- O'Neill, R. V., J. W. Elwood, and S. G. Hildebrand. 1979. Theoretical implications of spatial heterogeneity in stream ecosystems. pp. 79-101. IN G. S. Innis and R. V. O'Neill (eds.), Systems Analysis of Ecosystems. International Cooperative Publishing House, Fairfield, Maryland.
- O'Neill, R. V., R. H. Gardner, and J. H. Carney. 1982. Parameter constraints in a stream ecosystem model: Incorporation of a priori information in Monte Carlo error analysis. Ecol. Modelling 16:51-65.
- Pales, J. C., and C. D. Keeling. 1965. The concentration of atmospheric carbon dioxide in Hawaii. J. Geophys. Res. 70:6053-6076.
- Parnas, H., and J. Radford. 1974. A decomposition submodel. US/IBP Desert Biome Research Memorandum 74-64. Utah State University, Logan.
- Parton, W. J. 1976. Abiotic submodel. pp. 12-61. IN G. W. Cole (ed.), ELM: Version 2.0. Range Science Department, Science Series No. 20., Colorado State University, Fort Collins.
- Parton, W. J. 1978. Abiotic section of ELM. pp. 31-53. IN G. S. Innis (ed.), Grassland Simulation Model. Springer-Verlag, New York.

- Parton, W. J., and J. S. Singh. 1976. Simulation of plant biomass on a shortgrass and a tallgrass prairie with emphasis on belowground processes. US/IBP Grassland Biome Tech. Rep. No. 300. Colorado State University, Fort Collins.
- Parton, W. J., and J. S. Singh. 1984. Adapting a biomass simulation model to a tropical grassland. *Ecol. Modelling* 23:151-163.
- Parton, W. J., J. S. Singh, and D. C. Coleman. 1978. A model of production and turnover of roots in a shortgrass prairie. *J. Appl. Ecol.* 44:515-542.
- Pearman, G. I., and D. J. Beardsmore. 1984. Atmospheric carbon dioxide measurements in the Australian region: Ten years of aircraft data. *Tellus* 36B:1-24.
- Pearman, G. I., and P. Hyson. 1980. Activities of the global biosphere as reflected in atmospheric CO<sub>2</sub> records. *J. Geophys. Res.* 85:4468-4474.
- Pearman, G. I., and P. Hyson. 1981a. The annual variation of atmospheric CO<sub>2</sub> concentration observed in the Northern Hemisphere. *J. Geophys. Res.* 86:9839-9843.
- Pearman, G. I., and P. Hyson. 1981b. A global atmospheric diffusion simulation model for atmospheric carbon studies. pp. 227-240. IN B. Bolin (ed.), *Carbon Cycle Modelling - SCOPE 16*. John Wiley and Sons, New York.
- Pearman, G. I., P. Hyson, and P. J. Fraser. 1983. The global distribution of atmospheric carbon dioxide: 1. Aspects of observations and modeling. *J. Geophys. Res.* 88:3581-3590.
- Peterson, J. T., W. D. Komhyr, T. B. Harris, and L. S. Waterman. 1982. Atmospheric carbon dioxide measurements at Barrow, Alaska, 1973-1979. *Tellus* 34:166-175.
- Prentice, K. C. 1986. The influence of the terrestrial biosphere on seasonal atmospheric carbon dioxide: An empirical model. Ph.D. dissertation, Columbia University.
- Reichle, D. E. 1981. *Dynamic Properties of Forest Ecosystems*. Cambridge University Press, Cambridge, United Kingdom.
- Reichle, D. E., R. V. O'Neill, and J. S. Olson (eds.). 1973. *Modeling Forest Ecosystems*. EDFB-IBP-73-7. Oak Ridge National Laboratory, Oak Ridge, Tennessee.

- Reiter, E. R. 1971. Atmospheric Transport Processes. Part 2: Chemical Tracers. U.S. Atomic Energy Commission, Division of Technical Information, Springfield, Virginia.
- Rozanov, Y. A. 1969. Probability Theory: A Concise Course (rev. English ed.). R. A. Silverman (tr., tr. ed.). Dover Publications, Inc., New York.
- Rydin, B. E. 1981. Hydrology of northern tundra. pp. 115-137. IN L. S. Bliss, O. W. Heal, and J. J. Moore (eds.), Tundra Ecosystems: A Comparative Analysis. Cambridge University Press, Cambridge, United Kingdom.
- SAS Institute Inc. 1982. SAS User's Guide: Basics, 1982 Edition. SAS Institute Inc., Cary, North Carolina.
- Sieler, W., and P. J. Crutzen. 1980. Estimates of gross and net fluxes of carbon between the biosphere and the atmosphere from biomass burning. Climatic Change 2:207-247.
- Smith, O. L. 1980. The influence of environmental gradients on ecosystem stability. Am. Nat. 116:1-24.
- Sollins, P., W. F. Harris, and N. T. Edwards. 1976. Simulating the physiology of a temperate deciduous forest. pp. 173-218. IN B. C. Patten (ed.), Systems Analysis and Simulation in Ecology, Vol. 4, Academic Press, New York.
- Sollins, P., D. E. Reichle, and J. S. Olson. 1973. Organic matter budget and model for a southern Appalachian Liriodendron forest. EDFB-IBP-73-2. Oak Ridge National Laboratory, Oak Ridge, Tennessee.
- Spiegel, M. R. 1975. Schaum's Outline of Theory and Problems of Probability and Statistics. McGraw-Hill Book Company, New York.
- Stringer, E. T. 1972. Techniques of Climatology. W. H. Freeman and Company, San Francisco.
- Tanaka, M., T. Nakazawa, and S. Aoki. 1983. Concentration of atmospheric carbon dioxide over Japan. J. Geophys. Res. 88:1339-1344.
- Tiwari, J. L., and J. E. Hobbie. 1976. Random differential equations as models of ecosystems: Monte Carlo simulation approach. Math. Biosci. 28:25-44.
- Tucker, C. J., J. R. G. Townsend, and T. E. Goff. 1985. African land-cover classification using satellite data. Science 227:369-375.

- Tucker, C. J., I. Y. Fung, C. D. Keeling, and R. H. Gammon. 1986. Relationship between atmospheric CO<sub>2</sub> variation and a satellite-derived vegetation index. *Nature* 319:195-199.
- Turner, F. B., and J. F. McBrayer (eds.). 1974. Rock Valley validation site. US/IBP Desert Biome Research Memorandum 74-2. Utah State University, Logan.
- U.S. Department of Commerce. 1968. Climate Atlas of the United States. U.S. Department of Commerce, Washington, D.C.
- Valentine, W. 1974. Terrestrial model: Plant processes (Version IV). US/IBP Desert Biome Research Memorandum 74-50. Utah State University, Logan.
- Vollenvieder, R. A. 1970. Models for calculating integral photosynthesis and some implications regarding structural properties of the community metabolism of aquatic ecosystems. pp. 455-472. IN Prediction and Measurement of Photosynthetic Productivity. Pudoc, Wageningen, The Netherlands.
- Walter, H. 1985. Vegetation of the Earth and Ecological Systems of the Geo-Biosphere. 3rd Ed. Springer-Verlag, New York.
- Whittaker, R. H., and G. E. Likens. 1973. Carbon in the biota. pp. 281-302. IN G. M. Woodwell and E. V. Pecan (eds.), Carbon and the Biosphere. CONF-720510. National Technical Information Center, Springfield, Virginia.
- Whittaker, R. H., and G. E. Likens. 1975. The biosphere and man. pp. 305-328. IN H. Lieth and R. H. Whittaker (eds.), Primary Productivity of the Biosphere. Springer-Verlag, New York.
- Wilson, M. F., and A. Henderson-Sellers. 1985. A global archive of land cover and soils data for use in general circulation climate models. *J. Climatol.* 5:119-143.
- Woodwell, G. M. 1983. The blue planet: Of whales and parts and man. pp. 2-10. IN H. A. Mooney and M. Gordon (eds.), Disturbance and Ecosystems: Components of Response. Springer-Verlag, Berlin.
- Woodwell, G. M., and R. H. Whittaker. 1968. Primary production in terrestrial ecosystems. *Amer. Zoologist* 8:19-30.
- Woodwell, G. M., R. A. Houghton, and N. R. Tempel. 1973. Atmospheric CO<sub>2</sub> at Brookhaven, Long Island, New York: Patterns of variation up to 125 meters. *J. Geophys. Res.* 78:932-940.

- Woodwell, G. M., J. E. Hobbie, R. A. Haughton, J. M. Melillo, B. Moore, B. J. Peterson, and G. R. Shaver. 1983. Global deforestation: Contribution to atmospheric carbon dioxide. *Science* 222:1081-1086.
- Ziegler, B. P. 1978. Persistence and patchiness of predator-prey systems induced by discrete event population exchange mechanisms. *J. Theor. Biol.* 67:687-713.

APPENDIX



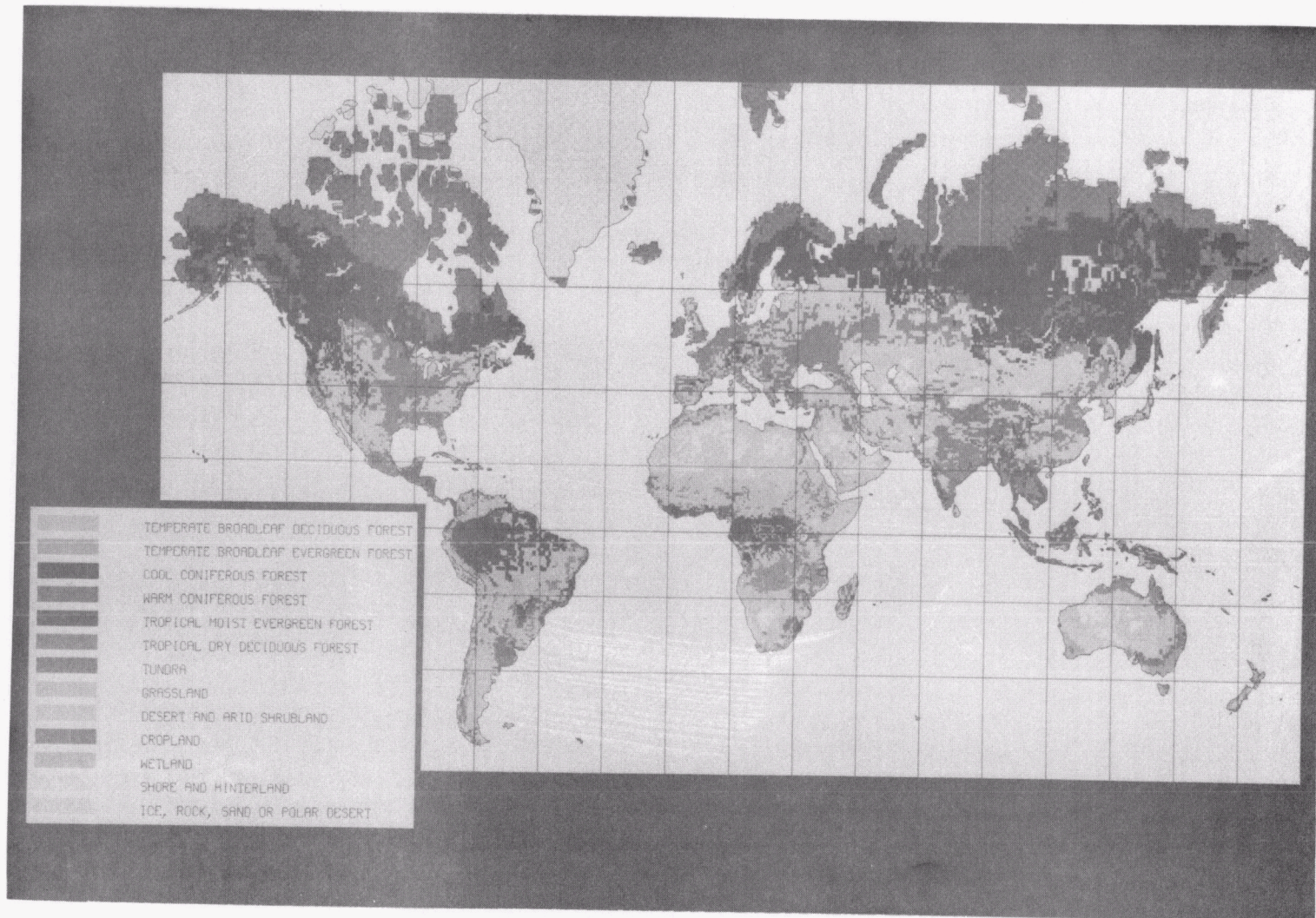


Plate 3.1 World map of the model biomes



## INTERNAL DISTRIBUTION

- |        |                  |        |                               |
|--------|------------------|--------|-------------------------------|
| 1.     | S. I. Auerbach   | 21.    | A. M. Perry, Jr.              |
| 2.     | V. H. Dale       | 22-26. | W. M. Post                    |
| 3-7.   | D. L. DeAngelis  | 27-28. | D. E. Reichle                 |
| 8.     | W. R. Emanuel    | 29.    | M. G. Turner                  |
| 9.     | M. P. Farrell    | 30.    | CDIC Files                    |
| 10.    | S. G. Hildebrand | 31.    | Central Research Library      |
| 11.    | M. A. Huston     | 32-46. | ESD Library                   |
| 12-16. | A. W. King       | 47-48. | Laboratory Records Department |
| 17.    | L. K. Mann       | 49.    | Laboratory Records, RC        |
| 18.    | R. J. Norby      | 50.    | ORNL Patent Office            |
| 19.    | P. J. Mulholland | 51.    | ORNL Y-12 Technical Library   |
| 20.    | R. V. O'Neill    |        |                               |

## EXTERNAL DISTRIBUTION

52. Thomas V. Armentano, Director, Biotic Resources Program, Holcomb Research Institute, Butler University, 4600 Sunset Avenue, Indianapolis, IN 46208
53. Jugo Aselmann, Max-Planck-Institut für Chemie (Otto-Hahn-Institut), P.O.B. 3060, Saarstrabe 23, D 65 Mainz, FEDERAL REPUBLIC OF GERMANY
54. Robert B. Bacastow, Geological Research Division, Scripps Institution of Oceanography, University of California, 2314 Ritter Hall, A-020, La Jolla, CA 92093
55. Roger G. Barry, Director, World Data Center-A for Glaciology, Cooperative Institute for Research in Environmental Sciences (CIRES), Campus Box 449, University of Colorado, Boulder, CO 80309-0449
56. Peter J. Beckett, Department of Biology, Laurentian University, Sudbury, Ontario P3E 2C6, CANADA
57. Robert A. Berner, Department of Geology and Geophysics, Kline Geology Laboratory, Yale University, 210 Whitney Avenue, New Haven, CT 06511
58. R. P. Berube, Office of Environmental Guidance and Compliance, EH-23, U.S. Department of Energy, Washington, DC 20585
59. Bert Bolin, Arrhenius Laboratory, Department of Meteorology, University of Stockholm, S-106 91 Stockholm, SWEDEN
60. C. M. Borgstrom, Director, Office of NEPA Project Assistance, EH-25, U.S. Department of Energy, Washington, DC 20585
61. Philippe Bourdeau, Head of Environment, Raw Materials and Materials Technology, Commission of the European Communities, Rue de la Loi 200, Wetstraat 200, 1049 Brussels, BELGIUM
62. Peter G. Brewer, Department of Chemistry, Woods Hole Oceanographic Institution, Woods Hole, MA 02543

63. Wallace S. Broecker, Lamont-Doherty Geological Observatory of Columbia University, Palisades, NY 10964
64. H. Bröhl-Kerner, Institut für Physikalische Chemie der Universität, P.O. Box 11 19 32, D-6000, Frankfurt 11, FEDERAL REPUBLIC OF GERMANY
65. Sandra Brown, Department of Forestry, University of Illinois, 110 Mumford Hall, 1301 West Gregory Drive, Urbana, IL 61801
66. Robert H. Byrne, Department of Marine Science, University of South Florida, 140 Seventh Avenue South, St. Petersburg, FL 33701
67. J. Thomas Callahan, Associate Director, Ecosystem Studies Program, National Science Foundation, Room 336, 1800 G Street, NW, Washington, DC 20550
68. Chen-Tung Arthur Chen, College of Oceanography, Oregon State University, Corvallis, OR 97331
69. Edward E. C. Clebsch, Department of Botany, University of Tennessee, Knoxville, TN 37996
70. Roger C. Dahlman, Carbon Dioxide Research Division, Office of Basic Energy Sciences, Room J-311, Code ER-12, U. S. Department of Energy, Washington, DC 20545
71. Prof. Dr. Egon T. Degens, SCOPE/UNEP International Carbon Center, Geologisch-Paläontologisches Institut und Museum, Universität Hamburg, Bundesstrasse 55, D-2000 Hamburg 13, FEDERAL REPUBLIC OF GERMANY
72. Ellen R. M. Druffel, Department of Chemistry, Woods Hole Oceanographic Institution, Woods Hole, MA 02543
73. Arthur C. Echternacht, Department of Zoology, University of Tennessee, Knoxville, TN 37996
74. James A. Edmonds, Battelle Memorial Institute, Pacific Northwest Laboratories, 2030 M Street, NW, Washington, DC 20036
75. Ian G. Enting, Commonwealth Scientific and Industrial Research Organization (CSIRO), Division of Atmospheric Research, Private Bag No. 1, Mordialloc, Vic. 3195, AUSTRALIA
76. Paul G. Falkowski, Department of Applied Science, Oceanographic Sciences Division, Brookhaven National Laboratory, Associated Universities, Inc., Upton, Long Island, NY 11973
77. G. J. Foley, Office of Environmental Process and Effects Research, U.S. Environmental Protection Agency, 401 M Street, SW, RD-682, Washington, DC 20460
78. Roger J. Francey, Commonwealth Scientific and Industrial Research Organization (CSIRO), Division of Atmospheric Research, Private Bag No. 1, Mordialloc, Vic. 3195, AUSTRALIA
79. Hans D. Freyer, Institut für Chemie, Der Kernforschungsanlage Jülich GmbH, Institut 2, Chemie Der Belasteten Atmosphäre, Postfach 1913, D-5170 Jülich, FEDERAL REPUBLIC OF GERMANY
80. Inez Yau-Sheung Fung, NASA Goddard Space Flight Center, Institute for Space Studies, 2880 Broadway, New York, NY 10025
81. Richard M. Gammon, PMEL/NOAA, U.S. Department of Commerce, Building 3, 7600 Sand Point Way, NE, Seattle, WA 98115

82. Robert M. Garrels, Department of Marine Science, University of South Florida, 140 Seventh Avenue South, St. Petersburg, FL 33701
83. M. Patricia Gildea, Complex Systems Research Center, O'Kane House, University of New Hampshire, Durham, NH 03824
84. C. R. Goldman, Professor of Limnology, Director of Tahoe Research Group, Division of Environmental Studies, University of California, Davis, CA 95616
85. Lou Gross, Department of Mathematics, University of Tennessee, Knoxville, TN 37996
86. Thomas J. Gross, Carbon Dioxide Research Division, Office of Basic Energy Sciences, Code ER-12, U.S. Department of Energy, Washington, D.C. 20545
87. Charles A. S. Hall, University of Montana Biological Station, Flathead Lake, East Shore, Big Fork, MT 59911
88. W. Franklin Harris, Executive Office to the Assistant Director for Biological, Behavioral, and Social Sciences, National Science Foundation, 1800 G Street, NW, Room 1140, Washington, DC 20550
89. Henry G. Hengeveld, CO<sub>2</sub>/Climate Advisor, Canadian Climate Centre, Environment Canada, 4905 Dufferin Street, Downsview, Ontario M3H 5T4, CANADA
90. Rafael Herrera, Centro de Ecologica, Institus Venezolano de Investigaciones Cientificas, Caracas 1010, VENEZUELA
91. Bruce B. Hicks, Director, Atmospheric Turbulence and Diffusion Division, National Oceanic and Atmospheric Administration, U.S. Department of Commerce, P.O. Box E, Oak Ridge, TN 37831
92. Richard A. Houghton, The Ecosystems Center, Marine Biological Laboratory, 167 Water Street, Woods Hole, MA 02543
93. J. W. Huckabee, Manager to Project Manager, Ecological Studies Program to Environmental Assessment Department, Electric Power Research Institute, 3412 Hillview Avenue, P.O. Box 10412, Palo Alto, CA 94303
94. Boyd A. Hutchison, Atmospheric Turbulence and Diffusion Division, National Oceanic and Atmospheric Administration, U.S. Department of Commerce, P.O. Box E, Oak Ridge, TN 37831
95. Paul G. Jarvis, Department of Forestry and Natural Resources, University of Edinburgh, Edinburgh EH9 3JU, Scotland, UNITED KINGDOM
96. Carl F. Jordan, Senior Ecologist, The Institute of Ecology, University of Georgia, Athens, GA 30602
97. George Y. Jordy, Director, Office of Program Analysis, Office of Energy Research, ER-30, G-225, U.S. Department of Energy, Washington, DC 20545
98. Charles D. Keeling, Scripps Institution of Oceanography, University of California-San Diego, 2314 Ritter Hall, A-020, La Jolla, CA 92093
99. Tim Kittel, CIRA, Foothills Campus, Colorado State University, Ft. Collins, CO 80523

100. Acad. K. Ya. Kondratyev, USSR Academy of Sciences, Chief, Laboratory of Remote Sensing, Institute for Lake Research, Jevastyanov Street, 9, 196199 Leningrad, USSR
101. F. A. Koomanoff, Director, Carbon Dioxide Research Division, Office of Basic Energy Sciences, Room J-309, Code ER-12, U.S. Department of Energy, Washington, DC 20545
102. Vladimir Kremsa, Institute of Landscape Ecology, Czechoslovak Academy of Sciences, Na sadkach 702, 370 05 Ceske Budejovice, CZECHOSLOVAKIA
103. Radomir Lakusie, Katedra za Ekologiju, Prirodno-Matematicki Fakultet Sarajevo, 71000 Sarajevo, Vojvode Putnika 43a, YUGOSLAVIA
104. John A. Laurmann, Executive Scientist, Engineering Sciences, Gas Research Institute, 8600 West Bryn Mawr Avenue, Chicago, IL 60631
105. Prof. Dr. Helmut Lieth, Fachbereich Biologie/Chemie der Universität Osnabrück, Postfach 4469, Barbarastraße 11, D-4500 Osnabrück, FEDERAL REPUBLIC OF GERMANY
106. Austin Long, Department of Geosciences, Laboratory of Isotope Geochemistry, The University of Arizona, Tucson, AZ 85721
107. Ariel E. Lugo, Project Leader, U.S. Department of Agriculture, Forest Service, Southern Forest Experiment Station, Institute of Tropical Forestry, P.O. Box AQ, Rio Piedras, PR 00928
108. C. J. Mankin, Director, Oklahoma Geological Survey, The University of Oklahoma, 830 Van Vleet Oval, Room 163, Norman, OK 73019
109. Gregg Marland, Oak Ridge Associated Universities, Institute for Energy Analysis, P.O. Box 117, Oak Ridge, TN 37831
110. Steven M. Martin, Department of Fisheries and Wildlife Sciences, School of Forestry and Wildlife Resources, Virginia polytechnic Institute and State University, Blacksburg, VA 24061
111. Helen McCammon, Director, Ecological Research Division, Office of Health and Environmental Research, ER-75, Department of Energy, Washington, DC 20545
112. James J. McCarthy, Director, Museum of Comparative Zoology, Harvard University, Cambridge, MA 02138
113. V. Rick McDaniel, Department of Biological Sciences, Arkansas State University, P.O. Box 599, State University, AR 72467
114. Jerry M. Melillo, Director, Ecosystem Studies Program, Room 336m 1800 G. Street, NW, National Science Foundation, Washington, DC 20005
115. Liliane Merlivat, Departement de Physico-Chimie, CEA-CENS, B.P. No. 2, 91191 Gif-Sur-Yvette Cedex, FRANCE
116. Berrien Moore III, Director, Complex Systems Research Center, Science and Engineering Building, College Road, University of New Hampshire, Durham, NH 03824
117. Hans Oeschger, Physikalisches Institut, Universität Bern, Sidlerstrasse 5, CH-3012 Bern, SWITZERLAND

118. Jerry S. Olson, Eblen Cave Road, Box 361A, Route 2, Lenoir City, TN 37771
119. William S. Osburn, Jr., Ecological Research Division, Office of Health and Environmental Research, Office of Energy Research, MS-E201, EV-33, Room F-216, Department of Energy, Washington, DC 20545
120. H. Gote Ostlund, Rosenstiel School of Marine and Atmospheric Science, Tritium Laboratory, University of Miami, 4600 Rickenbacker Causeway, Miami, FL 33149
121. John J. Pastor, Natural Resources Research Institute, University of Minnesota, 3151 Miller Trunk Highway, Duluth, MN 55812
122. Eldor A. Paul, Department of Crop and Soil Sciences, Michigan State University, East Lansing, MI 48824-1114
123. Graeme I. Pearman, Commonwealth Scientific and Industrial Research Organization (CSIRO), Division of Atmospheric Research, Private Bag No. 1, Mordialloc, Victoria 3195, AUSTRALIA
124. Ralph M. Perhac, Director, Environmental Assessment Department, Electric Power Research Institute, 3412 Hillview Avenue, P.O. Box 10412, Palo Alto, CA 94303
125. James T. Peterson, Director, Geophysical Monitoring for Climatic Change, U.S. Department of Commerce, National Oceanic and Atmospheric Administration, Environmental Research Laboratories, 325 Broadway, Boulder, CO 80303
126. Roger R. Revelle, Program in Science, Technology, and Public Affairs (Q-060), Scripps Institution of Oceanography, University of California-San Diego, La Jolla, CA 92093
127. John F. Richards, Department of History, Duke University, 6727 College Station, Durham, NC 27708
128. Michael R. Riches, Carbon Dioxide Research Division, Office of Basic Energy Sciences, Code ER-12, U.S. Department of Energy, Washington, D.C. 20545
129. Ralph M. Rotty, Department of Mechanical Engineering, University of New Orleans, Lakefront, New Orleans, LA 70148
130. Jorge L. Sarmiento, Director, Geophysical Fluid Dynamics Program, Princeton University, James Forestal Campus, P.O. Box 308, Princeton, NJ 08542
131. William H. Schlesinger, Department of Botany, Duke University, Durham, NC 27706
132. Jakob Schwander, Department of Geological Sciences, Faculty of Natural Sciences and Mathematics, State University of New York at Buffalo, 4240 Ridge Lea Road, Buffalo, NY 14226
133. Steven W. Seagle, Biological Research Laboratories, 130 College Place, Syracuse University, Syracuse, NY 13244-1220
134. Ulrich Siegenthaler, Physikalisches Institut, Universität Bern, Sidlerstrasse 5, CH-3012 Bern, SWITZERLAND
135. Michael A. Spanner, NASA/Ames Research Center MS 242-4, Moffet Field, CA 94035

136. R. J. Stern, Director, Office of Environmental Compliance, MS PE-25, FORRESTAL, U.S. Department of Energy, 1000 Independence Avenue, SW, Washington, DC 20585
137. Boyd R. Strain, Phytotron, Department of Botany, Duke University, Durham, NC 27708
138. Minze Stuiver, Director, Isotope Laboratory, Department of Geological Sciences, Quaternary Research Center, AK-60, University of Washington, Seattle, WA 98195
139. Eric T. Sundquist, Water Resources Division, U.S. Department of the Interior, U.S. Geological Survey, 431 National Center, MS-431, Reston, VA 22092
140. Yu. M. Svirezhev, Computer Center, USSR Academy of Sciences, Moscow, USSR
141. Taro Takahashi, Associate Director, Lamont-Doherty Geological Observatory of Columbia University, Palisades, NY 10964
142. J. R. Toggweiler, Geophysical Fluid Dynamics Program, Princeton University, James Forrestal Campus, P.O. Box 308, Princeton, NJ 08542
143. Christopher Uhl, College of Science, Department of Biology, 202 Buckhout Laboratory, The Pennsylvania State University, University Park, PA 16802
144. James A. Viecelli, Associate Division Leader, T Division, Physics Department, Lawrence Livermore National Laboratory, P.O. Box 808 (L-71), Livermore, CA 94550
145. Leonard H. Weinstein, Program Director of Environmental Biology, Boyce Thompson Institute for Plant Research, Cornell University, Ithaca, NY 14853
146. Ray F. Weiss, Geological Research Division, A-020, Scripps Institution of Oceanography, University of California-San Diego, P.O. Box 1529, La Jolla, CA 92093
147. James W. C. White, Lamont-Doherty Geological Observatory of Columbia University, Palisades, NY 10964
148. Frank J. Wobber, Division of Ecological Research, Office of Health and Environmental Research, Office of Energy Research, Department of Energy, Washington, DC 20545
149. M. Gordon Wolman, Department of Geography and Environmental Engineering, The Johns Hopkins University, Baltimore, MD 21218
150. C. S. Wong, Chief, Ocean Chemistry Division and Marine Carbon Research Centre, Institute of Ocean Sciences, 9860 W. Saanich Road, P.O. Box 6000, Sidney, British Columbia V8L 4B2, CANADA
151. Robert W. Wood, Director, Division of Physical and Technological Research, Department of Energy, Washington, DC 20545
152. George M. Woodwell, Director, The Woods Hole Research Center, P.O. Box 296, Woods Hole, MA 02543
153. Zu Yuangang, Botanical Laboratory, Department of Forestry, Northeast Forestry University, Harbin, CHINA
154. Paul J. Zinke, Department of Forestry and Natural Resources, Mulford Hall, University of California-Berkeley, Berkeley, CA 94720

- 155. Office of Assistant Manager for Energy Research and Development, Oak Ridge Operations, P.O. Box E, Department of Energy, Oak Ridge, TN 37831
- 156-185. Technical Information Center, Oak Ridge, TN 37831

